Vol. 277, No. 1, May 15, 1993

ISSN 0003-2670

ANALYTICA CHIMICA ACTA

An international journal devoted to all branches of analytical chemistry

ELSEVIER

ANALYTICA CHIMICA ACTA

Scope. *Analytica Chimica Acta* publishes original papers, preliminary communications and reviews dealing with every aspect of modern analytical chemistry. Reviews are normally written by invitation of the editors, who welcome suggestions for subjects. Preliminary communications of important urgent work can be printed within four months of submission, if the authors are prepared to forego proofs.

Submission of Papers

Americas

Prof. Harry L. Pardue
Department of Chemistry
1393 BRWN Bldg, Purdue University
West Lafayette, IN 47907–1393
USA
Tel:(+1-317) 494 5320
Fax:(+1-317) 496 1200

Computer Techniques

Prof. J.T. Clerc
Universität Bern
Pharmazeutisches Institut
Baltzerstrasse 5, CH-3012 Bern
Switzerland
Tel:(+41-31) 654171
Fax:(+41-31) 654198

Other Papers

Prof. Alan Townshend
Department of Chemistry
The University
Hull HU6 7RX
Great Britain

Tel:(+44-482) 465027
Fax:(+44-482) 466410

Prof. Willem E. van der Linden
Laboratory for Chemical Analysis
Department of Chemical Technology
Twente University of Technology
P.O. Box 217, 7500 AE Enschede
The Netherlands
Tel:(+31-53) 892629
Fax:(+31-53) 356024

Prof. Paul Worsfold
Dept. of Environmental Sciences
University of Plymouth
Plymouth PL4 8AA
Great Britain

Tel:(+44-752) 233006
Fax:(+44-752) 233009

Submission of an article is understood to imply that the article is original and unpublished and is not being considered for publication elsewhere. *Anal. Chim. Acta* accepts papers in English only. There are no page charges. Manuscripts should conform in layout and style to the papers published in this issue. See inside back cover for "Information for Authors".

Publication. *Analytica Chimica Acta* appears in 14 volumes in 1993. The subscription price for 1993 (Vols. 267–280) is Dfl. 4214.00 plus Dfl. 462.00 (p.p.h.) (total approx. US$ 2672.00). *Vibrational Spectroscopy* appears in 2 volumes in 1993. The subscription price for *Vibrational Spectroscopy* (Vols. 4 and 5) is Dfl. 700.00 plus Dfl. 66.00 (p.p.h.) (total approx. US$ 437.75). The price of a combined subscription (*Anal. Chim. Acta* and *Vib. Spectrosc.*) is Dfl. 4592.00 plus Dfl. 528.00 (p.p.h.) (total approx. US$ 2925.75). All earlier volumes (Vols. 1–266) except Vols. 23 and 28 are available at Dfl. 259.50 (US$ 148.25), plus Dfl. 18.00 (US$ 10.25) p.p.h., per volume. The Dutch guilder price is definitive. The U.S. dollar price is subject to exchange-rate fluctuations and is given only as a guide. Subscriptions are accepted on a prepaid basis only, unless different terms have been previously agreed upon.
Our p.p.h. (postage, packing and handling) charge includes surface delivery of all issues, except to subscribers in the U.S.A., Canada, Australia, New Zealand, China, India, Israel, South Africa, Malaysia, Thailand, Singapore, South Korea, Taiwan, Pakistan, Hong Kong, Brazil, Argentina and Mexico, who receive all issues by air delivery (S.A.L.–Surface Air Lifted) at no extra cost. For Japan, air delivery requires 25% additional charge of the normal postage and handling charge; for all other countries airmail and S.A.L. charges are available upon request.

Subscription orders. Subscription orders can be entered only by calendar year and should be sent to: Elsevier Science Publishers B.V., Journals Department, P.O. Box 211, 1000 AE Amsterdam, The Netherlands. Tel: (+31-20) 5803 642, Telex: 18582, Telefax: (+31-20) 5803598, to which requests for sample copies can also be sent. Claims for issues not received should be made within six months of publication of the issues. If not they cannot be honoured free of charge. Readers in the U.S.A. and Canada can contact the following address: Elsevier Science Publishing Co. Inc., Journal Information Center, 655 Avenue of the Americas, New York, NY 10010, U.S.A. Tel: (+1-212) 6333750, Telefax: (+1-212) 6333990, for further information, or a free sample copy of this or any other Elsevier Science Publishers journal.
Advertisements. Advertisement rates are available from the publisher on request.

Detailed "Instructions to Authors" for *Analytica Chimica Acta* was published in Volume 256, No. 2, pp. 373–376. Free reprints of the "Instructions to Authors" of *Analytica Chimica Acta* and *Vibrational Spectroscopy* are available from the Editors or from: Elsevier Science Publishers B.V., P.O. Box 330, 1000 AH Amsterdam, The Netherlands. Telefax: (+31-20) 5862845.

US mailing notice – Analytica Chimica Acta (ISSN 0003-2670) is published biweekly by Elsevier Science Publishers (Molenwerf 1, Postbus 211, 1000 AE Amsterdam). Annual subscription price in the USA US$ 2672.00 (subject to change), including air speed delivery. Second class postage paid at Jamaica, NY 11431. *USA Postmasters*: Send address changes to Anal. Chim. Acta, Publications Expediting, Inc., 200 Meacham Av., Elmont, NY 11003. Airfreight and mailing in the USA by Publication Expediting.

ANALYTICA CHIMICA ACTA

An international journal devoted to all branches of analytical chemistry

(Full texts are incorporated in CJELSEVIER, a file in the Chemical Journals Online database available on STN International; Abstracted, indexed in: Aluminum Abstracts; Anal. Abstr.; Biol. Abstr.; BIOSIS; Chem. Abstr.; Curr. Contents Phys. Chem. Earth Sci.; Engineered Materials Abstracts; Excerpta Medica; Index Med.; Life Sci.; Mass Spectrom. Bull.; Material Business Alerts; Metals Abstracts; Sci. Citation Index)

VOL. 277 NO. 1 CONTENTS MAY 15, 1993

(Continued overleaf)

Contents (continued)

ANALYTICA CHIMICA ACTA
VOL. 277 (1993)

ANALYTICA CHIMICA ACTA

An international journal devoted to all branches of analytical chemistry
Revue internationale consacrée à tous les domaines de la chimie analytique
Internationale Zeitschrift für alle Gebiete der analytischen Chemie

Anal. Chim. Acta, Vol. 277 (1993)

ELSEVIER, Amsterdam–London–New York–Tokyo

0003-2670/93/$06.00

This issue is printed on acid-free paper.

PRINTED IN THE NETHERLANDS

Analytica Chimica Acta, 277 (1993) 1–8
Elsevier Science Publishers B.V., Amsterdam

Evaluation of flow-injection techniques for microwave plasma torch atomic emission spectrometry

Yolanda Madrid [1], Min Wu, Qinhan Jin [2] and Gary M. Hieftje

Department of Chemistry, Indiana University, Bloomington, IN 47405 (USA)

(Received 15th January 1993)

Abstract

Flow injection (FI) sample introduction was coupled with a recently developed atomic emission source, the microwave plasma torch (MPT), operating at 200 W with Ar as the plasma gas. The use of FI in conjunction with an ultrasonic nebulizer was compared with direct nebulization; parameters taken into consideration include carrier solution flow-rate, aerosol carrier gas flow-rate, sample volume, dispersion coefficients and the effect of two easily ionized concomitant elements. Detection limits and precision of the FI technique were assessed for four sample-loop volumes: 75, 200, 250 and 500 μl. Flow injection was found to offer several advantages over continuous sample introduction: rapid sample throughput and a reduction of memory effects without a loss in sensitivity or precision. Furthermore, by appropriate choice of sample dispersion, a significant reduction of the Na and K interferences can be achieved without a substantial deterioration in sensitivity. An FI system incorporating a microcolumn of bonded silica with octadecyl functional groups was used to determine Cu in synthetic sea water. The sample preconcentration time was one minute at a sample solution flow-rate of 1.0 ml min^{-1}; pure ethanol was used as the eluent. The detection capability in this preconcentration mode was approximately 25 times better than that offered by a comparable continuous nebulization system. The detection limit for Cu was 0.16 ng ml^{-1}, the relative standard deviation at 500 ng ml^{-1} was about 3.2%, and recovery rates were in the 94–97% range.

Keywords: Atomic emission spectrometry; Flow injection; Microwave plasma torch technique; On-line sorbent extraction; Preconcentration; Waters

The low-power microwave-induced plasma (MIP) has become of interest as an excitation source for atomic emission spectrometry (AES) because it provides high sensitivity for a wide range of elements and is inexpensive and simple to operate. The major limitations of using an MIP as an emission source for AES are its low tolerance to the introduction of aqueous samples and a susceptibility to interferences caused by easily ionized elements (EIEs).

The first problem can be overcome or reduced by approaches such as separating the solvent vapor from the analyte material, pre-vaporizing (or atomizing) the analyte species from the sample, employing higher microwave power levels or changing the process by which power is transferred to the plasma (for example, through modification of the cavity or plasma torch design). The second limitation can be controlled by matching the matrix of the standards to that of the sample, by using standard additions, and sometimes by dilution of the sample solution.

Recently a relatively powerful new excitation source, supported by a microwave plasma torch

Correspondence to: G.M. Hieftje, Department of Chemistry, Chemistry Building, Indiana University, Bloomington, IN 47405 (USA).

[1] On leave from Department of Analytical Chemistry, Faculty of Chemistry, Complutense University, Madrid (Spain).

[2] On leave from Department of Chemistry, Jilin University, Changchun 130023 (China).

(MPT), has been developed in this laboratory [1]. This new source offers some very attractive features as an excitation source. Unlike conventional microwave induced plasma (MIP) supporting structures, the MPT assembly possesses a configuration similar to that of the inductively coupled plasma (ICP) torch, consisting of three concentric metal tubes. The plasma formed by the MPT is a flame-like discharge and has a central channel. This configuration makes it possible to introduce aqueous aerosols and molecular species directly into the discharge. Preliminary studies have served to illustrate its capabilities as an atomic emission source [1,2] and as an element-selective detector for gas chromatography (GC) and capillary supercritical fluid chromatography (SFC) [3]. However, as with other microwave induced plasmas, interferences caused by easily ionized elements (EIEs) are significant also in the microwave plasma torch.

It would seem that a combination of flow injection and on-line preconcentration could overcome or reduce the limitations of the MPT as an emission source for AES. Furthermore, the combination FI-MPT could provide the same advantages that have been reported when FI is coupled with flame atomic absorption spectrometry (FAAS) or ICP-AES [4–6].

Although FI methods have been extensively applied to ICP-AES and FAAS, very little has been done so far in coupling FI to an MIP. Gehlhausen and Carnahan [7] determined aqueous fluorine by coupling FI with a He-MIP using an ultrasonic nebulizer. The system operated at 500 W and utilized a modified TM_{010} resonator cavity with a demountable plasma torch. Detection limits (35 ppm F) and the effect of three easily ionized elements and pH were reported. The use of FI reduced both memory effects and analysis time.

The present study explores the attractiveness of the FI mode of sample introduction used with microwave plasma torch emission spectrometry. The effect of operating parameters was investigated and the performance of the system in terms of interferences, sensitivity and detection limits for copper were compared to that obtained with a comparable continuous-mode sample introduction system.

Additionally, a flow-injection on-line preconcentration system was employed to determine Cu in synthetic sea water by MPT-AES. Silica with bonded octadecyl functional groups (reversed-phase C_{18}) was selected as the sorbent material and sodium diethyldithiocarbamate (DDC) was used as the chelating agent. After the sample

TABLE 1

Instrumentation

Components	Model	Manufacturer
Torch	MPT	Laboratory built [1]
Microwave generator	Modified model [8] 420-1	Micro-Now Instrument Co.
Feedback stabilization system		Laboratory built [8]
Nebulizer	Ultrasonic nebulizer desolvation system	Laboratory built
Gas handling	602 Rotameters	Matheson Co.
Lens	50 mm diam., 350 mm focal length, quartz	
Monochromator	Model 270, 0.35 m focal length, ruled grating, 1200 grooves/mm, blaze wavelength: 500 nm, $f/6.8$, slit width 20 μm, slit height 12 mm	
Photomultiplier	1P28A, 800 V	RCA Co.
High voltage, PMT power supply	Model EU 42A, 300–1400 V	Heath Co.
Current amplifier	Model 427	Keithley Instruments
Data acquisition board	Lab ViewII software; Model MB-M10-16X1-18 interface board	National Instruments
Computer	Macintosh II fx	

loading (preconcentration) period, the Cu–DDC complex was eluted directly by pure ethanol and introduced into the MPT by means of an ultrasonic nebulizer equipped with a desolvation system. This arrangement enabled the determination of Cu in synthetic sea water with high precision and accuracy; it also suggests a promising future for the MPT as a detector for liquid chromatography because of its high sensitivity and tolerance to the introduction of molecular species.

EXPERIMENTAL

The components of the system are listed in Table 1 and are described below in some detail. The operating conditions are as listed in Table 2 unless otherwise stated.

Flow injection

The transient signal described later was produced by introducing a sample plug into the carrier stream by flow injection. In the load position of the pneumatically actuated injection valve, the carrier liquid (distilled and deionized water) flows from a peristaltic pump directly through an ultrasonic nebulizer to the plasma while the sample is simultaneously drawn into the sample loop. When the valve is rotated, the path of the carrier liquid is redirected to flow through the sample loop, thereby carrying the sample plug into the MPT. The PTFE tubing used for connections has an inner diameter of 0.5 mm and an outer diameter of 1.5 mm. Four different sample loops were used, with volumes of 75, 200, 250 and 500 μl.

TABLE 2

Operating conditions for the Ar-MPT

Microwave frequency	2450 MHz
Forward power	200 W
Reflected power	0 W
Plasma viewing mode	Side-on
Plasma viewing position	0–24 mm above top of torch
Plasma support gas flow-rate	550 ml min^{-1}
Sample carrier gas flow-rate	300 ml min^{-1}
Desolvation tube temperature	120°C
Cooling water for desolvation	0°C

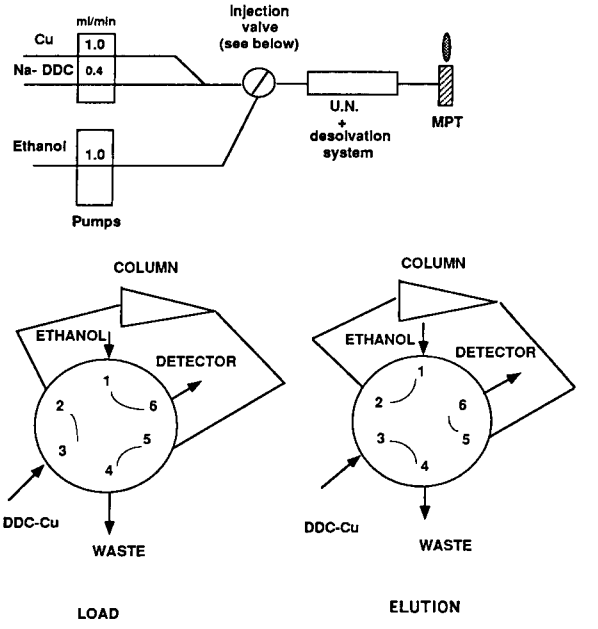

Fig. 1. Schematic diagram of the on-line preconcentration flow injection manifold. U.N. is an ultrasonic nebulizer, DDC–Cu is the copper complex of diethyldithiocarbamate formed by adding Na–DDC to the sample solution.

The FI on-line column preconcentration manifold is illustrated in Fig. 1 and is based on the work previously reported by Fang et al. [9]. The sample loop on the FI valve was replaced by a sorbent extraction column made by packing C_{18}-bonded silica into sections of plastic Eppendorf pipette tips having 5-mm i.d. at one end, 4-mm i.d. at the other and a 15-mm length. The packing was held in place by small plugs of plastic foam.

To minimize dispersion, the column was arranged in the manifold so the sample and the reagent stream flowed from the narrower end of the column (i.e., the pipette tip) to the broader and the eluent passed in the reverse direction. Dispersion was further reduced by using the shortest possible length of 5-mm i.d. tubing.

The DDC solution (0.5 mg ml^{-1}) was introduced at 0.4 ml min^{-1} and mixed with the sample in a reaction coil (4 cm × 0.5 mm i.d.). After the loading period (1 min), the valve was rotated and pure ethanol was pumped through the column at an elution flow-rate of 1.0 ml min^{-1}.

Sample introduction

To introduce sample solutions directly into the plasma a continuous-flow ultrasonic nebulizer equipped with a desolvation system was used. The design of the ultrasonic nebulizer was based on the model of Fassel and Bear [10]. The operating conditions of the ultrasonic nebulizer and desolvation system are compiled in Table 2.

Emission measurements

The Ar plasma system consisted of a microwave plasma torch with structure and dimensions as described elsewhere [1], powered by a modified Micro-Now Model 420-1 microwave generator [8]. The power delivered to the MPT was controlled by a feedback circuit developed recently in this laboratory [8]. The Cu I 324.7 nm line was monitored with a conventional optical system (see Table 2).

All data collection was performed with a Macintosh IIfx computer using LabView II software (National Instruments, Austin, TX) and a National Instruments A/D board (Model NB-M10-16XL-18).

Reagents

All reagents were of analytical-reagent grade and demineralized water was used throughout. The diethylammonium diethyldithiocarbamate (Fluka) solution (0.5 mg ml^{-1}) was prepared by dissolving the reagent in an aqueous 0.01 M acetic acid–0.02 M ammonium mixture (pH 9.2). Standard solutions of copper were prepared by diluting a 1000 mg ml^{-1} stock solution (Johnson Matthey Electronics). A synthetic sea-water matrix containing 35 000 mg l^{-1} sodium chloride, 1300 mg l^{-1} magnesium, 400 mg l^{-1} calcium was prepared and acidified to pH 2 after being spiked with the analyte.

RESULTS AND DISCUSSION

Optimization of experimental parameters

To achieve the best possible analytical performance, several experimental parameters were optimized: carrier solution flow-rate, aerosol carrier gas flow-rate, volume of sample injected and FI tubing length (which controls sample dispersion).

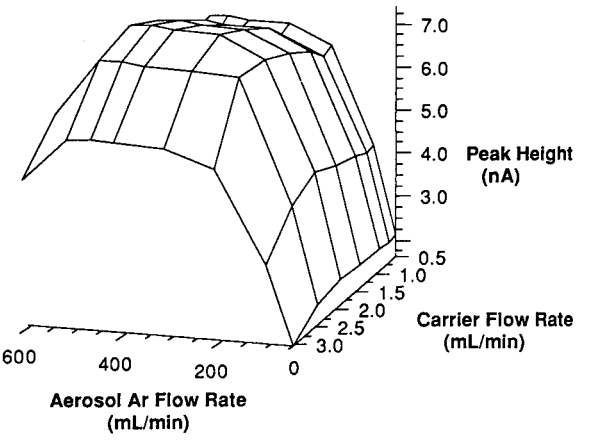

Fig. 2. Effect of the carrier stream and aerosol carrier gas flow-rate on FI-MPT signal for a 5 μg ml^{-1} Cu solution.

Figure 2 shows the influence of carrier solution and aerosol carrier gas flow-rates on FI peak height for a 5.0 μg ml^{-1} Cu solution. The interaction between the two factors is taken into consideration by mapping the entire three-dimensional response surface. Interestingly, changes in the carrier solution flow-rate within the range 0.5–2.0 ml min^{-1} caused only small variations in signal magnitude. However, sharper but smaller peaks were obtained at carrier stream flows above 2.0 ml min^{-1}. The flow of Ar through the ultrasonic nebulizer was explored over the range from 250 to 500 ml min^{-1}. The reproducibility was found to deteriorate and noise was elevated at flow-rates above 400 ml min^{-1}. The range of optimal conditions was very broad for both parameters, indicating that careful control of either is not particularly critical.

Figure 3 illustrates the influence of sample-loop volume on the signal from 5 μg ml^{-1} Cu. The peak height initially increases with sample volume but levels off past a loop volume of 250 μl. A 500-μl sample loop produced a signal about 85% of that obtained during continuous nebulization (0.026 μA).

The effect of the dispersion-tube length over the range of 5 to 30 cm was also investigated and found to be relatively small. This lack of effect is

likely due to the relatively large dead volume of the ultrasonic nebulizer/ desolvation system, which dominates the dispersion process. Dispersion coefficients of the combined system were computed by comparing the peak-height signal produced by a 75-μl injection loop to the steady-state signal generated by the same sample solution; the resulting dispersion factor was 3.

A problem noted during use of the ultrasonic nebulizer was its memory effect. The decay time for that system, defined as the time required for an analyte signal to drop to 1% of its maximum value, was 5 min. In contrast, the decay time of the FI arrangement was only 1 min. As a consequence, with the FI unit a sample can be introduced into the plasma every 1–2 min compared with the 3–5 min required for direct continuous nebulization.

Table 3 lists 3σ detection limits obtained under optimized conditions for each of the four different sample-loop volumes and also for continuous nebulization. Each value is the average of 10 runs collected in two sets. The concentration of Cu used to compute the detection limits was 5.0 μg ml^{-1}. As the volume of the sample loop increases, detection limits obtained with FI sample introduction approach those measured with continuous nebulization. Results for the 500-μl sample loop are indistinguishable from those obtained with continuous sample introduction.

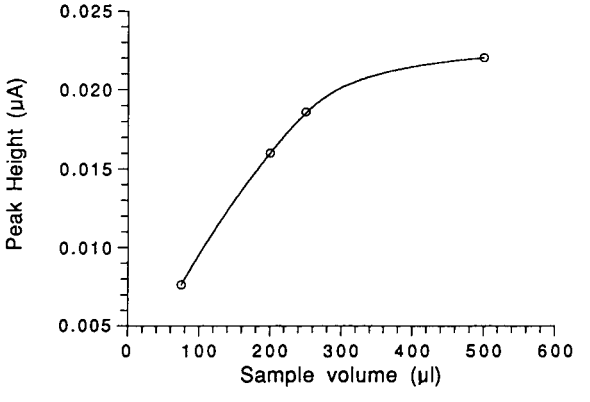

Fig. 3. Effect of the sample volume on FI peak signal from 5 μg ml^{-1} Cu. Carrier stream flow-rate, 1.0 ml min^{-1}; aerosol gas flow-rate, 300 ml min^{-1}. Others conditions are as in Tables 1 and 2. Signal from continuous-flow sample introduction was 0.026 μA.

TABLE 3

Detection limits and precision obtained with the MPT, for flow injection (FI) and continuous flow (Cont.) sample introduction

Sample Introduction	Sample loop volume (μl)	Detection limits (ng ml^{-1})	Precision (%R.S.D.) [a]
FI	75	13.5	1.8
FI	200	9.0	1.6
FI	250	6.4	1.5
FI	500	4.5	1.8
Cont.		4.0	2.1

[a] Obtained for 5 μg ml^{-1} Cu solution.

Table 3 also includes precision values calculated from the same set of data used to compute the detection limits. No significant differences were observed between the results obtained with continuous nebulization and those measured with FI sample introduction.

Interferences

Among the more significant shortcomings of many atomic emission sources are interferences caused by easily ionized elements (EIEs). This problem is particularly serious in most microwave-induced plasmas, in which a low gas temperature produces inefficient desolvation and vaporization of sample aerosol. Results in the literature on this subject are contradictory and indicate that the presence of EIE elements sometimes causes an enhancement and sometimes a suppression of the analyte signal; results seem to be highly dependent on the sample-introduction method and plasma conditions [11–13].

In the present study, the influence of two EIE elements on the performance of the MPT were evaluated using both continuous nebulization and FI sample introduction. Sodium and potassium were chosen to represent EIE elements since they are present in a wide variety of natural matrices: animal and plant materials, blood, sea water and geological samples. No attempts were made to elucidate the fundamental influence of either EIE on the excitation and atomization processes.

Figure 4 shows the effect of increasing concentrations of Na (Fig. 4a) and K (Fig. 4b) on the

signal from 5 μg ml^{-1} Cu using continuous nebulization and flow injection (75-μl sample loop) with the MPT. In the continuous mode an EIE-induced suppression of the Cu signal was obtained for both Na and K. Interestingly, for concentrations of K and Na above 500 ppm, the central channel of the MPT plasma became visibly narrower. The suppression caused by the added Na or K might therefore be related to their influence on the plasma volume; the expanded plasma that exists in the presence of the EIE might resist penetration by sample material, so sample atomization and excitation are less efficient. This hypothesis is in agreement with the experimental results of Selby et al. [13].

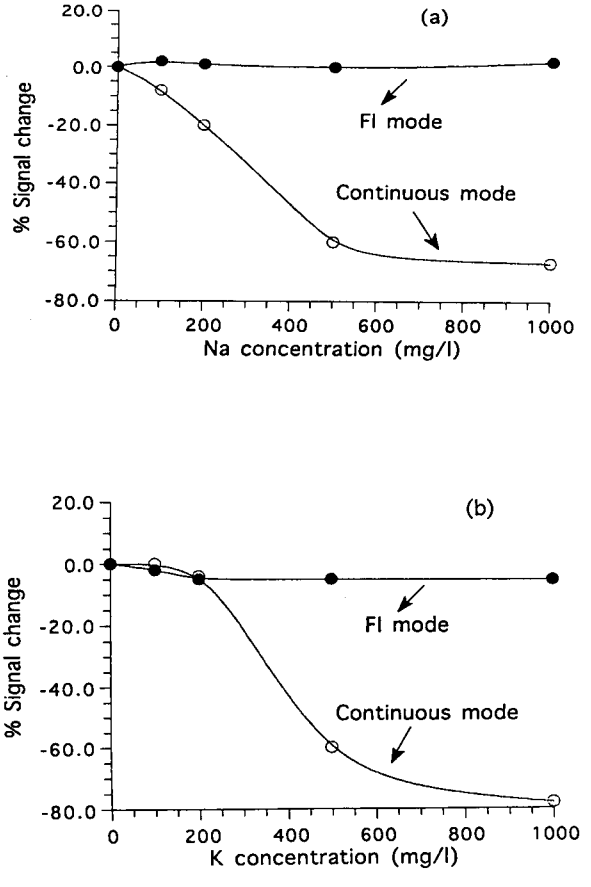

Fig. 4. Effect of Na (a) and K (b) concentration on the signal from 5 μg ml^{-1} Cu in continuous and flow-injection modes. Loop size, 75 μl. Conditions as in Fig. 3. The Cu I 324.7 nm line was used.

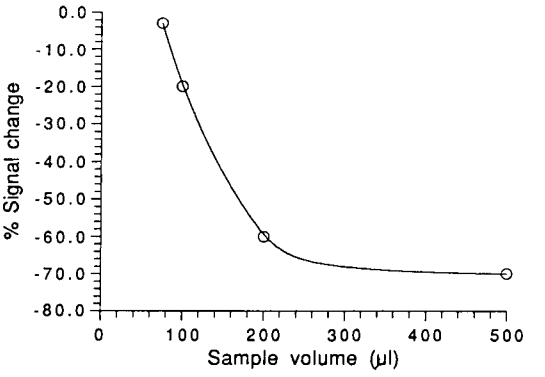

Fig. 5. Effect of FI sample-loop volume on the signal from 5 μg ml^{-1} Cu in the presence of 1000 μg ml^{-1} Na. Conditions as in Fig. 3.

In contrast, the FI mode (with a 75-μl sample loop) is virtually interference-free (cf. Fig. 4). Of course, this freedom from interference might be a result simply of sample dilution (dispersion) in the FI system. To explore this possibility, the same study was carried out but with larger sample-loop volumes. As can be seen from Fig. 5, the 500-μl sample loop produced a suppression of the Cu I signal that was similar to that observed in the conventional mode. Thus it seems that the reduction of interferences by FI is due at least in part to dilution. Yet, by appropriately choosing the dispersion of the FI system, a significant reduction of interferences caused by added Na and K can be achieved without a substantial loss in sensitivity (cf. Table 3). Although manual dilution could be used in a continuous sample-introduction system to eliminate interferences similarly, the procedure would be much longer and more laborious than the "automated" dilution by FI.

Preconcentration flow injection

Although flow injection can reduce the severity of EIE interferences by diluting the sample, even the slight loss in resulting sensitivity can render the method inadequate for the determination of trace elements in pure materials and natural waters. To overcome this limitation, on-line sorbent extraction was explored as a vehicle for preconcentration of copper. This approach has been successfully applied to atomic absorp-

tion spectrometry [9,14–16] and offers several advantages over the kinds of preconcentration media most commonly used: ion exchangers and chelating agents covalently bound on a solid support [15].

In the present study, silica bonded with octadecyl functional groups (reversed-phase C_{18}) was selected as the sorbent material and sodium diethyldithiocarbamate (DDC) was used as a chelating agent for copper. The sorbed DDC–Cu complex was subsequently eluted into the FI-MPT system by pure ethanol. The experimental set up is shown in Fig. 1 and was the same as that reported by Fang et al. [9]. No effort was expended in optimization of the on-line preconcentration system or column design; only the parameters that affect the microwave plasma torch itself were studied: ethanol concentration, eluent flow-rate and acidity.

Previous results [9] showed that quantitative elution of the retained DDC–Cu complex was achieved only when pure ethanol was used for elution. Unfortunately, microwave plasmas usually exhibit a low tolerance to the introduction of water vapor and molecular species. In order to assess the ability of the MPT to handle the required amount of organic solvent, the emission signal from 5 μg ml^{-1} Cu was monitored while a Cu solution was introduced continuously in either water or ethanol as the carrier. Under the same operating conditions, the steady-state signal obtained with ethanol was 30% lower than that produced with water as a carrier. The precision for 10 determinations using water and ethanol was 2.3% and 2.1% (R.S.D.), respectively. Further, the time needed to reach steady state was the same with either ethanol or water as the carrier; also, no significant differences were found in the decay times (5 and 5.2 min for water and ethanol, respectively).

The same experiment was carried out but in the FI mode, using a 75-μl loop. The dispersion of the FI signal was 3.1 and 3.5 for water and ethanol, respectively, and the decay times were 1.8 and 2.0 min. The precision for 10 determinations of Cu by FI using both ethanol and water was 2.5% and 3% (R.S.D.), respectively.

As expected, the MPT can handle large amounts of ethanol without being extinguished (after 6 h running) and without a substantial deterioration in its performance. These results suggest a promising future for the MPT as an atomic-emission detector for liquid chromatography.

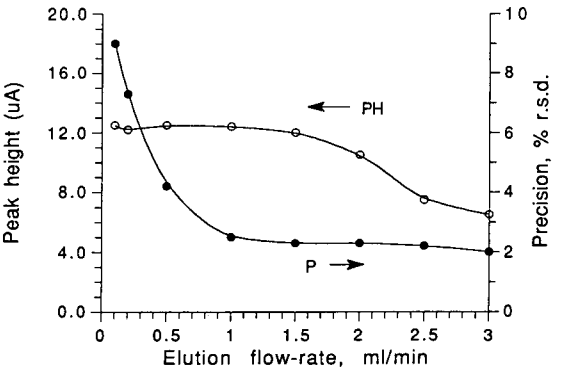

Fig. 6. Effect of eluent flow-rate on peak height (PH) and precision (P) for on-line sorbent extraction preconcentration of Cu (0.5 μg ml^{-1}) with the FI manifold in Fig. 1. Preconcentration period, 1 min. Sample flow-rate, 1.0 ml min^{-1}.

The effect of eluent flow-rate on FI peak height and precision for the measurement of 0.5 μg ml^{-1} Cu (following preconcentration) is shown in Fig. 6. The signal remains essentially constant over the eluent flow range from 0.2 to 2.0 ml min^{-1} but precision is degraded considerably at elution flow-rates below 0.5 ml min^{-1}. Another unfavorable aspect of the lower flow-rates is that the elution peak was broader and even split occasionally into double peaks. As a result, the highest sample-introduction frequency is reduced. An elution flow-rate of 1.0 ml was selected as being optimal, considering overall performance and economy of reagents.

In order to evaluate the effect of solution pH on the response of the preconcentration column, the pH of the initial copper solution was adjusted within the pH range of 1.0–6.0. The results revealed that the peak signals for copper are not influenced appreciably by acidity over the tested range.

Table 4 compiles the enrichment factor, detection limit, precision and maximum sampling frequency for the on-line FI preconcentration determination of Cu by MPT-AES. Its recovery in

TABLE 4

Performance of the on-line sorbent extraction preconcentration MPT system (preconcentration period, 1 min)

Enrichment factor	25
R.S.D. (%) ($n = 10$)	2.3
Recovery from sea water [a] (%)	93–97
Sampling frequency	30 per h
Detection limit (3 σ)	0.16 ng ml^{-1}

[a] Spiked with 0.5 μg ml^{-1} Cu.

synthetic sea water is also cited. The recovery of Cu in synthetic sea water was in the range 93–97% without dilution of the sample. Clearly, the on-line sorbent extraction preconcentration system overcomes one of the principal shortcomings of microwave induced plasmas, while providing a sample enrichment factor of 25.

Conclusions

The present study suggests that the principles and techniques of FI can be exploited to improve the performance and extend the capabilities not only of the microwave plasma torch but also of other, more conventional microwave plasmas. The combination of flow injection with on-line preconcentration is shown to alleviate or even eliminate two of the major limitations of microwave induced plasmas: low tolerance to the introduction of aqueous samples and interferences caused by easily ionized elements. Further, the fact that the MPT can handle large amounts of ethanol without a significant deterioration in analytical performance indicates that it is extremely attractive as an element-selective detector for liquid chromatography, especially for the determination and speciation of non-metals.

Supported in part by the National Institutes of Health through grant R01 GM 46853 and by the National Science Foundation through grant CHE 90-20631. One of the authors (Y. Madrid) wishes to thank the Spanish Ministry of Education and Science for support through a postdoctoral fellowship.

REFERENCES

1 Q. Jin, C. Zhu, M.W. Borer and G.M. Hieftje, Spectrochim. Acta, 46B (1991) 417.
2 Q. Jin, C. Zhu, K. Brushwyler and G.M. Hieftje, Applied Spectrosc., 44 (1990) 183.
3 Q. Jin, F. Wang, C. Zhu, D.M. Chambers and G.M. Hieftje, J. Anal. Atom. Spectrom., 5 (1990) 487.
4 K.R. Brushwyler, L.D. Carter and G.M. Hieftje, Appl. Spectrosc., 44 (1990) 1483.
5 Z. Fang and B. Welz, J. Anal. Atom. Spectrom., 4 (1989) 83.
6 J.F. Tyson, Spectrochim. Acta Rev., 14 (1991) 169.
7 J.M. Gehlhausen and J.W. Carnahan, Anal. Chem., 61 (1989) 674.
8 M.W. Borer, R.E. Ensman, Y. Madrid and G.M. Hieftje, Appl. Spectrosc., 46 (1992) 1162.
9 Z. Fang, T. Guo and B. Welz, Talanta, 38 (1991) 613.
10 V.A. Fassel and B.R. Bear, Spectrochim. Acta, 41B (1986) 1089.
11 Q. Jin, H. Zhang, Y. Duan, A. Yu, Y. Ren, X. Zhang, H. Lu and S. Yu, Microchemical J., 44 (1991) 153.
12 M.H. Abdallah, S. Coulombe, J. Mermet and J. Hubert, Spectrochim. Acta, 37B (1982) 583.
13 M. Selby, R. Rezaaiyaan and G.M. Hieftje, Appl. Spectrosc., 41 (1987) 761.
14 M. Sperling, X. Yin and B. Welz, Spectrochim. Acta, 46B (1991) 1789.
15 J. Ruzicka and A. Arnald, Anal. Chim. Acta, 216 (1989) 243.
16 Z. Fang, M. Sperling and B. Welz, J. Anal. Atom. Spectrom., 5 (1990) 639.

Analytica Chimica Acta, 277 (1993) 9–24
Elsevier Science Publishers B.V., Amsterdam

Mass transfer kinetics for analytical enrichment and sample preparation using supported liquid membranes in a flow system with stagnant acceptor liquid

Jan Åke Jönsson, Per Lövkvist, Gudjón Audunsson [1] and Göran Nilvé

Department of Analytical Chemistry, University of Lund, P.O. Box 124, S-221 00 Lund (Sweden)

(Received 5th October 1992)

Abstract

Supported liquid membranes in a flow system have been utilized for selective sample enrichment, clean up and field sampling, prior to the application of chromatographic and spectrometric analytical methods. For similar objectives, supported liquid membranes may be combined with a number of other analytical systems. The technique has a wide range of applications, especially in the fields of environmental analysis and bioanalysis. This paper presents the theoretical principles for the technique and the mass transfer kinetic equations relevant to most applications. Guidelines for the optimization of experimental conditions and physical dimensions of the extraction devices are discussed.

Keywords: Flow system; Kinetic methods; Mass transfer kinetics; Supported liquid membranes

Liquid membranes, i.e., organic liquids in contact with two separated aqueous phases, have many technical applications, as summarized recently [1,2]. Typically, the technique is used for extraction and re-extraction of various substances for purification and enrichment purposes in production or waste water treatment. One of the configurations used is the supported liquid membrane, where the organic liquid is entrapped in a porous membrane, separating the two aqueous phases.

As originally described by Audunsson [3] and recently reviewed [4], this configuration can be used in a flow system connected to an analytical instrument for various sample handling operations, such as clean-up of complicated biological matrices, trace-level enrichment and time-integrating environmental field sampling. Typically, the aqueous donor phase containing the sample is continuously pumped, while the acceptor phase is stagnant. In a variation of the technique, which could be called selective dialysis, the acceptor phase is also pumped.

Analytical applications of the supported liquid membrane technique, studied up to now, include amines in urine [5] and in blood plasma [6], acidic herbicides in water [7–10] and carboxylic acids in manure [11]. Current, yet unpublished work, involves heavy metals and chlorophenols in water and pharmaceutical substances in biological samples.

The liquid membrane equipment has been connected on-line to a UV detector [3], a gas chromatograph [5,6] and a liquid chromatograph

Correspondence to: J.Å. Jönsson, Department of Analytical Chemistry, University of Lund, P.O. Box 124, S-22100 Lund (Sweden).

[1] Present address: Icelandic Fisheries Laboratories R.F., P.O. Box 1390, Skulagata 4, 121 Reykjavik (Iceland).

[7,10], or off-line with manual transfer of sample to liquid chromatography [8] or gas chromatography [11]. In current work, it is also used prior to atomic absorption spectrometry and ion chromatography.

This paper is intended to describe the basic principles of the supported liquid membrane technique for analytical sample handling with a stagnant acceptor liquid. The mass transfer kinetics, treated here for cases of concern in practical applications, results in expressions describing how the extraction efficiency depends on experimental parameters. These expressions are helpful when various experimental parameters are optimized.

THEORY

General

The membrane, commonly a porous PTFE membrane impregnated with an organic liquid immiscible with water, is mounted between two plates with machined grooves of rectangular cross-section. These grooves form narrow channels, through which aqueous solutions are pumped. For practical reasons, the channels are often arranged in a spiral pattern, but for the purpose of developing a suitable theory for the process, the channels may be considered to be straight. In Fig. 1, the relevant dimensional parameters are illustrated.

The system thus comprises two aqueous liquid phases: the donor phase (D), which occupies the upper part of the channel and the acceptor phase (A) which occupies the lower part. These phases are separated by the non-aqueous membrane phase (M).

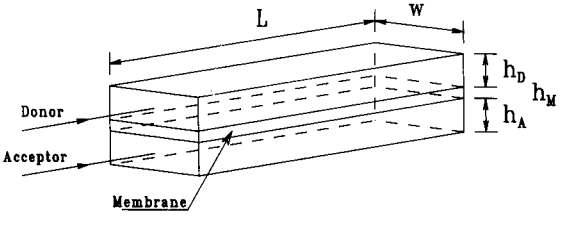

Fig. 1. Dimensions of the membrane channel. L = Length and w = width of the channel; h_D, h_M and h_A = height (thickness) of the donor channel, membrane, and acceptor channels, respectively.

In typical applications, the sample to be processed is pumped through the donor channel, while the acceptor phase is stagnant and collects the extracted analyte. After the sample has passed the membrane separator module, the entire volume of the stagnant acceptor phase is transferred to the equipment used for final analysis. In some cases the whole of the acceptor phase is utilized for analysis and the total amount of analyte collected is of interest. In other cases, the acceptor phase is pumped, after the extraction is completed, through the analytical instrument, e.g., a spectrophotometric detector or an interface for gas or liquid chromatography. Here, the concentration profile in the acceptor phase is of interest.

Analyte molecules are transported from the donor phase to the acceptor phase by diffusion through the membrane. For this to be efficient, the solute must be in an *active* form in the donor phase, i.e., a form that permits it to be dissolved in the organic membrane phase. After diffusion to the acceptor phase, the solution has to be converted to an *inactive* form and "trapped" if it is to be prevented from diffusing back into the membrane. With a stagnant acceptor phase, the total concentration of the analyte can be increased to levels higher than that in the original sample, leading to efficient enrichment.

Apart from the composition of the membrane phase, the selectivity of the mass transfer process relies on the possibility to transform the analytes of interest between active and inactive forms in the required sequence, preferably leaving interfering compounds in an inactive form.

In Table 1, some examples of active and inactive forms are given. Amines, for example, can efficiently be extracted (and enriched) from a donor phase of high pH to an acceptor phase with a lower pH. Acidic compounds are not extracted at these conditions, but compounds which are neutral in both aqueous phases may distribute between all phases, approaching equal activities in the phases. By pumping a pure solution through the donor channel in a separate washing operation after the passage of the sam-

TABLE 1
Examples of active and inactive forms of certain analyte types

Analyte type	Active form	Inactive form
Amines	Uncharged	Protonated (ammonium ions)
Organic acids	Undissociated	Dissociated acids
Metal ions	Neutral complexes	Charged complexes
Metal ions	Neutral complexes	Uncomplexed metal ions
Ionic compounds	Ion pairs	Free ions (counter ions inactivated)

ple, neutral compounds can be washed from the acceptor phase [3–5].

The selectivity and efficiency further depend on the composition of the organic membrane liquid [6,7], as the transport rate is related to the partition coefficient of the analyte between the aqueous and organic phases (this will be detailed below). The incorporation of selective carrier molecules into the liquid membrane, often described in the technical literature [1,2], may be advantageous. However, since the liquid membrane is used in a flow system, i.e., with large aqueous to organic volume ratios, it is imperative that all the components of the membrane phase are insoluble in water. Therefore, the addition of selective complexing agents to the aqueous phases is probably the most practical means of achieving increased selectivity and efficiency.

Mass transfer kinetics

To develop the mass transfer kinetic equations, we consider the overall mass transfer as three serial mass transfer processes. Assuming equilibrium at the donor–membrane interface and between the active and inactive forms of the analyte, the mass transfer in the donor phase is described by the following equations (see the list at the end of the paper for an explanation of all the symbols):

$$J_D = k_D \alpha_D (C_D - C_{DM})$$
$$J_D^i = k_D^i (1 - \alpha_D)(C_D - C_{DM}) \quad (1)$$

α_D is the fraction of the total analyte that is in active form in the donor phase, i.e., in such a form that it may transverse the membrane ($0 \leq \alpha_D \leq 1$). It is assumed that the conditions are such that α_D is constant throughout the donor phase, also in the vicinity of the membrane surface. Typically α_D is close to unity. The distribution constant, K_D, is equal to the partition coefficient $K_P = [A]_{org}/[A]_{aq}$, where A is the analyte in its active form. With a carrier B in the membrane, forming a complex AB with the analyte, K_D is given by:

$$K_D = K_P(K_C[B]_{org} + 1)$$
$$K_C = \frac{[AB]_{org}}{[A]_{org}[B]_{org}} \quad (2)$$

The mass transfer coefficient for the active form in the donor phase is derived from the penetration theory as [3,12]:

$$k_D = \sqrt{\frac{3D_D f_D}{2\pi x}} \quad (3)$$

An analogous expression is valid for the inactive form. It is to be noted that k_D decreases along the donor channel from an initially very high value.

The fluxes for the membrane and acceptor phases may be written analogously to Eqn. 1, noting that no inactive form of the analyte exists in the membrane phase:

$$J_M = k_M(K_D \alpha_D C_{DM} - K_A \alpha_A C_{MA})$$
$$J_A = k_A \alpha_A (C_{MA} - C_A)$$
$$J_A^i = k_A^i (1 - \alpha_A)(C_{MA} - C_A) \quad (4)$$

α_A is assumed to be constant throughout the acceptor phase, even at high degrees of enrichment. In typical applications, α_A is close to zero. For the mass transfer in the membrane phase, the film theory for mass transfer [12] gives:

$$k_M = \frac{D_M \epsilon}{\zeta h_M} \quad (5)$$

An expression for the mass transfer coefficient in the stagnant acceptor phase can be derived from Fick's second law (see Appendix A). This leads to a constant k_A according to the following expression:

$$k_A = 3\frac{D_A}{h_A} \quad (6)$$

The total flux of analyte from the bulk of the donor phase to the bulk of the acceptor phase is described by

$$J = k\left(\alpha_D C_D - \alpha_A \frac{K_A}{K_D} C_A\right) \quad (7)$$

where k is the overall mass transfer coefficient. Implicit in this equation is zero flux ($J = 0$) between all bulk phases at equilibrium. Thus, at steady state mass transfer it holds that:

$$J = J_D + J_D^i = J_M = J_A + J_A^i \quad (8)$$

The further treatment can be simplified by introducing α'_D and α'_A, the fractions of the total flux that represents the active form of the analyte in the donor and acceptor phases, respectively.

$$\alpha'_j = \frac{J_j}{J_j + J_j^i} = \frac{k_j \alpha_j}{k_j \alpha_j + k_j^i (1 - \alpha_j)}, \; j = A, D \quad (9)$$

If the mass transfer coefficients for inactive and active forms are equal, it follows that α and α' are equal. In most cases, this probably is a valid approximation. Note that α'_A and α'_D are independent of x, which is easily demonstrated by substitution Eqns. 3 and 6 into Eqn. 9.

From Eqns. 1, 4, 7–9, an expression for the overall mass transfer coefficient can be derived:

$$\frac{1}{k} = \frac{\alpha'_D}{k_D} + \frac{1}{k_M K_D} + \frac{\alpha'_A K_A}{k_A K_D} \quad (10)$$

The mass transfer model described here is similar to that developed by Audunsson [3,13], but that treatment was limited to the case when the analytes (amines) were entirely in active (neutral) form in the donor phase, and entirely in the inactive (protonated) form in the acceptor phase. This is referred to as *complete trapping*. The conditions for complete trapping correspond to $\alpha_D = 1$ and $\alpha_A = 0$. The introduction of optional values for these parameters in the present treatment permits modelling of more general experimental conditions. As expected, if $\alpha_A = 0$, Eqn. 10 is reduced to the corresponding expression given in Ref. 3. By suitable extension of the treatment above, it is possible to include other kinetic parameters, such as rate constants for the transfer of analyte across a phase boundary or for reactions between active and inactive forms. If such rate constants are independent of position and time, their inclusion will not change the overall appearance of Eqn. 10. For example, to include the effects of slow mass transfer over the aqueous-organic interfaces instead of assuming instantaneous equilibria as in Eqns. 1 and 4, the following terms should be added to the right side of Eqn. 10:

$$\frac{1}{k_{1D}} + \frac{K_A}{K_D}\frac{1}{k_{1A}} \quad (11)$$

In the present treatment, such considerations are conveniently taken into account by the modification of the parameter b (see Eqn. 14 below), but in other treatments of similar problems [12], equilibrium across the interface is usually assumed. In the case of protonation/deprotonation reactions, the reaction between active and inactive forms of the analyte is much faster than mass transfer and may therefore be neglected. However, when working with e.g. metal chelating reactions, additional terms may have to be included in Eqn. 10.

Below, it is assumed that $K_D = K_A = K$. This is often the case, as the composition of the two aqueous phases is usually similar. However, if for example the ionic strengths of the donor and acceptor phases are different, the assumption may not be valid. As is seen from Eqns. 7 and 10, the condition of unequal K_D and K_A has mathematically the same effect as a change in α_A. Therefore, in the theoretical treatment, inequality of partition coefficients may be taken care of by suitable adjustment of the effective value of α_A in cases of incomplete trapping, i.e., when $\alpha_A > 0$.

The overall mass transfer coefficient given by Eqn. 10 reveals some practically important limiting conditions. If the solubility of the analyte in the membrane is relatively large (or if reactions enhancing extractability occurs in the membrane), K is large and the mass transfer in the donor phase is rate-determining (donor-controlled conditions). On the other hand, with decreasing solubility in the membrane, the resistance to mass transfer in the membrane becomes more important ($k \to Kk_M$ as $K \to 0$) and finally dominate the overall resistance to mass transfer; membrane-controlled conditions.

TABLE 2

Different variations of the mass balance problem

Case	Characteristics	Comments
I	$\alpha_A > 0$, $k = f(x)$	Active solute in acceptor, expected dependence of k on x
II	$\alpha_A = 0$, $k = f(x)$	Complete trapping, i.e., no active solute in acceptor, expected dependence of k on x This case was solved in Ref. 3 and 13
III	$\alpha_A > 0$, k = constant	Active solute in acceptor, no dependence of k on x
IV	$\alpha_A = 0$, k = constant	No active solute in acceptor, no dependence of k on x

General mass balance equations

With the donor phase flowing in the x-direction (flow velocity f_D) and disregarding diffusion in that direction, the mass balance equation in the donor phase is:

$$\frac{\partial C_D}{\partial t} = -f_D\frac{\partial C_D}{\partial x} - \frac{k}{h_D}(\alpha_D C_D - \alpha_A C_A) \qquad (12)$$

With a stagnant acceptor phase, no convective transport in the x-direction takes place, resulting in the following mass balance equation in the acceptor phase:

$$\frac{\partial C_A}{\partial t} = \frac{k}{h_A}(\alpha_D C_D - \alpha_A C_A) \qquad (13)$$

Thus, a system of two partial differential equations is obtained, which together with different assumptions about initial and boundary conditions, leads to a number of possible cases. Those of practical relevance are summarized in Table 2. These cases are distinguished by the degree of trapping (α_A) and by the dependence of k on x. As will appear below, no special considerations have to be made regarding the value of α_D.

RESULTS AND DISCUSSION

Solution of mass balance equations

To develop general expressions for the concentration profiles in the donor and acceptor phases, the partial differential Eqns. 12 and 13 must be solved, taking into account that the overall mass transfer coefficient, k, is dependent on x. This dependence is described by Eqn. 10 and it can be expressed using the temporary constants a and b (cf. Eqns. 3, 5 and 6) as:

$$k = \frac{a}{b+\sqrt{x}},\quad a = \frac{1}{\alpha'_D}\sqrt{\frac{3D_D f_D}{2\pi}}$$

$$b = a\left(\frac{1}{Kk_M} + \frac{\alpha'_A}{k_A}\right) \qquad (14)$$

The relevant initial and boundary conditions are as follows:

$$\begin{aligned} &C_D = 0,\ C_A = 0 \quad && t = 0\ \forall\ x \\ &C_D = C_I && t > 0 \wedge x = 0 \end{aligned} \qquad (15)$$

C_I is the concentration of analyte in the incoming sample. The concentration in both channels is initially zero and the front of the sample moves along the donor channel with linear velocity f_D. After the time $t_0 = L/f_D$, the front has reached the end of the channel and the following concentration profile $[C_D = C_I\mathscr{P}_D(x, t)]$ is developed, expressed here as a power series in the variable $\tau = t - t_0$ (see Appendix B and the list of symbols):

$$\mathscr{P}_D(x, t) = \exp\left(-2\beta_D a\sqrt{x}\right)\cdot\left(\frac{\sqrt{x}}{b}+1\right)^{2\beta_D ab} \times\left(1 + \tau c_1 + \tau^2 c_2 + \tau^3 c_3 + \ldots\right) \qquad (16)$$

$$c_1 = \frac{2a^2\alpha_A\beta_D}{h_A}\left[\ln\left(\frac{\sqrt{x}}{b}+1\right) - \frac{\sqrt{x}}{\sqrt{x}+b}\right]$$

$$c_2 = \frac{c_1^2}{4} - \frac{a^3\alpha_A^2\beta_D x}{2bh_A^2(\sqrt{x}+b)^2}$$

$$c_3 = \frac{c_1 c_2}{3} - \frac{c_1^3}{18} + \frac{a^4\alpha_A^3\beta_D x(\sqrt{x}+3b)}{18b^2h_A^3(\sqrt{x}+b)^3} \qquad (17)$$

For the acceptor phase, the concentration profile $[C_A = C_I \mathscr{P}_A(x, t)]$ is given by:

$$\mathscr{P}_A(x, t) = \frac{a\alpha_D}{bh_A}\exp(-2\beta_D a\sqrt{x}) \times\left(\frac{\sqrt{x}}{b}+1\right)^{2\beta_D ab-1} \times\tau(1+\tau d_1+\tau^2 d_2+\tau^3 d_3+\ldots) \quad (18)$$

$$d_1 = \frac{a^2\alpha_A\beta_D}{h_A}\left[\ln\left(\frac{\sqrt{x}}{b}+1\right)-\frac{2a\beta_D\sqrt{x}+1}{2a\beta_D(\sqrt{x}+b)}\right]$$

$$d_2 = \frac{d_1^2}{3}-\frac{a^2\alpha_A^2(2a\beta_D x-b)}{12bh_A^2(\sqrt{x}+b)^2}$$

$$d_3 = \frac{d_1 d_2}{2}-\frac{d_1^3}{9} + \frac{a^3\alpha_A^3(a\beta_D x^{3/2}+3ab\beta_D x-b^2)}{72b^2h_A^3(\sqrt{x}+b)^3} \quad (19)$$

Case I. The complicated expressions above (Eqns. 16–19) are valid for the general case. The more constrained conditions appearing in cases II–IV permit substantial simplifications as described below. The total amount of analyte (n_A) accumulated in the acceptor phase can be derived by integrating C_A over the entire channel length. However, it is more easily evaluated from the difference between the amount of analyte entering the donor channel ($tF_D C_I$) and the amount of analyte leaving the donor channel. This also gives the extraction efficiency $E(t)$, i.e., the fraction of the analyte pumped into the donor channel that is transferred to the acceptor after a certain time. Thus, the following equations, valid for all cases, are obtained:

$$n_A = F_D\left(tC_I - \int_0^t C_D(L, u)\,du\right) = tF_D C_I E$$

$$E = 1-\frac{1}{t}\int_0^t \mathscr{P}_D(L, u)\,du \quad (20)$$

In this general case, the extraction efficiency decreases with time as a significant concentration of analyte in the acceptor phase is built up.

Case II. In case II, it is assumed that the solute is immediately and completely transferred to its inactive form in the acceptor phase, and thereby prevented from passing back into the membrane and subsequently to the donor phase. This is more or less valid in many practical applications of the technique. Using the notation above, the condition corresponds to $\alpha_A = 0$, so Eqn. 16 is simplified to:

$$\mathscr{P}_D(x) = \exp(-2\beta_D a\sqrt{x})\left(\frac{\sqrt{x}}{b}+1\right)^{2\beta_D ab} \quad (21)$$

The acceptor phase concentration profile is found from Eqn. 18 with $\alpha_A = 0$:

$$C_A = \tau C_I\frac{Kk_M\alpha_D}{h_A}\exp(-2\beta_D a\sqrt{x}) \times\left(\frac{\sqrt{x}}{b}+1\right)^{2\beta_D ab-1} \quad (22)$$

This equation (with $\alpha_D = 1$) was presented earlier [3] in a slightly different form.

The maximum acceptor phase concentration is found at the beginning of the channel. If the stagnant acceptor phase is subsequently moved with flow velocity f_A from the membrane separator unit, the concentration profile leaving the membrane unit is given by Eqn. 22, after exchanging x for t/f_A, where t is the time from the start of the transfer. As the concentration profile will be broadened by dispersion in the tubings, Eqn. 22 does not accurately describe the profile observed with, e.g., a flow photometer. This has been extensively discussed in Ref. 3, where the following approximate relation for the maximum of the observed profile was given:

$$C_P^{max} = k_1\exp\left(\frac{k_2}{\sqrt{f_D}}\right) \quad (23)$$

Here k_1 and k_2 are independent of f_D.

The total amount of analyte (n_A) accumulated in the acceptor phase, as well as the extraction efficiency E are given by Eqn. 20, but in this case $\mathscr{P}_D$ is independent of t. Concequently, n_A increases linearly with time, the extraction efficiency E is constant and Eqn. 20 is simplified to:

$$n_A = tF_D C_I E$$

$$E = [1-\mathscr{P}_D(L, t)] \quad (24)$$

Case III. This case implies a constant mass transfer coefficient in the donor phase, independent of the position along the channel. It is valid when the solubility of the analyte in the membrane phase is small. As was seen above in the discussion of Eqn. 10, this leads to membrane-controlled conditions where the mass transfer coefficient has the product Kk_M as a limit. The concentration profile in the donor phase is found by simplification of Eqns. 16 and 17:

$$\mathscr{P}_D(x, t) = \exp(-k\beta_D x) \times \left[1 + \tau\frac{k^2\alpha_A\beta_D x}{h_A} - \tau^2\frac{k^3\alpha_A^2\beta_D x}{2h_A^2} \times \left(1 - \frac{k\beta_D x}{2}\right) + \ldots\right] \quad (25)$$

The amount of accumulated analyte, n_A, and the extraction efficiency, E, are also here given by Eqn. 20. The concentration in the acceptor phase is found by simplification of Eqns. 18 and 19:

$$C_A = C_I\frac{k\alpha_D}{h_A}\exp(-k\beta_D x) \times\tau\left[1 - \tau\frac{k\alpha_A}{2h_A}(1 - k\beta_D x) + \tau^2\frac{k^2\alpha_A^2}{6h_A^2}\left(1 - 2k\beta_D x + \tfrac{1}{2}k^2\beta_D^2 x^2\right) + \ldots\right] \quad (26)$$

Case IV. For the most simple case, where $\alpha_A = 0$ and k is independent of x (i.e., a combination of cases II and III), C_D and C_A exponentially decrease along the donor and acceptor channels:

$$\mathscr{P}_D(x) = \exp(-k\beta_D x)$$

$$C_A = \tau C_I\frac{k\alpha_D}{h_A}\exp(-k\beta_D x) \quad (27)$$

Influence of the degree of trapping (α_A)

If trapping is complete ($\alpha_A = 0$), the concentration profile in the donor channel is constant with time, leading to a constant extraction efficiency and a linear increase of the concentration in the acceptor channel with time (Eqns. 21, 22 and 24). These conditions are obviously desirable in practical applications of the technique. With incomplete trapping, the extraction efficiency will decrease with time until a sufficient concentration in the acceptor channel is reached, representing equilibrium concentrations of the analyte in all three phases and, consequently, zero flux.

In order to illustrate this behaviour, model calculations (using Eqns. 16, 17 and 20) have been performed for some typical cases. In Fig. 2, calculated curves of E versus L are presented for different enrichment times and $\alpha_A = 0.01$. The other parameters used in the calculation are given in the first row of Table 3.

It is seen that for a given channel length L, the efficiency decreases with time, as active analyte builds up on the acceptor side. Even with this relatively small value of α_A, significant changes in E will be observed after only a few minutes enrichment time.

For other values of $\alpha_A > 0$, similar curves are observed. The rate of decrease of E versus time

TABLE 3

Parameter values used in Figs. 2–4

Row	D_A, D_D, D_M ($cm^2\ s^{-1}$)	F_D ($cm^3\ min^{-1}$)	h_A, h_D (cm)	h_M (cm)	K	α_A	α_D	L (cm)	w (cm)
1	5×10^{-6}	0.50	0.025	0.006	1	0.01	1.0	v [a]	0.15
2	8×10^{-6}	0.20	0.025	0.006	10.1	v	v	15	0.15
3	8×10^{-6}	0.25	0.025	0.006	0.18	v	v	15	0.15

[a] v = Varied.

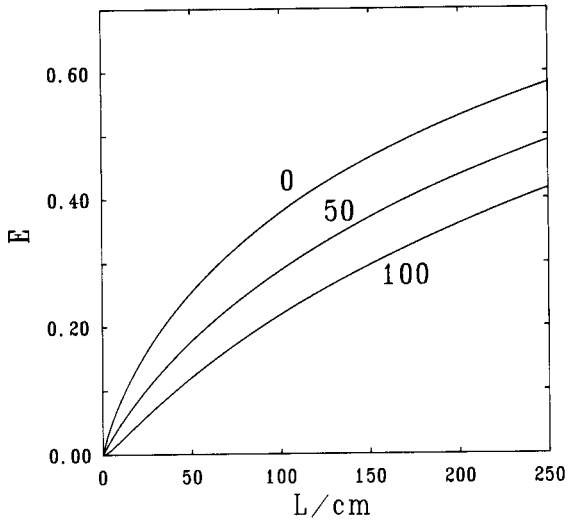

Fig. 2. Extraction efficiency E for $\alpha_A = 0.01$ versus channel length L after 0, 50 and 100 min. Other parameters as given in row 1 of Table 3.

is roughly proportional to α_A, i.e., the efficiency curve (E vs. L) after 10 min with $\alpha_A = 0.1$ is similar to that shown in the figure for 100 min with $\alpha_A = 0.01$. A reasonable criterion for sample preparation applications, is a relative decrease of E amounting to 1% per hour. This leads to a maximum value for $\alpha_A(\alpha_{A,crit})$ of about 5×10^{-4}. For the application of the liquid membrane technique for field sampling [8,9], where extraction times may be several days, the criterion of 1% loss per hour is not stringent enough and smaller values of $\alpha_{A,crit}$ must be used.

These calculations can not be extended to much longer times than shown in Fig. 2, due to the form of Eqn. 16 where the time series does not always converge (especially close to $x = 0$).

Using a spreadsheet program, E and dE/dt are easily calculated. In this way it is found that $\alpha_{A,crit}$, as defined above, in typical cases is between 10^{-4} and 10^{-3}.

In the case of acidic or basic analytes, the value of α_A is controlled by the pH in the acceptor phase. For a monoprotonic base, α_A is given by:

$$\alpha_A = \frac{K_a}{[H^+] + K_a} \qquad (28)$$

Hence, the condition $\alpha_A < 5 \times 10^{-4}$ is equivalent to $pH < pK_a - 3.3$ in the acceptor phase. For an acid, the corresponding condition is $pH > pK_a + 3.3$. These requirements are in agreement with experimental observations made earlier [5,6].

Influence of α_D

For membrane-controlled conditions, the parameter α_D influences the extraction efficiency in a roughly proportional manner, i.e., if $\alpha_D = 0.5$, the efficiency is about half of the value when $\alpha_D = 1$. With increasing influence of the mass transfer in the donor phase, the relative efficiency increases. Therefore, a safe criterion is that $\alpha_D > 0.99$, which leads to maximum 1% loss of efficiency. For bases, this corresponds (cf, Eqn. 28) to $pH > pK_a + 2$ in the donor phase, and for acids to $pH < pK_a - 2$.

Experimental study of the influence of α_A and α_D

An experimental investigation of the extraction efficiency as a function of both donor and acceptor phase pH was made for the extraction of phenol using an *n*-undecane membrane. By means of Eqns. 16 and 20 above, theoretical relationships were calculated and compared with the experimental data. α_A and α_D were calculated using Eqn. 28 with pK_a for phenol equal to 9.9 [14]. The other parameters used are listed in Table 3 (row 3). The diffusion coefficients were estimated by means of the Stokes–Einstein equation [12]. The partition coefficient (0.18) was determined by liquid chromatographic analysis of a water phase containing 2 mg l^{-1} phenol and 0.2 M H_2SO_4 before and after shaking with *n*-undecane.

First, the extraction efficiency was determined at different values of pH in the acceptor phase and for three different enrichment times. The variation of the acceptor pH was made while keeping the ionic strength constant. The donor phase was 0.2 M H_2SO_4, where α_D is practically unity. The results are shown in Fig. 3. For the shortest enrichment time, the calculation of E converges in the whole range of $0 < \alpha_A < 1$, and the calculated curve agrees reasonably well with the experimental points. For longer enrichment

times, the calculation can only be performed in a part of the pH range, due to the convergence problem mentioned above.

Furthermore, the pH of the donor phase was varied with the acceptor phase consisting of 0.1 M NaOH ($\alpha_A \approx 0$). Also in this case, the theoretically calculated curve and the experimental results agreed.

In Ref. 5 an experimental investigation of the extraction efficiency as a function of both donor and acceptor phase pH was presented for the extraction of triethylamine (TEA) (Fig. 3 in Ref. 5). Also here, it is possible to compare experimental data with predictions from Eqns. 16 and 20.

The measurements of E were described in Ref. 5. When the acceptor pH was varied, the donor phase was 0.8 M NaOH, giving $\alpha_D \approx 1$. Similarly, the donor phase pH was varied with an acceptor phase of 0.5 M H_2SO_4 ($\alpha_A \approx 0$). All variations of pH were made at constant ionic strength. The pK_a was 11.0 and the partition coefficient K was 10.1 [5].

As seen in Fig. 4, a satisfactory agreement between the theoretically calculated curve and the experimental results was obtained when the acceptor pH was varied. The curve for variation of the donor pH agreed, however, with the experiments only if an effective pK_a value of 13.3 was assumed, (i.e., higher than the literature value). This is probably due to the fact that the ionic strength of the donor solution was as high as 1.3 M [5].

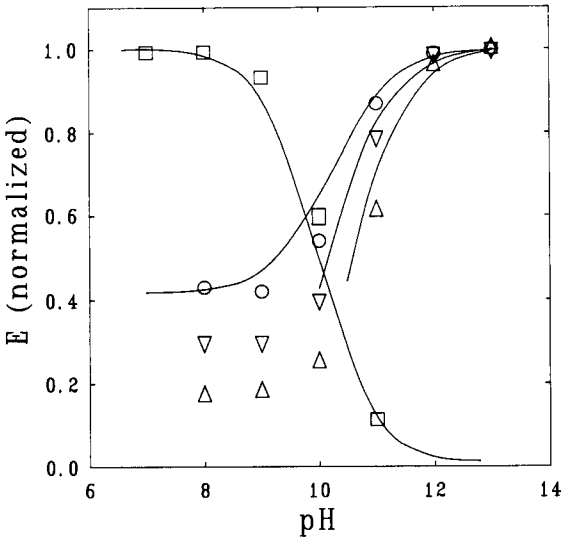

Fig. 3. Normalized extraction efficiency for phenol vs. donor pH (□) and acceptor pH after 4 (○), 8 (▽) and 16 (△) minutes. Points are experimental data, curves are calculated as described in the text.

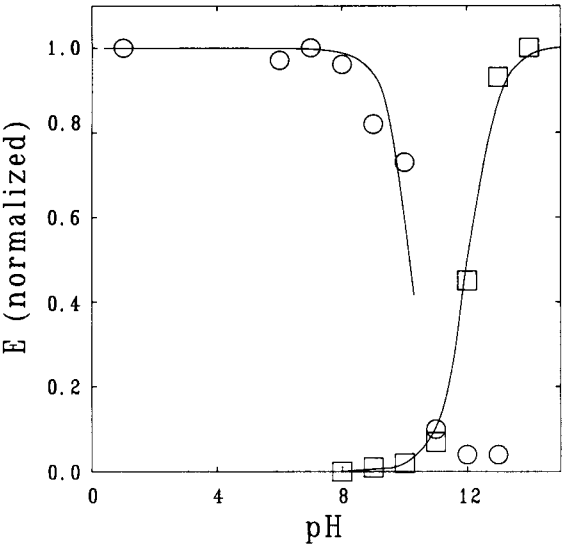

Fig. 4. Normalized extraction efficiency for triethylamine vs. pH in the donor (□) and the acceptor phase (○) after 5 min enrichment. Points are experimental data [5], curves are calculated as described in the text.

Comparing Figs. 3 and 4, it is seen that the theoretical donor curve is centered around pH = pK_a in the phenol case, where the mass transfer is membrane-controlled due to the low K value. In the TEA case, a higher K value leads to donor-controlled conditions and a correspondingly increased mass transfer as both the active and the inactive forms of the solute contribute the total mass transfer when $\alpha_D < 1$ (cf., Eqn. 1). Therefore, the theoretical curve is shifted to lower pH values (more efficient extraction) relative to the effective pK_a.

Influence of mass transfer parameters

For general discussions about the influence of various parameters on the extraction efficiency,

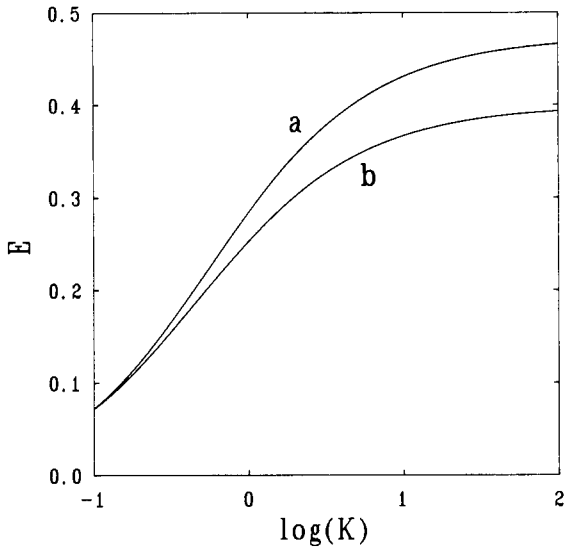

Fig. 5. Influence of the partition coefficient K on the extraction efficiency E. Calculated from Eqn. 20 with (a) $D_D = 8 \times 10^{-6}$ cm^2 s^{-1} and (b) $D_D = 5 \times 10^{-6}$ cm^2 s^{-1}, $\alpha_A = 0$ and $\alpha_D = 1$, while other parameters are given in row 2 of Table 3.

we assume that $\alpha_A = 0$ and $\alpha_D = 1$, i.e., that Eqn. 21 applies to the donor phase concentration profile.

In practice, the value of K can vary over several orders of magnitude from below 0.1, where the resistance to mass transfer is mainly in the membrane to over 50, where the resistance to mass transfer is mainly in the donor phase. The range within which the diffusion coefficient falls, is usually considerably smaller.

The influence of these parameters on the extraction efficiency is illustrated in Fig. 5, where curve a is calculated by Eqn. 21, using parameter values in row 2 of Table 3 ($\alpha_A = 0$, $\alpha_D = 1$). Curve b is calculated with the same parameters as curve a, except that the value of D_D is 5×10^{-6} instead of 8×10^{-6} as in curve a. At low values of K, the efficiency is low, and a change in D_D has little effect: the total mass transfer is controlled by mass transfer in the membrane phase. When K is higher than, say, 10, a further increase in K has little effect, and the total mass transfer is mostly controlled by mass transfer in the donor phase. Changes in D_D then become significant.

Influence of physical dimensions

Equation 21 can be written in terms of three independent variables: the reduced flow-rate $\phi = F_D/Lw$, h_D/D_D, and Kk_M, i.e.,

$$\mathscr{P} = \exp\left[\frac{3D_D}{\pi h_D K k_M} \ln\left(1 + K k_M \sqrt{\frac{2\pi h_D}{3D_D \phi}}\right) - \sqrt{\frac{6D_D}{\pi h_D \phi}}\right] \quad (29)$$

Thus, the length or width of the channel and the donor flow-rate are inversely related, and an increase of the channel length or area is equivalent to a corresponding decrease of the donor flow-rate. Generally, an increase in ϕ leads to lower efficiency.

In Fig. 6, the influence of ϕ on the efficiency is illustrated in two cases: curve a, calculated from Eqn. 29 with parameters from row 2 of Table 3 ($\alpha_A = 0$, $\alpha_D = 1$) represents donor-controlled conditions. Curve b, calculated with the same parameters as curve a, except that $K = 0.1$, represents membrane-controlled conditions, leading to a substantially lower efficiency. As ϕ ap-

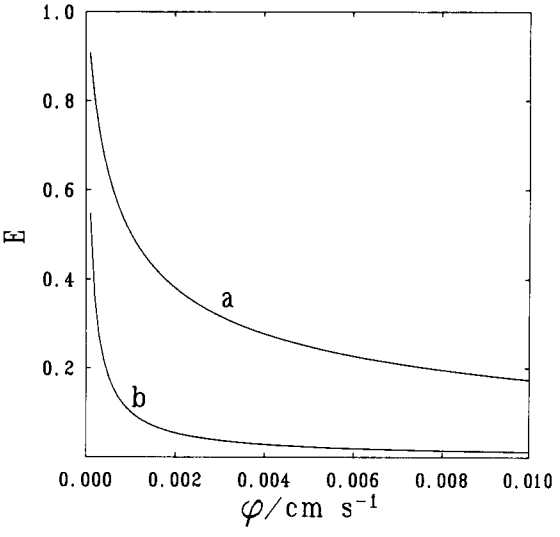

Fig. 6. Influence of the reduced flow-rate ϕ on the extraction efficiency E. Calculated from Eqn. 28 with (a) $K = 10.1$ and (b) $K = 0.1$. Other parameters are given in row 2 of Table 3.

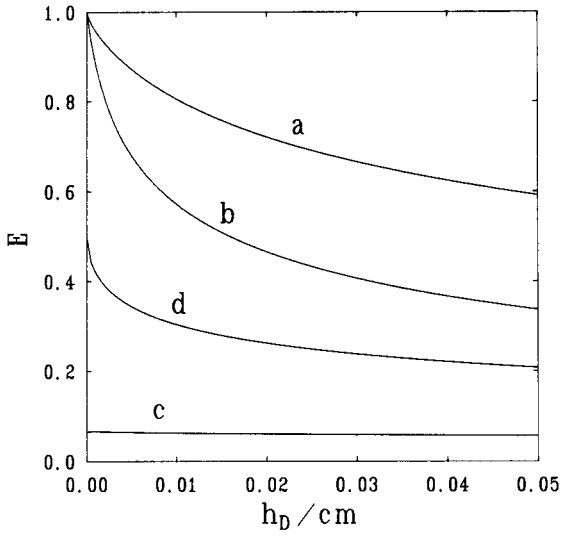

Fig. 7. Dependence of the extraction efficiency, E, on depth of the donor channel, h_D. Efficiency is calculated by Eqn. 18 and 20 with (a) $L = 250$ cm and other parameters as in row 1 of Table 3, (b) parameters as in row 2, (c) parameters as in row 3 and (d) $K = 1$ and other parameters as in row 3. In all cases, $\lambda_A = 0$ and $\alpha_D = 1$.

proaches zero, the efficiency approaches unity independently of K.

The depth of the donor channel affects the efficiency in a more complex manner. Figure 7 shows how h_D influences the efficiency.

It is seen that the efficiency generally increases when h_D is decreased. In curve c, where the overall mass transfer efficiency is very small (due to a low value of K), the mass transfer is almost entirely controlled by mass transfer in the membrane phase. At these conditions, the efficiency is very low and almost independent of h_D, even when h_D approaches zero. Only when the total mass transfer is predominantly controlled by mass transfer in the donor phase, shown by curves a and b, does E approach unity when h_D becomes infinitely small. The value of E at infinitely small h_D, can be derived from Eqn. 29, giving:

$$\lim_{h_D \to 0} E = 1 - \exp\left(-\frac{Kk_M}{\phi}\right) \qquad (30)$$

Optimization for obtaining maximal efficiency

In many applications of the liquid membrane technique, maximal efficiency is desired. This is especially important when the available sample volume is limited, as is often the case in sample clean-up work, particularly when the sample requires further processing after the treatment with the liquid membrane technique.

The first step in a strategy to obtain a high efficiency is to select chemical conditions in the three phases that ascertains as high K as possible (preferable $K > 10$) and to assure complete trapping, i.e., $\alpha_A < 0.001$ and $\alpha_D > 0.99$. The diffusion coefficient in the donor phase should be as large as possible; it may be influenced by, e.g., the viscosity of the sample solution or chemical interactions with matrix constituents. A somewhat lowered efficiency was noted in the extraction of amines from urine and blood plasma as compared to aqueous solutions [5,6]. Difficulties related to both viscosity and chemical interactions with matrix constituents may be solved (at the cost of increased processing time) by appropriate dilution of the sample prior to membrane workup [5].

Secondly, the dimensions of the membrane extractor should be adjusted to the demands of the subsequent processing. As mentioned above, efficiency increases with membrane area Lw. The upper limit of this area will be set by the volume of acceptor phase (Lwh_A) that is compatible with the receiving equipment. Thus, to achieve maximum membrane area, while keeping the acceptor volume at minimum, h_A should be minimized. This is in turn limited by the shallowest groove that is possible to machine (in the order of 0.10 mm).

There is no theoretical optimum for the relation between L and w, i.e., of the geometry of the membrane surface, and its shape is not critical. The channels are usually machined in a relatively long and narrow spiral or in a meandering fashion, which prevents stagnant spots to occur.

From the discussion above, it is clear that the maximum efficiency is obtained if the depth of the donor channel (h_D) is as close to zero as possible. Thus, it should generally be selected as small as mechanically possible.

Finally, the optimal donor flow rate, F_D, should be selected. From Fig. 6, it is seen that maximum efficiency is obtained when F_D is decreased to

low values, obviously at the expense of time. Assume that the volume of sample to be processed is V and that the maximum acceptable time is t_{max}. A part of this time [$t_0 = (Lwh_D)/F_D$] is needed to transport the trailing end of the sample plug through the channel, assuring that the entire sample contacts the whole membrane surface. The optimum flow-rate that can be used is therefore:

$$F_D = \frac{V + Lwh_D}{t_{max}} \quad (31)$$

Optimization for maximal extraction efficiency with multiple passages of the same sample portion

If the experimental arrangements permit, the sample to be extracted can be passed through the donor channel several times, either by recycling or by a "push–pull" operation. By increasing the flow-rate in proportion to the number of passages, the total processing time may be kept constant. Thus, it is of interest to compare the extraction efficiency obtained in normal operation with that obtained after two passages with double donor flow-rate, etc.

If the extraction efficiency during the first passage is E, a fraction $1 - E$ of the total analyte amount remains in the outlet of the donor channel. This is then extracted again, and after the second passage, $(1 - E)^2$ of the initial analyte amount remains. Thus, the overall extraction efficiency, E_n, after n passages is

$$E_n = 1 - (1 - E)^n \quad (32)$$

In Table 4, results of calculations for two typical cases are shown. The hold-up time t_0 is neglected. It is seen that a higher overall efficiency can be obtained by increasing the donor flow-rate and at the same time increase the number of passages over the membrane. The total contact time is the same, but the mass transfer in the donor phase will be more efficient as the flow-rate increases (cf., Eqn. 3). This effect is only of significance with donor-controlled conditions; if the mass transfer is entirely membrane-controlled, only the contact time determines the degree of enrichment, which is seen as a much smaller influence of the number of passages on the overall efficiency in the last column of Table 4.

TABLE 4

Overall extraction efficiency E_n after different number of passages (n) through the donor channel
(Conditions as in rows 2 and 3 of Table 3. F_D is n times the F_D in Table 3, making the total enrichment time constant for all values of n)

n	E_n (row 2)	E_n (row 3)
1	0.43	0.096
2	0.54	0.101
5	0.68	0.108
10	0.78	0.112

Optimization for maximal accumulation factor

In most environmental applications, the main objective is the enrichment of an analyte present in low concentration. If the volume of the available sample is not limiting, it is preferable to maximize the accumulation factor per unit time, E_a, where:

$$E_a = \frac{n_A}{tC_I} = EF_D \quad (33)$$

As in the previous case, the entire acceptor volume is assumed to be transferred to final analysis. In many cases, the acceptor volume is not critical, provided that the entire sample is transferred. This is for example the case when the technique is used for field sampling [8,9], where the entire acceptor phase is transferred to a precolumn after the enrichment is completed. The entire amount of accumulated analyte is subsequently injected onto the chromatographic column.

In Fig. 8, $E_a = EF_D$ is plotted versus F_D for the same cases as in Fig. 6. It is seen that when donor-controlled conditions prevail (curve a) much better accumulation rates are obtained compared to when membrane-controlled conditions dominate (curve b). Apart from choosing as favourable chemical conditions as possible, the product membrane area, Lw, should be as large as possible, leading to a small ϕ for a given F_D (cf. Eqn. 29).

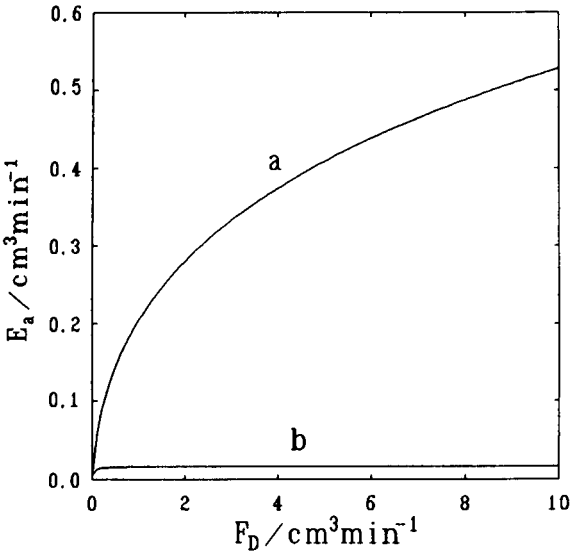

Fig. 8. Influence of the flow-rate on the accumulation factor E_a. Calculated from Eqns. 28 and 31 with (a) $K = 10.1$ and (b) $K = 0.1$. Other parameters as given in row 2 of Table 3.

The value of the accumulation factor, E_a, increases with increasing flow-rates, as demonstrated in Fig. 8. At increasing flow-rates, the extraction efficiency, E, decreases (cf., Fig. 6), but for the purpose of high accumulation rates, larger through-put of sample is beneficial, counteracting the low efficiency. At very high flow-rates, E_a approaches the value $LwKk_M$, which thus becomes the maximum accumulation factor possible. As seen in Fig. 8 (curve b) the maximum value (0.018) is reached for low flow-rates at membrane-controlled conditions, while at donor-controlled conditions (curve a) the limiting value (1.818) is reached only at unrealistically high flow-rates.

Efficiency, E, and thereby the accumulation factor E_a increase with decreased donor channel depths, h_D, according to Fig. 7. However, h_D does not limit the value of E_a at large flow-rates as it does for E, but only the slope of the curves in Fig. 8. For example, E_a corresponding to curve a in Fig. 8 increases by ca. 40% when h_D is decreased to 0.01 cm (from 0.025 cm) at $F_D = 10$ cm^3 s^{-1}. This increase is expected when h_D is decreased under donor-controlled conditions. Unfortunately, a decreased h_D, leads to an increased pressure drop across the donor channel, which limits the maximum attainable flow-rate and thus E_a. As the pressure drop for a slit-shaped channel is inversely proportional to h_D^3 [14], it is more beneficial to increase h_D and thereby permit larger donor flow-rates (8 times higher if h_D is doubled). This will eventually result in turbulent flow, which will further increase the extraction efficiency due to improved mixing in the donor channel.

By increasing the w to L ratio, the pressure drop will also be decreased, permitting a higher donor flow-rate, but without the possibility of turbulent flow. In any case, the price to be paid for a high donor flow rate and thus a higher accumulation factor is a larger consumption of sample.

Many co-workers contributed to various aspects of the liquid membrane technique and they are gratefully acknowledged. These include G. Bremle, L. Grönberg, H. Irth, B. Lindegård, L. Mathiasson, M. Knutsson, M. Papantoni, R. Stebbins and J. Trocewicz. Financial support for projects leading to the present work has been obtained from the Swedish Natural Science Research Council, the Swedish Council for Forestry and Agricultural Research, the Swedish Environmental Protection Agency, the Swedish Work Environment Fund, the Swedish Institute and the Crafoord Foundation.

LIST OF SYMBOLS

a, b	temporary constants (see Eqn. 14)
c_1, c_2, c_3	temporary constants (see Eqns. 16, 17)
d_1, d_2, d_3	temporary constants (see Eqns. 18, 19)
C_j	total concentration of analyte in phase j (A, D, DM, MA)
C_I	concentration of analyte in sample to be extracted
C_p^{max}	maximum of observed concentration profile in the acceptor phase
D_j	diffusion coefficient for active form of analyte in phase j (A, D, M)
E	extraction efficiency
E_a	accumulation factor (see Eqn. 33)

E_n extraction efficiency after n passages (see Eqn. 32)
f_j linear flow velocity in phase j (A, D)
F_j volume flow-rate in phase j (A, D)
h_j height (thickness) of phase j (A, D, M)
J overall flux
J_j flux in phase j (A, D, M)
K effective partition coefficient
K_a dissociation constant
K_j partition coefficient between organic phase and phase j (A, D)
K_C complexation constant (see Eqn. 2)
K_P partition coefficient
k overall mass transfer coefficient
k_j mass transfer coefficient in phase j (A, D, M)
k_1, k_2 parameters in Eqn. 23
L length of the channels
n number of passages over the membrane (see Eqn. 32)
n_A amount of accumulated analyte in acceptor phase
$\mathscr{P}_j$ concentration profile in phase j (A, D)
t time from start of experiment
t_0 time for transport through the donor channel (L/f_D)
t_{max} maximum enrichment time (see Eqn. 31)
V volume of sample
w width of the channels
x distance from inlet end of donor channel
α_j fraction of solute in active form in phase j (A, D)
α'_j fraction of the total flux due to the active form in phase j (A, D)
β_j $\alpha_j/(h_j f_j)$
Γ gamma function
ϵ membrane porosity
ζ membrane tortuosity
τ $t - t_0$
ϕ reduced flow ($F_D/(Lw)$)

Subscripts

A acceptor phase
D donor phase
M membrane phase
DM donor phase, close to membrane surface
MA acceptor phase, close to membrane surface

Superscript

i refers to the inactive form of the analyte

APPENDIX A

Lateral diffusion in the acceptor phase

The diffusion of active analyte laterally from the membrane surface into the bulk of the stagnant acceptor phase is described by Fick's second law applied to a finite region [12]:

$$\frac{\partial C}{\partial t} = D\frac{\partial^2 C}{\partial z^2} \quad 0 \le z \le h \tag{A1}$$

For simplicity, C is written instead of $\alpha_A C_A$ for the acceptor phase concentration of the active form of the analyte, D instead of D_A, and h instead of h_A. z is the direction towards the membrane surface, viz. $z = h$ is the position of the membrane surface. Eqn. A1 is subject to the following initial and boundary conditions:

$$\begin{aligned} &C = 0 && \text{at } t = 0 \\ &C = C_0(t) && \text{at } z = h \\ &\frac{\partial C}{\partial z} = 0 && \text{at } z = 0 \end{aligned} \tag{A2}$$

Here, it is necessary to take into account that the concentration at the surface is a function of time, resulting in a slightly more complicated solution than standard treatments of this problem (see, e.g., p. 308 in Ref. 16). The Laplace transform of the differential equation is (s is the Laplace variable and an overscore denotes Laplace transform):

$$\frac{\partial^2 \overline{C}}{\partial z^2} = \frac{s}{D}\overline{C}, \quad \begin{aligned} &\overline{C} = \overline{C_0} && \text{at } z = h \\ &\frac{\partial \overline{C}}{\partial z} = 0 && \text{at } z = 0 \end{aligned} \tag{A3}$$

The solution in the Laplace domain is:

$$\overline{C} = \overline{C_0}\frac{\cosh(qz)}{\cosh(qh)}, \quad q = \sqrt{\frac{s}{D}} \tag{A4}$$

To obtain an expression for the mass transfer coefficient, k, Fick's first law and the definition of mass transfer coefficients are applied:

$$J = D\left.\frac{\partial C}{\partial z}\right|_{z=h} = k[C_0(t) - \langle C\rangle] \qquad \text{(A5)}$$

Here, $\langle C\rangle$ is the average (bulk) concentration in the channel:

$$\langle C\rangle = \frac{1}{h}\int_0^h C\,\mathrm{d}z \qquad \text{(A6)}$$

Thus the mass transfer coefficient is given by

$$k = \frac{D}{C_0(t) - \langle C\rangle}\left.\frac{\partial C}{\partial z}\right|_{z=h} \qquad \text{(A7)}$$

In order to proceed, it is necessary to find, by suitable manipulations and inversions of Laplace transforms, expressions for the quantities in Eqn. A7. First, the form of the function $C_0(t)$ must be defined. In normal enrichment applications, the surface concentration will increase nearly linearly with time. Therefore, the following equation is assumed:

$$C_0(t) = C_1 t^p;\ \overline{C_0} = C_1\frac{\Gamma(p+1)}{s^{p+1}} \qquad \text{(A8)}$$

The parameter p is approximately unity, Γ denotes the gamma function and C_1 is a constant. By standard procedures, it is then possible to find the Laplace transforms of the derivative of C with z and of $\langle C\rangle$. This has been carried out for $p = 0.5$, 1 and 1.5. The inversion of the transforms is straightforward after McLaurin expansion (as described in Ref. 16), but the resulting expressions are complex and it is not necessary to reproduce them here. By means of the inverse transforms and Eqn. A7, k can be calculated numerically for realistic values of D, h and t. It is then found that, irrespective of the value of p, the mass transfer coefficient decreases from an initially high value to the constant value:

$$k = 3\frac{D}{h} \qquad \text{(A9)}$$

within a time that is short in comparison with typical enrichment times.

As an example, with $p = 1.0$, $D = 10^{-5}$ cm^2 s^{-1} and $h = 0.025$ cm, k is found to be 246×10^{-5} cm s^{-1} after 3 s, 121×10^{-5} cm s^{-1} after 100 s and 120×10^{-5} cm s^{-1} according to Eqn. A9.

APPENDIX B

Solution of the mass balance equation for enrichment with a stagnant acceptor phase

The Laplace transforms of Eqns. 12 and 13, considering the initial conditions in Eqn. 15 are:

$$s\overline{C_D} = -f_D\frac{\partial\overline{C_D}}{\partial x} - \frac{k}{h_D}(\alpha_D\overline{C_D} - \alpha_A\overline{C_A}) \qquad \text{(B1)}$$

$$s\overline{C_A} = \frac{k}{h_A}(\alpha_D\overline{C_D} - \alpha_A\overline{C_A}) \qquad \text{(B2)}$$

By eliminating $\overline{C_A}$ from these equations, the following equation is obtained for the donor phase:

$$f_D\frac{\partial\overline{C_D}}{\partial x} + s\left[1 + \frac{h_A k\alpha_D}{h_D(sh_A + k\alpha_A)}\right]\overline{C_D} = 0 \qquad \text{(B3)}$$

The Laplace transform of the boundary condition in Eqn. 15 is:

$$\overline{C_D} = \frac{C_I}{s},\ x = 0 \qquad \text{(B4)}$$

Considering that k depends on x according to Eqn. 14, the solution in the Laplace domain to Eqn. B3 is given by:

$$\overline{C_D} = \frac{C_I}{s}\exp\left(-2a\beta_D\sqrt{x} - x\frac{s}{f_D}\right) \times\left(1 + \frac{h_A s\sqrt{x}}{sh_A b + a\alpha_A}\right)^{2\beta_D(sh_A b + a\alpha_A)/h_A s} \qquad \text{(B5)}$$

From Eqn. B2, the corresponding equation for the acceptor phase is found:

$$\overline{C_A} = \frac{k\alpha_D}{sh_A + k\alpha_A}\overline{C_D} \qquad \text{(B6)}$$

By expanding Eqns. B5 and B6 into McLaurin series, the solutions in the time domain can be found as time series expansions, as presented in Eqns. 16–19.

REFERENCES

1 R.D. Noble and J.D. Way (Eds.), Liquid Membranes. Theory and Applications (ACS Symposium Series, Vol. 347), ACS, Washington, DC, 1987.
2 T. Araki and H. Tsukube (Eds.), Liquid Membranes, Chemical Applications, CRC Press, Boca Raton, FL, 1990.
3 G. Audunsson, Anal. Chem., 58 (1986) 2714.
4 J.Å. Jönsson and L. Mathiasson, Trends Anal. Chem., 11 (1992) 106.
5 G. Audunsson, Anal. Chem., 60 (1988) 1340.
6 B. Lindegård, J.Å. Jönsson and L. Mathiasson, J. Chromatogr., 573 (1992) 191.
7 G. Nilvé, G. Audunsson and J.Å. Jönsson, J. Chromatogr., 471 (1989) 151.
8 L. Mathiasson, G. Nilvé and B. Ulén, Int. J. Environ. Anal. Chem., 45 (1991) 117.
9 M. Knutsson, G. Nilvé, L. Mathiasson and J.Å. Jönsson, J. Agric. Food Chem., 40 (1992) 2413.
10 G. Nilvé and R. Stebbins, Chromatographia, 32 (1991) 269.
11 L. Mathiasson, M. Knutsson, G. Bremle and L. Mårtensson, Swedish J. Agric. Res., 21 (1991) 147.
12 E.L. Cussler, Diffusion. Mass Transfer in Fluid Systems, Cambridge University Press, Cambridge, 1984.
13 G.A. Audunsson, Trace Analysis of Amines by GLC with Special Emphasis on Sample Pretreatment, Particularly Supported Liquid Membranes, Thesis, University of Lund, 1987.
14 R.C. Weast (Editor), CRC Handbook of Chemistry and Physics 70th edn., CRC Press, Boca Raton, FL, 1989.
15 J. Happel and H. Brenner, Low Reynolds Number Hydrodynamics, Martinus Nijhoff, Dordrecht, 1983, p. 34.
16 H.S. Carslaw and J.C. Jaeger, Conduction of Heat in Solids, Clarendon Press, Oxford, 1959.

Analytica Chimica Acta, 277 (1993) 25–30
Elsevier Science Publishers B.V., Amsterdam

On-line real-time detection method for trace Cl^- in aqueous solution

Akyhiro Iwata and Chiyoe Yamanaka

Department of Chemistry, Institute for Laser Technology, Nakoji 3-11-20, Amagasaki, Hyogo 661 (Japan)

Nobuaki Nakashima and Yasukazu Izawa

Institute of Laser Engineering, Osaka University, Yamada-Oka 2-6, Suita, Osaka 565 (Japan)

(Received 2nd December 1992)

Abstract

An on-line real-time detection method for Cl^- in aqueous solution was developed in which the concentration of Cl^- was determined by measuring the absorbances of Cl^-, e^- and Cl_2^- which were formed by ArF laser irradiation. A linear relationship between absorbance and concentration was confirmed. The calibration graphs were linear for about two orders of magnitude above the detection limit. A detection limit of 1×10^{-5} M was achieved.

Keywords: UV–Visible spectrophotometry; Chloride; Laser flash photolysis; Waters

On-line real-time measurements without pretreatment have been a key factor for detecting trace species in primary cooling water of nuclear power stations. For the primary cooling water, measurements should be automated in order to protect the analyst from exposure to radiation and for rapid detection, and should be carried out in a cooling tube without waste fluid, which must be treated as radioactive waste. However, none of the previous methods for detecting Cl^- in aqueous solution can satisfy these requirements. For example, ion chromatography cannot measure in real time without producing waste fluid. An ion-selective electrode is unsuitable for analysis in the cooling tube because of deterioration of the electrode. Therefore, a purely optical method would be the most suitable for detecting contaminants in the primary cooling water.

Correspondence to: A. Iwata, Department of Chemistry, Institute for Laser Technology, Nakoji 3-11-20, Amagasaki, Hyogo 661 (Japan).

Using laser-induced fluorescence, contaminants in aqueous solution have been easily detected with high sensitivity if the inorganic ions are luminescent. However, Cl^- does not fluoresce in the UV and visible regions. On the other hand, Cl^- in aqueous solution absorbs UV radiation of wavelength shorter than ca. 200 nm and has an absorption maximum at 174 nm [1]. The short-wavelength side of the absorption band overlaps with the long-wavelength side of the strong absorption of water. Therefore, it is not easy to determine the concentration of Cl^- by the direct measurement of its absorption. The laser flash photolysis method has been successfully applied to Cl^- detection. In aqueous solution, Cl, e^- and Cl_2^- are formed by flash photolysis [2] and pulse radiolysis [3] in the following reactions:

$$Cl^- \rightarrow Cl + e^- \quad (1)$$

$$Cl^- + Cl \rightarrow Cl_2^- \quad (2)$$

In this work, it was confirmed that the reactions occur with ArF laser irradiation using laser flash photolysis and it was demonstrated that the concentration of Cl^- can be determined by measuring the absorbance of these three products. The laser flash photolysis method for Cl^- detection is applicable to on-line real-time measurement without pretreatment. Further, the method can be applied to other halogen ions, except F^-.

EXPERIMENTAL

Apparatus

Figure 1 shows the experimental set-up. It consisted of a photolysis laser, a monitoring source, a sample cell, lenses, a monochromator, detectors and analysis devices. An ArF laser [Lambda Physik EMG201MSC, λ = 193 nm, pulse width = 30 ns (FWHM)] was used as the photolysis laser. The laser energies were measured using a joule meter (Gentec ED-500) and a laser energy meter (Gentec EM-1). The measured laser energies were used for correcting the fluctuation of signals, which was caused by the fluctuation of laser energies. The cross-sectional area of the laser was 1.5 cm^2. A quartz sample cell was irradiated with the laser light. The effective optical path length of the quartz sample cell was 30 mm, and slits (3 mm × 1 mm) were placed on the ends of the sample cell. The monitoring light source was a xenon lamp (EG&G XFX265), which was operated in a pulsed mode (FWHM = 10 μs). The light was at 90° with respect to the laser light and was focused into the sample cell by a convex quartz lens, L_1, with a focal length of 10 cm. The light passing through the sample cell was focused into the monochromator (Jovin Yvon H-10UV) by a convex quartz lens, L_2, with a focal length of 40 cm. The monitoring light intensity through the monochromator was detected by a photomultiplier (Hamamatsu Photonics R758). As required, a band pass filter and a neutral density filter were placed in front of the monochromator. The photolysis laser, the xenon lamp and the oscilloscope were triggered by a digital pulse generator (Stanford Research System DG-535). The trigger signal was adjusted to the maximum intensity of the xenon lamp light. A digital oscilloscope (Tektronix 2440) was used to convert the photomultiplier output into digital form. Through a GP-IB interface, these data were transferred to a computer (NEC PC-9801VM) where the signals were averaged.

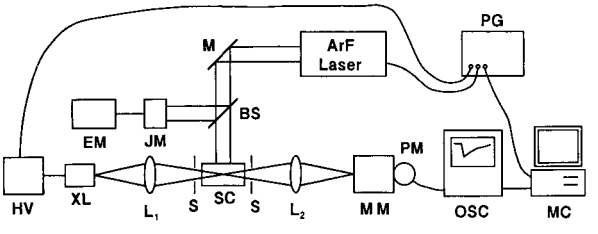

Fig. 1. Experimental set-up for the detection of Cl^-. M, mirror; BS, beam splitter; JM, joule meter; EM, laser energy meter; SC, sample cell; S, slit; L_1, L_2, lenses; HV, high-voltage power supply; XL, xenon lamp; MM, monochromator; PM, photomultiplier; OSC, oscilloscope; MC, microcomputer; PG, pulse generator.

Procedure

A 0.1 M Cl^- stock standard solution was diluted to 200 ml with distilled water. The sample cell was filled with the sample solution. The laser was operated in the single-shot mode. The sample solution was renewed for each shot. All measurements were done at 23°C.

Reagents

Distilled water was purchased from Wako and sodium chloride from Matsunaga Chemical. These reagents were of guaranteed grade and were used as received.

RESULTS AND DISCUSSION

Transient signals and spectra

The absorption spectra of Cl, e^- and Cl_2^- in aqueous solution have maxima at 320 nm ($\epsilon_{320} \leqslant$ 5000 l mol^{-1} cm^{-1}) [4], 720 nm (ϵ_{720} = 18500 l mol^{-1} cm^{-1} [5] and 340 nm (ϵ_{340} = 8800 l mol^{-1} cm^{-1}) [6], respectively. Figure 2 shows oscilloscope traces at 320, 340 and 720 nm for the

1×10^{-3} M Cl^- solution. At 320 and 340 nm, the signals have two components which are due to Cl and Cl_2^-. The rate constant of Cl is much faster than the observation range (1 μs); therefore, the rise curve is equal to the integration of the laser pulse. Cl_2^- formation is a diffusion-controlled reaction and depends on the concentration of Cl^-. The lifetime of Cl_2^- was much longer than the observation range. The two components at 340 nm fit the following equation:

$$A(t) = \int_0^t \phi W(t') a \exp[-k(t-t')]\, dt' + \int_0^t \phi W(t') b\{1 - \exp[-k(t-t')]\}\, dt' \quad (3)$$

where $A(t)$ is the observed absorbance at 340 nm, ϕ is the quantum yield of Cl, k is the formation rate constant of Cl_2^-, $W(t')$ is the time profile of the excitation laser pulse and a and b are the constants corresponding to the molar absorptivities (ϵ) of Cl and Cl_2^-, respectively. The first term represents the absorbance of Cl and the second term the absorbance of Cl_2^-. Figure 3 shows the analysed curves which were calculated from Eqn. 3. From the analysis, b/a was 1.61. This is smaller than the theoretical value of 1.76, which is calculated under the assumption that all Cl was converted to Cl_2^-, taking $\epsilon_{Cl} = 5000$ l mol^{-1} cm^{-1}. In other words, the conversion efficiency from Cl to Cl_2^- is 0.91. The calculated rate constant, k, was 1.92×10^{10} l mol^{-1} s^{-1}, which was a reasonable value for a diffusion-controlled reaction and agreed approximately with the previously reported value of 2.1×10^{10} l mol^{-1} s^{-1} [6]. Thus, reactions 1 and 2 were confirmed.

At 720 nm, the high absorbance value is due to the hydrated electron, e^-. The lifetime of e^-

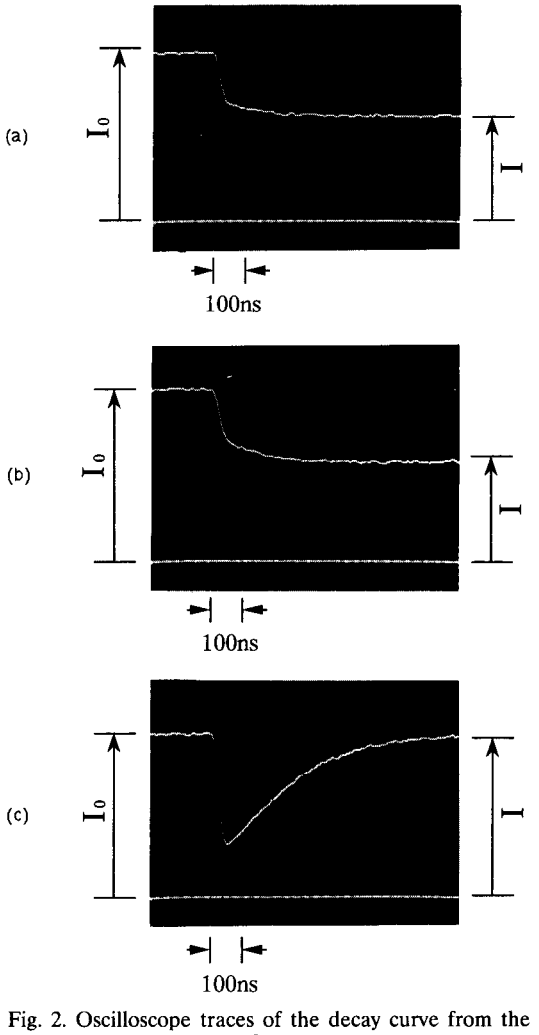

Fig. 2. Oscilloscope traces of the decay curve from the laser flash photolysis of 1×10^{-3} M Cl^- in aqueous solution at (a) 320, (b) 340 and (c) 720 nm. I_0, monitoring light intensity before the laser irradiation; I, monitoring light intensity after the laser irradiation.

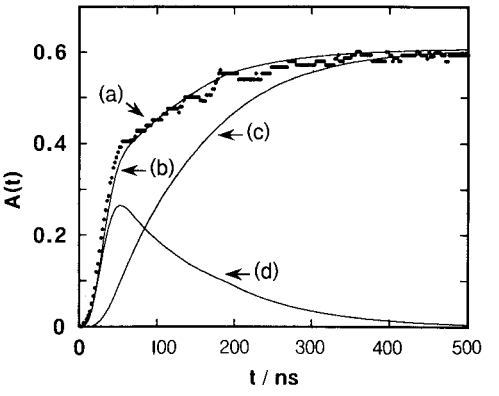

Fig. 3. Two-component analysis of the oscilloscope trace at 340 nm: (a) observed rise curve (dotted line); (b) fitted rise curve (solid line); (c) rise curve of Cl_2^-; (d) rise and decay curve of Cl.

depends on the concentration of O_2 in the sample solution. In the presence of O_2, the following reaction occurs:

$$O_2 + e^- \rightarrow O_2^- \quad (4)$$

For 0.01 M Cl^-, the lifetime of e^- was 120 ns for O_2-saturated solution, whereas it was 1.5 μs for N_2-saturated solution. However, the reactions did not prevent the detection of Cl^-.

Figure 4 shows the absorption spectra of transient species in aqueous solution. At 50 ns after the laser irradiation, two peaks appeared at 320 and 720 nm. The former agrees with the absorption maximum of Cl and the latter is attributable to e^-, based on correspondence with previous report [4,5]. At 500 ns after laser irradiation, the absorption of the e^- had almost disappeared. The absorption spectrum of Cl_2^- was observed. The absorption spectrum has been reported for flash photolysis [2] and pulse radiolysis [3,6].

Laser power dependence

The dependence of the absorbance at 720 nm on the laser fluence has a simple proportional relationship at fluences ≤ 50 mJ cm^{-2}. This indicates that the reaction is a one-photon process. If the laser light was focused into the sample cell, a multiphoton process or a breakdown was caused. All of the absorbances were measured in the range of a one-photon process in this study.

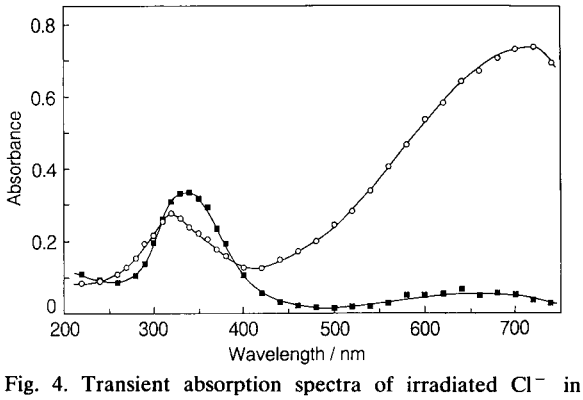

Fig. 4. Transient absorption spectra of irradiated Cl^- in aqueous solution (○) 50 ns after the laser pulse and (■) 500 ns after the laser pulse.

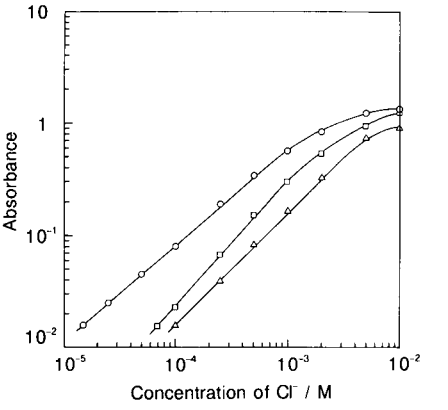

Fig. 5. Calibration graphs for Cl^- constructed by measuring the absorbance at (○) 720, (△) 320 and (□) 340 nm.

Calibration and detection limit

The calibration graphs are shown in Fig. 5. The detection limits, which were defined as the concentration at a signal-to-noise ratio of 2, were 1×10^{-4}, 7×10^{-5} and 1.5×10^{-5} M at 320, 340 and 720 nm, respectively. The values at 340 and 720 nm were obtained with a laser fluence of 46 mJ cm^{-2} and that at 320 nm with a laser fluence of 33 mJ cm^{-2}. The absorbances at 320 and 720 nm were measured 50 ns after the laser irradiation and that at 340 nm 500 ns after the laser irradiation. At 720 nm, the highest sensitivity was obtained. At 320 and 340 nm, the selectivity with an identical laser fluence will be approximately the same. The calibration graphs were linear for about two orders of magnitude above the detection limit.

With a high concentration of Cl^-, all laser light is absorbed on the irradiated surface of the solution; this leads to saturation of the absorption and to a deviation from the linear relationship.

In the measurement of the absorbance at 340 nm, after averaging the signals 50 times, a concentration of 1×10^{-5} M was detected, which corresponds to an absorbance of 1.8×10^{-3}.

Application to other halogen ions

The proposed method for Cl^- detection can be applied for other halogen ions, except F^-. Br^-

reacts according to the following schemes with flash photolysis [2] and pulse radiolysis [7]:

$$Br^- \rightarrow Br + e^- \quad (5)$$

$$Br + Br^- \rightarrow Br_2^- \quad (6)$$

Br^- has absorption maxima at 175 nm ($\epsilon_{175} = 5 \times 10^3$ l mol^{-1} cm^{-1}), 186 nm ($\epsilon_{186} = 1.35 \times 10^4$ l mol^{-1} cm^{-1}) and 198 nm ($\epsilon_{198} = 1.3 \times 10^4$ l mol^{-1} cm^{-1}) [1]. Therefore, ArF laser irradiation will induce reactions 5 and 6. The absorption maxima of Br and Br_2^- are at 275 nm [4] and 360 nm [7], where the molar absorptivities are 3500 [4] and 1.2×10^4 l mol^{-1} cm^{-1} [7], respectively. The concentration of Br^- can be determined by measuring the absorption of the products.

I^- shows reactions similar to those of Cl^- with flash photolysis [2] and pulse radiolysis [8]:

$$I^- \rightarrow I + e^- \quad (7)$$

$$I + I^- \rightarrow I_2^- \quad (8)$$

I^- has absorption maxima at 183 nm ($\epsilon_{183} = 4 \times 10^3$ l mol^{-1} cm^{-1}), 196 nm ($\epsilon_{196} = 1.32 \times 10^4$ l mol^{-1} cm^{-1}) and 228 nm ($\epsilon_{228} = 1.29 \times 10^4$ l mol^{-1} cm^{-1}) [1]. Therefore, with I^-, reactions 7 and 8 can be induced not only by ArF laser irradiation but also by KrCl (222 nm) and KrF (248 nm) laser irradiation. The absorption maxima of I and I_2^- are at 260 nm ($\epsilon_{260} = 1.04 \times 10^3$ l mol^{-1} cm^{-1}) [9] and 380 nm ($\epsilon_{380} = 1.4 \times 10^4$ l mol^{-1} cm^{-1}) [10], respectively. I^- will be detectable by measuring these absorptions.

Selectivity

It is possible to detect Cl^- in aqueous solution without other ions that absorb at 193 nm. In the presence of such other ions, the absorption at several wavelengths needs to be measured using multivariate analysis. However, in the presence of ions that have strong absorption at 193 nm, it is difficult to detect Cl^- with high sensitivity.

In the presence of ions that form e^- by ArF laser irradiation, it is impossible to distinguish Cl^- from these ions by the measurement of absorbance due to e^-. However, measurement of all the ions that form e^- by ArF laser irradiation is possible.

Further improvements

Improvements in the detection limit require a decrease in noise and an increase in the signal intensity. A major source of noise is the photomultiplier. A good noise reduction method is to average the signals. By averaging 100 times, the signal-to-noise ratio will theoretically be improved tenfold. In the present experiments, the sensitivity was improved sevenfold by averaging 50 times. Therefore, the experimental results were in good agreement with the theoretical values. It is possible to operate the system at more than 10 Hz, and real-time measurement is expected.

The intensity fluctuation of a Xenon lamp also influences the detection limit. If a stable light source is used, for example, a helium–neon laser (632.8 nm) or helium–cadmium laser (325 nm), the noise can be reduced and high sensitivity can be obtained.

Using a quartz sample cell with a long optical path is another simple method of improvement. Further, a multireflection method using a probe laser leads to higher sensitivity.

By irradiation with high laser energy, a lower concentration of Cl^- can be detected. However, an extremely high laser energy may cause a multiphoton process or breakdown.

As the temperature of the solution is raised, the molar absorptivities of Cl^- become high. The molar absorptivities of Cl^- at 190 nm are 4700, 7800 and 11300 l mol^{-1} cm^{-1} at 20, 40 and 60°C, respectively [11]. Therefore, a higher sensitivity can be obtained by raising the temperature of the solution.

If these improvements are introduced, the detection limit of 10^{-6} M, which is the minimum requirement for the analysis of primary cooling water, can be bettered.

The authors thank Mr. M. Kusaba for helpful discussions about the experimental set-up. This work was financially supported in part by Kansai Electric Power.

REFERENCES

1 G.J. Ferraudi, Elements of Inorganic Photochemistry, Wiley-Interscience, New York, 1988, p. 142.

2 L.I. Grossweiner and M.S. Matheson, J. Phys. Chem., 61 (1957) 1089.
3 M. Anbar and J.K. Thomas, J. Phys. Chem., 68 (1964) 3829.
4 A. Treinin and E. Hayon, J. Am. Chem. Soc., 97 (1975) 1716.
5 E.J. Hart and J.W. Boag, J. Am. Chem. Soc., 84 (1962) 4090.
6 G.G. Jayson, B.J. Parsons and A.J. Swallow, J. Chem. Soc., Faraday Trans., 69 (1973) 1597.
7 D. Zehavi and J. Rabani, J. Phys. Chem., 76 (1972) 312.
8 J.K. Thomas, Trans. Faraday Soc., 61 (1965) 702.
9 P. Fornier de Violet, R. Bonneau and J. Joussot-Dubien, J. Chim. Phys., 70 (1973) 1404.
10 A. Treinin and E. Hayon, Int. J. Radiat. Phys. Chem., 7 (1975) 387.
11 D. Wu, D. Wong and B. Di Bartolo, J. Photochem., 14 (1980) 303.

Analytica Chimica Acta, 277 (1993) 31–39
Elsevier Science Publishers B.V., Amsterdam

Fast neutral beam Fourier transform ion cyclotron resonance mass spectrometry for analysis of insulating and conductive materials

Patrick A. Limbach, Hyun Sik Kim, Nicholas C. Hill [1] and Alan G. Marshall

Department of Chemistry, 120 West 18th Avenue, The Ohio State University, Columbus, OH 43210 (USA)

(Received 2nd November 1992; revised manuscript received 30th November 1992)

Abstract

The use of an autoneutralizing fast neutral SF_6 beam (FNB) for secondary ion quadrupole mass spectrometry of refractive samples has been demonstrated previously. Here, we demonstrate the FNB technique for generation and high-resolution Fourier transform ion cyclotron resonance (FT-ICR) mass spectrometric detection of ions from a wide variety of samples. The fast neutral beam generates abundant secondary ions from both conductive and insulating samples for detection in an open-ended ICR ion trap, as demonstrated by representative mass spectra of methyl stearate, fluorocarbon polymers, gramicidin S, and fullerenes. Optimization of the FNB-FT-ICR-MS experiment is discussed in detail, with particular emphasis on analysis of insulating materials which are not readily analyzed by ion-bombardment secondary ion mass spectrometry.

Keywords: Mass spectrometry; Fast neutral beam; Fourier transform ion cyclotron resonance mass spectrometry; Insulator; Secondary ion mass spectrometry; SIMS; FTMS; FT-ICR

Analytical uses of Fourier transform ion cyclotron resonance mass spectrometry (FT-ICR-MS) have been the subject of several recent reviews [1–12]. Advantages of FT-ICR-MS include extremely high mass resolving power, high mass accuracy, MS^n experiments, and nondestructive ion detection. However, high mass resolving power (10^5–10^6 at $m/z \leq 1000$) requires low (10^{-8}–10^{-9} Torr) pressure, whereas several of the currently popular ionization sources [e.g., fast atom bombardment (FAB) and electrospray] operate optimally at several orders of magnitude higher pressure.

Correspondence to: Professor Alan G. Marshall, Department of Chemistry, The Ohio State University, 120 West 18th Avenue, Columbus, OH 43210 (USA). A.G.M. is also a member of the Department of Biochemistry.

[1] Present address: Tosoh SMD Inc., 3515 Grove City Road, Grove City, OH 43123 (USA).

The general solution to the problem of differential pressure between the ion source and mass analyzer is to separate the two functions in spatially distinct regions. In a "dual trap", the "source" and "analyzer" regions are separated by a conductance limit wall through whose small central aperture ions may transit from "source" to "analyzer" [13]. The dual trap can maintain a pressure ratio of about a factor of up to 100–500 between the source and analyzer regions. A greater pressure differential requires more than two stages of differential pumping, which is typically achieved by moving the ion source outside the solenoidal magnet. Ions may then be injected into the ion trap inside the solenoidal magnet by: (a) passage through rf-only quadrupole rods [14–18]; (b) acceleration and focusing with electrostatic lenses [19–22]; or (c) entrainment in a supersonic jet (of, e.g., helium) [23]. Although each of these methods succeeds in forcing or

focusing ions to trajectories close to the magnetic field symmetry axis (z-axis) to circumvent the "magnetic mirror" effect [24,25], some fraction of the ions is always lost in transit, and (in pulsed injection) quadrupole-stability and time-of-flight effects [20,26] can lead to mass discrimination in attempts to inject ions of a wide mass-to-charge ratio into the ion trap.

Ionization methods in which ions are formed in or near the ion trap (e.g., electron ionization, chemical ionization, laser desorption/ionization [7], and Cs^+ "static" secondary ionization [27,28]) avoid these problems and are therefore in general preferable to external formation of ions, provided that the desired ions can be generated by those methods. Moreover, ions formed near the ion trap are already confined laterally by the strong magnetic field, and are therefore more easily directed and transmitted to the ion trap, as in a recent electrospray ion source operating inside a high-field solendoial magnet [29]. In this work, we try to combine the advantages of external and internal ionization: the ion source is removed from the high vacuum chamber of the mass analyzer in order to optimize production of the primary ionizing beam; the beam is focussed, differentially pumped, and directed into the bore of the solenoidal magnet; and ions are desorbed near the ion trap to facilitate efficient capture of secondary ions at low pressure for optimal FT-ICR mass analysis.

The fast neutral beam ionization source allows for the production of a focused and rasterable primary beam. This beam may be used for secondary ion mass spectrometry with the FT-ICR mass spectrometer as the detector. The FNB ionization source is a "soft" ionization source and has desorption characteristics similar to those of Cs^+ ion sources previously used with FT-ICR-MS [27,28]. However, the fast neutral beam source has the advantage that sample charging is reduced because the primary ionizing beam is neutral. Thus, analysis of insulating materials may be improved with this primary ionization source relative to Cs^+ sources.

Delmore and co-workers [30–33] at the Idaho National Engineering Laboratory originally developed a fast neutral beam gun that generates a high-velocity SF_6^- ion beam. SF_6^- is chosen, because a significant fraction of the accelerated (to several keV translational energy) SF_6^- ions autodissociates (to SF_6 and an electron) during the time it takes for those ions to travel ~ 2 m from the source to the sample. Thus, autodetachment of the electron from SF_6^- ions which have been formed, accelerated, focused, and rastered (laterally) leaves a *neutral* SF_6 beam which retains the focus of the original ion beam (because of the much greater mass of SF_6 compared to an electron). The neutral beam exhibits the same ionization characteristics as an ion beam, with respect to sputtering of a sample surface and generation of secondary ions for subsequent mass analysis. In that spirit, the neutral beam flux may be stated in units of the "equivalent current" of a similar number of singly-charged primary ions.

Based on a series of experiments in which a fast neutral SF_6 beam was interfaced to a quadrupole mass analyzer, Delmore and coworkers [30–33] were quick to point out the special advantage of a neutral beam source for analysis of electrically insulating samples, due to reduced electrical charging at the sample surface. In experiments with a prototype fast neutral beam (FNB) source interfaced to an FT-ICR mass analyzer [34], we noted the additional advantage for FT-ICR-MS that the neutral beam passes unaffected through the fringe field of a solenoidal magnet, thereby allowing the ion source to be moved outside the magnet without any magnetic mirror reflection of primary beam ions. Yet another advantage of a polyatomic SF_6 beam is that the molecular beam produces a greater secondary ion yield than an atomic (e.g., Cs^+) beam of the same momentum [35].

EXPERIMENTAL

Ionization method

A schematic diagram of a fast neutral beam generator and its interface to an FT-ICR mass spectrometer is shown in Fig. 1. The operation and instrumental configuration of the FNB-FT-ICR instrument have been described previously [34]. Briefly, the 5–15 keV SF_6^- beam source is

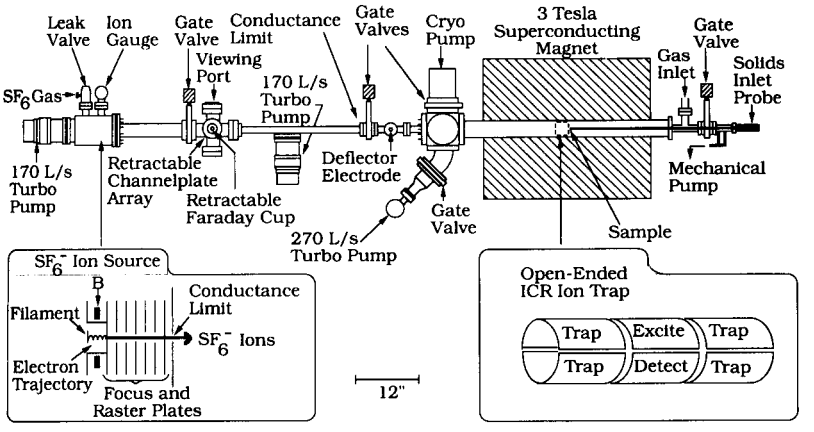

Fig. 1. Schematic diagram of a fast neutral primary SF_6 beam source and its interface to an FT-ICR mass spectrometer. Primary beam formation is external to the magnet. The neutral beam is focused and accelerated to impact on a solid-sample insertion probe located on the far side of the ICR ion trap. Typical working pressure is $\sim 1 \times 10^{-5}$ Torr in the source housing and $1\text{–}2 \times 10^{-8}$ Torr in the ICR ion trap.

formed by electron attachment to neutral SF_6 gas molecules; the ion beam is then focused and rastered to strike a solids insertion probe positioned adjacent to the ion trap. The source housing is ~ 2 m from the ion trap and is separated from the mass spectrometer by two 1.0-mm conductance limits that allow the source housing to be operated at 10^{-5} Torr while the mass spectrometer pressure is maintained at $\sim 1\text{–}2 \times 10^{-8}$ Torr. The key feature here is the formation of the SF_6^- beam at high pressure outside the magnet; after the beam is focused and accelerated toward the bore of the solenoidal magnet, the SF_6^- beam partially autoneutralizes to leave a neutral beam of SF_6 molecules whose trajectories are unaffected by the magnetic field. Because the electron mass is only 10^{-4} of the SF_6 mass, autoneutralization does not affect the trajectory of the original SF_6^- ion, and the neutral beam retains the focus of the original SF_6^- beam. A primary ion plus neutral equivalent current of hundreds of picoamperes can be focused to a spot diameter of a few mm, to produce a primary beam current density of ~ 10 nA/cm^2.

Fourier transform ion cyclotron resonance mass spectrometer

The FT-ICR mass spectrometer is comprised of a Nicolet FTMS-1000 data station to control signal generation, data acquisition, and data processing; a custom built vacuum system; and an Oxford 3-tesla magnet (Oxford Instruments, Osney Mead). A manual insertion solids sample probe is mounted at the opposite end of the vacuum chamber from the beam entrance. The vacuum chamber was roughed with a Balzers (Hudson, NH) 270 L/s turbomechanical pump. A CTI Cryogenics (Waltham, MA) CryoTorr-8 cryopump produced a base pressure of 3×10^{-10} Torr before sample analysis. A 5.08 cm (o.d.) $\times$ 15.24 cm (axial) elongated cylindrical open ended ion trap [36,37] centered at the highest-field point within the solenoidal magnet was used to trap, excite and detect the secondary ions.

Mass spectra

SF_6 (99.99%) was obtained from Matheson Gas Products (Secaucus, NJ); methyl stearate (> 99%) and gramicidin S from Sigma (St. Louis, MO); Teflon® was obtained in tape form. Fullerene-containing toluene extracts of soot prepared by the Krätschmer Huffman method [38] were a gift from R. Ziolo (Xerox). Each sample was dissolved in a suitable solvent (if necessary) and placed onto the probe tip [in some cases with a cellulose matrix (Kim-Wipe®) fastened to the probe tip] before insertion into the vacuum chamber. The probe was then inserted to an initial

position ~ 1 cm from the end of the rear trap electrodes. The neutral beam ion optical element voltages were adjusted appropriately, and the beam focused so that it would pass through the trap and impact upon the probe tip. Generally, focusing of the beam was determined by maximizing the observed FT-ICR mass spectral magnitude-mode peak height from K^+ ions in the sample or by maximizing the signal from the sample of interest. The observed signal was further optimized by moving the probe closer or farther from the rear trap electrodes, typically ~ 1–2 cm for most of the work reported here. The desorbed ions were then captured in the ion trap where they were subjected to the usual FT-ICR-MS experimental event sequence: quench period to remove any unwanted ions; delay period to allow a new population of ions to accumulate in the trap; and then excitation followed by detection. The event sequence was typically repeated 50–100 times to acquire mass spectra with acceptable signal-to-noise ratio. Chirp excitation (2 MHz bandwidth, sweep rate varying from 1200 to 800 Hz/μs over a period of 1.67–2.5 ms) was used, except for methyl stearate, for which single-frequency resonant dipolar excitation (500 μs at 4.2 V) was used. Direct-mode detection (64 K time-domain data points), padded with an additional 64 K zeroes, exponentially apodized (to enhance spectral peak height-to-noise ratio) and then Blackman-Harris apodized (to reduce peak overlap resulting from magnitude-mode Lorentzian line shape), was followed by fast Fourier transform, magnitude calculation, and frequency-to-mass conversion [39] to yield a mass spectrum.

RESULTS AND DISCUSSION

Primary beam intensity

In this work, we implemented a number of improvements on the previously described prototype FNB-FT-ICR mass spectrometer [34]. For example, the previous instrument configuration limited the primary beam equivalent ion current to ~ 10 pA. Because secondary ion yield is in general proportional to the primary ion beam current [40], it is desirable to increase the primary ion current while retaining low pressure in the mass spectrometer. We therefore chose to increase the conductance limit aperture area at the exit of the SF_6 ion source by a factor of four (from 0.5 mm to 1.0 mm i.d.); the primary ion plus neutral equivalent current (as measured on a Faraday cup placed in the beam path) thereby increased approximately tenfold. The increase in the primary ion current is due to the larger area of the conductance limit and to the ease of maximizing the larger spot size. Unfortunately, the pressure in the mass spectrometer also rose to a level ($\sim 1 \times 10^{-7}$ Torr) unsuitable for ultrahigh-resolution mass analysis. We therefore added another stage of differential pumping to the beam line; the pressure in the mass analyzer was thereby reduced to $1–2 \times 10^{-8}$ Torr.

Pulsed vs. continuous primary beam

Another improvement included changing the beam from a continuous to a pulsed source in order to take advantage of the inherently pulsed nature of the FT-ICR mass spectrometer. A small switching circuit was triggered from the Nicolet 1280 computer. The final lens element (y-raster) was pulsed from 0 to 500 V in order to allow the beam to enter the mass spectrometer during ion accumulation and subsequently be deflected away during the excitation, detection and quench events. Figure 2 shows the marked (66%) improvement in mass resolving power for pulsed vs. continuous beam operation: mass resolving power for SF_6^- increases from 268 000 to 445 000 presumbly due to the reduction of the interaction between the trapped ion packet and the primary beam.

Open-ended cylindrical ion trap

Beu and Laude [36,37] recently reintroduced the open-ended trap previously used in single-ion measurements [41,42] for use in FT-ICR-MS, for improved efficiency of capture of externally injected ions. Such a trap may particularly improve trapping retention of high-mass ions [43]. We therefore constructed an elongated cylindrical open ended ion trap for the present experiments. Moreover, the increased detection sensitivity of an elongated ion trap [44] and (slight) additional

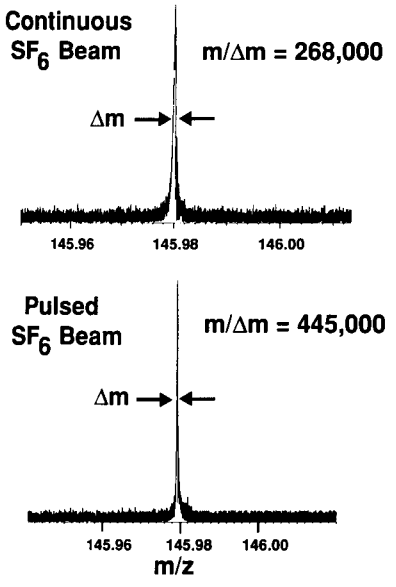

Fig. 2. Comparison of experimental FNB-FT-ICR magnitude-mode mass spectra of SF_6^- for continuous (top) and pulsed (bottom) primary beam. In the lower spectrum, the primary beam is deflected away from the ion trap during excitation and detection, resulting in significantly enhanced mass resolving power. Primary beam conditions: beam energy, 7.5 keV; beam duration, 5 s.

increase in detection sensitivity for a cylindrical trap over a tetragonal trap of the same aspect ratio [44,45] are well documented. Experimentally, we observed a very substantial improvement in detected secondary ion signal for an elongated, open-ended, cylindrical trap compared to our prior cubic trap. First, the open-ended trap provides a completely unobstructed path for the primary ions and neutrals to strike the solids probe surface. Second, the open-ended trap increases the acceptance angle (measured relative to the z-axis) of secondary ions which can be captured in the ion trap; thus, ions which are initially formed off-axis may still be trapped. Finally, with the open-ended ion trap, the probe bias voltage and position may be varied in order to increase the detected ion signal. For example, the probe could be placed inside the outer trap electrode cylinder to increase the number of ions reaching the central cylinder for excitation and detection; alternatively, moving the probe away from the outer trap cylinder (i.e., outside of the main trapping field) exposes the secondary ions to a decelerating force (due to the static trapping field) whose magnitude depends on the probe position. Based on these experiments, the open-ended ion trap proves to be the trap of choice for the present FNB-FT-ICR-MS analysis.

Fullerenes

The effectiveness of the various above-listed instrumental improvements is nicely illustrated by FNB-FT-ICR mass spectral analysis of fullerene-containing soot obtained by toluene extraction from arc-welding of graphite rods. Without the above-listed modifications, no detectable fullerene signal could be obtained, presumably due to too-low primary ion plus neutral equivalent current and/or inefficient capture of desorbed ions. Following the above-listed modifications, Fig. 3 shows a strong signal from C_{60}^+ (m/z 720) and a weaker signal from C_{70}^+ (m/z 840) from a benzene solution of soot evaporated onto the solids insertion probe tip. The isotope relative abundances for $^{12}C_{60}^+$ and $^{13}C^{12}C_{59}^+$ are as expected, as are the relative abundances of C_{60}^+ and C_{70}^+

Methyl stearate

Methyl stearate was examined because it produces abundant molecular ions by any of several other ionization methods, and is often used as a

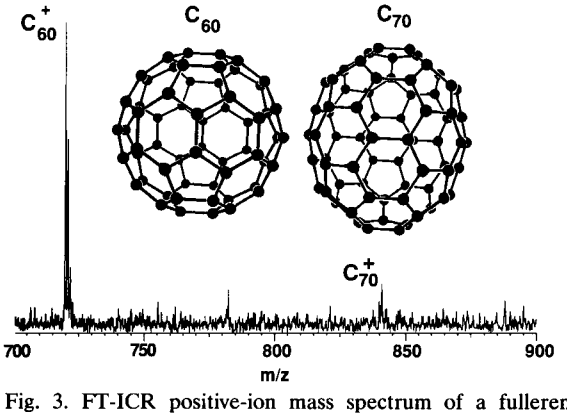

Fig. 3. FT-ICR positive-ion mass spectrum of a fullerene sample obtained from toluene-extracted soot from arc-welded graphite. Primary beam conditions: beam energy, 8 keV; beam duration, 2 s. The sample in benzene solution was evaporated onto an aluminum probe tip. C_{60}^+ and C_{70}^+ are clearly evident.

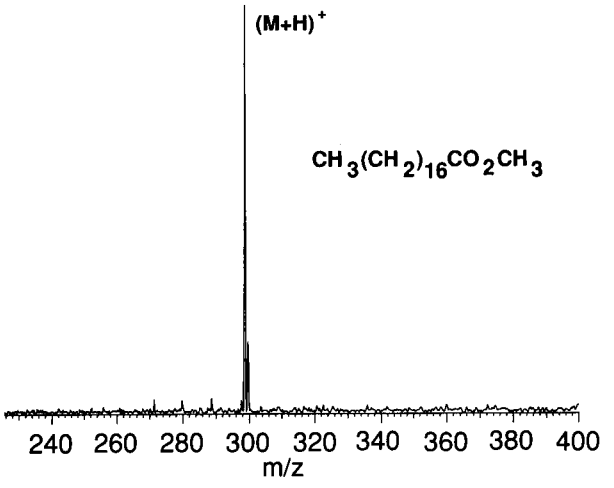

Fig. 4. FT-ICR broadband mass spectrum of methyl stearate ionized without a matrix. The sample was dissolved in methylene chloride and evaporated onto an aluminum probe tip. Primary beam conditions: beam energy, 10 keV; beam duration, 3 s. The main peak in the mass spectrum is from protonated molecular ions, $(M+H)^+$.

sensitivity test for mass spectrometers. Figure 4 shows the FNB-FT-ICR mass spectrum of methyl stearate dissolved in methylene chloride and evaporated onto the aluminum probe tip with no added matrix. The predominant signal is from the protonated molecular ion, $(M + H)^+$ at m/z 299. Although single-frequency resonant excitation was used to generate this particular spectrum, broadband excitation (not shown) showed a virtual lack of fragmentation of this sample. Variation of the beam accelerating voltage (5–10 keV) did not affect the fragmentation pattern.

Gramicidin S

Gramicidin S is a cyclic peptide which has become a standard sample for demonstrating peptide analytical performance in mass spectrometry. Figure 5 is the FNB-FT-ICR mass spectrum of gramicidin S dissolved in methanol and evaporated onto a cellulose matrix (Kim-Wipe tissue paper) previously attached to the probe tip by wrapping the probe tip and securing with an encircling metal strip. Abundant protonated molecular ions, $(M + H)^+$, and several ionic fragments are readily observed. The cellulose matrix was essential for generation and detection of ions of $m/z > 300$. In the future we plan to investigate the role of the matrix in the production of ions from this and similar biological samples. The most abundant fragment ions are quite similar to those observed by FT-ICR-MS by Cs^+ ionization [28], fast atom bombardment [46], and laser desorption [47]. The presently observed fragmentation pattern suggests that FNB-FT-ICR-MS could be useful for peptide sequencing, since most of the fragment ions are N-terminal fragments corresponding to B-type ions [48]. There was no significant overlap between the relatively low-abundance cellulose matrix ions and the gramicidin fragment ions. Finally, it is noteworthy that the protonated molecular ion was readily observed by FNB-FT-ICR-MS without the addition of glutathione or salts to the sample solution, as for some other prior ionization methods [28].

Teflon®

The fast neutral beam is uniquely suited for analysis of *electrically insulating materials*. Because the beam autoneutralizes on its way from the source to the sample target, a neutrals-only SF_6 primary beam is available for secondary ion generation. The obvious advantage of a neutrals-only beam, as previously noted by Appelhans et

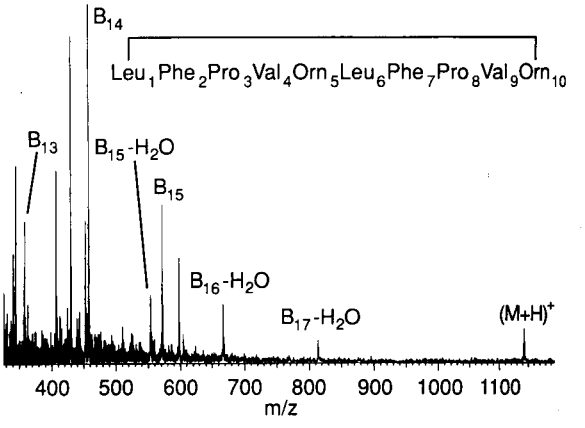

Fig. 5. FT-ICR broadband positive-ion mass spectrum of the cyclic peptide, gramicidin S. The sample was dissolved in methanol before evaporation onto a cellulose matrix. Primary beam conditions: beam energy, 7.2 keV; beam duration, 2.5 s. Abundant molecular ions are evident, along with several N-terminus-type fragment ions: B_{xy} denotes a B-type fragment [48] extending from amino acid residues x to y.

al. [31] and Delmore et al. [32] is that surface charging from the primary beam may be reduced without the need for external neutralization devices [40]. The primary beam consisted of an approximately 50:50 mixture of neutrals and ions as calculated from electron autodetachment lifetime and the flight time of the primary beam. Even with the resulting large negative-ion current, Teflon, $[C_xF_y]$, with $y \approx 2x$, was easily analyzed, as shown by the FNB-FT-ICR mass spectrum of a Teflon film (Fig. 6). At low trapping voltage (e.g., 2 V in Fig. 6), oligomeric species up to m/z 581 are observed; at higher trapping voltage (8 V, not shown), the FNB-FT-ICR mass spectrum shows oligomers up to m/z 1531.

The upward extension in mass range of detectable positive ions on increase in trapping voltage corroborates the results of Amster et al. [28], who postulated that surface charging was a problem in trapping of the secondary ions. As noted

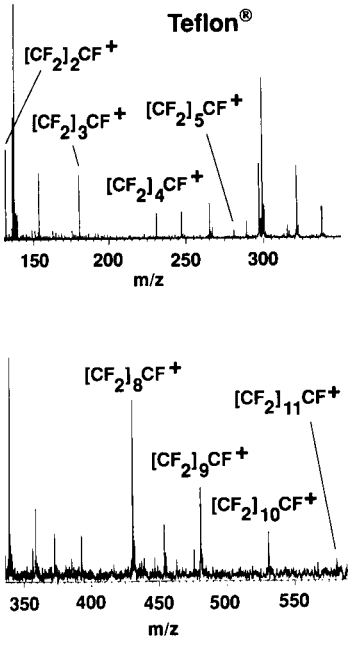

Fig. 6. FT-ICR mass spectra of Teflon®. Top: broadband positive-ion mass spectrum of a Teflon film. Teflon tape was attached directly to the probe tip and bombarded with a 10-keV beam for 5 s per scan. Bottom: same mass spectrum showing easily detectable fluorocarbon fragment ions up to m/z 581. The mass range may be extended either by increasing the trapping voltage or by reducing the ion content in the primary beam (see text).

by a reviewer, a heavier ion may have a larger kinetic energy which necessitates a higher trapping voltage. Variation of the primary beam composition (ion/neutral content) may help to determine the source of the increase in ion axial energy. Preliminary measurements suggest that the upper mass limit may be further extended by reducing the number of negative ions in the primary beam; however, under those conditions, contaminants in the vacuum chamber (from previous sample matrices) were also readily detected, thereby limiting the available dynamic range.

Previous FNB-FT-ICR mass spectra of Teflon obtained with a prototype instrument were limited to relatively low-mass polymer fragments, because attempts to lower the beam current (to reduce sample surface charging) led to long beam period (to generate a detectable signal), and the resultant ion-molecule reactions of the trapped ions produced $C_xF_y^+$ clusters that were no longer representative of the original polymer structure. The higher primary ion plus neutral equivalent current of the present instrument allows for shorter beam period, and a more readily interpretable fragmentation pattern. Future FT-ICR analysis of other insulating materials (e.g., polyethylene terphthalates, with similarly severe surface charging effect) with a neutrals-only beam appears especially attractive.

Additional considerations

For a neutrals-only primary beam, sample charging of electrically insulating samples is greatly reduced, thereby largely eliminating the need for additional compensation devices (e.g., electrons flooding the sample surface [49], pulsed extraction devices [50]) to neutralize the sample surface charging. Even if some sample charging occurs, the voltages applied to the probe and to the rear trapping electrodes may easily be adjusted to lower the additional translational energy acquired by the secondary ions as they are repelled from the (positively) charged surface. Moreover, because the secondary ions are initially formed in a strong magnetic field, the cyclotron motion of the secondary ions will largely prevent them from escaping in directions perpendicular to the magnetic field direction. In addi-

tion, the open-ended ion trap facilitates entry of ions formed initially off-axis into the ion trap, thereby increasing the population of detectable ions. Finally, even if ions enter the trap off-axis, they may be driven ("shrink-wrapped") back to the center of the trap by the application of resonant or stored-waveform [51] based rf-electric quadrupolar excitation of *xy* [52–54] or *xz* [55] symmetry.

Pulsing the primary beam source (as demonstrated here) to reduce ion formation during the (potentially) long FT-ICR excitation and detection periods and/or use of a "storage" trap [26,56,57] to increase the duty cycle of the experiment should also improve FNB-FT-ICR-MS performance. Here, we showed that the addition of an involatile cellulose matrix neither degrades the mass spectral resolving power nor produces significant "chemical noise" from ions derived from the matrix itself. If another more reactive matrix were needed, its "chemical noise" could be removed by SWIFT [58] multiple selective simultaneous ejection of unwanted matrix peaks.

Conclusions

Secondary ion mass spectra of high signal-to-noise ratio and ultrahigh mass resolving power have been obtained from a fast neutral beam ionization source FT-ICR mass spectrometer. The signal-to-noise ratio and molecular weight range of analysis have been extended by a factor of at least 5 over those of a prior prototype instrument [34]. Routine analysis of thermally fragile materials is now feasible. FNB-FT-ICR-MS is uniquely advantageous for high-resolution mass spectral analysis of electrically insulating materials. General considerations for optimizing routine FNB-FT-ICR secondary ion mass analysis have been presented.

The authors thank A. Appelhans and S. Guan for their helpful advice and instructions. We thank R. Ziolo (Xerox) for providing a toluene extract of soot from arc-welded graphite rods. The authors also thank T. Hickey and K. Tewell of the O.S.U. machine shop for design and construction of the open-ended ion trap. The authors especially thank T. Ricca for his help with various aspects of electronics design, construction, testing, and troubleshooting. Financial support was provided by the National Science Foundation (CHE-9021058) and the Ohio State University.

REFERENCES

1 A.G. Marshall, Adv. Mass Spectrom., 11A (1989) 651.
2 P. Sharpe and D.E. Richardson, Coord. Chem. Rev., 93 (1989) 59.
3 S. Ghaderi, Ceram. Trans., 5 (1989) 73.
4 C.L. Wilkins, A.K. Chowdhury, L.M. Nuwaysir and M.L. Coates, Mass Spectrom. Rev., 8 (1989) 67.
5 B.S. Freiser, Chemtracts Anal. Phys. Chem., 1 (1989) 65.
6 B.S. Freiser, in Bonding Energies in Organometallic Compounds, Vol. 428, Am. Chem. Soc., Washington, DC, 1990, p. 55.
7 D.M. Lubman (Ed.), Lasers in Mass Spectrometry, Oxford University Press, New York, 1990.
8 D.A. Laude Jr. and J.D. Hogan, Technisches Messen, 57 (1990) 155.
9 B. Asamoto and R.C. Dunbar, Analytical Applications of Fourier Transform Ion Cyclotron Resonance Mass Spectrometry, VCH, New York, 1991.
10 J.E. Campana, Proc. SPIE Applied Spectroscopy in Material Science, (1991) 138.
11 L.M. Nuwaysir and C.L. Wilkins, Proc. SPIE Applied Spectroscopy in Material Science, (1991) 112.
12 A.G. Marshall and L. Schweikhard, Int. J. Mass Spectrom. Ion Proc., 118/119 (1992) 37.
13 D.P. Littlejohn and S. Ghaderi, U.S.A. Pat., 4,581,533, issued 8 April, 1986
14 R.T. McIver, Jr., R.L. Hunter and W.D. Bowers, Int. J. Mass Spectrom. Ion Processes, 64 (1985) 67.
15 D.F. Hunt, J. Shabanowitz, J.R.I. Yates, N.-Z. Zhu, D.H. Russell and M.E. Castro, Proc. Natl. Acad. Sci. USA, 84 (1987) 620.
16 B.H. Wang, I.J. Amster, F.W. McLafferty and I.B. Brown, Int. J. Mass Spectrom. Ion Proc., 100 (1990) 51.
17 J.A. Carroll, L. Ngoka, S. McCullough, E. Gard, A.D. Jones and C.B. Lebrilla, Anal. Chem., 63 (1991) 2526.
18 K.D. Henry, J.P. Quinn and F.W. McLafferty, J. Am. Chem. Soc., 113 (1991) 5447.
19 J.M. Alford, P.E. Williams, D.J. Trevor and R.E. Smalley, Int. J. Mass Spectrom. Ion Proc., (1986) 33.
20 P. Kofel, M. Allemann, H. Kellerhals and K.-P. Wanczek, Int. J. Mass Spectrom. Ion Proc., 72 (1986) 53.
21 P. Kofel and T.B. McMahon, Int. J. Mass Spectrom. Ion Proc., 98 (1990) 1.
22 M.P. Irion, A. Selinger and R. Wendel, Int. J. Mass Spectrom. Ion Proc., 96 (1990) 27.
23 S. Maruyama, L.R. Anderson and R.E. Smalley, Rev. Sci. Instrum., 61 (1990) 3686.
24 F.F. Chen, Introduction to Plasma Physics, Plenum, New York, 1974.

25 R.T. McIver, Jr., Int. J. Mass Spectrom. Ion Proc., 98 (1990) 35.
26 S.A. Hofstadler and D.A. Laude, Jr., Anal. Chem., 63 (1991) 2001.
27 M.E. Castro and D.H. Russell, Anal. Chem., 56 (1984) 578.
28 I.J. Amster, J.A. Loo, J.J.P. Furlong and F.W. McLafferty, Anal. Chem., 59 (1987) 313.
29 S.A. Hofstadler and D.A. Laude, Jr., Proc. 39th Am. Soc. Mass Spectrom. Ann. Conf. on Mass Spectrom. Allied Topics, Nashville, TN, 1991, p. 1538.
30 J.E. Delmore, U.S.A. Pat. 4,649,279, issued 10 March, 1987.
31 A.D. Appelhans, J.E. Delmore and D.A. Dahl, Anal. Chem., 59 (1987) 1685.
32 J.E. Delmore, A.D. Appelhans, R.E.I. Shomo and D.A. Dahl, Biomed. Environ. Mass Spectrom., 16 (1988) 237.
33 J.E. Delmore, A.D. Appelhans and D.A. Dahl, Rev. Sci. Inst., 61 (1990) 633.
34 N.C. Hill, P.A. Limbach, R.E. Shomo, A.G. Marshall, A.D. Appelhans and J.E. Delmore, Rev. Sci. Instrum., 62 (1991) 2612.
35 A.D. Appelhans and J.E. Delmore, Anal. Chem., 61 (1989) 1087.
36 S.C. Beu and D.A. Laude, Jr., Int. J. Mass Spectrom. Ion Proc., 112 (1992) 215.
37 S.C. Beu and D.A. Laude, Jr., Anal. Chem., 64 (1992) 177.
38 W. Krätschmer, L.D. Lamb, K. Fostiropooulos and D.R. Huffman, Nature (London), 347 (1990) 354.
39 E.B. Ledford, Jr., D.L. Rempel and M.L. Gross, Anal. Chem., 56 (1984) 2744.
40 A. Benninghoven, F.G. Rudenauer and H.W. Werner, Secondary Ion Mass Spectrometry, Wiley, New York, 1987.
41 J. Byrne and P.S. Farago, Proc. Phys. Soc., 86 (1965) 801.
42 G. Gabrielse, L. Haarsma and S.L. Rolston, Int. J. Mass Spectrom. Ion Proc., 88 (1989) 319.
43 C.L. Holliman, D.L. Rempel and M.L. Gross, J. Am. Soc. Mass Spectrom., 3 (1992) 460.
44 P.B. Grosshans, P.J. Shields and A.G. Marshall, J. Chem. Phys., 94 (1991) 5341.
45 E.N. Nikolaev and M.V. Gorshkov, Int. J. Mass Spectrom. Ion Proc., 64 (1985) 115.
46 C.B. Lebrilla, D.T.S. Wang, T.J. Mizoguchi and R.T. McIver, Jr., J. Am. Chem. Soc., 111 (1989) 8593.
47 L.M. Nuwaysir and C.L. Wilkins, in D.M. Lubman (Ed.), Lasers and Mass Spectrometry, Oxford University Press, New York, 1990, p. 291.
48 K. Biemann, Biomed. Environ. Mass Spectrom., 16 (1988) 99.
49 B. Hagenhoff, D. van Leyen, E. Niehuis and A. Benninghoven, J. Vac. Sci. Technol. A, 7 (1989) 3056.
50 A.D. Appelhans, D.A. Dahl and J.E. Delmore, Rapid. Commun. Mass Spectrom., 3 (1989) 356.
51 A.G. Marshall, T.-C.L. Wang and T.L. Ricca, J. Am. Chem. Soc., 107 (1985) 7893.
52 G. Savard, S. Becker, G. Bollen, H.-J. Kluge, R.B. Moore, L. Schweikahrd, H. Stolzenberg and U. Wiess, Phys. Lett. A, 158 (1991) 247.
53 L. Schweikhard, S. Guan and A.G. Marshall, Int. J. Mass Spectrom. Ion Proc., 120 (1992) 71.
54 S. Guan and A.G. Marshall, J. Chem. Phys., (1993) in press.
55 S. Guan, X. Xiang and A.G. Marshall, Int. J. Mass Spectrom. Ion Proc., (1993) in press.
56 P. Kofel, M. Allemann, H.P. Kellerhals and K.-P. Wanczek, Int. J. Mass Spectrom. Ion Proc., 87 (1989) 237.
57 H. Schnatz, G. Bollen, P. Dabkiewicz, P. Egelhof, F. Kern, H. Kalinowsky, L. Schweikhard, H. Stolzenberg and H.-J. Kluge, Nucl. Instrum. Methods, A251 (1986) 17.
58 T.-C.L. Wang, T.L. Ricca and A.G. Marshall, Anal. Chem., 58 (1986) 2935.

Analytica Chimica Acta, 277 (1993) 41–54
Elsevier Science Publishers B.V., Amsterdam

Gas chromatography–tandem mass spectrometry implemented on a bench-top quadrupole ion trap-based instrument using random noise to effect collision-induced dissociation

Gary J. Van Berkel and Douglas E. Goeringer

Analytical Chemistry Division, Oak Ridge National Laboratory, Oak Ridge, TN 37831-6365 (USA)

(Received 11th December 1992; revised manuscript received 22nd December 1992)

Abstract

A simple and effective method for collision-induced dissociation (CID), implemented through application of random noise to an end-cap electrode, allows gas chromatography (GC)–tandem mass spectrometry (MS–MS) experiments to be performed on a commercial bench-top quadrupole ion trap mass spectrometer. Details of the random noise CID experiment, the characteristics of the noise spectrum, and the effect of varying noise spectrum and ion trap parameters on MS–MS spectra are discussed using *N,N*-diethylaniline as a model compound. Compromises to the technique imposed by current software flexibility limitations are also discussed. GC–MS–MS spectra, generated using random noise CID, are shown for methamphetamine and amphetamine ionized via isobutane chemical ionization.

Keywords: Gas chromatography–mass spectrometry; Collision-induced dissociation; Diethylaniline; Tandem MS; Quadrupole ion trap

The first commercial quadrupole ion trap [1], based on the mass selective instability mode of operation and using helium as a bath gas to improve mass resolution and trapping efficiency [2], was introduced in 1983 as an inexpensive and sensitive mass spectrometric (MS) detector for gas chromatography (GC) employing in situ electron ionization (EI). Since that time the analytical capabilities of the quadrupole ion trap have advanced rapidly (for recent reviews see Refs. 3–8). Some of these new capabilities and reasons for rapid advancement include, for example, in situ chemical ionization (CI) [9], automatic gain control (AGC) in EI [10] and automatic reaction control (ARC) in CI [11], axial modulation [12], the capability for tandem mass spectrometry (MS–MS) [13] and MS^n (where $n > 2$) [14,15] employing collision-induced dissociation (CID), mass-to-charge range extension [16], interfacing of external ion sources to the trap [17–19], and high mass resolution [20–23]. Incorporation of many of these advances into commercial versions of bench-top quadrupole ion trap GC–MS systems (e.g., CI, AGC, ARC, and axial modulation on the Finnigan MAT ITS40 and Varian Saturn) has increased their performance as highly sensitive, mass-specific detectors for GC. Detection limits in the low picogram range are now routine for both EI and CI using these bench-top GC–MS ion traps, and detection limits of 0.5 pg of analyte injected have been reported using EI with the more sophisticated Finnigan-MAT ion trap mass

Correspondence to: G.J. Van Berkel, Analytical Chemistry Division, Oak Ridge National Laboratory, Oak Ridge, TN 37831-6365 (USA).

spectrometer (ITMS) [24]. Incorporation of these and other advances into the ITMS has transformed it into an extremely versatile research-grade mass spectrometer (see e.g., Refs. 6 and 8).

A logical next step in the advancement of quadrupole ion traps as detectors for GC is implementation of routine methods for inducing fragmentation so as to perform MS–MS analyses. Product ion MS–MS spectra, for example, may increase detection specificity and can be used in quantitative analyses [25]. The protocol for MS–MS has been well established in the ITMS with single-frequency CID being the most generally employed method to promote fragmentation [13–15,26–28]. Using this method, CID is accomplished via the application of a discrete supplementary radio-frequency (rf) signal to the end-cap electrodes to kinetically excite ions stored in the trap at their mass-to-charge dependent frequencies of motion. The kinetically excited ions undergo energetic collisions with the helium bath gas (present in the trap at a pressure of ca. 1 mTorr) thereby inducing fragmentation.

This same means used to perform MS–MS experiments on the ITMS could be incorporated into the commercial bench-top instruments, but the complex and time consuming "tuning" involved in optimizing CID for a particular ion has hindered this development. Ion excitation and fragmentation with single-frequency CID is dependent upon the parent ion mass-to-charge ratio, the amplitude of the rf trapping voltage applied to the ring electrode, the frequency, amplitude and duration of the supplementary rf signal, the number of ions in the trap, and the tendency of the particular ion for fragmentation. Since ion acceleration is mass-to-charge dependent, the parent ion mass-to-charge ratio must be known in advance. That is, MS–MS experiments employing single-frequency CID cannot be pre-optimized for unknowns and at present cannot be optimized on the chromatographic time scale (i.e., on the fly). A second limitation arises in the absence of measures, viz., AGC in EI and ARC in CI, to adjust ionization conditions to keep the number of ions in the trap constant during elution of the analyte. The presence of other ions of like charge in the trap can establish a dc field strong enough to shift significantly the frequencies of ion motion [3]. As a result of these "space charge" effects, optimum tuning conditions are not constant as the peak elutes because the number of ions in the trap is changing. In addition, due to the relatively slow nature of parent ion internal energy deposition and the fact that product ions are not subsequently kinetically excited, conventional single-frequency CID typically leads to the formation of only one or a few different product ions [13–15]. Therefore, structural information inherent in the MS–MS spectrum may be limited. The use of MS^n experiments to increase structural information is possible, in principle, but usually not feasible in on-line applications.

Other researchers have investigated means to circumvent some of the problems mentioned above. For example, Yates et al. [29] have used rapid frequency preramps over a narrow mass range to determine empirically the parent ion resonant frequency in an automated fashion. They also investigated the use of a supplementary rf signal with a range in frequency of 10 kHz, which, under their experimental conditions, corresponded to a mass-to-charge range of 1.7. Penman et al. [30], with a similar automated approach, used a dc voltage ramp applied to the ring electrode during application of the supplementary rf signal to the end-caps as a means to shift the secular frequency of the ions at a particular m/z into resonance with the applied frequency. While all three approaches deal effectively with the space charge problem, they still require the parent ion mass-to-charge ratio to be known in advance and do not deal with the limited structural information inherent in typical signal-frequency CID spectra. The stored waveform inverse Fourier transform (SWIFT) method [31], currently used in conjunction with Fourier transform ion cyclotron resonance (FT-ICR) mass spectrometry, represents another possible approach. Because of the extreme specificity and flexibility with which it enables the excitation signal to be tailored, the SWIFT technique should prove extremely effective in dealing with such problems. In fact, Julian et al. [32] have recently demonstrated that broad band excitation is possible in the quadrupole ion trap using the same

techniques developed for FT-ICR. However, the advantages of this and similar broad band excitation techniques may be offset by their cost and complexity of implementation.

Ijames and Wilkins [33] and Marshall et al. [34] have examined the use of random noise excitation in the detection segment of FT-ICR mass spectrometry. Recently, our group demonstrated that random noise applied to the end-caps of a quadrupole ion trap is an effective means for CID of trapped ions that is largely independent of the analyte mass-to-charge ratio and the number of ions in the trap [35]. This new CID methodology provides a simple means to overcome the problems of space charge, the need for frequency tuning, the limited fragmentation, and the inability to fragment compounds of unknown mass-to-charge ratio inherent in the single-frequency CID method. In this paper, the random noise CID methodology is used to implement MS–MS capability on a commercially available bench-top GC–MS quadrupole ion trap. Equipment and parameters involved in implementation and optimization of this capability on the bench-top instrument are discussed using the compound *N,N*-diethylaniline to illustrate. Limits to the experiment, imposed for the most part by instrumental software constraints, are also discussed. GC–MS–MS spectra generated using random noise CID are shown for methamphetamine and amphetamine ionized via isobutane CI.

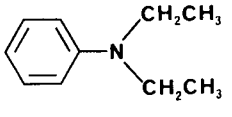

N,N-diethylaniline
(MW = 149)

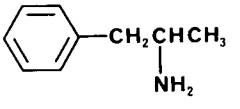

amphetamine
(MW = 135)

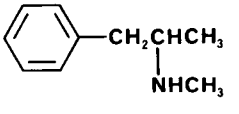

methamphetamine
(MW = 149)

EXPERIMENTAL

Instrumentation

A commercial bench-top quadrupole ion trap, the Finnigan-MAT ITS40 (San Jose, CA), equipped with a Varian Model 3400 GC (Walnut Creek, CA) was used in these experiments. The GC column used was a 12 m × 0.22 mm i.d. aluminum clad HT5 column with a 0.1 μm film thickness (Scientific Glass Engineering, Austin, TX). Research grade helium (99.9999%, Alphagaz, Morrisville, PA) was used as the carrier gas and adjusted to give a flow rate of about 1.0 ml/min. In the case of methamphetamine, splitless injections of 1 μl were performed manually with the chromatograph held at 50°C for 2 min and then ramped to 280°C at a rate of 25°C/min and held at this temperature for 0.8 min. For the methamphetamine–amphetamine mixture, splitless injections of 1 μl were performed manually with the chromatograph held at 50°C for 1 min and then ramped to 280°C at a rate of 50°C/min and held at this temperature for 0.4 min. The temperature of the injector and transfer line in both cases were maintained at 280°C and the ion trap was held at 220°C. For experiments involving *N,N*-diethylaniline, the calibration compound inlet line on the ITS40 was used to introduce the analyte into the vacuum chamber.

Ionization of the analytes was carried out using EI or isobutane (Linde, Danbury, CT) CI. Electron ionization mass spectra were acquired using the instrument supplied EI scan function with the AGC feature turned on. The scan function used to carry out CI-MS and CI-MS–MS was the nominal CI-MS scan function provided with the instrument, but used without the ARC feature. As shown in Fig. 1, when used with ARC off, the CI scan function consists of four segments, namely, (1) reagent gas ionization, (2) reagent gas reaction, (3) ejection of reagent gas ions, and (4) mass spectrum acquisition. The duration and amplitude of the rf trapping voltage in the first two segments, which, as listed in Table 1, can be preset within limits via the instrument software, are important variables in the experiment. To perform CI, the rf trapping voltage in segment 1 is set low (typically equivalent to a low

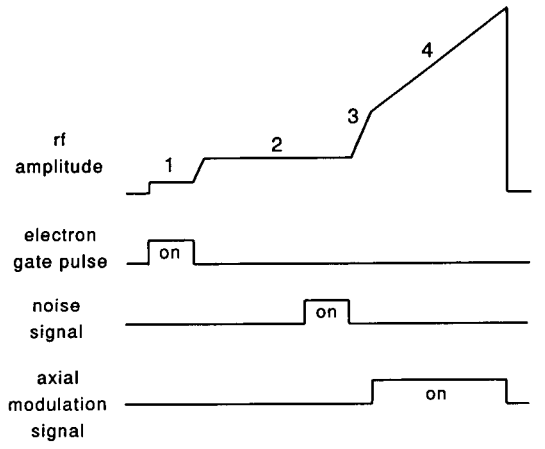

Fig. 1. Four segment scan function used to carry out the CI-MS and CI-MS–MS experiments. Individual time segments are (1) reagent gas ionization, (2) reagent gas reaction/random noise CID, (3) ejection of reagent gas ions, and (4) mass spectrum acquisition.

mass cutoff corresponding to m/z 5) to trap only the reagent gas ions formed by the electron pulse. Higher mass analyte ions formed by EI at these low trapping levels are lost from the trap. The segment 2 time period is used to allow the reagent ions created in segment 1 to react with the neutral analyte to form analyte ions. The rf trapping voltage is set in this segment to a level that optimizes formation of analyte ions, which in these cases was equivalent to a low mass cutoff of m/z 35. To perform MS–MS experiments, the random noise signal was applied to the end-cap during the final 10–20 ms of this segment. Software imposed limitations on the amplitude of the rf trapping voltage during this segment, the need to trap both the reagent ions and analyte ions formed, and the necessity of applying the noise signal during this segment, combine to compromise, to a degree, random noise CID on the bench-top instrument (vide infra). Each of the GC–MS–MS spectra shown in the Results and discussion section is the result of a single ionization event followed by application of the noise signal and finally the mass analysis.

TABLE 1

Variable parameter settings for segments 1 and 2 in the CI scan function [a]

Segment	rf Amplitude low-mass cutoff (m/z)	Time (ms)
1	1–50 (5)	0.01–2.5 (2.5)
2	1–50 (35)	1–100 (100)

[a] Numbers in parentheses indicate typical values used in these experiments.

Random noise collision-induced dissociation

A broadband noise generator (Model NC6103, NoiseCom, Paramus, NJ) with a flat power spectrum (±1.0 dB) from 10 Hz–500 kHz served as the random noise signal source for these experiments. Noise amplitude could be attenuated in steps of 0.1 dB via manual controls on the noise generator. The noise signal was gated on (10–20 ms) by a variable-delay pulse generator (Model 6040, Berkeley Nucleonics, Richmond, CA) which was triggered by the ITS40 electron gate signal. The delay interval between the electron gate pulse and the noise gating pulse was adjusted using an oscilloscope so that the random noise signal was activated near the end of segment 2. Output from the noise generator was sent through a variable-bandpass low-pass filter (Model 7A22 plug-in, Tektronix, Beaverton, OR) and then amplified by 50 dB (Model 2100L, Electronic Navigation Industries, Rochester, NY) before being applied to one end-cap electrode; the standard axial modulation signal was applied to the other end-cap (i.e., the monopolar excitation mode was employed for both axial modulation and random noise CID).

Samples

Methamphetamine hydrochloride and amphetamine sulfate standards (1.0 mg/ml in methanol) were obtained from Sigma (St. Louis, MO). Stock solutions were prepared from these standards by serial dilution in HPLC-grade hexane (EM Science, Gibbstown, NJ). *N,N*-Diethyaniline was obtained from Chem Service (West Chester, PA).

RESULTS AND DISCUSSION

Current versions of the commercial bench-top GC–MS ion traps are not configured to perform MS–MS experiments largely because of the complexity of implementing such an experiment using single-frequency CID. Even with the more sophisticated ITMS, the practicality of GC–MS–MS experiments is generally limited to the analysis of targeted compounds having standards which allow pre-optimization of conditions. The use of random noise CID in GC–MS–MS experiments reduces this complexity making such experiments more routine. The less sophisticated software of the bench-top ion trap does, however, impose some limitations on the experiment not experienced when using the ITMS.

Implementation and characterization of random noise CID

Ion trapping in the quadrupole ion trap is achieved by application of a radio frequency (rf) voltage to the ring electrode. A static dc potential may also be added but is not required for trapping. Conditions for stable ion motion in the device, which correspond to solutions of the Mathieu equation, can be plotted parametrically. The parameters a_u and q_u (u represents the radial (r) or axial (z) dimension) are proportional to the dc and rf amplitude, respectively, and inversely related to the mass-to-charge ratio (m/z), frequency of the rf signal, and the end-cap and ring electrode spacing and size. Thus, adjustment of the values for the above variables determines the stable range of mass-to-charge ratios for the ion trap. Neglecting low-amplitude oscillations at the frequency of the applied rf voltage (micromotion), trapped ions can be considered to experience simple harmonic motion (macromotion) simultaneously in the r- and z-directions. For a particular set of experimental conditions, ions of different mass-to-charge are characterized by a unique frequency of macromotion termed the secular frequency. The secular frequency is proportional to q_u and thus has an inverse dependence on mass-to-charge. The amplitude of the z-macromotion of an ion can be increased via resonance absorption of energy from a supplementary rf signal, of the same frequency as the secular frequency of the ion, applied to the end-caps. As the amplitude of the secular motion grows, collisions between the kinetically excited ions and the He bath gas become more energetic thereby increasing the ion internal energy and ultimately leading to fragmentation. This process is the basis for CID in the quadrupole ion trap.

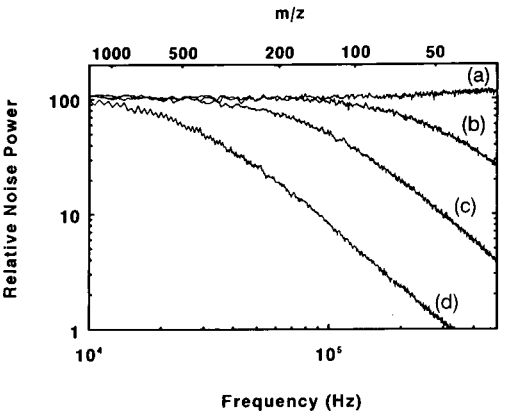

Fig. 2. Relative noise power versus frequency (lower abscissa) as a function of the −3 dB roll-off frequency for the individual filter: (a) no filter, (b) 300 kHz filter, (c) 100 kHz filter, and (d) 30 kHz filter. The upper abscissa indicates mass-to-charge values for trapped ions corresponding to the secular frequencies on the lower abscissa for a low mass cutoff corresponding to m/z 35.

The efficacy of a broadband excitation signal, that is, random noise, in overcoming similar problems in analytical MS–MS applications on the ITMS has been shown [35]. The operational basis of random noise CID can be better understood by reference to Fig. 2. The lower and upper abscissae of Fig. 2 indicate a portion of the secular frequency and corresponding mass-to-charge range, respectively, for trapped ions when a fixed rf amplitude of approximately 400 V (low-mass cutoff of m/z 35) is used. Curve a in Fig. 2 is a plot of relative signal power versus frequency (and therefore also m/z) for the unfiltered random noise signal as applied to one of the end-caps. Although the instantaneous noise spectrum is composed of random frequencies, when evaluated over the ion excitation period the noise signal is essentially continuous and broadband covering the range of secular frequencies corre-

sponding to a mass-to-charge range of 10–650. As a result, prior knowledge of target ion m/z is unnecessary for ion excitation, since ions over that entire mass-to-charge range can undergo simultaneous, non-mass specific kinetic excitation and fragment. Also, difficulties in MS–MS optimization resulting from space-charge related shifts in secular frequency are eliminated. In addition, first-generation product ions subsequently become resonant, undergo kinetic excitation, and may also fragment; such fragmentation may continue for several generations of ions. The result is that a random-noise MS–MS spectrum may yield significantly more structural information than the single-frequency counterpart. The technique is straightforward to implement on the ITMS and has been used by our group to study a wide variety of ions generated by EI, CI, glow discharge ionization, laser desorption, and electrospray ionization [35–37].

Regardless of whether single-frequency or random-noise resonance excitation is used to effect CID, several important variables are shared by the two techniques. These variables are the amplitude and duration of excitation, the amplitude of the fundamental rf signal applied to the ring electrode during resonance excitation, which is proportional to q_z, application of the excitation signal to one (monopolar excitation) or both end-caps (in-phase: quadrupolar excitation or 180° out-of-phase: dipolar excitation), and the helium bath gas pressure. The spectral properties of the random noise signal can also be expected to influence CID results and in some instances its broadband nature can be problematic. For example, the exclusive production of low mass-to-charge ratio ions, which can result from excessive fragmentation, may actually reduce the amount of structural information obtained. In addition, low mass-to-charge ions attain higher frequency oscillations of greater amplitude than ions of relatively higher mass-to-charge at a fixed low mass rf cutoff. Consequently, under conditions which are optimum for parent ion fragmentation using random noise, product ions may undergo excessive fragmentation or attain kinetic energies which lead to ejection from the ion trap.

Fortunately, the aforementioned problems can be moderated by tailoring the properties of the excitation signal via attenuation of signal power and bandwidth limiting techniques. A simple approach to tailoring the properties of the excitation signal is to use adjustable filtering of the random noise signal. The effect of low-pass filters having −3 dB points of 300, 100, and 30 kHz on the fixed-attenuation random noise is demonstrated by curves b–d, respectively, in Fig. 2. For each filter the noise power rolls off at 20 dB/decade at frequencies above the −3 dB point. Ion acceleration and kinetic energy are expected to diminish for ions with m/z values below the mass-to-charge ratio corresponding to the roll-off frequency. Although not shown in the plot, frequency spectra were also obtained for increasing amounts of random noise attenuation at fixed filtering; such curves were parallel to and negatively offset from those shown. Thus, increasing the noise attenuation, i.e., reducing the noise power, should result in a reduction in kinetic energy over the entire mass-to-charge range of trapped ions.

The protonated molecule of *N,N*-diethylaniline (m/z 150), formed via isobutane CI, was used to investigate the effect of modifying the random-noise excitation signal characteristics and varying the fundamental rf voltage applied during resonance excitation (i.e., the low mass cutoff) on the resultant product ion spectra. Due to constraints imposed by the bench-top instrument software and in order to simplify the random-noise experiments, only monopolar excitation of fixed duration (10 ms) was used and the helium pressure (ca. 1 mTorr) was kept constant. Shown in Fig. 3 are the relative abundances of $(M + H)^+$ (m/z 150) and the product ions at m/z 148, 120 and 94, formed via random-noise CID at a fixed rf amplitude (low mass cutoff = m/z 35) as a function of increasing noise signal power. The four separate plots in each figure represent results obtained by filtering the noise with the 1 MHz, 300 kHz, 100 kHz and 30 kHz low-pass filters. Single-frequency CID studies with the ITMS established the major genealogy of these ions as shown in Scheme 1. The parent ion plot (Fig. 3a) features a series of sigmoidal curves while the product ion plots (Fig. 3b–d) are peak-

m/z 150 → m/z 148 → m/z 120
m/z 135 → m/z 107
m/z 122 → m/z 120, 94
m/z 94 → m/z 77

Scheme 1.

shaped. Essentially only the protonated parent molecules are initially formed and trapped. Product ions do not appear until their precursor ions attain sufficient internal energy to dissociate. (The low abundance of m/z 148 at low noise power levels is probably the result of fragmentation of the parent ion due to the energetics of the isobutane proton transfer reaction.) Thus, coincident with the reduction in parent ion intensity is the increase in product ion intensities. However, both parent and product ions can be ejected from the trap if their kinetic energy exceeds the trapping potential well depth. This, along with successive sequential fragmentation of the product ions, explains the loss of product ion intensity at higher noise powers. The shifting of peak maxima to higher noise powers as the product ions decrease in mass is a result of the sequential nature of the fragmentation process (see Scheme 1) and the related energetics. That is, the plots in Fig. 3 are essentially breakdown curves with increasing noise power proportional to precursor ion internal energy necessary for product ion formation.

The shift in peak intensity and position for an individual ionic species shown in Fig. 3 as a function of the low-pass filter used in the experiment is a consequence of the particular precursor/product ion secular frequencies. Formation of a particular product ion requires that sufficient internal energy is acquired by the precursor ion to dissociate, which in turn requires sufficient noise power at the secular frequency of the precursor. As was shown in Fig. 2, the individual filters attenuate the noise power to varying degrees with respect to frequency. The secular frequencies for m/z 150, 148, 120, and 94 under the conditions of this experiment are approximately 83, 84, 104, and 135 kHz, respectively. Therefore, the 1 MHz and 300 kHz filters, which have little attenuation effect in the frequency region of these ions (Fig. 2), change only slightly the positions of the parent/product ion curves. However, the 100 kHz and 30 kHz filters significantly attenuate the noise power in this frequency range and thus, the curves for parent ion dissociation and production ion formation are shifted towards higher noise powers. Furthermore, the increase in noise power observed between the curves associated with the 30 kHz and 300 kHz filters in each plot parallels the difference in noise powers seen at the corresponding secular frequencies in Fig. 2b and d. It is also noteworthy that for a given filter setting, the optimum noise power (i.e., the power associated with each peak maximum) increases with successive generations of ions. This is logical as the formation of each succeeding product ion in the fragmentation sequence presumably requires higher internal energy in its precursor ion. Consequently, the appearance (i.e., the relative intensities of each ion) of the MS–MS spectra can be altered by the filter/attenuation combination selected. Presumably more precise control over MS–MS spectra can be attained by using filters which exhibit sharper roll-off at the cut-off frequency.

As demonstrated by the data shown in Fig. 4, the amplitude of the rf potential applied to the ring electrode during application of the noise signal also influences the CID spectrum obtained. These data were acquired under the same conditions as those shown in Fig. 3, but the low mass cutoff during segment 2 in the scan function in this case was equivalent to m/z 45. The main differences between these plots and those in Fig. 3 are the increased noise power necessary for parent ion diminution and the appearance of product ions, and the increased relative abundances of the products. Elevating the rf amplitude causes q_z and the secular frequency for ions of a given mass-to-charge to increase. The effect of this change in secular frequency in reference to Fig. 2 would be to shift the mass-to-charge abscissa to the right. The secular frequencies of m/z 150, 148, 120, and 94 at this new low mass cutoff are 108, 109, 136, and 176 kHz, respectively. As such the ions are moved into the frequency region that is more severely attenuated by the filtering, thereby requiring more noise power to dissociate the parent/precursor ions. The increased intensity of the product ions formed is

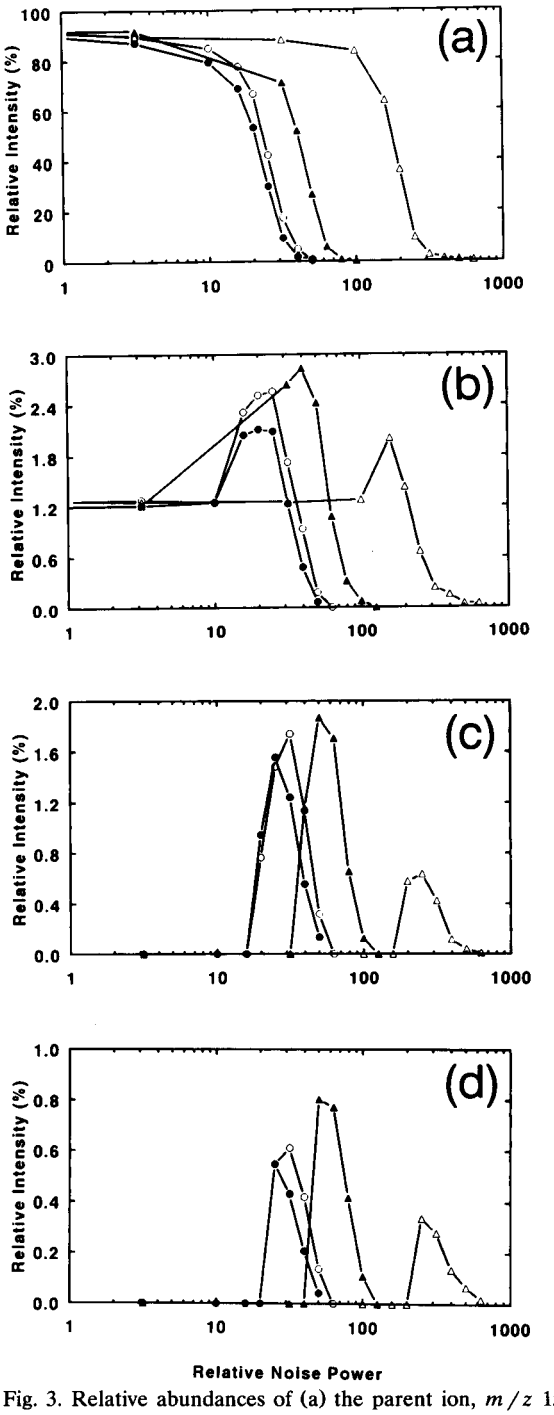

Fig. 3. Relative abundances of (a) the parent ion, m/z 150, and major product ions (b) m/z 148, (c) m/z 120, and (d) m/z 94 formed via random-noise CID of *N,N*-diethylaniline at a fixed rf amplitude (low mass cutoff = m/z 35) as a function of relative noise signal power. The separate plots in each figure were obtained by filtering the noise with 1 MHz (●), 300 kHz (○), 100 kHz (▲) and 30 kHz (△) low-pass filters.

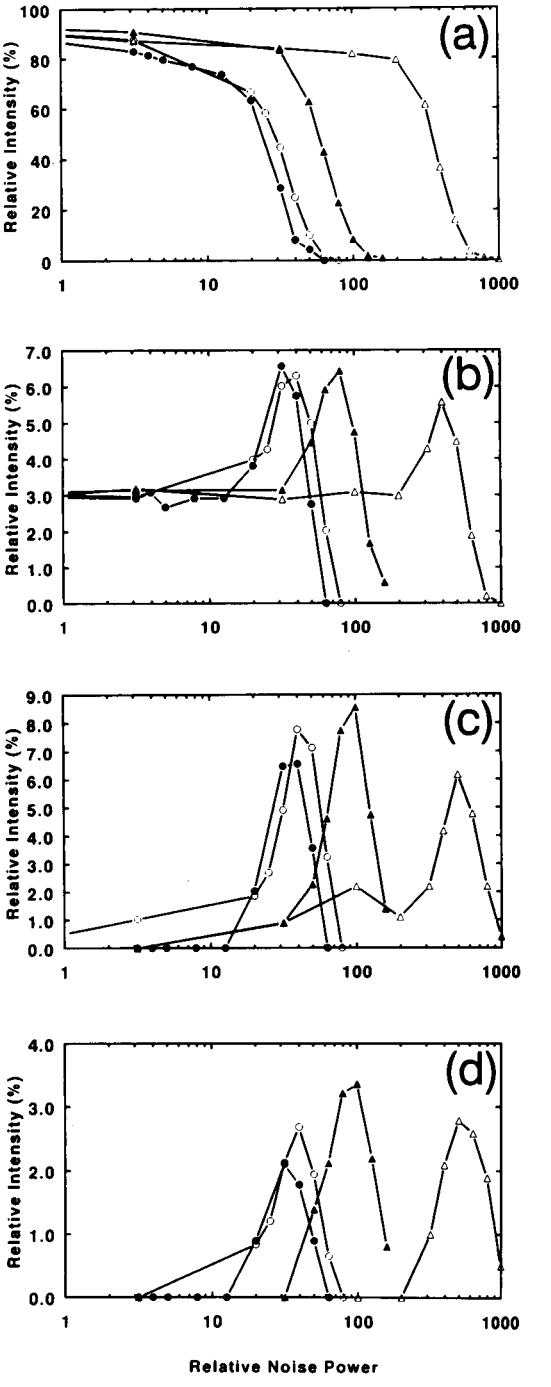

Fig. 4. Relative abundances of (a) the parent ion, m/z 150, and major product ions (b) m/z 148, (c) m/z 120, and (d) m/z 94 formed via random-noise CID of *N,N*-diethylaniline at a low mass rf cutoff corresponding to m/z 45 as a function of relative noise signal power. The separate plots in each figure were obtained by filtering the noise with 1 MHz (●), 300 kHz (○), 100 kHz (▲) and 30 kHz (△) low-pass filters.

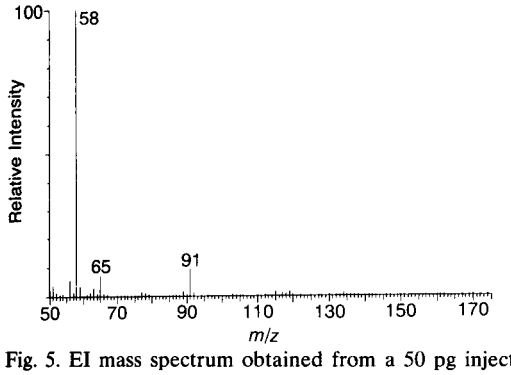

Fig. 5. EI mass spectrum obtained from a 50 pg injection of methamphetamine.

explained by the increased well-depth at the higher low mass cutoff that results in better trapping efficiency. Although trapping efficiency of the product ions from noise CID is greater at the higher low mass cutoff, the formation of the parent ion is less efficient. Since both creation of the parent ion and the CID process must be carried out in the same segment of the scan function, a compromise low mass cutoff of m/z 35 affords better ionization efficiency while still allowing the acquisition of the noise CID spectrum.

On the basis of the above discussion, it is apparent that the best MS–MS spectra using random noise CID will probably be attained when noise power and filtering, and q_z are customized for a particular analyte or analytes within a predetermined range of m/z values. Random noise CID is, therefore, not a truly "universal" or non-mass selective CID method. Nonetheless, the elimination of frequency tuning along with the need for only approximate adjustment of q_z and random noise amplitude for effective fragmentation over a selected m/z range makes this CID methodology much more amenable to on-line GC–MS–MS applications, especially those involving the separation of multiple components, than single-frequency CID.

GC-MS–MS using random noise CID

The particular scenario used here to demonstrate the application of random noise CID in GC–MS–MS on the bench-top ion trap involves the analysis of amphetamines. Amphetamines as a compound class, when ionized by EI, tend to fragment extensively such that no molecular species is readily discernable in the spectrum and only low mass fragment ions, offering little useful structural information, are observed [38,39]. This behavior is demonstrated by the EI spectrum of methamphetamine shown in Fig. 5. A molecular species is absent from the spectrum so that the molecular weight of the compound cannot be determined. Without knowledge of the molecular weight or compound class, the low mass fragment ions at m/z 91 and 58 provide little structural information. In such a case, CI is often used to form a molecular species so as to determine molecular weight. This is demonstrated in Fig. 6 which shows ion current profiles and the isobutane CI mass spectrum obtained from the injection of 50 pg of methamphetamine. (Because of the nature of this compound, the eluting peak is

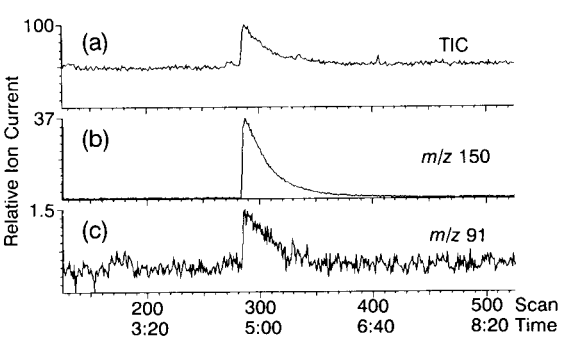

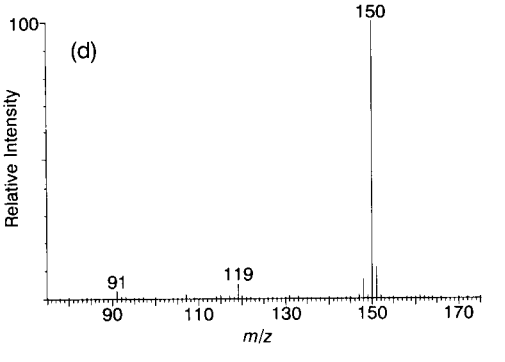

Fig. 6. Total ion current (a) and extracted ion current profiles for (b) m/z 150 and (c) m/z 91 from the isobutane CI analysis of 50 pg of methamphetamine. (d) Background subtracted, averaged isobutane CI mass spectrum of methamphetamine.

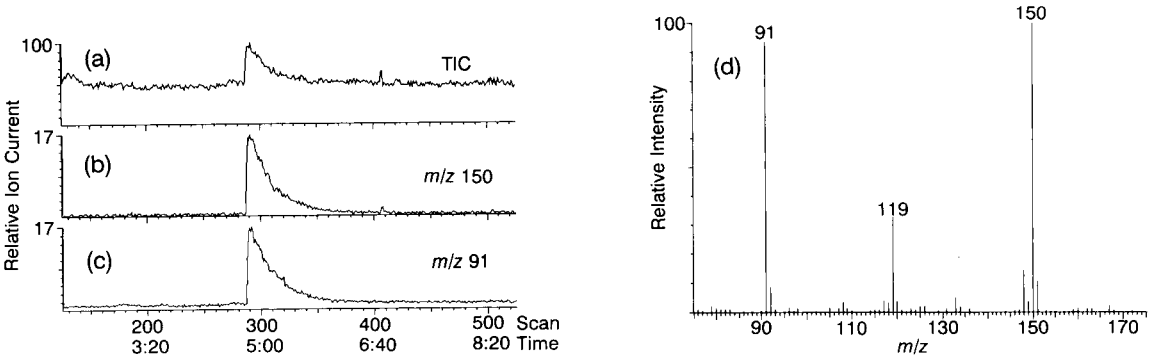

Fig. 7. Total ion current (a) and extracted ion current profiles for (b) m/z 150 and (c) m/z 91 from the isobutane CI, random noise CID analysis of 50 pg of methamphetamine. (d) Background subtracted, averaged isobutane CI random noise MS–MS spectrum of methamphetamine. A fixed power noise signal, filtered with the 100 kHz low-pass filter, was applied for 20 ms.

quite broad. Typically nitrogen bases of this type are derivatized before analysis to improve the chromatography and detection, but for the purposes of this work the relatively poor peak shape is acceptable.) The major peak in the CI mass spectrum (Fig. 6d) at m/z 150 corresponds to $(M + H)^+$ providing the molecular weight of the compound. The two ions of low abundance, m/z 119 and m/z 91, as the MS–MS spectra below will demonstrate, result from fragmentation of $(M + H)^+$ due to the energetics of the isobutane proton transfer reaction. It should be noted that methane CI of methamphetamine produces more fragmentation than isobutane CI while ammonia CI produces less as expected from the energetics of their respective proton transfer reactions [40]. Although ammonia might be a "softer" and more selective reagent gas for ionization in this analysis, the need to carry out the MS–MS experiment at sufficiently high q_z (i.e., preferably $\geqslant 0.25$), as was described above, does not allow this low molecular weight reagent gas to be used since the ability to tailor the scan function is limited. A q_z of 0.25 for m/z 150, for example, corresponds to a low mass rf cutoff equivalent to m/z 37.5 which is too high to trap NH_4^+ (m/z 18). In any case, the molecular weight from the CI mass spectrum along with the fragment ion information from the EI mass spectrum, does provide a great deal of information regarding the nature of this compound.

A more direct method to obtain structural information is to acquire the product ion MS–MS spectrum of the protonated molecule. By using a

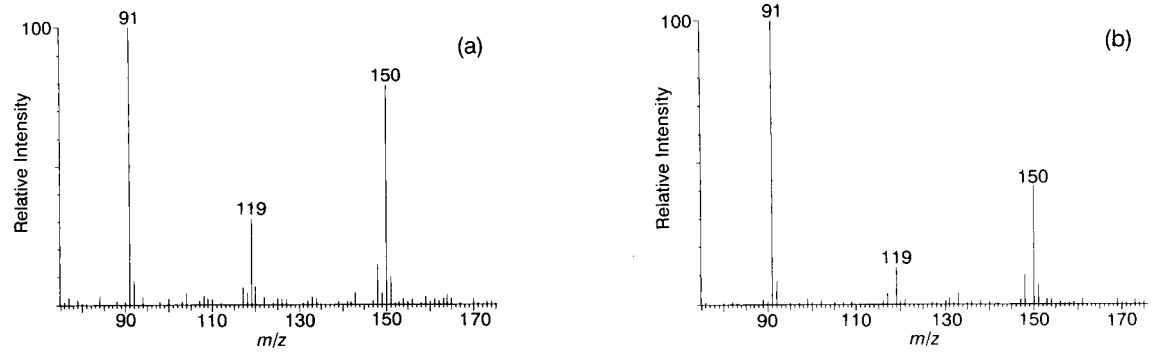

Fig. 8. Background subtracted, averaged isobutane CI random noise MS–MS spectra of 50 pg of methamphetamine obtained using a noise signal, filtered with the 100 kHz low-pass filter, 2 dB (i.e., 58%) greater in power than the signal used in the acquisition of the spectrum shown in Fig. 7. The two spectra correspond to application of the noise signal for (a) 10 ms and (b) 20 ms, respectively.

reagent gas that provides "soft" ionization, little fragmentation occurs obviating the need for ion isolation prior to MS–MS. Fig. 7 shows the ion current profiles and the isobutane CI-MS–MS spectrum, generated using random noise CID, from a 50 pg injection of methamphetamine. The major fragment ions are m/z 119 and m/z 91 corresponding to the loss of CH_5N from the protonated molecule and the loss of C_2H_4 from the ion at m/z 119, respectively. This spectrum is more informative than the CI mass spectrum since the fragment ions are much more intense and are known to arise from the molecular species rather than from some co-eluting species.

Several settings of the noise amplitude and duration can be used to achieve similar MS–MS spectra as demonstrated by a comparison of the MS–MS spectrum in Fig. 7 and the MS–MS spectra obtained under different noise conditions shown in Fig. 8. As these spectra demonstrate, the product of noise signal duration and amplitude, i.e., the noise "fluence", determines the extent of fragmentation when holding all other variables constant. Typically, longer times at a given noise power results in more extensive fragmentation.

A major advantage of random noise CID over single frequency CID is the potential for acquisition of MS–MS spectra of each component in a separated mixture without the need for parameter tuning for each individual compound. This potential is demonstrated in Fig. 9 which shows the extracted ion current profiles and random noise MS–MS spectra acquired during an on-line separation of methampethamine and amphetamine. In order to fragment both compounds efficiently, a compromise combination of noise filtering and attenuation, at a fixed low mass cutoff (i.e., m/z 35), was determined based on experiments performed using three different noise filters, viz., 30, 100, and 300 kHz. Note that these two compounds produce product ions with the same mass-to-charge ratio. Although no frequency tuning is necessary in this experiment, noise power must be adjusted for compounds of different mass-to-charge ratio because of the m/z dependence of q_z. For a fixed low mass cutoff, as the mass-to-charge of an ion decreases, q_z for

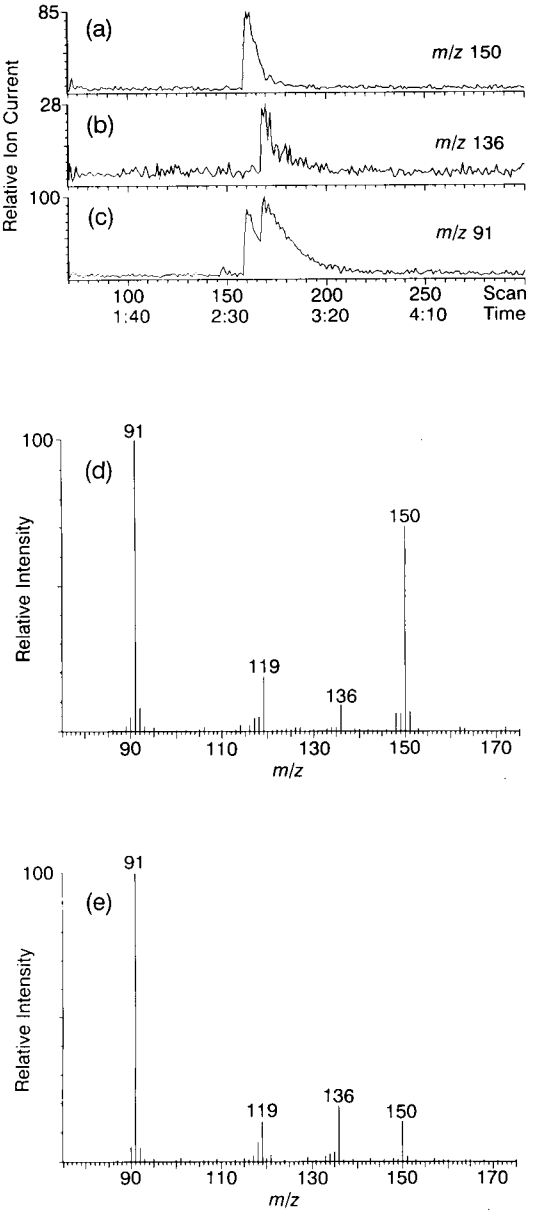

Fig. 9. Extracted ion current profiles for the protonated molecules of (a) methamphetamine (100 pg) and (b) amphetamine (200 pg) and (c) their major fragment ion m/z 91 obtained from the random noise CID analysis of a methamphetamine–amphetamine mixture. The noise signal, filtered with the 30 kHz low-pass filter, was of the same power as that used to acquire the spectra in Fig. 8 and was applied for 10 ms. (d) Background subtracted, averaged isobutane CI random noise MS–MS spectrum of methamphetamine. (e) Background subtracted, averaged isobutane CI random noise MS–MS spectrum of amphetamine.

that ion increases. Noise power must therefore be attenuated for lower m/z ions to avoid excessive fragmentation and potential ion ejection. A simple and cost effective means to accomplish this is through the use of the low pass filters described above. With such filtering, for a fixed low mass cutoff and noise attenuation the actual noise power applied to the end-cap decreases as m/z decreases. This allows for an m/z window where compounds can be fragmented without any subsequent parameter tuning. An additional complicating factor is the propensity for a given compound to fragment. This means that even if two parent ions are close in mass-to-charge, significantly more internal energy may be required for dissociation of one analyte compared with the other. In the present example, amphetamine is more extensively fragmented than methamphetamine under the same experimental conditions.

The data in Fig. 9 also point out the greater demand on separation efficiency imposed by the use of the random noise CID methodology for MS–MS. Since this excitation method is non-mass selective, coeluting compounds or compounds not completely separated will each be excited and fragment as they elute. As such, the MS–MS spectra at a given point in time are a convolution consisting of each molecular species and their respective product ions. For the case of methamphetamine and amphetamine shown, the two components are not completely separated, and therefore, the molecular species (m/z 150 and 136, respectively) and product ions at m/z 119 and 91, which are formed from both parent ions, are observed in each of the two MS/MS spectra (Fig. 9d and e). If two species co-elute the situation is more complicated as the respective parent and fragment ions cannot be determined. One method to at least determine the coeluting species in a peak is to alternately turn the noise signal off and on. In this way mass spectra and MS–MS spectra can be acquired in an alternate fashion as the peak elutes from the column. This allows confirmation of molecular weight and the purity of the peak (i.e., the CI mass spectra) as well as providing structural information (i.e., the MS–MS spectra). Unfortunately, the software does not allow alternation between different scan functions in a repetitive manner. We have, however, with the ITMS used a frequency divider circuit, triggered by the electron gate-pulse, to gate the noise on every other mass scan, rather than changing scan functions [37]. All spectra acquired are collected into one data file using this method, but the data can be deconvoluted into mass spectra and MS–MS spectra and moved to separate data files subsequent to acquisition. This same technique in principle can be used on the bench-top ion trap to alternately acquire mass spectra and random noise MS–MS spectra. However, our attempts to use such an approach were only partially successful, presumably due to a problem with synchronization between data acquisition and transfer to the disk. The standard acquisition software apparently stores spectral data obtained during a chromatographic run in buffer memory. When the memory becomes full the data are written to a disk file; to avoid loss of information, the data acquisition process continues during the disk transfer. Examination of such disk files revealed the expected pattern of alternating mass and MS–MS spectra for data obtained prior to the initial data transfer. Spectra corresponding to data acquired subsequent to that transfer appeared to be some type of average of the mass and MS–MS spectra.

Conclusions

The application of random noise to the end-cap of a bench-top quadrupole ion trap mass spectrometer allows GC–tandem mass spectrometry experiments to be carried out without complex and time-consuming frequency tuning. Although the method relaxes tuning requirements compared to single frequency CID, prior knowledge of the mass-to-charge range of the ions of interest allows for the selection of the optimum low mass cutoff, or q_z, for efficient fragmentation and product ion storage. As such the method is not a truly "universal" CID method, but a compromise set of parameters should be able to be selected in most cases that affords collection of MS–MS spectra of eluting species within a predetermined mass-to-charge range. The main limitations to this method at present result from the limited flexibility of scan function parameters on the

bench-top instrument. The addition, for example, of an independent time segment for random noise CID, after the reagent gas reaction segment, with no limitation in low mass cutoff would greatly enhance the utility of the method.

The assistance of K.G. Asano (ORNL) with acquisition of MS–MS spectra on the ITMS and with maintenance and operation of the ITS40 is acknowledged. This research was sponsored by Grant No. R01GM45372 from the National Institutes of Health.

REFERENCES

1 S.A. Borman, Anal. Chem., 55 (1983) 726A.
2 G.C. Stafford, P.E. Kelley, J.E.P. Syka, W.E. Reynolds and J.F.J. Todd, Int. J. Mass Spectrom. Ion Proc., 60 (1984) 85.
3 R.E. March and R.J. Hughes, Quadrupole Storage Mass Spectrometry, Wiley, New York, 1989.
4 R.G. Cooks and R.E. Kaiser, Jr., Acc. Chem. Res., 23 (1990) 213.
5 B.D. Nourse and R.G. Cooks, Anal. Chim. Acta, 228 (1990) 1.
6 R.G. Cooks, G.L. Glish, S.A. McLuckey and R.E. Kaiser, Jr., Chem. Eng. News, 69 (1991) 26.
7 R.E. March, Org. Mass Spectrom., 26 (1991) 625.
8 G.L. Glish and S.A. McLuckey, Int. J. Mass Spectrom. Ion Proc., 106 (1991) 85.
9 J.S. Brodbelt, J.N. Louris and R.G. Cooks, Anal. Chem., 59 (1987) 1278.
10 G.C. Stafford, D.M. Taylor, S.C. Bradshaw, J.P.E. Syka and M. Uhrich, in Proceedings of the 35th ASMS Conference on Mass Spectrometry and Allied Topics, Denver, CO, May 24–29, 1987, American Society for Mass Spectrometry, East Lansing, MI, p. 775.
11 M. Weber-Grabau, P.E. Kelley, J.E.P. Syka, S.C. Bradshaw and J.S. Brodbelt, in Proceedings of the 35th ASMS Conference on Mass Spectrometry and Allied Topics, Denver, CO, May 24–29, 1987, American Society for Mass Spectrometry, East Lansing, MI, p. 1114.
12 M. Weber-Grabau, P.E. Kelley, S.C. Bradshaw and D.J. Hoekman, in Proceedings of the 36th ASMS Conference on Mass Spectrometry and Allied Topics, San Francisco, CA, June 5–10, 1988, American Society for Mass Spectrometry, East Lansing, MI, p. 1106.
13 J.N. Louris, R.G. Cooks, J.E.P. Syka, P.E. Kelley, G.C. Jr. Stafford and J.F.J. Todd, Anal. Chem., 59 (1987) 1677.
14 J.N. Louris, J.S. Brodbelt-Lustig, R.G. Cooks, G.L. Glish, G.J. Van Berkel and S.A. McLuckey, Int. J. Mass Spectrom. Ion Processes, 96 (1990) 117.
15 S.A. McLuckey, G.L. Glish and G.J. Van Berkel, Int. J. Mass Spectrom. Ion Processes, 106 (1991) 213.
16 R.E. Kaiser, J.N. Louris, J.W. Amy and R.G. Cooks, Rapid Commun. Mass Spectrom., 3 (1989) 225.
17 J.N. Louris, J.W. Amy, T.Y. Ridley and R.G. Cooks, Int. J. Mass Spectrom. Ion Processes, 88 (1989) 97.
18 S.A. McLuckey, G.L. Glish and K.G. Asano, Anal. Chim. Acta, 225 (1989) 25.
19 G.J. Van Berkel, G.L. Glish and S.A. McLuckey, Anal. Chem., 62 (1990) 1284.
20 R.E. Kaiser, R.G. Cooks, G.C. Stafford, J.E.P. Syka and P.H. Hemberger, Int. J. Mass Spectrom. Ion Processes, 106 (1991) 79.
21 J.C. Schwartz, J.E.P. Syka and I. Jardine, J. Am. Soc. Mass Spectrom., 2 (1991) 198.
22 D.E. Goeringer, S.A. McLuckey and G.L. Glish, in Proceedings of the 39th ASMS Conference on Mass Spectrometry and Allied Topics, Nashville, TN, May 19–24, 1991, American Society for Mass Spectrometry, East Lansing, MI, p. 532.
23 D.E. Goeringer, W.B. Whitten, J.M. Ramsey, S.A. McLuckey and G.L. Glish, Anal. Chem., 64 (1992) 1434.
24 B.L. Kleintop, R.A. Yost and C.R. Abolin, J. Am. Soc. Mass Spectrom., 3 (1992) 85.
25 K.L. Busch, G.L. Glish and S.A. McLuckey, Mass Spectrometry/Mass Spectrometry: Techniques and Applications of Tandem mass Spectrometry, VCH, New York, 1988.
26 R.J. Strife and J.R. Simms, Anal. Chem., 61 (1989) 2316.
27 J.V. Johnson, R.A. Yost, P.E. Kelley and D.C. Bradford, Anal. Chem., 62 (1990) 2162.
28 R.J. Strife and J.R. Simms, J. Am. Soc. Mass Spectrom., 3 (1992) 372.
29 N.A. Yates, R.A. Yost, S.C. Bradshaw and D.B. Tucker, in Proceedings of the 39th ASMS Conference on Mass Spectrometry and Allied Topics, Nashville, TN, May 19–24, 1991, American Society for Mass Spectrometry, East Lansing, MI, p. 132.
30 A.D. Penman, J.F.J. Todd, D.A. Thorner and R.D. Smith, Rapid Commun. Mass Spectrom., 4 (1990) 415.
31 A.G. Marshall, T.-C.L. Wang and T.L. Ricca, J. Am. Chem. Soc., 107 (1985) 7893.
32 R.K. Julian, K. Cox and R.G. Cooks, in Proceedings of the 40th ASMS Conference on Mass Spectrometry and Allied Topics, Washington, DC, May 31–June 5, 1992, American Society for Mass Spectrometry, East Lansing, MI, p. 943.
33 C.F. Ijames and C.L. Wilkins, Chem. Phys. Lett., 108 (1984) 58.
34 A.G. Marshall, T.-C.L. Wang and T.L. Ricca, Chem. Phys. Lett., 108 (1984) 63.
35 S.A. McLuckey, D.E. Goeringer and G.L. Glish, Anal. Chem., 64 (1992) 1455.
36 D.E. Goeringer, D.M. Chambers and S.A. McLuckey, in Proceedings of the 40th ASMS Conference on Mass Spectrometry and Allied Topics, Washington, DC, May 31–June 5, 1992, American Society for Mass Spectrometry, East Lansing, MI, in press.

37 G.J. Van Berkel, R.S. Ramsey, S.A. McLuckey and G.L. Glish, in Proceedings of the 40th ASMS Conference on Mass Spectrometry and Allied Topics, Washington, DC, May 31–June 5, 1992, American Society for Mass Spectrometry, East Lansing, MI, in press.
38 D.A. Cowan and G. Woffendin, Spectra, 11 (1988) 4.
39 H.K. Lim, C.O. Sakashita and R.L. Foltz, Spectra, 11 (1988) 10.
40 A.G. Harrison, Chemical Ionization Mass Spectrometry, CRC Press, Boca Raton, FL, 1983.

Analytica Chimica Acta, 277 (1993) 55–60
Elsevier Science Publishers B.V., Amsterdam

Chemiluminescence reaction of thiazide compounds with tris(2,2′-bipyridine)ruthenium(III)

John A. Holeman and Neil D. Danielson

Department of Chemistry, Miami University, Oxford, OH 45056 (USA)

(Received 12th October 1992; revised manuscript received 9th December 1992)

Abstract

The chemiluminescence reaction of five thiazide diuretic compounds with tris(2,2′-bipyridine)ruthenium(III) is studied by flow injection over a range of pH values of the carrier stream. The optimum pH range was generally 4–6. One compound, hydroflumethiazide, could be detected at the 0.06 pmole (1 ng ml^{-1}) level. The detection limits for hydrochlorothiazide and cyclothiazide were at 1–2 pmole (13 and 41 ng ml^{-1}, respectively). Two other compounds, chlorothiazide and trichlormethiazide, are only detectable at $\mu g\ ml^{-1}$ levels. Hydrochlorothiazide was quantified with a 103% recovery from a pharmaceutical capsule.

Keywords: Flow injection; Chemiluminescence; Diuretics; Thiazide compounds; Tris(2,2′-bipyridine)ruthenium(III)

Chemiluminescence (CL) has been recently reviewed as a simple but good detection method for selected analytes by either flow injection or liquid chromatography (LC) [1]. One chemiluminescent reaction which has received renewed attention is that involving tris(bipyridine)ruthenium(III) [$Ru(bpy)_3^{3+}$] and some reducing agent, generally an organic amine. Danielson and coworkers [2–6] first showed this reaction had broad applicability to the chemiluminescent determination of aliphatic amines by either flow injection [2] or LC [3]. Tertiary amines such as tripropylamine were particularly reactive and could be determined at the pmole level. Pharmaceutical products containing antibiotics such as erythromycin [4] or clindomycin [5] which each had a tertiary amine group in their structure could be assayed using $Ru(bpy)_3^{3+}$ CL. Amino acids particularly those having a secondary amine group such as proline could also be determined at the 20 pmole level [6]. Detection limits of primary amino acids could be markedly improved at alkaline reaction pH values [7,8]. Immobilization of $Ru(bpy)_3^{3+}$ on a Nafion coated carbon electrode has permitted the facile reuse of this chemiluminescent reagent [9]. Application of a 1.3-V potential to the carbon electrode would convert the $Ru(bpy)_3^{2+}$ reaction product back to the reactive $Ru(bpy)_3^{3+}$. Detection limits for oxalate, alkylamines, and NADH were determined to be at the low μM level by flow injection.

Although most simple aliphatic amines appear to react readily with $Ru(bpy)_3^{3+}$, it is still difficult to predict which organic compounds with more complicated structures will generate CL. One early chemiluminescent study of hydralazine mentioned briefly that hydrochlorothiazide reacted with $Ru(bpy)_3^{3+}$ to give a strong emission signal [10]. However, no quantitative results were reported and other thiazide drugs in this same class were not considered. The quantitation of

Correspondence to: N.D. Danielson, Department of Chemistry, Miami University, Oxford, OH 45056 (USA).

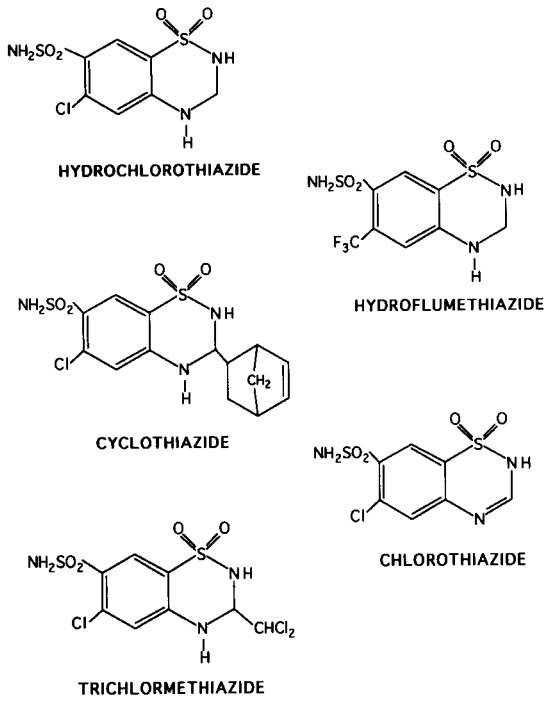

Fig. 1. Structures of five thiazide pharmaceutical compounds.

these compounds is important since they are used pharmaceutically as diuretics for the treatment of hypertension and other disorders [11,12].

This report will describe the feasibility of using flow injection with $Ru(bpy)_3^{3+}$ to determine five thiazide diuretic compounds (Fig. 1) by CL. All but cyclothiazide are found in commercial pharmaceutical products. An initial aspect of this work was to study which common functional groups present in the thiazide structure may be primarily responsible for the chemiluminescent response. Most of the research focused on a chemiluminescent reactivity comparison of these five thiazide compounds, with respect to pH and detection limit. The sensitivity response tend to vary between different thiazide compounds with linear calibration curves over several orders of magnitude. Hydrochlorothiazide, the most commonly available of the five thiazide compounds, was quantitatively determined in a pharmaceutical product by this flow injection–CL technique.

EXPERIMENTAL

All solutions were prepared using water from a Barnstead E-pure system and reagent grade acetonitrile. The pH of sample carrier streams ranged from pH 3 to 10. Phosphate salts were used for pH buffers 3.0, 6.5, and 8.0. Acetate salts were used for solutions buffered at pH 4.0 and 5.5 and borate salts for solutions buffered at pH 9.0 and 10.0. All buffer concentrations were 0.3 M except for the borate buffers which were 0.02 M. The 1.0 mM ruthenium oxidation reagent was prepared from tris(2,2′-bipyridyl)ruthenium(II) chloride hexahydrate [$Ru(bpy)_3^{2+}$] (Aldrich, Milwaukee, WI) with 0.05 M sodium sulfate or an equivalent concentration of acetate supporting electrolyte buffer at pH 5.5. The $Ru(bpy)_3^{2+}$ reagent was oxidized to $Ru(bpy)_3^{3+}$ with a Princeton Applied Research (Princeton, NJ) Model 174A polarographic analyzer using a platinum gauze working electrode, a platinum auxiliary electrode, and a silver wire reference electrode. Oxidation of the $Ru(bpy)_3^{2+}$ solution was performed at a potential of 1.0 V over a 30–45 min period with helium gas continuously bubbling through the solution to provide mixing as well as to remove oxygen. The helium also cooled the reagent solution in about 60 min to 14°C when the supporting electrolyte was sodium sulfate and to 19°C when acetate buffered the solution. During all analytical work, the voltage from the potentiostat was maintained at the electrolysis cell to ensure stability of the $Ru(bpy)_3^{3+}$ concentration.

Hydrochlorothiazide, hydroflumethiazide, chlorothiazide, and trichlormethiazide were obtained from Sigma (St. Louis, MO). Tetramethylene sulfone, benzenesulfonamide, 1,2,3,4-tetramethylquinoline, and 4-amino-6-chloro-1,3-disulfonamide were purchased from Aldrich. The cyclothiazide was a gift from Eli Lilly (Indianapolis, IN). A sample of 50 mg hydrochlorothiazide pharmaceutical tablets was obtained from Geneva Generics (Broomfield, CO).

All analytical results were generated by flow injection. The instrumentation consisted of a Beckman (Fullerton, CA) Model 110A HPLC pump to propel the sample carrier stream and an Alitea (Seattle, WA) Model C-4A peristaltic

pump to deliver the ruthenium oxidizing reagent. Before injection of the first sample, the peristaltic pump was turned on for a 10–15 min period to remove any unoxidizied ruthenium reagent within the reagent intake filter. A Scientific Systems (State College, PA) Model LP-21 pulse damper was positioned between a Rheodyne (Cotati, CA) Model 1040A injector with a 20-μl loop and the Beckman pump. A low dead volume Kel-F (0.012 in. through-hole) union tee allowed mixing of the sample and reagent together before entering the detector. The light emitted was measured in an 8-μl flowcell housed in a Waters 420-AC fluorescence detector. The Kel-F union tee was connected to the detector with a 25×0.5 mm i.d. piece of PTFE tubing to minimize the time between reaction and detection. Optimum flow-rates determined for the sample carrier and $Ru(bpy)_3^{3+}$ streams to be 1.0 ml min^{-1} and 0.4 ml min^{-1}, respectively, were similar to previous work [5]. At this combined flow-rate of 1.4 ml min^{-1}, the time between reaction and detection was calculated to be about 2 s. Residence time of the solution in the flow cell was calculated to be 0.34 s. Signal responses were measured on a Model 5000 Fisher recorder. The flow-injection instrument could generate data for about 3.5 h before the $Ru(bpy)_3^{3+}$ solution reservoir needed to be replenished.

The hydrochlorothiazide tablet was first crushed and the powder then transferred to a 100-ml volumetric flask. Then the contents were dissolved in acetonitrile–water (50:50). This solution was filtered to removed the binder and then quantitatively diluted to a calculated concentration.

RESULTS AND DISCUSSION

An initial study was focused on determining the reactive portion of the hydrochlorothiazide compound. This evaluation was done by selecting compounds that contain similar functional groups to that of hydrochlorothiazide. A negative (quenching) response was observed for the synthetic starting material for hydrochlorothiazide, 4-amino-6-chloro-1,3-benzenedisulfonamide. This precursor compound possesses a primary amine aromatic substituent which may cause quenching of the reaction [8]. This quenching phenomenon was also observed for aniline and *N*-methylaniline under acidic, neutral, and basic pH conditions of the carrier stream. The compound 1,2,3,4-tetrahydroquinoline was chosen for its similarity to hydrochlorothiazide with respect to the cyclic aliphatic secondary amine positioned adjacent to the aromatic ring. An analogous aromatic compound with two cyclic aliphatic secondary amines in its structure was not commercially available. This tetrahydroquinoline compound showed a quenching (negative) response over the entire pH scale studied. The compound tetramethylene sulfone was used as a representative compound to determine the reactivity of the sulfone substituent. A concentration of at least 6000 μg ml^{-1} was required in order to see a light emission signal. Benzenesulfonamide which represents the aromatic sulfonamide functional group provided a much improved response with a detection limit of 130 μg ml^{-1}. In general, the chemiluminescent reactivity for all of the above representative compounds did not come close to that measured for hydrochlorothiazide, at the low ng ml^{-1} level. Subsequently, we as well as others [9] have found it more difficult to predict whether a compound having several nitrogen containing functional groups will undergo $Ru(bpy)_3^{3+}$ CL. Hexamethylenetetramine having several tertiary amines in its structure surprisingly could not be detected. Although methylacetamide [CH_3NH-$(C{=}O)CH_3$] did not chemiluminesce well [6], barbituric acid could be detected at the sub-ppm levels [13]. Further work in predicting good candidates for $Ru(bpy)_3^{3+}$ is underway.

The effect of pH on the chemiluminescent signal for all thiazide compounds was studied from pH 3–9 using a variety of carrier stream buffers with the $Ru(bpy)_3^{3+}$ reagent prepared in two types of electrolyte. The pH of the mixed carrier and reagent stream was unchanged from that of the carrier stream itself in all cases. The detection limit results for hydroflumethiazide, hydrochlorothiazide, and cyclothiazide using a sodium sulfate $Ru(bpy)_3^{3+}$ electrolyte are shown in Fig. 2. Optimum pH values were generally

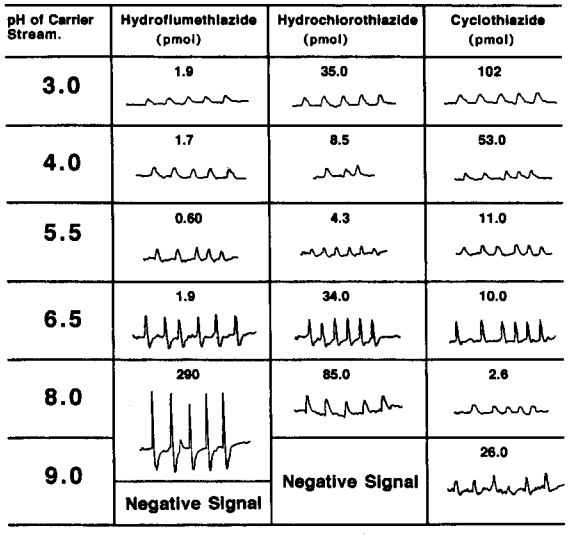

Fig. 2. Detection limit data of three thiazide compounds at various pH values. The 1 mM $Ru(bpy)_3^{3+}$ solution was prepared in 0.05 M sodium sulfate.

observed under slightly acidic conditions for hydroflumethiazide and hydrochlorothiazide but cyclothiazide tended to be more reactive at higher pH. Hydroflumethiazide was about six times more reactive than hydrochlorothiazide and about twenty times more reactive than cyclothiazide at pH 5.5. At pH 8, the best detection limit for cyclothiazide was comparable to that for hydrochlorothiazide at pH 5.5. When hydrochlorothiazide and hydroflumethiazide were allowed to react under basic conditions, the signal response decreased substantially. The pK_a values for hydrochlorothiazide are 7.9 and 9.2, and those for hydroflumethiazide are 8.9 and 10.7. Apparently, the optimum reaction pH for thiazides does not have to be near or above the pK_a values for the amine groups. Reference pK_a values for cyclothiazide could not be obtained.

The detection limits for these three thiazide drugs as well as those for trichlormethiazide and chlorothiazide were examined in the acid pH range using an acetate buffer as the supporting electrolyte for $Ru(bpy)_3^{3+}$ (Table 1). Substantially better detection limits are seen for hydrochlorothiazide, hydroflumethiazide, and cyclothiazide using acetate buffer as compared to using sodium sulfate as the electrolyte. Hydroflumethiazide could be detected at the 0.1 pmole level while the detection limits for hydrochlorothiazide and cyclothiazide were about 1 and 2 pmole, respectively. Previously, hydrochlorothiazide has been detected at 50 ng ml^{-1} using LC with UV detection [14,15] and at 15 ng ml^{-1} using LC with photolysis electrochemical detection [16]. If methylation of hydrochlorothiazide is carried out first, detection limits by gas chromatography are in the 10 ng ml^{-1} range [17]. Our detection limits of 10 ng ml^{-1} can be considered comparable to those found previously for hydrochlorothiazide. In addition, the selectivity of chemiluminescent detection for hydrochlorothiazide is probably superior to the other previously cited methods. The reactivity for cyclothiazide seemed to improve under acidic conditions if the $Ru(bpy)_3^{3+}$ reagent was in an acetate buffered solution of pH 5.5. In fact, optimum pH conditions using an acetate buffer tended to shift for all three highly reactive thiazide compounds to more acidic conditions compared to results found in Fig. 2. The detection limits for trichlormethiazide and chlorothiazide were significantly higher (in mg ml^{-1} region)

TABLE 1

Detection limits of five thiazide compounds as a function of pH
(Carrier stream = 0.05 M acetate buffer. Reagent stream = 1.0 mM $Ru(bpy)_3^{3+}$ in 0.05 M acetate buffer, pH 5.5. nd = Not determined)

pH Carrier stream	Hydroflu-methiazide (pmol)	Hydrochloro-thiazide (pmol)	Cyclo-thiazide (pmol)	Trichlor-methiazide (pmol)	Chloro-thiazide (pmol)
3.0	0.11	2.1	4.2	100	7780
4.0	0.060	0.87	2.1	100	6900
5.5	0.11	2.1	2.1	120	4870
6.5	nd	nd	nd	2840	14500

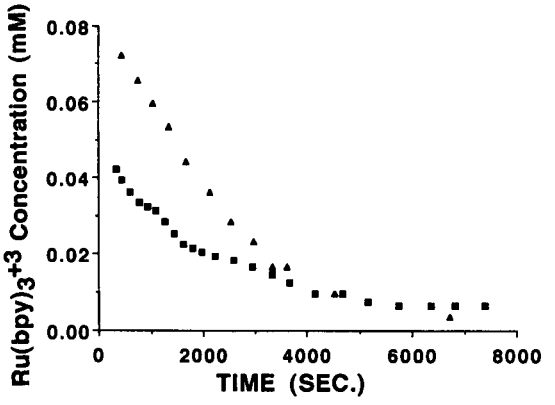

Fig. 3. Concentration vs. time stability curves for $Ru(bpy)_3^{3+}$ prepared in two different electrolytes. ▲ = Acetate buffer; ■ = sodium sulfate.

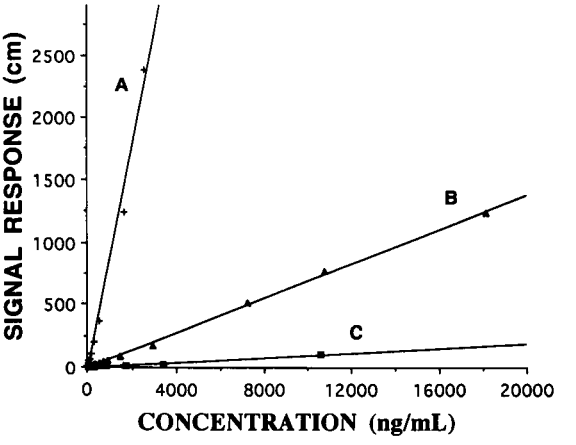

Fig. 4. Calibration curves of three sulfonamide pharmaceutical drugs: (A) hydroflumethiazide, (B) hydrochlorothiazide, (C) cyclothiazide. For A ($n = 10$), $y = -3.9\times10^{1}$ (+/−) $2.7\times10^{1} + 9.1\times10^{-1}$ (+/−) 3.0×10^{-2} z. For B ($n = 14$), $y = -4.2$ (+/−) $3.6 + 7.0\times10^{-2}$ (+/−) 6.0×10^{-4} z. For C ($n = 6$), $y = -9.5\times10^{-2}$ (+/−) $2.5 + 9.5\times10^{-3}$ (+/−) 5.5×10^{-4} z. y = peak height (cm); z = concentration (ng ml^{-1}). Reagent stream: 1.0 mM $Ru(bpy)_3^{3+}$ with 0.05 M acetate buffer (pH 5.5). Sample carrier stream: 0.3 M acetate buffer (pH 4.0).

than those for the other three thiazide drugs. Nitrogen heterocycles such as pyridine are previously known not to be as reactive as alkyl amines. Therefore, chlorothiazide was not expected to be as reactive as hydrochlorothiazide because of the double bond between the nitrogen and carbon atom. Based on the trichlormethiazide data, a strong electron withdrawing functional group on the carbon between the NH groups seemed to cause a reduced chemiluminescent reaction. Previously, it has been reported that electron withdrawing groups present in amino acids reduce $Ru(bpy)_3^{3+}$ CL [8]. The large alkyl substituent of cyclothiazide was found to cause no significant deleterious effect in reactivity. This result is also consistent with that reported previously [8].

Possibly the lower detection limits found for the thiazide compounds using the $Ru(bpy)_3^{3+}$ acetate solution were simply due to more efficient oxidation of $Ru(bpy)_3^{2+}$. Visible spectra of a 0.1 mM ruthenium reagent solution removed from

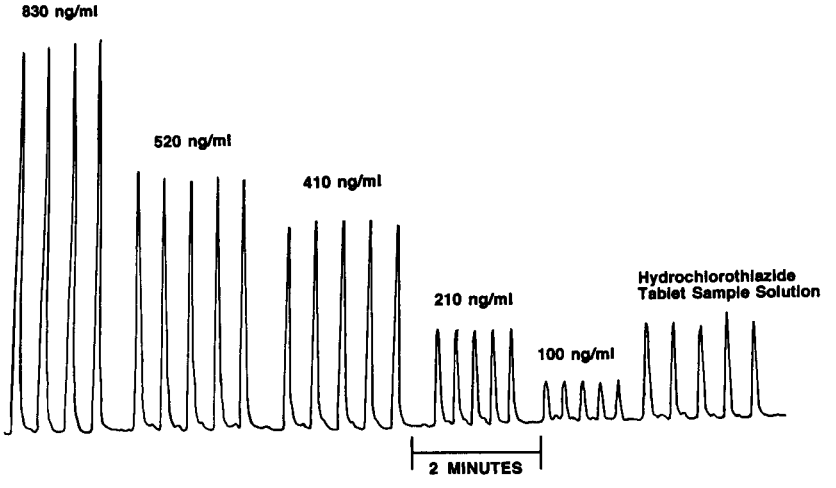

Fig. 5. Flow injection reproducibility of hydrochlorothiazide standards and samples.

the electrolysis cell were taken at 450 nm [the optimum wavelength for $Ru(bpy)_3^{2+}$] to measure the stability of a $Ru(bpy)_3^{3+}$ as a function of time. The results indicate that the concentration of $Ru(bpy)_3^{3+}$ in the acetate solution (buffered at pH 5.5) dropped more slowly than the $Ru(bpy)_3^{3+}$ solution with sodium sulfate as a function of time (Fig. 3). In addition, the coloration of the 1.0 mM $Ru(bpy)_3^{3+}$ acetate solution, after 30–45 min of oxidation, was greenish in color and partially transparent. Whereas, the 1.0 mM $Ru(bpy)_3^{3+}$ solution containing sodium sulfate was dark reddish brown and not transparent at all when compared to the initial solution of $Ru(bpy)_3^{2+}$. These data indicate that more of the $Ru(bpy)_3^{2+}$ had been electrochemically converted to $Ru(bpy)_3^{3+}$ ion using an acetate buffer and this solution is more stable. Therefore, more ruthenium oxidizing agent was present to react with the sample. This could also explain why detection limits are generally better in Table 1 as compared to Fig. 2.

Standard calibration curves were made for three of the most reactive thiazide compounds (Fig. 4). The sensitivity response for these three compounds could be ordered from cyclothiazide < hydrochlorothiazide < hydroflumethiazide. The linear ranges span several orders of magnitude with correlation coefficients of 0.993, 0.995, and 0.999 for the three compounds listed above, respectively.

The accuracy of this method was tested by determining the percent yield for a hydrochlorothiazide pharmaceutical product. This was accomplished by measuring the signal heights for five injections per standard. Then five injections were performed for a diluted hydrochlorothiazide sample. The precision for each of the five injected standards and samples ranged from 1.1 to 4.4% relative standard deviation (R.S.D.) (Fig. 5). For 50 mg hydrochlorothiazide tablets, the percent recovery for the four samples ranged from 99 to 104% with an average value of 103% with a 3% R.S.D.. These data are within the USP guidelines of a range from 93 to 107% [18].

Conclusion

This study indicates that thiazide compounds tend to vary in reactivity depending upon the molecular structure of the compound and types of substituents. Other thiazide diuretics available outside the U.S.A. [12,19] may also be amenable to sensitive detection using this chemiluminescent reaction. Visible spectroscopic analysis of the $Ru(bpy)_3^{3+}$ reagent tended to indicate a better yield when $Ru(bpy)_3^{2+}$ is oxidized under slightly acidic conditions compared to a neutral pH solution. Initial results for the quantitative determination of hydrochlorothiazide in a pharmaceutical product were found to be within the prescribed USP limits.

We thank Eli Lilly for the gift of cyclothiazide and Geneva Generics for sending the hydrochlorothiazide tablets. Financial support through a NIH AREA grant is gratefully appreciated.

REFERENCES

1 T.A. Nieman, in J.W. Birks (Ed.), Chemiluminescence and Photochemical Reaction Detection in Chromatography, VCH, New York, 1989, Chap. 4.
2 J.B. Noffsinger and N.D. Danielson, Anal. Chem., 59 (1987) 865.
3 J.B. Noffsinger and N.D. Danielson, J. Chromatogr., 387 (1987) 520.
4 N.D. Danielson, L. He, J.B. Noffsinger and L. Trelli, J. Pharm. Biomed. Anal., 7 (1989) 1281.
5 M.A. Targove and N.D. Danielson, J. Chromatogr. Sci., 28 (1990) 505.
6 L. He, K.A. Cox and N.D. Danielson, Anal. Lett., 23 (1990) 195.
7 S.N. Brune and D.R. Bobbitt, Talanta, 38 (1991) 419.
8 S.N. Brune and D.R. Bobbitt, Anal. Chem., 64 (1992) 166.
9 T.M. Downey and T.A. Nieman, Anal. Chem., 64 (1992) 261.
10 W.K. Nonidez and D.E. Leyden, Anal. Chim. Acta., 96 (1978) 401.
11 L.H. Werner, A. Halamandras, S. Ricca, L. Dorfman and G. deStevens, J. Am. Chem. Soc., 82 (1960) 1161.
12 R.O. Fullinfaw, R.W. Bury and R.F.W. Moulds, J. Chromatogr., 415 (1987) 347.
13 J.A. Holeman and N.D. Danielson, unpublished results.
14 M.J. Cooper, A.R. Sinaiko, M.W. Anders and B.L. Mirkin, Anal. Chem., 48 (1976) 1110.
15 A.S. Christophersen, K. Rasmussen and B. Salbesen, J. Chromatogr., 132 (1977) 91.
16 W.J. Bachman and J.T. Stewart, J. Chromatogr. Sci., 28 (1990) 123.
17 M.E. Sharp, J. Chromatogr. Sci., 11 (1987) 8.
18 The United States Pharmacopeia, USP, Rockville, MD, 19th edn. 1975, p. 236.
19 R.R. Brodie, L.F. Chasseaud, T. Taylor, D.A. O'Kelly and A. Darragh, J. Chromatogr., 146 (1978) 152.

Analytica Chimica Acta, 277 (1993) 61–65
Elsevier Science Publishers B.V., Amsterdam

Selective determination of L-ascorbic acid by a chemiluminescence method with ascorbate oxidase

K. Sato, Y. Chiba and S. Tanaka

Department of Fundamental Science, College of Science and Engineering, Iwaki Meisei University, Iwaki, Fukushima 970 (Japan)

(Received 24th July 1992; revised manuscript received 2nd December 1992)

Abstract

The determination of L-ascorbic acid by utilizing lucigenin chemiluminescence with ascorbate oxidase was studied. The dehydroascorbic acid produced by the enzymatic reaction of L-ascorbic acid and ascorbate oxidase was found to be a more effective activator than L-ascorbic acid for the lucigenin chemiluminescence reaction. The optimum pH, temperature and incubation time for the enzymatic reaction were 5.7, 30°C and 10 min, respectively. The calibration graph was linear over the range 0.14–50 μg ml^{-1}. The correlation coefficient for this line was 0.998. The detection limit (2σ) was 0.1 μg ml^{-1} and the relative standard deviation was 10% ($n = 5$) for a concentration of 0.14 μg ml^{-1}. This method was applied to the determination of L-ascorbic acid in commercially available drugs and health drinks.

Keywords: Chemiluminescence; Enzymatic methods; Ascorbic acid; Beverages; Health drinks

The use of chemiluminescence (CL) methods for the determination of organic species has been extensively investigated by numerous workers. The most notable characteristic of CL methods is the higher sensitivity compared with other analytical methods, such as spectrophotometric or spectrofluorimetric methods [1]. Luminol and lucigenin are popular CL reagents in the field of clinical chemistry. Whereas the luminol CL reaction has been widely utilized in the determination of numerous inorganic and organic species [2–7], the lucigenin CL reaction has mainly been employed in the determination of organic reducing compounds [8–10].

Lucigenin was used as a CL agent in this work for the selective determination of L-ascorbic acid (AA), as the AA–lucigenin CL reaction is well known to give a very strong CL signal [11]. However, in general, a CL method is not selective for a particular analyte. In application to real samples, the analytes must be separated from each other and/or converted into a species that is effective in producing a CL response. Liquid chromatography (LC) with CL detection has been used for the determination of several organic compounds [12]. In this instance, the concentration of analytes can be individually determined by a postcolumn CL reaction, but the LC conditions, e.g., eluent, and flow-rate, must be optimized for the separation of the analytes from other substances present in a real sample, otherwise, individual analytes cannot be determined accurately. Only a few studies utilizing a CL method coupled with an enzymatic reaction [5,6] for the analysis of real samples, have been reported. This CL method is very simple and rapid, and also has high selectivity.

In this laboratory, it was found that the lucigenin CL intensity for dehydroascorbic acid (DHAA) was much higher than that for AA. It

Correspondence to: K. Sato, Department of Fundamental Science, College of Science and Engineering, Iwaki Meisei University, Iwaki, Fukushima 970 (Japan).

was considered that this phenomenon could be applied to the selective determination of AA, i.e., the amount of AA should be determinable from the difference between the AA and DHAA CL intensities after the enzymatic reaction

$$AA + 1/2\ O_2 \xrightarrow{\text{ascorbate oxidase}} DHAA + H_2O \quad (1)$$

This work was undertaken to develop a CL method for the simple and selective determination of AA by the use of the enzymatic reaction with ascorbate oxidase (AAOD) based on the lucigenin CL reaction. In addition, the proposed method was applied to the determination of AA in commercially available drugs and health drinks.

EXPERIMENTAL

Reagents

Analytical-reagent grade chemicals were used. Lucigenin was purchased from Boehringer (Mannheim, Germany). A stock standard solution of lucigenin (1×10^{-3} M) was prepared in redistilled water and stored in a dark bottle at 5°C. A 1×10^{-4} M working standard solution of lucigenin was prepared on the day of use by dilution of the 1×10^{-3} M stock standard solution. A solution of AA (Kanto Chemical) was prepared by dissolution in distilled water just prior to use. AAOD (from *Cucurbita* species) was obtained from Boehringer. A 7 U ml^{-1} AAOD solution was prepared in 0.1% gelatin aqueous solution which was adjusted to pH 5.6 with 0.1 M acetate buffer solution.

Apparatus

CL measurements were made with a Model UPD-8000 luminometer (Meiden). The enzymatic reaction was run in a BT-23 water-bath incubator (Yamatokagaku) at 30°C.

Procedure

All of the procedures were carried out in a batchwise operation. The enzymatic reaction (Eqn. 1) of AA and AAOD was achieved by the method of Dawson and Magee [13] and run in a glass tube (105 mm × 12 mm id.). The solutions of AA (0.5 ml) and AAOD (0.5 ml), 2.0 ml of 0.2 M phosphate buffer solution (pH 5.7) and 0.5 ml of gelatin solution (5 mg ml^{-1}) were mixed in the glass tube. After incubation at a constant temperature for 10 min, a 0.5-ml portion was placed in the sample cell. The cell was fitted in the sample holder of the luminometer and then solutions of lucigenin (1×10^{-4} M) and potassium hydroxide (0.5 M) were added automatically to the cell by the peristaltic pump inside the luminometer. The CL intensity was measured immediately for 30 s. In addition, a reference solution, i.e., AA solution without AAOD, was also prepared in a similar manner to the above and the CL intensity was measured. The amounts of AA were determined

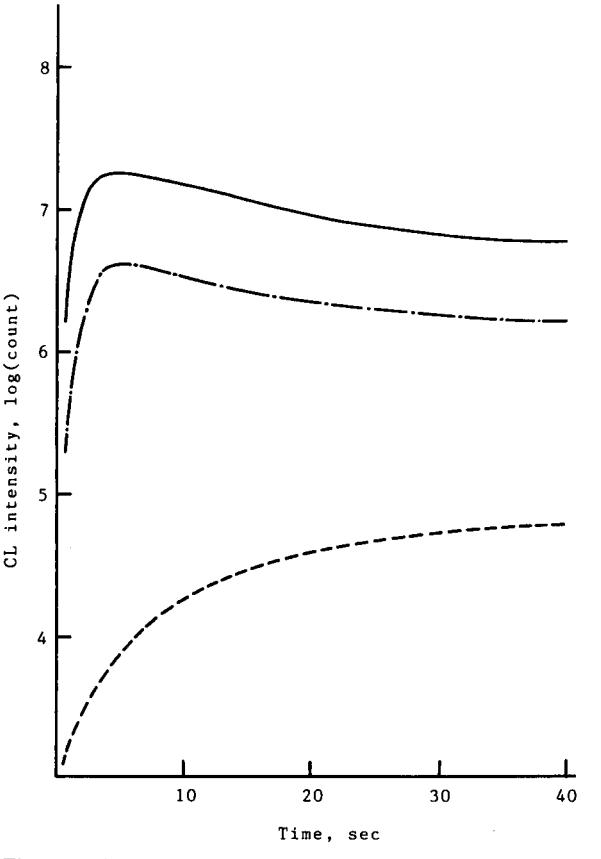

Fig. 1. Typical chemiluminescence response curves. Solid line, sample solution, 50 $\mu g\ ml^{-1}$ AA in the presence of 7 U ml^{-1} AAOD; dot-dashed line, reference solution, 50 $\mu g\ ml^{-1}$ AA solution; dashed line, blank solution. Sample volume, 1 ml.

by the difference in CL intensities with and without AAOD.

RESULTS AND DISCUSSION

CL reaction

In Fig. 1, typical curves of the CL response are shown for AA solution and blank solution. The CL response for the blank solution (in the absence of AA and AAOD) increased with time. The rate of the CL reaction is slower in the blank solution owing to be absence of a catalyst. The CL response curve for AA solution (without AAOD) showed a maximum intensity after ca. 4 s and then gradually decreased to an approximately constant CL intensity. The CL intensity was measured for 30 s in subsequent work.

Figure 1 also shows the CL response curve for the sample solution after the enzymatic reaction of AA and AAOD. The curve was similar to that for AA solution, but the CL intensity was much higher than that for AA. This effect was due to the production of DHAA from the enzymatic reaction of AA and AAOD. The results demonstrated that DHAA was more effective than AA in the lucigenin CL reaction.

Enzyme reaction

The appropriate conditions for the enzymatic reaction were studied.

The optimum pH region for the enzymatic reaction was investigated. As shown in Fig. 2, a maximum CL intensity (counts per 30 s) was obtained at pH values > 4. This result indicates that the amount of DHAA that was produced from the enzymatic reaction was a maximum in this pH range. Therefore, pH 5.7 was adopted according to the procedure described previously [13].

The effect of the incubation time on the enzymatic reaction was investigated. The CL intensity did not change during a period up to 45 min. The results suggested that DHAA was produced quantitatively for at least 2 min. The enzymatic reaction was carried out with incubation at vari-

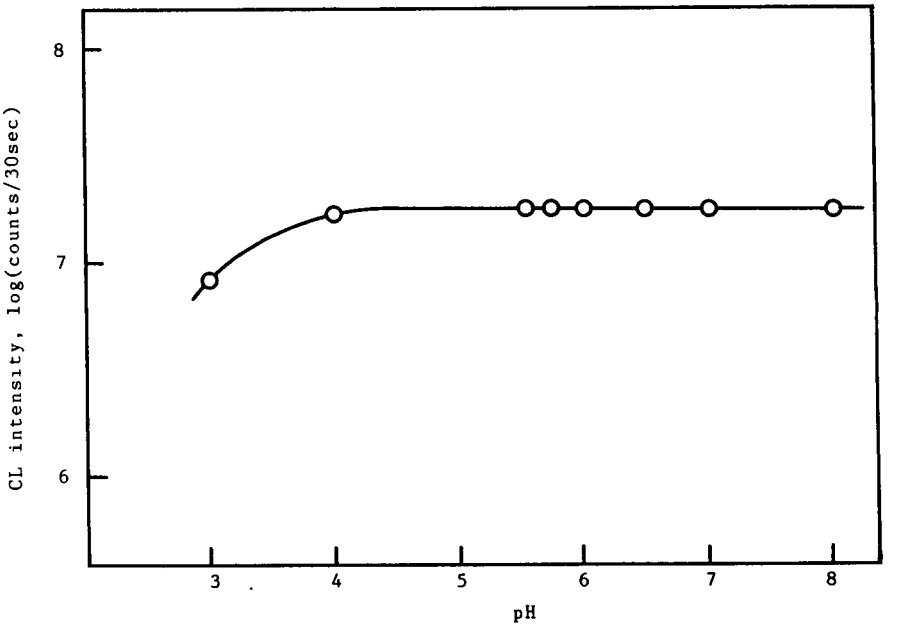

Fig. 2. Effect of pH on the enzymatic reaction of 50 μg ml^{-1} AA and 7 U ml^{-1} AAOD. Incubation time, 10 min; temperature, 30°C.

TABLE 1

Effect of foreign reductants on the determination of 50 μg ml^{-1} AA

Addition	Concentration (μg ml^{-1})	CL intensity [a] (counts per 30 s)	Relative intensity (%)
None	–	1.29×10^7	100
Glutathione	50	1.30×10^7	101
	500	1.30×10^7	101
	5000	1.25×10^7	97
Glucose	50	1.31×10^7	102
	500	1.32×10^7	102
	5000	1.31×10^7	102
Fructose	50	1.30×10^7	101
	500	1.31×10^7	102
	5000	0.83×10^7	64

[a] Means of five experiments (R.S.D.: < 6%).

ous temperatures, then the CL intensity was measured. A maximum CL intensity was observed in the range 20–50°C. Therefore, the enzymatic reaction was carried out for 10 min at 30°C. A test solution containing 50 μg ml^{-1} AA was allowed to react with several concentrations of AAOD. The results showed that a concentration of 0.3 U ml^{-1} AAOD was required for the enzymatic reaction and the CL intensity was not influenced by adding an excess of AAOD at least up to 17 U ml^{-1}. A 7 U ml^{-1} solution of AAOD was chosen for subsequent work because the AAOD was relatively unstable in aqueous solution.

Calibration and interferences

The log–log calibration graph for AA standard solution was obtained under the optimum conditions. The calibration graph was linear over the range 70 ng ml^{-1}–50 μg ml^{-1} and the linear regression equation of the best fit was $y = 1.22x + 5.94$, where x is log[AA, μg ml^{-1}] and y is log(CL intensity, counts per 30 s), i.e., the logarithm of the difference in CL intensity for AA before and after the enzymatic reaction with AAOD. The correlation coefficient for this line was 0.998. The detection limit (2σ) for AA was calculated from the standard deviation (σ, $n = 5$) of the reference CL intensity, i.e., the difference between the blank intensities in the presence and absence of AAOD, and was ca. 0.1 μg ml^{-1}. The relative standard deviation ($n = 5$) was less than 10% at an AA concentration of 0.14 μg ml^{-1}.

The effect of other organic reductants on the determination of 50 μg ml^{-1} AA was investigated. In the enzymatic reaction, these reductants were added to the AA solution, then the CL intensity was measured by the procedure described above. The results are given in Table 1.

TABLE 2

Analytical results for the determination of AA in health beverages

Sample [a]	Sample taken (ml)	Aliquot	AA added (μg)	AA found [b] (μg)	AA in sample (μg ml^{-1})	Recovery (%)	Titration method: [c] AA in sample (μg ml^{-1})
A	0.5	1/100	0	15.0	3000		
		1/100	25	40.2		101	3240
		1/25	0	60.9	3050		
B	0.5	1/250	0	22.3	11200		
		1/250	25	48.1		103	10600
		1/100	0	59.7	11900		
C	0.5	1/25	0	7.8	390		
		1/25	25	32.5		99	415
		1/10	0	18.3	366		
D	0.5	1/50	0	12.9	1290		
		1/50	25	38.7		103	–
		1/25	0	22.2	1110		

[a] A and B = drug samples; C and D = health drink samples. [b] Means of five experiments (R.S.D.: < 6%). [c] 2,6-Dichloroindophenol titration method [14].

Glutathione and glucose did not interefere in concentrations up to at least a 100-fold excess over AA. Although the CL intensity was affected by adding 5000 μg ml^{-1} of fructose, no influence on the AA determination was observed with a ten-fold excess of fructose.

Sample analysis

The proposed method was applied to the determination of AA in two commercially available drugs and in two health-oriented drinks. The drugs are health beverages for promoting nutrition, and amounts of vitamin C indicated on the label of each container were 300 mg per 100 ml and 500 mg per 50 ml, respectively. The drink samples are health drinks containing natural food fibre and vitamin C. The samples were thoroughly degassed under reduced pressure and 0.5 ml was dissolved immediately in distilled water. A suitable aliquot of the sample solution was pipetted into the glass tube and the enzymatic reaction with AAOD and CL measurement were carried out by the procedure described above. The results are summarized in Table 2.

The concentrations of AA for drug samples A and B agreed with the label values. The recoveries of AA for all the samples tested were 99–103%.

Further, the 2,6-dichloroindophenol tritration method [14] was applied in order to compare the results with those of the proposed method (Table 2). For these samples, there was a difference of 6–11% between the results obtained by the proposed and the titration methods. These results are considered to be satisfactory.

It is concluded that the proposed method is able to determine AA selectively and is applicable to analyses of practical samples, such as fruits or vegetables.

The authors are grateful to the Sasakawa Scientific Research of the Japan Science Society for financial support granted through Project No. 3-056.

REFERENCES

1 K. Van Dyke (Ed.), Biochemiluminescence and Chemiluminescence: Instruments and Applications, Vol. 1, CRC, Boca Raton, FL, 1985, p. 188.
2 D.E. Bause and H.H. Patterson, Anal. Chem., 51 (1979) 2288.
3 S. Nakahara, M. Yamada and S. Suzuki, Anal. Chim. Acta, 141 (1982) 255.
4 D. Pilosof and T.A. Nieman, Anal. Chem., 54 (1982) 1698.
5 A. Taniguchi, Y. Hayashi and H. Yuki, Anal. Chim. Acta, 188 (1986) 95.
6 P. Jones, T. Williams and L. Ebdon, Anal. Chim. Acta, 217 (1989) 157.
7 K. Sato and S. Tanaka, Anal. Chim. Acta, 236 (1990) 459.
8 R.L. Veazey and T.A. Nieman, Anal. Chem., 51 (1979) 2092.
9 W.L. Hinze, T.E. Reihe, H.N. Singh and Y. Baba, Anal. Chem., 56 (1984) 2180.
10 M. Maeda and A. Tuji, Anal. Sci., 2 (1986) 183.
11 J.R. Totter, Photochem. Photobiol., 22 (1975) 203.
12 R.L. Veazey and T.A. Nieman, J. Chromatogr., 200 (1980) 153.
13 C.R. Dawson and R.J. Magee, Methods Enzymol., 2 (1955) 831.
14 T. Nagahara, H. Iwao and S. Kubo, Shokuhin Bunseki-Hou (Analytical Methods for Food) Shibata, Tokyo, 1988, p. 232.

Analytica Chimica Acta, 277 (1993) 67–72
Elsevier Science Publishers B.V., Amsterdam

Catalytic behaviour of iron(II)–oxime complexes in the chemiluminescence reaction of luminol with hydrogen peroxide

Yun-Xiang Ci, Jian-Ke Tie, Feng-Ji Yao, Zhao-Lan Liu, Sa Lin and Wei-Qing Zheng

Department of Chemistry, Beijing University, Beijing 100871 (China)

(Received 26th August 1992)

Abstract

Chemiluminescence produced by the catalytic effect of iron(II)–oxime complexes on the oxidation of luminol by hydrogen peroxide was studied. This is a very fast chemiluminescence reaction and the emission spectrum is similar to that of peroxidase-catalysed chemiluminescence. Different kinds of iron(II)–oxime complexes were compared and it was found that the symmetrical dioxime complex (four nitrogen ligands) has a higher catalytic activity than the asymmetric monooxime complex (two nitrogen and two oxygen ligands). The presence of EDTA can greatly accelerate the chemiluminescence reaction, which was considered to be a result of the formation of a mixed-ligand complex. Other homologues of EDTA were tested and showed different degrees of enhancement. Optimum conditions for the chemiluminescence reactions were examined. Combined with a flow-injection technique, trace amounts of hydrogen peroxide (2×10^{-7}–1×10^{-4} M) and, using glucose oxidase, glucose (0.79–160 μg ml^{-1}) can be determined by using the iron(II)–dimethylglyoxime complex as a typical catalyst. The detection limit of hydrogen peroxide was 1.3×10^{-8} M. The relative standard deviation was 1% for the determination of 2×10^{-7} M H_2O_2 ($n = 11$). The feasibility of utilizing the proposed method for the determination of glucose in human serum was examined.

Keywords: Catalytic methods; Chemiluminescence; Flow injection; Fluorimetry complexes; Glucose; Iron–oxime; Serum

Chemiluminescence (CL) has become attractive for analytical detection because of the very low detection limits and wide working ranges that can be achieved while using relatively simple instrumentation. The chemiluminescent reaction of luminol with hydrogen peroxide catalysed by haeme catalysts such as peroxidase and microperoxidase is widely used in biochemistry and clinical chemistry [1–3]. However, enzymes are expensive and their solutions are unstable. An alternative is to seek an understanding of the enzyme behaviour and thus provide a substitute for such enzymes. Metalloporphyrins (M–Pr) were first investigated and successfully used in spectrophotometric [4,5], fluorimetric [6–8], and chemiluminescent [9–11] determinations. In the search for models with similar chemical and physical properties, e.g., coordination atoms and number, geometry, redox and magnetic properties, to those of the metal–porphyrin complexes, the peroxidic activity of metal–oxime complexes was studied in this work.

It is reasonable to consider that a metal–oxime complex consists of a planar group of the cation and two oxime molecules, as is found in the nickel–dimethylglyoxime (DMG) complex [12], very similar to M–Pr. Evidence supporting the suggested structure and its properties for combin-

Correspondence to: Yun-Xiang Ci, Department of Chemistry, Beijing University, 100871 Beijing (China).

ing with molecular oxygen has been obtained through the study of the Fe–DMG complex [13,14], and some bases, e.g., pyridine, can combine with Fe–DMG just like iron(II) porphyrins.

This paper reports a study of the catalytic activity of Fe–oxime complexes in the luminol–H_2O_2 CL system. Combined with a flow-injection system, it was applied to the determination of glucose in human serum.

EXPERIMENTAL

Apparatus

The flow system used for flow-injection analysis was identical with that used previously [15]. CL intensity was monitored with a GD-1 luminometer (Northwest Research Institute of Geology) and the signal was recorded with a Type 3056 pen recorder. CL spectra were recorded with a Shimadzu RF-540 spectrofluorimeter.

Reagents

All chemicals (analytical-reagent grade) were purchased from Beijing Chemical Works and all aqueous solutions were prepared with distilled water (doubly deionized water was distilled in a Model SYZ-550 sub-boiling quartz evaporator).

For the preparation of Fe–oxime complexes, 8.6×10^{-3} mol of $FeCl_2$ were dissolved in the minimum volume of 0.5 M HCl and the solution was added to 70 ml of ethanol containing 1.7×10^{-2} mol of oxime. The mixture was stirred for about 30 min at room temperature. Ethanol and water were removed by heating with aspiration (the temperature should not exceed 40°C), giving a brown residue. Fe–oxime stock solutions (0.02 M) were prepared by dissolving the product in distilled water (for the Fe–DMG complex) or dissolving in a minimum volume of ethanol and diluted with water (for Fe–furildioxime, –nioxime (–cyclohexane-1,2-dione dioxime) and –salicylaldoxime complexes) and stored in a brown flask.

Hydrogen peroxide solutions were prepared by dilution of a 30% solution (titrated with standard $KMnO_4$) immediately prior to use.

Glucose oxidase (EC 1.1.3.4) (Chinese Science Academy Microbiology Institute) was used as a dilute solution (1 U ml^{-1}) prepared from a 250 U ml^{-1} stock standard solution. Horseradish peroxidase (EC 1.11.1.7) (Merck) was applied at 2.16 U ml^{-1}. Glucose solution was prepared by dissolving glucose in distilled water to give a concentration of 0.01 M.

Luminol was dissolved in 0.10 M NaOH solution to give a 0.025 M stock standard solution. A working standard solution was prepared by diluting the stock standard solution with 0.10 M Na_2HPO_4–NaOH buffer solution (pH 10.0) containing 6×10^{-5} M EDTA.

Procedure

Luminol and Fe–oxime reagent solutions were pumped and mixed by one peristaltic pump of the Intelligent Flow Injection Sampler (Xi'an Spring Institute) and delivered directly to the flow cell. A different concentration of H_2O_2 solution was pumped by another pump and certain amount of H_2O_2 (150 μl) was injected into the luminol–Fe–oxime stream automatically. Peak heights of the emission spectrum were used for determination.

RESULTS AND DISCUSSIONS

Catalytic behaviour of Fe–oxime complexes

The CL emission spectra of luminol–H_2O_2 CL catalysed by Fe–oxime complexes were measured in the spectrofluorimeter as described previously [10]. Figure 1 shows a typical emission spectrum of Fe–DMG and horse radish peroxidase (HRP)-catalysed CL reaction. They have the same emission spectrum. It was found that EDTA can dramatically accelerate the CL reaction. The dependence of the CL intensity on the concentration of EDTA in the Fe–DMG system is shown in Fig. 2. It features a maximum at 10^{-5} M EDTA. Optimum concentrations of EDTA in other CL systems are given in Table 1. The influence of other homologous of EDTA on the Fe–DMG–luminol–H_2O_2 CL reaction were tested and showed different degrees of enhancement (Table 2).

Benfis et al. [16] have demonstrated that small amounts of a lipophilic carboxylic acid and a heterocyclic nitrogen base (serving as the axial

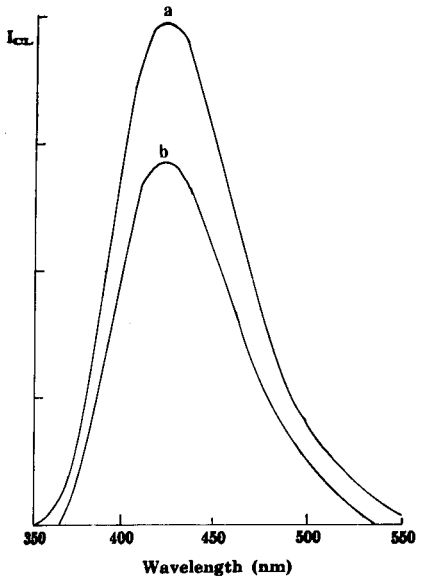

Fig. 1. CL emission spectra of (a) Fe–DMG- and (b) HRP-catalysed luminol–H_2O_2 CL reaction.

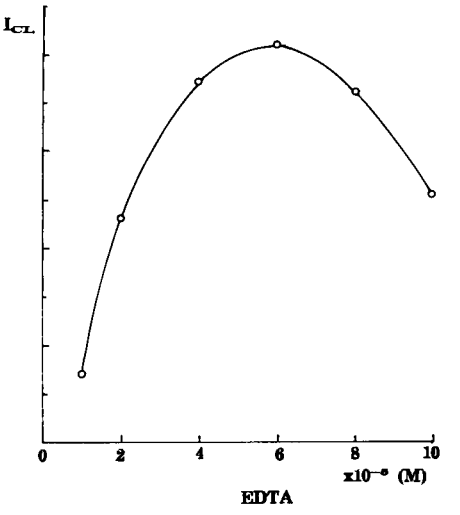

Fig. 2. Dependence of CL intensity on concentration of EDTA [Fe–DMG] = 1×10^{-4} M; [luminol] = 5×10^{-4} M; [H_2O_2] = 1×10^{-5} M; pH = 10.2.

ligand) strongly accelerate the hydrogen peroxide oxygenation of alkanes catalysed by manganese tetraarylporphrins. It has been reported that the peroxidic activity of Mn–$TPPS_4$ is greatly inhibited when two axial coordination sites of the metalloporphyrin are occupied by pyridine or an amino acid [15,17]. Therefore, the enhancement mechanism of EDTA on this CL system was considered to involve the formation of a mixed-ligand complex in which EDTA serves as the axial ligand. A detailed explanation still needs further investigation. In order to confirm that the CL reaction is induced by the Fe–oxime complex

TABLE 1

Optimum conditions and the linear ranges for Fe–oxime complex-catalysed luminol–H_2O_2 chemiluminescence reactions.

Complex	EDTA (M)	pH	Luminol (M)	Fe–oxime (M)	Linear range (M)
Fe–DMG	6×10^{-5}	10.00	5×10^{-4}	3×10^{-5}	2×10^{-7}–1×10^{-4}
Fe–nioxime	5.5×10^{-3}	10.60	9×10^{-4}	5×10^{-5}	1×10^{-7}–1×10^{-5}
Fe–furildioxime	6×10^{-4}	10.00	3×10^{-4}	4.3×10^{-5}	2×10^{-7}–1×10^{-5}
Fe–salicylaldoxime	4×10^{-4}	10.25	3×10^{-4}	4.1×10^{-4}	2×10^{-7}–6×10^{-6}

TABLE 2

Enhancement by EDTA homologues of emission from Fe–DMG–luminol–H_2O_2CL system

Parameter	Enhancer [a]				
	EDTA	TTHA	NTA	DTPA	HEDTA
Optimum concentration (M)	6.0×10^{-5}	8.0×10^{-4}	2.2×10^{-2}	2×10^{-3}	1.2×10^{-3}
Magnitude of enhancement (-fold)	290	123	50	9	8.3

[a] EDTA = ethylenediamine tetraacetic acid; TTHA = triethylenetetraaminehexaacetic acid; NTA = nitrilotriacetic acid; DTPA = diethylenetriaminepentaacetic acid; HEDTA = hydroxyethylenediaminetriacetic acid.

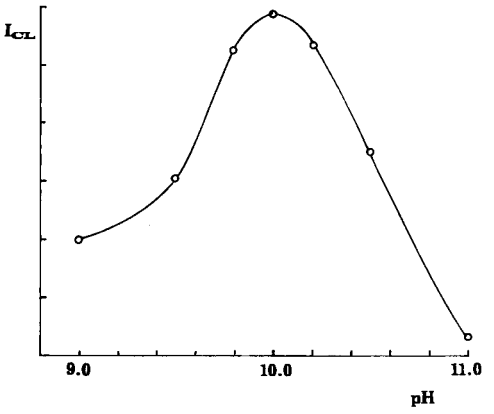

Fig. 3. CL intensity–pH profiles. [Fe–DMG] = 1×10^{-4} M; [luminol] = 5×10^{-4} M; [H_2O_2] = 1×10^{-5} M; [EDTA] = 6×10^{-5} M.

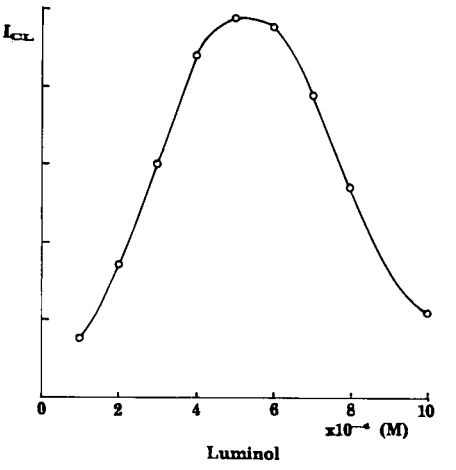

Fig. 4. Effect of luminol concentration on CL intensity. [Fe–DMG] = 1×10^{-4} M; [H_2O_2] = 1×10^{-5} M; [EDTA] = 6×10^{-5} M; pH = 10.0.

not by the Fe–EDTA complex or Fe(II) itself, 1×10^{-4} M Fe–EDTA, Fe(II) and Fe–DMG as catalysts were tested under the same reaction conditions and the relative CL intensities were 0, 13 and 50, respectively.

Optimization of reaction conditions

The effect of pH plays a key role in Fe–oxime complex-catalysed luminol CL reactions as with most other catalysts. Figure 3 shows the pH dependence of the CL intensity from the Fe–DMG-induced luminol CL reaction. It features a maximum at pH 10.00. As the pH increases, the emission decreases drastically and at pH 11.50 precipitation occurs because of the decomposition of the Fe–DMG complex. The optimum pH values of other CL reaction systems are given in Table 1. Based on these data, pH 10.00 (0.1 M Na_2HPO_4–NaOH buffer) was selected as the optimum pH.

The effects of the concentrations of luminol and the Fe–DMG complex on the CL intensity are shown in Figs. 4 and 5. As is evident, maximum emission occurred when the concentrations of luminol and Fe–DMG were 5×10^{-4} and 1×10^{-4} M, respectively. The optimum concentrations of luminol and other Fe–oxime complexes were tested and are given in Table 1.

Under these optimum conditions, the catalytic activities of Fe–DMG, nioxime, furildioxime and –salicylaldoxime complexes in the luminol–H_2O_2 CL reaction were compared. The relatively CL intensities were 100, 40, 38.5 and 1.5, respectively. The Fe–salicylaldoxime complex has much lower catalytic activity than the others. This suggested that four nitrogen ligands are necessary for the metal–oxime complexes to show peroxidic activity, as with metal–porphyrin chelates.

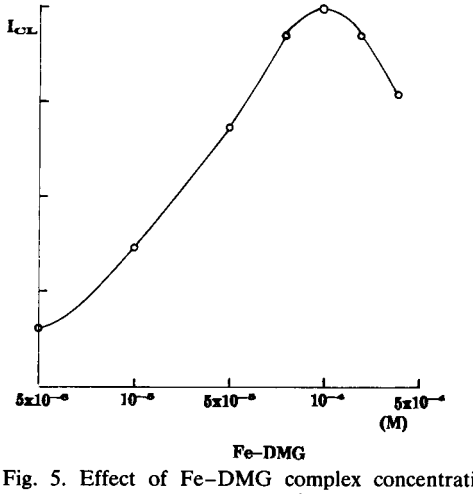

Fig. 5. Effect of Fe–DMG complex concentration on CL intensity. [Fe–DMG] = 1×10^{-4} M; [luminol] = 5×10^{-4} M; [H_2O_2] = 1×10^{-5} M; pH = 10.0.

TABLE 3

Effect of foreign ions on the determination of 4×10^{-6} M H_2O_2 under the optimum conditions

Ion added	Maximum tolerance ratio of ion to H_2O_2 (molar ratio) [a]
K^+, Na^+, CL^-, F^-, NO^{3-}, SO_4^{2-}, Br^-	>1000
I^-	250
Mg^{2+}, Ca^{2+}	30
Ba^{2+}	20
NH_4^+	15
Zn^{2+}, Cu^{2+}	10
Mn^{2+}	5
Al^{3+}, Co^{2+}, Cr^{3+}, Fe^{3+}, Pb^{2+}	2.5
Ni^{2+}	1
Fe^{2+}	0.025

[a] The ions in the stated ratio caused a relative error of less than 5%.

Calibration graphs for hydrogen peroxide

After establishing the effect of the different parameters on the Fe–oxime–luminol–H_2O_2 CL system, the calibration graphs for the determination of hydrogen peroxide were obtained using the optimum reaction conditions. The range of linearity for the relationship between the relative CL intensity and the concentration of hydrogen peroxide is given in Table 1. The Fe–DMG complex has a relatively wider linear range, and it was chosen as a catalyst for the analytical application study. The relative standard deviation was 1% for the determination of 2×10^{-7} M H_2O_2 ($n=11$), and the limit of determination was 1.3×10^{-8} M H_2O_2 using Fe–DMG as the catalyst.

Interferences

The interference effect of foreign ions on the determination of H_2O_2 (4×10^{-6} M) in the Fe–DMG–luminol–H_2O_2 CL system was studied and the results are summarized in Table 3. When added at levels greater than those given, all the ions listed caused negative errors.

Determination of glucose in human serum

A brief study was made of the feasibility of utilizing the glucose–glucose oxidase reaction coupled with the Fe–DMG–luminol–H_2O_2 CL reaction system as a means of determining glucose. Considering the interferences of metal ions in human serum, 1×10^{-5} M EDTA was added to the samples as the final concentration. GOD at 0.01 U ml^{-1} and 30 min were selected as the optimum conditions for the glucose oxidation reaction. A calibration graph was prepared by using glucose standards. The linear range for the determination of glucose was 0.79×160 $\mu g\ ml^{-1}$ and the correlation coefficient was 0.9999 ($n=6$). In order to compensate for any interference in the samples, a calibration graph for glucose in human serum was prepared. The calibration graph was translated through the origin and was used for the determination of glucose in human serum. The results are given in Table 4.

TABLE 4

Determination of glucose in human serum [a]

Sample No.	Glucose added ($\mu g\ ml^{-1}$)	Glucose found ($\mu g\ ml^{-1}$)	Recovery (%)	Concentration of glucose in serum ($mg\ ml^{-1}$)
1	0.0	8.12		
	3.96	12.05	99	0.81
2	0.0	7.93		
	3.96	11.85	99	0.79
3 [b]	0.0	20.02		
	7.93	27.94	100	2.00
4 [b]	0.0	20.02		
	7.93	28.73	110	2.00

[a] Each sample was analysed three times. The results given are averages. [b] Serum samples from diabetic subjects.

This work was supported by the National Natural Science Foundation of China.

REFERENCES

1 W.G., Wood, in S.B. Pal (Ed.), Immunoassay Technology, Vol. 1, De Gruyter, Berlin, New York, 1985, p. 105.
2 G.H.G. Thorpe and L.J. Kricka, Methods Enzymol., 133 (1986) 331.
3 J.P. Gosling, Clin. Chem., 36 (1990) 1408.
4 T. Satio, S. Nakashima, M. Mifune, J. Odo, Y. Tanaka, M. Chikuma and H. Tanaka, Anal. Chim. Acta, 172 (1985) 285.

5 T. Saito, M. Mifune, S. Nakashima, Y. Tanaka, M. Chikuma and H. Tanaka, Chem. Pharm. Bull., 34 (1986) 5016.
6 Y.X. Ci and F. Wang, Mikrochim. Acta, I (1990) 63.
7 Y.X. Ci, L. Chen and W.B. Chang, Microchem. J., 45 (1992) 72.
8 G.F. Zhang and P.K. Dasgupta, Anal. Chem., 64 (1992) 517.
9 T. Hara, M. Toriyawa and K. Tsukagoshi, Bull. Chem. Soc. Jpn., 56 (1983) 2267.
10 Y.X. Ci, H.B. He, W.B. Chang and J.S. Liu, Anal. Chim. Acta, 237 (1990) 497.
11 Y. Ikariyama, S. Suzuki and M. Alzawa, Anal. Chem., 54 (1982) 1126.
12 L.E. Godycki and R.E. Rundle, Acta Crystallogr., 6 (1953) 487.
13 J.F. Drake and R.J.P. Williams, Nature, 182 (1958) 1084.
14 B.A. Jillot and R.J.P. Williams, J. Chem. Soc., (1958) 462.
15 Y.X. Ci, J.K. Tie, Q.W. Wang and W.B. Chang, Anal. Chim. Acta, 269 (1992) 109.
16 S. Benfis, A. Maiocchi, A. Moggi, F. Montanari and S. Quici, J. Chem. Soc., Chem. Commun., (1990) 1794.
17 F. Wang and Y.X. Ci, Analyst, 116 (1991) 297.

Analytica Chimica Acta, 277 (1993) 73–78
Elsevier Science Publishers B.V., Amsterdam

Formation of fluorescent complexes of Eu(III) and Sm(III) with β-diketones and trioctylphosphine oxide in oil–water microemulsions

Hitoshi Watarai and Koko Ogawa

Department of Chemistry, Faculty of Education, Akita University, Akita 010 (Japan)

Nobuo Suzuki

Department of Chemistry, Faculty of Science, Tohoku University, Sendai 980 (Japan)

(Received 9th July 1992; revised manuscript received 9th December 1992)

Abstract

Synergistic enhancement of the fluorescence of Eu(III) and Sm(III) by the addition of β-diketones (HL) and trioctylphosphine oxide (TOPO) was observed in single-phase oil–water microemulsions composed of water–sodium dodecyl sulphate–butan-1-ol–heptane. The synergistic phenomena were attributable to the formation of the ternary complexes $ML_3(TOPO)_2$, where M = Eu(III) or Sm(III), in the microemulsion droplets and the formation constants were determined. Microslide electrophoresis of the microemulsion systems confirmed the solubilization of the complexes into the droplets.

Keywords: Electrophoresis; Fluorimetry; Europium; Microemulsions; Microslide electrophoresis; Samarium

Microemulsions are microheterogeneous media composed of water, a surfactant, a cosurfactant and oil that exhibit characteristic properties such as optical transparency, thermodynamic stability, low viscosity and high solubilization power. The structure of microemulsions depends on the composition: oil–water (o/w) microemulsions with a water-rich composition and water–oil (w/o) microemulsions with an oil-rich composition. The hydrodynamic diameter of oil droplets in o/w microemulsions or water droplets in w/o microemulsions is smaller than 500 nm. Recently, w/o microemulsions have been utilized as organic phases in the liquid–liquid extraction of metal ions [1,2] and proteins [3] and as mobile phases in liquid chromatography [4,5]. In contrast to w/o microemulsions, studies on the application of o/w microemulsions in separation chemistry are limited. Tondre and Canet [6] studied the complexation of Ni(II) in o/w microemulsions in order to discuss the extraction mechanism. Recently, capillary electrophoresis using o/w microemulsions as electrophoretic media was demonstrated [7].

In order to assess the advantages of microemulsions as solvents in analytical separation methods, further extensive studies on the solubilization mechanism of various kinds of compounds are required. Previously, the solubilization mechanism of β-diketones in some different types of o/w microemulsions was reported [8]. In this study, adduct formation between the β-diketone complexes of Eu(III) and Sm(III) with trioctylphosphine oxide (TOPO) in o/w microemulsions composed of water–sodium dodecyl sul-

Correspondence to: H. Watarai, Department of Chemistry, Faculty of Education, Akita University, Akita 010 (Japan).

phate (SDS)–butan-1-ol–heptane was investigated by means of spectrofluorimetry. The fluorescence characteristics of the β-diketonatolanthanide adduct complexes are of interest in relation to fluorescent probes in biomedical systems and in the trace determination of lanthanides [9].

EXPERIMENTAL

Chemicals

Chemicals were of analytical-reagent grade. Water was purified by using a Millipore Milli-QII system after conventional distillation.

Stock solutions of Eu(III) and Sm(III) were prepared by dissolving the corresponding oxides (both from Wako) in perchloric acid. Thenoyltrifluoroacetone (TTA) (Wako) and 2-naphthoyltrifluoroacetone (NFA) (Aldrich) were purified by sublimation under reduced pressure, 4 mmHg at 37–40°C and 1 mmHg at 50–60°C, respectively. TOPO, Dotite and SDS (Wako) were used as received.

The o/w microemulsions (ME) used in most experiments were prepared by mixing water, SDS, butan-1-ol and heptane (89.3 : 3.3 : 6.6 : 0.8, w/w). In addition, o/w ME of other compositions and SDS micelle solution were used to examine the effect of solvent composition. All of the solvents contained 0.01 M $NaClO_4$ and 0.02 M CH_3COONa and the pH was controlled by the addition of small amounts of 0.1 M $HClO_4$ or 0.1 M NaOH.

Apparatus

Fluorescence and excitation spectra were recorded on a Hitachi Model 650-40 spectrofluorimeter. The fluorescence spectra and intensity were all uncorrected. The variation in the intensity of the excitation light from day to day was less than 4%, which was confirmed by monitoring the fluorescence intensity of Rhodamine B aqueous solution, excited at 350 nm and observed at 580 nm. UV–visible spectra were measured by means of a Jasco Uvidec 430 spectrophotometer.

Microslide electrophoresis of metal complexes using ME as solvents was carried out with the apparatus shown in Fig. 1. After the microslide (Vitro Dynamic), of dimensions 10 or 30 cm long, 50 × 500 μm inside section and 150 × 600 μm outside section, had been filled with ME, a sample ME solution including Eu^{3+} or Sm^{3+}, TTA and TOPO was introduced at the cathodic end to a length of ca. 5 mm by a capillary action, and both ends of the microslide were inserted into the silicone solvent reservoirs filled with the ME of TTA and TOPO as shown in Fig. 1. A d.c. voltage was applied by the power supply (Toyo Kagaku Elepos PS-2510) (0–2500 V) between the platinum electrodes and the current was monitored by a Takeda Riken SER multimeter. The migration rate of the lanthanides was determined by measuring the migration distance of the red fluorescent spot of the complex in a certain period from 1.5 to 6 min under irradiation with UV radiation from a Tokyo Kogaku Topcon PAN UV lamp. Heat generated in the microslide was removed by an air fan in a thermostated room at 25 ± 1°C. The use of a microslide was superior to a filter-paper or a polymer-coated fused-silica capillary for the purposes of observation of the fluorescence of the discrete migration spot over the whole length and effective heat dispersion.

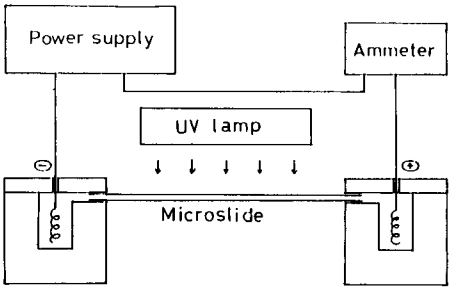

Fig. 1. Schematic diagram of the apparatus for microemulsion microslide electrophoresis.

RESULTS AND DISCUSSION

Fluorescence spectra of Eu(III) and Sm(III)

The hydrated Eu(III) and Sm(III) ions and their β-diketone complexes were virtually nonfluorescent in ME, because of the quenching

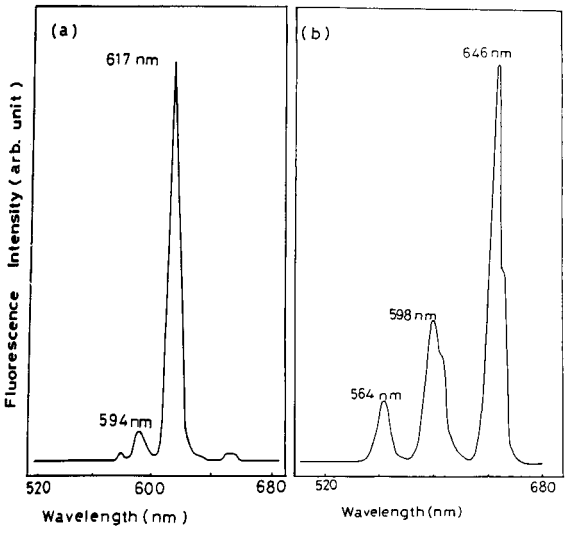

Fig. 2. Fluorescence spectra of (a) $[Eu^{3+}] = 2.85 \times 10^{-7}$ M, $[TTA] = 5.52 \times 10^{-6}$ M, $[TOPO] = 5.86 \times 10^{-4}$ M, pH = 6.4 and (b) $[Sm^{3+}] = 5.80 \times 10^{-6}$ M, $[TTA] = 2.76 \times 10^{-4}$ M, $[TOPO] = 5.86 \times 10^{-4}$ M, pH = 6.5 in ME. Excitation wavelengths were 350 nm for Eu(III) and 347 nm for Sm(III).

activity of hydration water molecules. When TOPO was added to the solution, however, the characteristic fluorescence spectra assigned to the unhydrated metal ions could be observed, as shown in Fig. 2. The fluorescence enhancing effect of TOPO was dependent on the solvent, as shown in Fig. 3. SDS micelle solution was effective only at higher TOPO concentrations. The ME of lower organic composition (ME A) was better than that of higher organic composition (ME B), when compared at the same concentrations of Eu(III), TOPO and β-diketone. Therefore, the former was used as a solvent for the quantitative study of complex formation.

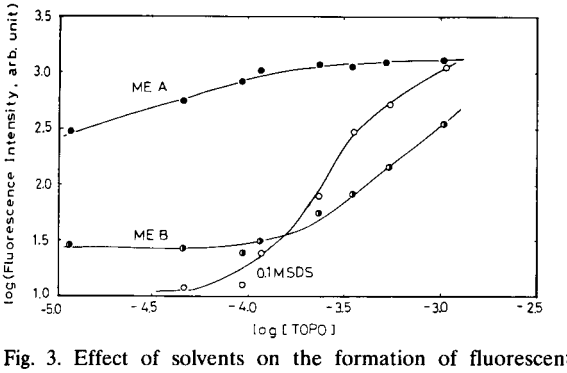

Fig. 3. Effect of solvents on the formation of fluorescent Eu(III) complex. Conditions: ME A, H_2O–SDS–butan-1-ol–heptane (89.30:3.31:6.61:0.80), and ME B, H_2O–SDS–butan-1-ol–heptane (65.14:9.30:18.59:6.97); $[Eu^{3+}] = 1.14 \times 10^{-5}$ M; $[NFA] = 2.99 \times 10^{-5}$ M; pH = 6.0.

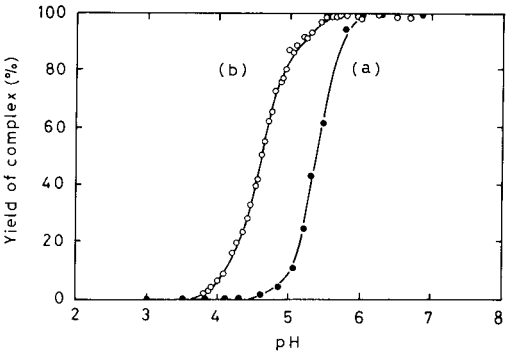

Fig. 4. Variation of the yield of the fluorescent Eu(III) complexes with pH represented by the percentage fluorescence intensity. At pH > 6, the formation of the complexes was assumed to be complete. (a) $[Eu^{3+}] = 1.50 \times 10^{-5}$ M, $[TTA] = 2.76 \times 10^{-5}$ M, $[TOPO] = 5.86 \times 10^{-4}$ M; (b) $[Eu^{3+}] = 5.12 \times 10^{-5}$ M, $[NFA] = 2.19 \times 10^{-5}$ M, $[TOPO] = 5.86 \times 10^{-4}$ M.

Adduct formation in microemulsion

The dependence of the fluorescence intensity of Eu(III) and Sm(III) on pH is shown in Fig. 4. The sigmoidal curves are understood as being analogous to extraction curves which are usually plotted as percentage extraction versus pH for chelate extraction of metal ions. The dependences of the fluorescence intensity on the β-diketone and the metal ion concentration suggested that the molar ratio of the β-diketonate anion to the metal ion in the fluorescent complex was 3:1. In Fig. 5, the points of intersection of the straight lines clearly indicate the ratios $[Eu^{3+}]:[TTA] = 1:3$ and $[Eu^{3+}]:[NFA] = 1:3$.

The relationship between the fluorescence intensity and the TOPO concentration is discussed on the basis of the equation

$$ML_{3,o} + mS_o \rightleftharpoons ML_3S_{m,o} \quad (1)$$

where M and S refer to the metal ion and TOPO, respectively, and the subscript o represents the

oil droplets. The adduct formation constant is defined by

$$\beta_{s,m} = \frac{(ML_3S_m)_o}{(ML_3)_o(S)_o^m} \quad (2)$$

where ( ) refers to the local concentration in the pseudo-organic phase.

Provided that the concentration of the β-diketone is sufficiently high to "extract" quantitatively the metal ion into the oil droplets, the total concentration of metal ion, $[M]_T$, and the total concentration of TOPO, $[S]_T$, are represented by

$$[M]_T = (ML_3)_o\phi + (ML_3S_m)_o\phi \quad (3)$$

$$[S]_T = (S)_o\phi + m(ML_3S_m)_o\phi \quad (4)$$

where ϕ is the volume fraction of the organic component in the o/w microemulsion.

The observed fluorescence intensity, I_F, is represented by

$$I_F = \Phi_o(ML_3)_o\phi + \Phi_m(ML_3S_m)_o\phi \quad (5)$$

where Φ_o and Φ_m are the apparent quantum yields under the present instrumental conditions. When the following relationships are defined:

$$I_F = I_{Fo} \text{ when } (ML_3)_o = [M]_T/\phi \quad (6)$$

$$I_F = I_{Fm} \text{ when } (ML_3S_m)_o = [M]_T/\phi \quad (7)$$

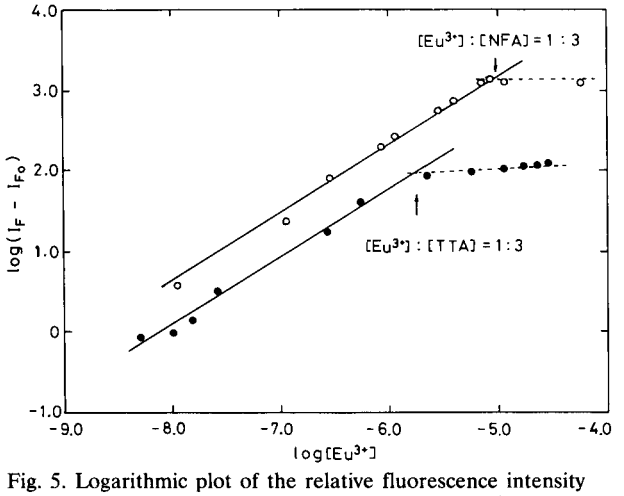

Fig. 5. Logarithmic plot of the relative fluorescence intensity against Eu(III) concentration. [TOPO] = 5.86×10^{-4} M. ● = [TTA] = 5.52×10^{-6} M; ○ = [NFA] = 2.99×10^{-5} M. The two concentrations of Eu^{3+} denoted by arrows correspond to one third of the TTA and NFA concentrations, respectively.

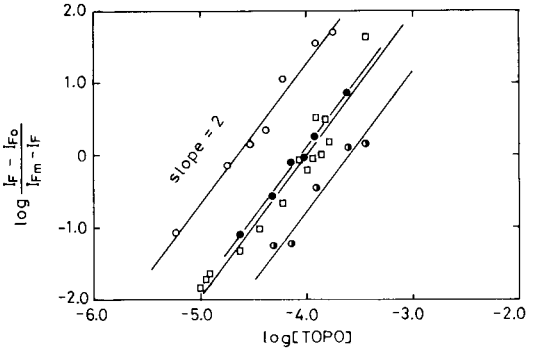

Fig. 6. Analyses of the adduct formation equilibria in o/w microemulsion. ○ = $[Eu^{3+}] = 1.71\times10^{-6}$ M, [TTA] = 5.52×10^{-6} M, pH = 6.5; □ = $[Eu^{3+}] = 6.83\times10^{-7}$ M, [NFA] = 2.19×10^{-6} M, pH = 6.3; ○ = $[Sm^{3+}] = 5.80\times10^{-6}$ M, [TTA] = 5.53×10^{-6} M, pH = 6.5; ● = $[Sm^{3+}] = 5.79\times10^{-6}$ M, [NFA] = 2.19×10^{-6} M, pH = 6.5.

the apparent quantum yields are given by

$$\Phi_o = I_{Fo}/[M]_T \quad (8)$$

$$\Phi_m = I_{Fm}/[M]_T \quad (9)$$

Equations 2–9 lead to the final equation provided that $(S)_o$ is much larger than $(ML_3S_m)_o$:

$$\log\left(\frac{I_F - I_{Fo}}{I_{Fm} - I_F}\right) = m\ \log[S]_T + \log\ \beta_{s,m} - m\ \log\ \phi \quad (10)$$

According to Eqn. 10, the experimental data were analysed as shown in Fig. 6. From the slopes of the straight lines, the value of m in each instance was confirmed to be 2 and the values of the adduct formation constants were determined from the intercepts given in Table 1 for Eu(III) and Sm(III) systems. The result that the values of log

TABLE 1

The adduct formation constants in o/w microemulsion droplets at 25°C [a]

β-Diketone	pK_a	log $\beta_{s,2}$	
		Eu(III)	Sm(III)
TTA	6.17 [b]	7.23 ± 0.53	6.37 ± 1.04
NFA	6.27 [c]	6.13 ± 0.62	6.03 ± 0.36

[a] H_2O : SDS: butan-1-ol : heptane = 89.30 : 3.31 : 6.61 : 0.80 (wt%). [b] Ref. 13. [c] Ref. 14.

$\beta_{s,2}$ in TTA systems are larger than those in NFA systems may reflect the difference between the pK_a values for TTA and NFA. The result that log $\beta_{s,2}$ for Eu(III) is higher than that for Sm(III) is also consistent with the general tendency observed in the extraction of lanthanides [10]. The values of log $\beta_{s,2}$, however, are 2–3 orders smaller than those reported for ordinary solvent extraction systems employing TOPO as synergist [11]. This may be partly due to the solvation of butan-1-ol with the β-diketonates or TOPO in the microemulsion droplets.

Microemulsion microslide electrophoresis

The electrophoretic measurements of Eu(III) and Sm(III) complexes revealed that the red fluorescence zone, the adduct complex, migrated from the negative end to the positive end. This means that the negatively charged microemulsion droplets into which the complex was incorporated has migrated, because the complex itself has no charge. Hence the solubilization of the fluorescent adduct complex was unambiguously confirmed. The microslides treated with HNO_3 (1 : 1) gave a faster migration velocity than those treated with 0.1 M NaOH, as shown in Fig. 7. This result implies that the acid treatment depressed the electroosmotic flow which works in the direction opposite to the electrophoretic force. The magnitude of the average migration velocity of 0.78 ± 0.20 cm min^{-1}, observed under the present conditions of a 10-cm acid-treated microslide, 610–750 V and 0.1 mA, corresponds to an average electrophoretic mobility of $(1.9 \pm 0.4) \times 10^{-8}$ m^2 s^{-1} V^{-1}, which is close to the values reported for sulphonated polystyrene latex and oil drops adsorbed by carboxylic acid [12]. The phenomenon that the neutral metal complexes can migrate according to the solubilization into the microemulsion droplets by an electrophoretic force will be applicable with many other metal–chelate systems as an analytical separation method that can be called microemulsion extraction electrophoresis.

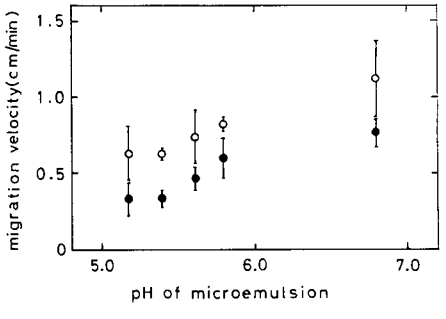

Fig. 7. Migration velocities of Eu(III)–TTA–TOPO complex at various pH values which were observed in microemulsion microslide electrophoresis. The microslide was immersed overnight in (○) HNO_3 (1+1) or (●) 0.1 M NaOH before being washed with water and filled with the pH-controlled microemulsion. Conditions: $[Eu^{3+}] = 1.71 \times 10^{-6}$ M, [TTA] = 5.52×10^{-5} M, [TOPO] = 5.86×10^{-4} M, 10-cm microslide, applied voltage 610–750 V, current 0.1 mA.

Conclusion

The stoichiometric analyses of the formation of the fluorescent adduct complexes of Eu(III) and Sm(III) in SDS microemulsions and the observation of microslide electrophoresis of the adduct complexes in microemulsion systems revealed that the adduct formation occurred in the microemulsion droplets according to a mechanism analogous to the synergic extraction of metal ions. The adduct formation constants for TTA–TOPO and NFA–TOPO mixed-ligand systems were determined. The combination of microemulsion extraction and microslide electrophoresis is suggested as a promising separation method.

This research was supported by the Japan Association of Chemistry.

REFERENCES

1 P. Fourre, D. Bauer and J. Lemerle, Anal. Chem., 55 (1983) 662.
2 E. Paatero, J. Sjoblom and S.K. Datta, J. Colloid Interface Sci., 138 (1990) 388.
3 S.R. Dungan, T. Bausch, T.A. Hatton, P. Plucinski and W. Nitsch, J. Colloid Interface Sci., 145 (1991) 33.
4 A. Berthod, O. Nicolas and M. Porthault, Anal. Chem., 62 (1990) 1402.
5 R.W. Gale, J.L. Fulton and R.D. Smith, Anal. Chem., 59 (1987) 1977.
6 C. Tondre and D. Canet, J. Phys. Chem., 95 (1991) 4810.
7 H. Watarai, Chem. Lett., (1991) 391.

8 H. Watarai, M. Takano and N. Suzuki, Bull. Chem. Soc. Jpn., 65 (1992) 170.
9 T. Shigematu, M. Matsui and R. Wake, Anal. Chim. Acta, 46 (1969) 101.
10 S. Siekierski, J. Inorg. Nucl. Chem., 32 (1970) 519.
11 T. Sekine, S. Iwahori and R. Murai, J. Inorg. Nucl. Chem., 39 (1977) 363.
12 D.J. Shaw, Introduction to Colloid and Surface Chemistry, Butterworths, London, 1980.
13 E.M. Larsen and G. Terry, J. Am. Chem. Soc., 75 (1953) 1560.
14 H. Watarai, K. Kamada and S. Yokoyama, Solvent Extraction Ion Exch., 7 (1989) 361.

Analytica Chimica Acta, 277 (1993) 79–88
Elsevier Science Publishers B.V., Amsterdam

Synthesis and properties of hydrazones from 3- and/or 5-nitro-2-pyridylhydrazine and heterocyclic aldehydes, characterization of their complexes and extraction–spectrophotometric determination of traces of nickel with 2-pyridinecarbaldehyde 3,5-dinitro-2-pyridylhydrazone

Tsugikatsu Odashima and Hajime Ishii

Institute for Chemical Reaction Science, Tohoku University, Katahira, Aoba-ku, Sendai 980 (Japan)

(Received 11th September 1992)

Abstract

Four new hydrazones, 2-pyridinecarbaldehyde 3-nitro-2-pyridylhydrazone, 2-pyridinecarbaldehyde 3,5-dinitro-2-pyridylhydrazone (PA-3,5-NPH), 2-quinolinecarbaldehyde 5-nitro-2-pyridylhydrazone and 6-phenanthridinecarbaldehyde 5-nitro-2-pyridylhydrazone, were synthesized. Their properties and reactivities with metal ions and the properties of the resultant complexes were investigated spectrophotometrically and compared mutually and with those of 2-pyridinecarbaldehyde 5-nitro-2-pyridylhydrazone. Useful information on the molecular design of the hydrazone reagent was obtained. A highly sensitive and practical extraction–spectrophotometric method for the determination of nickel with PA-3,5-NPH was developed and applied successfully to the determination of nickel in steel samples.

Keywords: UV–Visible spectrophotometry; Complexation; Extraction; Hydrazones; Nickel

In the course of a series of studies on the synthesis of heterocyclic hydrazones as highly sensitive and/or selective reagents for metal ions and their analytical application, it was found that 2-pyridinecarbaldehyde 5-nitro-2-pyridylhydrazone (PA-5-NPH) is the most sensitive reagent for metal ions among the hydrazone reagents that have been reported and that it forms complexes having apparent molar absorptivities of the order of 10^5 l mol^{-1} cm^{-1} with copper(II) and nickel(II) [1]. This indicates that the introduction of a strongly electron-withdrawing nitro group into the 5-position of the pyridine ring in the hydrazine moiety of the hydrazone is very effective for enhancing its sensitivity as a spectrophotometric reagent, which was subsequently confirmed by Kanetake and Otomo [2] using a complex of di-2-pyridylmethanone 5-nitro-2-pyridylhydrazone with palladium(II). However, PA-5-NPH had the disadvantage that its solubility in organic solvents is poor, so it was not very easy to use.

In this work, four new hydrazones, 2-pyridinecarbaldehyde 3-nitro-2-pyridylhydrazone (PA-3-NPH), 2-pyridinecarbaldehyde 3,5-dinitro-2-pyridylhydrazone (PA-3,5-NPH), 2-quinolinecarbaldehyde 5-nitro-2-pyridylhydrazone (QA-5-

Correspondence to: H. Ishii, Institute for Chemical Reaction Science, Tohoku University, Katahira, Aoba-ku, Sendai 980 (Japan).

NPH) and 6-phenanthridinecarbaldehyde 5-nitro-2-pyridylhydrazone (PhA-5-NPH), were synthesized in order not only to improve the solubility of PA-5-NPH but also to obtain fundamental information on the molecular design of the highly sensitive and selective hydrazone reagent by clarifying the effect of the number and position of the nitro group introduced into the pyridine ring in the hydrazine moiety of the hydrazone and determining the effect of the magnitude of the hetero ring in the aldehyde moiety. The properties, characteristics and usefulness of the synthesized hydrazones as spectrophotometric reagents for metal ions were investigated in detail, the results being compared with one another and with those of PA-5-NPH and 2-pyridinecarbaldehyde 2-pyridylhydrazone (PAPH), the parent compound of the hydrazones studied in this work. Further, an extraction–spectrophotometric method for the determination of nickel with PA-3,5-NPH was developed.

EXPERIMENTAL

Synthesis of hydrazones

3-Nitro-2-pyridylhydrazine. 2-Chloro-3-nitropyridine (2.21 g, 0.01 mol) was dissolved in ethanol (100 ml) at room temperature. To this solution was added dropwise a solution of hydrazine monohydrate (7.5 g, 0.1 mol) with stirring. The mixture was stirred for additional 30 min at room temperature, allowed to stand overnight in a refrigerator, filtered and dried at 50°C under reduced pressure to yield a red precipitate, which was used without purification in the next step, the synthesis of PA-3-NPH.

3,5-Dinitro-2-pyridylhydrazine. 2-Chloro-3,5-dinitropyridine (0.41 g, 0.002 mol) was dissolved in ethanol (15 ml). To this solution was added dropwise 5 ml of ethanol containing hydrazine monohydrate (0.1 g, 0.002 mol) with cooling at about −70°C in a dry-ice–propan-2-ol bath and stirring. The mixture was stirred for additional 3 h under cooling, filtered and dried at 50°C under reduced pressure to yield a red precipitate, which was used without purification in the next step, the synthesis of PA-3,5-NPH.

5-Nitro-2-pyridylhydrazine [3], 2-quinolinecarbaldehyde [4] and 6-phenanthridinecarbaldehyde [5]. These were synthesized according to the literature methods using 2-chloro-5-nitropyridine, quinaldine and 2-aminodiphenyl, respectively, as starting materials.

Other raw materials for synthesis were obtained commercially.

PA-3-NPH and PA-3,5-NPH. PA-3-NPH was synthesized by refluxing equimolar amounts of 2-pyridinecarbaldehyde and 3-nitro-2-pyridylhydrazine in ethanol–water (4 + 1, v/v) for 3 h, and PA-3,5-NPH by refluxing equimolar amounts of 2-pyridinecarbaldehyde and 3,5-dinitro-2-pyridylhydrazine in ethanol for 3 h. Both products were recrystallized from each solvent used in the synthesis and dried at 110°C for 5 h under reduced pressure to yield yellow crystals.

QA-5-NPH and PhA-5-NPH. Both hydrazones were synthesized by refluxing equimolar amounts of 5-nitro-2-pyridylhydrazine and the corresponding aldehyde in ethanol for 2 and 1 h, respectively. The products were recrystallized from ethanol and 1,4-dioxane, respectively, and dried for 6 h under reduced pressure.

Reagents

Hydrazone solutions. Solutions of 1.5×10^{-3}–2.8×10^{-3} M in 1,4-dioxane and 1.5×10^{-4}–2.8×10^{-4} M in benzene were prepared and stored in amber-coloured bottles.

Standard nickel(II) solution. This was prepared by dissolving 2.5 g of nickel nitrate [$Ni(NO_3)_2 \cdot 6H_2O$] in about 100 ml of water, adding 10 ml of nitric acid (1 + 1) and diluting to 500 ml with water. This solution was standardized by EDTA titration with copper 1-(2-pyridylazo)-2-naphtholate (Cu-PAN) as an indicator. Working solutions were prepared by diluting this solution with water.

Other reagents and water used were the same as in previous work [6].

Procedures

Determination of acid dissociation constants. The acid dissociation constants of the synthesized hydrazones were determined spectrophotometri-

cally in aqueous 1,4-dioxane of various concentrations as described previously [1].

Determination of nickel with PA-3,5-NPH. Place a sample or standard solution containing up to 6 μg of nickel(II) in a 50-ml separating funnel. Add 2 ml of 1 M acetate buffer solution (pH 4.5) and 1 ml of 5% sodium thioglycollate solution and dilute to about 20 ml with water. Add 10 ml of 2.0×10^{-4} M PA-3,5-NPH solution in benzene and extract the nickel complex by shaking mechanically for 7 min. Measure the absorbance of the extract at 484 nm against a reagent blank using 1-cm cells.

Dissolution and pretreatment of iron and steel samples. The same procedure as described previously [7] was used.

RESULTS AND DISCUSSION

Identification of hydrazones

Infrared spectra of the synthesized hydrazones were measured with potassium bromide tablets in order to confirm their structures. The spectra had absorption peaks assigned to the stretching vibration of an azomethine bond (–N=C<) around 1600 cm^{-1} [8]. On the basis of this result and those of elemental analysis shown in Table 1, the synthesized hydrazones are presumed to have the structures shown in Table 1.

Properties and characteristics of hydrazones

PA-3-NPH, PA-3,5-NPH, QA-5-NPH, PhA-5-NPH and PA-5-NPH are yellow crystals that are insoluble in water, but soluble in weakly acidic

TABLE 1

Structures and properties of synthesized hydrazones

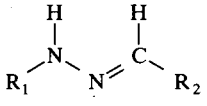

Hydrazone	R_1	R_2	M.p. (°C)	$\nu_{C=N}$ (cm^{-1})	Analysis (%) [a]		
					C	H	N
PA-3-NPH	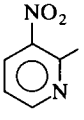		133–135	1597	54.54 (54.32)	3.77 (3.73)	28.60 (28.79)
PA-3,5-NPH	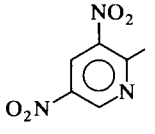		299–301	1615	45.33 (45.84)	2.84 (2.80)	28.84 (29.16)
QA-5-NPH	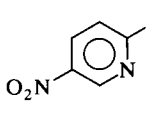	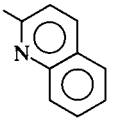	319–322	1590	61.35 (61.43)	3.74 (3.78)	23.88 (23.88)
PhA-5-NPH	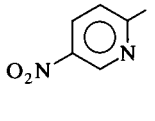	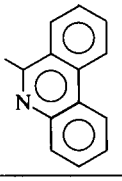	295–297	1590	66.30 (66.47)	3.86 (3.82)	20.24 (20.40)

[a] Experimental values, with calculated values in parentheses.

TABLE 2

Acid dissociation constants and molar absorptivities (ϵ) at the absorption maximum wavelength (λ_{max}) of the hydrazones in 1,4-dioxane [a]

Hydrazone	Acid dissociation constant			ϵ (l mol^{-1} cm^{-1})	λ_{max} (nm)
	pK_{a_1}	pK_{a_2}	pK_{a_3}		
PAPH	3.01	5.75	> 14	3.0×10^4	334
PA-3-NPH	< 1	3.90	> 14	2.4×10^4	329
PA-3,5-NPH	< 1	3.38	10.70	3.1×10^4	363
PA-5-NPH [b]	< 1	4.22	11.17	3.8×10^4	377
QA-5-NPH	< 1	4.19	11.20	5.1×10^4	383
PhA-5-NPH	< 1	4.16	11.17	4.4×10^4	391

[a] $I = 0.2$; $T = 25 \pm 0.1$°C. [b] Determined in previous work [1].

and alkaline solutions and organic solvents such as ethanol, 1,4-dioxane, benzene and chloroform. Solutions of the hydrazones in these organic solvents are stable for several months when stored in amber-coloured bottles. The solubility of the hydrazones in the above organic solvents increased in the sequence PhA-5-NPH < QA-5-NPH < PA-5-NPH < PA-3,5-NPH < PA-3-NPH < PAPH. This reveals that the introduction of a nitro group into the 5-position of the pyridine ring in the hydrazine moiety of PAPH causes a considerable decrease in solubility in organic solvents, but when it is introduced into the 3-position of the pyridine ring the decrease in solubility is small. Hence the poor solubility of PA-5-NPH in organic solvents, its major disadvantage, can be improved by introducing one more nitro group into the 3-position of the pyridine ring. Also, the substitution of the pyridine ring in the aldehyde moiety by a quinoline or phenanthridine ring was found to cause a decrease in the solubility of the hydrazone.

The acid dissociation equilibria of PA-3-NPH, PA-3,5-NPH, QA-5-NPH, PhA-5-NPH and PA-5-NPH can be expressed by Eqn. 1:

$$H_3L^{2+} \overset{K_{a_1}}{\rightleftharpoons} H_2L^{+} \overset{K_{a_2}}{\rightleftharpoons} HL \overset{K_{a_3}}{\rightleftharpoons} L^{-} \qquad (1)$$

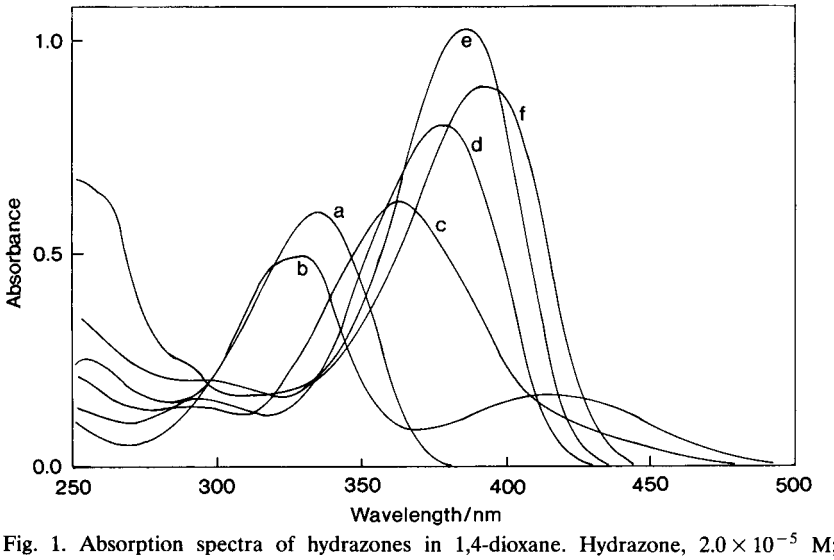

Fig. 1. Absorption spectra of hydrazones in 1,4-dioxane. Hydrazone, 2.0×10^{-5} M; reference, 1,4-dioxane. (a) PAPH; (b) PA-3-NPH; (c) PA-3,5-NPH; (d) PA-5-NPH; (e) QA-5-NPH; (f) PhA-5-NPH.

where L denotes the undissociable part of the hydrazone and K_{a_1}, K_{a_2} and K_{a_3} are the acid dissociation constants. The acid dissociation constants were evaluated by extrapolating the linear plots of apparent pK_a versus 1,4-dioxane concentration to the intercept. The apparent pK_a values were determined spectrophotometrically at an ionic strength of 0.2 at 25 ± 0.1°C and various 1,4-dioxane concentrations (10–40%, v/v). The results are given in Table 2 in comparison with those of PAPH and PA-5-NPH reported previously [1]. K_{a_1} and K_{a_2} may correspond to the deprotonations of the protonated pyridine nitrogen in the hydrazine moiety and the heterocycle nitrogen in the aldehyde moiety, respectively, whereas K_{a_3} corresponds to the deprotonation of the secondary amino group. As can be seen from Table 2, the inductive effect of the nitro group on the pyridine ring reflects the pK_a values of the hydrazones, that is, the introduction of a nitro group is very effective in decreasing the pK_a values of the hydrazones except for the pK_{a_3} value of PA-3-NPH, the magnitude of the decrease depending on the number and position of the nitro group introduced into the pyridine ring.

Figure 1 shows absorption spectra of PA-3-NPH, PA-3,5-NPH, QA-5-NPH and PhA-5-NPH in 1,4-dioxane, and those of PAPH and PA-5-NPH are also shown for comparison. Their absorption maxima and molar absorptivities are given in Table 2, which reveals that the absorption maximum wavelength was bathochromically shifted in the sequence PA-3-NPH < PAPH < PA-3,5-NPH < PA-5-NPH < QA-5-NPH < PhA-5-NPH and the molar absorptivity also increases in the same sequence except that the order of QA-5-NPH and PhA-5-NPH is reversed. Hence both the introduction of a nitro group into the 5-position of the pyridine ring and the substitution of the pyridine ring by a quinoline or phenanthridine ring are very effective for the bathochromic shift of the absorption maximum and for the increase in the molar absorptivity, whereas the introduction of a nitro group into the 3-position has a negative effect.

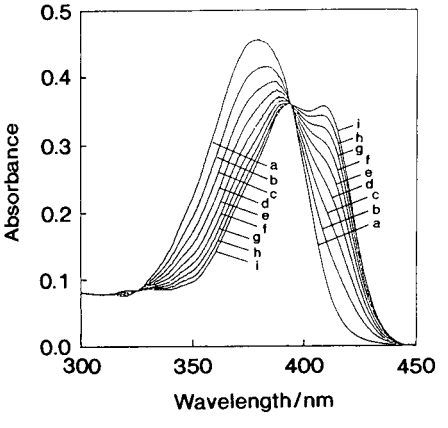

Fig. 2. Spectral changes of a benzene solution of QA-5-NPH when irradiated by a fluorescent light of 15 W about 15 cm distant from the solution. QA-5-NPH, 1.0×10^{-5} M; reference, benzene. Irradiation time: (a) 0; (b) 10; (c) 20; (d) 30; (e) 40; (f) 50; (g) 60; (h) 70; (i) 90 min.

Geometrical isomerization of hydrazones

Solutions of the synthesized hydrazones, especially QA-5-NPH solution, exhibits the spectral change shown in Fig. 2 when exposed to natural light or ultraviolet radiation. This spectral change may be attributed to the geometrical isomerization, from the *E*- (*anti*-) isomer to the *Z*- (*syn*-) isomer, of the hydrazone molecule [9,10]. As the *Z*-isomer does not react with metal ions, solutions of the synthesized hydrazones should be stored in amber-coloured bottles.

Reactivities with metal ions and extractabilities of the complexes

The reactivities of PA-3-NPH, PA-3,5-NPH, QA-5-NPH and PhA-5-NPH were investigated at an apparent pH of 4, 7 and 10 in 40% (v/v) aqueous 1,4-dioxane. The results indicated that these hydrazones, in addition to PA-5-NPH reported previously [1], react with cadmium(II), cobalt(II), copper(II), iron(II), mercury(II), nickel(II), palladium(II), zinc(II), etc., to form colored complexes. However, the reactivity of PA-3-NPH and QA-5-NPH seemed to be poor and the complexes of PhA-5-NPH were unstable. The apparent molar absorptivities of the metal complexes of these hydrazones increased in the sequence of PA-3-NPH < PA-3,5-NPH ≈ PA-5-NPH < QA-5-NPH < PhA-5-NPH.

These complexes were extracted into common organic solvents. Table 3 shows absorption maxima and apparent molar absorptivities of the complexes of the synthesized hydrazones extracted into benzene from aqueous solutions of pH 4, 7 and 10. The apparent molar absorptivities of the complexes of PA-3,5-NPH, QA-5-NPH, PhA-5-NPH and PA-5-NPH [1] are much higher than those of PA-3-NPH complexes. Especially the apparent molar absorptivities of the cadmium(II), copper(II), nickel(II) and zinc(II) complexes are very large, those of the first three complexes reaching ca. 10^5 l mol^{-1} cm^{-1}, whereas those of the PA-3-NPH complexes are about half those of the corresponding complexes of PA-3,5-NPH, PA-5-NPH, QA-5-NPH and PhA-5-NPH.

TABLE 3

Absorption maxima (λ_{max}) and apparent molar absorptivities (ϵ) of metal complexes extracted into benzene

Hydrazone	Complex	pH 4		pH 7		pH 10	
		λ_{max}(nm)	ϵ (l mol^{-1} cm^{-1})	λ_{max}(nm)	ϵ (l mol^{-1} cm^{-1})	λ_{max}(nm)	ϵ (l mol^{-1} cm^{-1})
PA-3-NPH	Cd(II)	–	–	476	7700	476	58700
	Co(II)	–	–	–	–	–	–
	Cu(II)	–	–	473	50100	473	59400
	Fe(II)	473	24000	473	30200	473	26000
	Hg(II)	–	–	473	9400	473	25600
	Ni(II)	–	–	478	57100	478	53200
	Pd(II)	541	9600	541	12600	541	13500
	Zn(II)	–	–	470	55400	470	62400
PA-3,5-NPH	Cd(II)	–	–	483	82500	483	100200
	Co(II)	471	26800	471	30900	471	51200
	Cu(II)	482	38500	482	107400	482	106700
	Fe(II)	450	49400	450	49100	450	48400
	Hg(II)	480	54100	480	62100	480	64300
	Ni(II)	484 461	100000 79000	–	–	–	–
	Pd(II)	528 497	10100 7900	480	3000	531 439	11000 16200
	Zn(II)	–	–	481	101500	481	99100
QA-5-NPH	Cd(II)	–	–	–	–	544	110000
	Co(II)	–	–	533	12600	533	60600
	Cu(II)	534	86400	534	118000	534	118000
	Fe(II)	–	–	–	–	–	–
	Hg(II)	542	8000	542	5900	–	–
	Ni(II) [a]	542	~47300	542	~53000	542	~113000
	Pd(II)	596 450	20000 11600	–	–	–	–
	Zn(II)	–	–	542	22100	542	30000
PhA-5-NPH	Cd(II)	–	–	558	114000	558	126000
	Co(II)	545	55500	545	57200	545	63400
	Cu(II)	546	110600	546	118800	546	118000
	Fe(II)	501	25100	501	28400	501	26700
	Hg(II)	555	10500	555	21200	555	12000
	Ni(II) [a]	556	~80800	556	~106300	556	~115700
	Pd(II)	616 461	17400 34200	616 461	33000 64900	616 461	32500 66000
	Zn(II)	–	–	554	116200	554	119200

[a] Unstable.

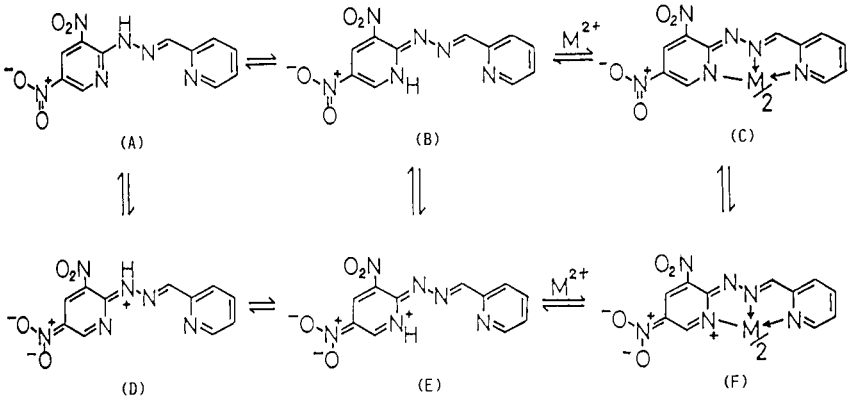

Fig. 3. Equilibria and resonances of PA-3,5-NPH and its metal complexes.

These results can reasonably be explained by assuming structures of the complexes as follows: the complexes of PA-3,5-NPH, QA-5-NPH, PhA-5-NPH and PA-5-NPH can predominatingly form so-called "charged quinone"-like structures [11,12], which have an extended conjugated system as shown in (F) in Fig. 3, by the inductive effect of a strong electron-withdrawing nitro group introduced into the 5-position of the pyridine ring in the hydrazine moiety of these hydra-

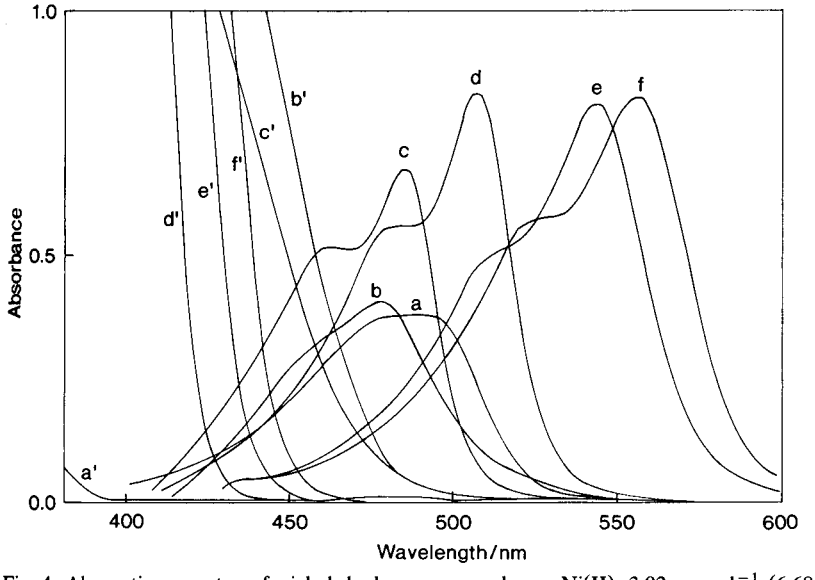

Fig. 4. Absorption spectra of nickel–hydrazone complexes. Ni(II), 3.92 μg ml^{-1} (6.68×10^{-5} M); sodium thioglycollate, 0.25% (w/v); shaking time, 15 min; reference, reagent blank. Other conditions (a'–f' are spectra of the corresponding reagent blanks against benzene):

	a	b	c	d	e	f
Hydrazone	PAPH	PA-3-NPH	PA-3,5-NPH	PA-5-NPH	QA-5-NPH	PhA-5-NPH
Concentration (10^{-4} M)	2.0	2.8	2.0	1.5	1.5	1.5
pH of aqueous phase	9.8	8.3	5.0	5.5	9.9	9.9

zones. On the other hand, the complexes of PA-3-NPH having a nitro group at the 3-position on the pyridine ring, and those of PAPH, the parent compound of the hydrazones discussed here, cannot form such structures. That is, the extremely high molar absorptivities of the complexes of PA-3,5-NPH, PA-5-NPH, QA-5-NPH and PhA-5-NPH compared with those of the complexes of PA-3-NPH and PAPH seem to attributable to the difference in their structures.

Metal complexes of PA-3,5-NPH, especially the nickel complex, were extracted into benzene from aqueous solutions of appreciably lower pH, than those of the other hydrazones, which may be due to PA-3,5-NPH having the smallest pK_a values among the synthesized hydrazones. Of the cobalt complexes, those of PA-3,5-NPH, QA-5-NPH and PhA-5-NPH were extracted into benzene, but those of the other hydrazones were scarcely or not extracted. This suggests that the cobalt in the extracted complexes is cobalt(II) in contrast to cobalt(III) in the complexes not extracted.

From the above results, PA-3,5-NPH seems to be the most balanced reagent for metal ions, especially for nickel(II), because it has a relatively high solubility in organic solvents, which makes it easy to use and forms a complex with an apparent molar absorptivity of the order of 10^5 l mol^{-1} cm^{-1}, although this value is smaller than those of the nickel complexes of PA-5-NPH, QA-5-NPH and PhA-5-NPH. In addition, the nickel–PA-3,5-NPH complex is extracted at the lowest pH among the nickel complexes of the synthesized hydrazones, as shows later in Fig. 5, from which PA-3,5-NPH was expected to be both selective and sensitive for nickel(II). Therefore, the complexation of PA-3,5-NPH with nickel(II) and the extraction of the resultant complex were investigated in detail in subsequent work, in order to develop a sensitive and selective method for the determination of nickel.

Studies on determination of nickel with PA-3,5-NPH

Extraction solvent. PA-3,5-NPH reacts with nickel(II) in weakly acidic media to form a red complex, which is insoluble in water but soluble in organic solvents such as benzene, chloroform and 4-methylpentan-2-one. Among these solvents, benzene was the most preferable because the benzene gave the highest molar absorptivity and showed the largest bathochromic shift in the absorption spectrum.

Absorption spectra. Figure 4 shows the absorption spectrum of the nickel–PA-3,5-NPH complex extracted into benzene, together with those of the nickel complexes of PAPH, PA-3-NPH, PA-5-NPH, QA-5-NPH and PhA-5-NPH measured for comparison. The absorption maximum wavelengths of these complexes, some of which are given in Table 3, were bathochromically shifted in the sequence PA-3-NPH < PAPH < PA-3,5-NPH < PA-5-NPH < QA-5-NPH < PhA-5-NPH. This sequence is consistent with that of the bathochromic shift in the absorption maxima of the hydrazones themselves, shown already. The PA-3,5-NPH complex has two absorption maxima, at 461 and 484 nm. These maxima and the shape of the absorption spectrum did not vary in the nickel to PA-3,5-NPH molar ratio range 1:20 to 20:1 and in the pH range 2.5–6.5, where the extraction was carried out. This suggests that only one species of the complex is extracted. For the determination of nickel the wavelength of 484 nm is preferable because at this wavelength the absorption due to PA-3,5-NPH itself is barely observed, higher sensitivity thus being obtained.

Effect of pH. Figure 5 shows the effect of pH on the extraction of the nickel–PA-3,5-NPH complex in comparison with that on the extraction of the complexes of PAPH, PA-3-NPH, PA-5-NPH, QA-5-NPH and PhA-5-NPH. The PA-3,5-NPH complex was quantitatively extracted at pH 4.0, a maximum and constant absorbance being obtained in the pH range 4.0–6.1. This pH is the lowest among not only the nickel–hydrazone complexes studied here but also those studied previously.

Extraction rate. The extraction of nickel into benzene was not as rapid as expected when it was extracted by shaking with a benzene solution of PA-3,5-NPH, but this extraction was considerably accelerated by the addition of a small amount of sodium thioglycollate. Under the recommended conditions, shaking for 5 min is sufficient, al-

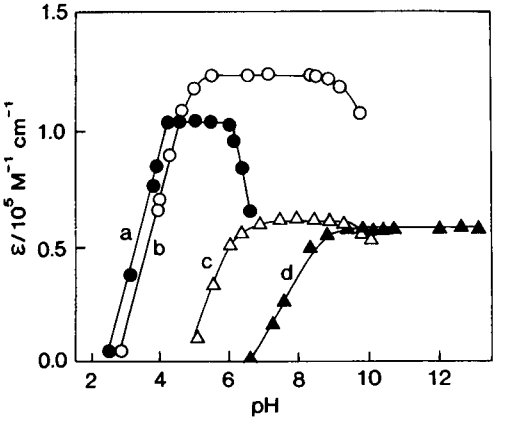

Fig. 5. Effect of pH on extraction of nickel–hydrazone complexes. Conditions (other conditions as in Fig. 4):

	a	b	c	d
Hydrazone	PA-3,5-NPH	PA-5-NPH	PA-3-NPH	PAPH
Concentration (10^{-4} M)	2.0	1.5	2.8	2.0
Wavelength (nm)	484	507	478	481

though the shaking time required for the quantitative extraction depends on the PA-3,5-NPH concentration, similarly to the extraction with PA-5-NPH reported previously [1].

Effect of other variations in extraction. The extraction of nickel was reproducible, almost all of the nickel(II) present in the aqueous phase being extracted by a single extraction. The absorbance of the extract remained almost constant even when the organic to aqueous phase volume was varied from 1:1 to 1:5. The complex extracted into benzene was stable, the absorbance of the extract remaining constant for at least 2 h.

Composition of the complex. The molar composition of the extracted complex was investigated by both the molar ratio and the continuous variation methods. Both methods revealed the formation of a 1:2 (metal:ligand) complex.

Calibration graph, sensitivity and precision. The calibration graph prepared by the proposed procedure was linear over the range 0.5–6 μg of nickel and passed through the origin. The equation for the line obtained by least-squares treatment was

$$[\text{Ni}\ (\mu\text{g})] = 5.82A \qquad (2)$$

where A is the absorbance. The apparent molar absorptivity and the sensitivity for an absorbance of 0.001 calculated from Eqn. 2 were 1.01×10^5 l mol^{-1} cm^{-1} and 0.58 ng cm^{-2}, respectively. The relative standard deviation was 0.97% when ten standard solutions containing 1.96 μg of nickel(II) were analysed.

Interferences by other ions and their removal. Cobalt(II), copper(II), iron(II and III), mercury (II), palladium(II) and citrate interfered considerably with the determination of nickel when no masking agent was added, because the cations form complexes with PA-3,5-NPH and citrate forms a complex with nickel(II), but other common ions did not interfere. Of the interfering cations, those except cobalt(II) could be masked almost completely by thioglycollate added as an accelerator for the complexation of nickel(II) with PA-3,5-NPH and/or the addition of a small amount of fluoride. The interference from cobalt(II) could not be removed.

TABLE 4

Determination of nickel in standard iron and steel samples

Sample [a]	Amount taken (g)	Ni content (%)	
		Proposed method	Certified value
Tungsten steel JSS-11a	0.5262	0.063	0.064
		0.064	
		0.065	
		Av. 0.064	
	0.9872	0.064	
		0.062	
		0.063	
		Av. 0.063	
Ferrophosphorus JSS-20	0.5047	0.018	0.019
		0.020	
		0.018	
		Av. 0.019	
	1.0010	0.020	
		0.020	
		0.019	
		Av. 0.020	

[a] JSS = Japanese Standard Sample.

Practical application. Nickel in iron and steel samples was determined by the proposed procedure. The results (Table 4) are in good agreement with certified values.

Conclusion

Four new hydrazones derived from PAPH were synthesized and their properties, reactivities and complexations with metal ions and the extraction of the resultant complexes were investigated and compared with one another and also with the results for PA-5-NPH and its complexes reported previously [1]. The following useful information for the molecular design of a hydrazone reagent was obtained: the introduction of a nitro group into the pyridine ring in the hydrazine moiety of PAPH lowers the pK_a values; its introduction into the 5-position of the pyridine ring brings about large increases in the molar absorptivities of the hydrazone and its metal complexes and bathochromic shifts in their absorption spectra, but at the same time brings about large decreases in the solubilities of the hydrazone and its complexes in organic solvents; its introduction into the 3-position is ineffective in increasing the molar absorptivities of the hydrazone and its complexes, but is effective for the suppression of the above decrease in solubilities of the hydrazone and its complexes; and substitution of the pyridine ring in the aldehyde moiety by a quinoline or phenanthridine ring is also effective in increasing the molar absorptivity and the bathochromic shift of the hydrazone and its metal complexes, but at the same time lowers the solubility of the hydrazone and its complexes. Further, among the hydrazones that have been studied here and previously, PA-3,5-NPH was found to be the most balanced, useful reagent for metal ions, especially nickel(II), in terms of sensitivity, selectivity and solubility, and a practical method for the determination of traces of nickel has been developed and applied to the analysis of real samples with satisfactory results.

The authors thank Dr. Katsunori Kohata of the National Research Institute of Vegetables, Ornamental Plants and Tea, Ministry of Agriculture, Forestry and Fisheries, for valuable advice on the synthesis of hydrazones. This work was supported in part by a Grant-in-Aid for Scientific Research No. 62550540 from the Ministry of Education, Science and Culture, Japan, for which the authors are grateful. Results of this work were presented in part at the 36th Annual Meeting of the Japan Society for Analytical Chemistry, October 1987.

REFERENCES

1 H. Ishii, T. Odashima and T. Hashimoto, Anal. Sci., 3 (1987) 347.
2 T. Kanetake and M. Otomo, Anal. Sci., 4 (1988) 411.
3 K. Kohata, Y. Kawamonzen, T. Odashima and H. Ishii, Bull. Chem. Soc. Jpn., 63 (1990) 3398.
4 H. Kaplan, J. Am. Chem. Soc., 63 (1941) 2654.
5 V. Zatka, J. Abraham, J. Holzbecher and D.E. Ryan, Anal. Chim. Acta, 54 (1971) 65.
6 T. Odashima, M. Yamada, N. Yonemori and H. Ishii, Bull. Chem. Soc. Jpn., 60 (1987) 3225.
7 H. Ishii, T. Odashima and T. Imamura, Analyst, 107 (1982) 885.
8 R.M. Silverstein and G.C. Bassler, Spectrometric Identification of Organic Compounds, Wiley, New York, 2nd edn., 1967 (translated by S. Araki and Y. Mashiko, Tokyo Kagaku Dojin, Tokyo, 1969), p. 102.
9 S. Kwon, M. Tanaka and K. Isagawa, Nippon Kagaku Kaishi, (1974) 1526.
10 T. Tsujikawa, E. Mizuta and M. Hayashi, Yakugaku Zasshi, 96 (1976) 125.
11 K. Toei, Anal. Sci., 3 (1987) 479.
12 S. Shibata and M. Furukawa, Bunseki Kagaku, 23 (1974) 1412.

Analytica Chimica Acta, 277 (1993) 89–95
Elsevier Science Publishers B.V., Amsterdam

Spectrophotometric method for the simultaneous determination of proteins and amino acids with *p*-benzoquinone

Dimas A.M. Zaia and Wagner J. Barreto

Department of Chemistry, State University of Londrina, 86051 Londrina, Pr. (Brazil)

Nilson J. Santos

Department of Food Technology and Drugs, State University of Londrina, 86051 Londrina, Pr. (Brazil)

Asae S. Endo

Department of Biochemistry, State University of Londrina, 86051 Londrina, Pr. (Brazil)

(Received 27th July 1992; revised manuscript received 19th November 1992)

Abstract

A spectrophotometric method for the simultaneous determination of proteins and total amino acids in mixtures is described, based on the observation that the products of the reaction between *p*-benzoquinone (PBQ) and proteins show an absorbance band at about 350 nm, whereas for most of the essential amino acids the absorbance band is at about 440 nm. Beer's law was obeyed by the products of the reaction between PBQ and 1:1 or 2:1 (w/w) mixtures of proteins and amino acids for a wide range of concentrations. The products of the reaction were stable for 2 h at either 5 or 30°C; shifts of the wavelength of maximum absorbance were not observed for up to 48 h after starting the reaction. The molar and specific absorptivities for several amino acids and proteins, respectively, were determined. The detection limit observed with the PBQ method was compared with those obtained with other methods. A recovery of about 100% was observed for both BSA and total amino acids when the PBQ method was applied to an amino acid–protein mixture resembling cerebrospinal fluid.

Keywords: UV–Visible spectrophotometry; Amino acids; Proteins

Quantitative analyses for proteins and amino acids are commonly used in clinical investigations, the food industry and research, but there is no routine spectrophotometric method for the simultaneous determination of both total proteins and amino acids in mixtures. Several spectrophotometric methods for the determination of proteins are currently in use [1–7]. For the determination of amino acids, the ninhydrin reaction is commonly employed [8,9].

Correspondence to: W.J. Barreto, Department of Chemistry, State University of Londrina, 86051 Londrina, Pr. (Brazil).

Lorentz and Flatter [10] used *p*-benzoquinone (PBQ) for the determination of total amino acids in blood plasma, serum and urine, observing that the product of the reaction absorbs at about 490 nm and follows Beer's law, at room temperature in phosphate buffer (pH 6.5). There is no agreement, however, about the product of the reaction between PBQ and amino acids [11,12].

In previous papers [13–15], the use of PBQ for the measurement of total proteins was reported, observing that the reaction product absorbs at about 350 nm and follows Beers's law. However, this reaction had to be carried out at 100°C for 20

min because at room temperature the reaction is too slow. When amino acids react with PBQ at 100°C, under the same conditions as used for the reaction between PBQ and proteins, the products of reaction show an absorbance band between 390 and 440 nm, which follows Beer's law. In this work, we have the possibility of using this difference in absorbance to develop a spectrophotometric method for the simultaneous determination of amino acids and proteins in mixtures was investigated, and this method was tested on samples of a mixture of amino acids and proteins.

EXPERIMENTAL

Ultraviolet and visible spectrophotometry were carried out on Varian DMS-80 and Hitachi Perkin-Elmer 139-0880 spectrophotometers.

Materials and reagents

Deionized water was used throughout.

A 0.1 M solution of PBQ (Riedel-de Haën) was prepared in dimethyl sulphoxide as described previously [13]. Standard glutamine (Merck) and bovine serum albumin (BSA) (Sigma, fraction V) solutions, each 0.3000 g l^{-1}, were prepared.

An amino acid solution was prepared that contained a mixture of amino acids (Glu, Gln, Asp, Gly, Ala, Ser, Thr, Lys, Arg, His, Val, Leu, Ile, Phe, Tyr and Met) in proportions similar to those observed in cerebrospinal fluid [16], with a total concentration of 200 μg ml^{-1}. A protein solution containing 0.4000 g l^{-1} of BSA was prepared. A mixed amino acid–protein was then prepared by mixing 100 ml of each of the above amino acid and protein solutions and adjusting the pH to 7.32 with 0.1 M NaOH solution (Merck). This mixed solution was divided into aliquots and stored at −20°C.

A 0.1 M phosphate (Na_2HPO_4–NaH_2PO_4) solution (pH 6.0) was used as a buffer.

Methods

Calibration. By dilution of the 0.3000 g l^{-1} standard solutions of BSA and glutamine, a calibration solution was prepared containing 60 and 30, 120 and 60, 180 and 90, and 240 and 120 μg

TABLE 1

Maximum absorbance of the products of the reaction between PBQ and proteins or amino acids [samples heated at 100°C for 20 min in a medium containing 1.0 mM PBQ in 0.1 M phosphate buffer (pH 6.0)]

Sample	Maximum (nm)	Sample	Maximum (nm)
Ala	390, 320, 280	BSA	350, 280
Arg	400, 320, 280	Casein	350, 280
Asn	390, 320, 280	Cytochrome *c*	407, 350, 285
Asp	390, 320, 280	Globulin	350, 280
Cys [a]	670, 350 [b], 280	HSA	350, 280
Gln	440, 320, 280	OA	350, 280
Glu	430, 320, 280	Pepsin	350, 280
Gly	430, 320, 280	Trypsin	350, 280
His	280		
Ile	430, 320, 280		
Leu	430, 320, 280		
Lys	430, 320 [b], 280		
Met	430, 320, 280		
Phe	430, 280		
Pro	590, 280		
Ser	430, 320, 280		
Thr	440, 320, 280		
Trp	440, 280		
Tyr	390, 280		
Val	430, 320, 280		

[a] Spectra of the product of reaction between PBQ and cysteine, obtained after separation of black precipitate. [b] High intensity.

ml^{-1} of BSA and Gln, respectively, in test-tubes, the final volume being completed to 5 ml with phosphate buffer. To each test-tube, plus a blank containing 5 ml of phosphate buffer, 50 μl of 0.1 M PBQ were added; the tubes were shaken, capped with glass marbles and incubated at 100°C for 20 min. The tubes were cooled to room temperature and the absorbances at 350 and 480 nm were read against the blank and used for construction of the calibration graphs for BSA and Gln, respectively.

Samples. To 1 ml of the amino acid–protein mixture, 4 ml of phosphate buffer and 50 μl of 0.1 M PBQ were added; the tubes were capped and heated at 100°C for 20 min as above, and the absorbances were read at 350 and 480 nm against the blank. These readings were interpolated on the calibration graphs for BSA and Gln for calculation of the total protein and amino acid concentrations in the sample.

RESULTS AND DISCUSSION

PBQ has been used previously for the determination of total proteins in skim milk (13), blood plasma (14) and rat tissues (15). Under the reaction conditions used, which include heating to

TABLE 2

Straight-line equations, number of experiments and range of linearity (Beer's law) for the products of reaction between PBQ and proteins, amino acids and 1:1 or 2:1 (w/w) mixtures of proteins to amino acids [sample heated at 100°C for 20 min in a medium containing 1.0 mM PBQ in 0.1 M phosphate buffer (pH 6.0)]

Sample	Straight-line equation: Y(absorbance) = mX (μg ml^{-1}) + b	No. of experiments	Range of linearity (μg ml^{-1})
Gln	$Y = 3.310 \times 10^{-3} X + 1.200 \times 10^{-3}$	14	0–120
Asn	$Y = 4.323 \times 10^{-3} X + 1.920 \times 10^{-2}$	5	0– 90
Glu	$Y = 2.628 \times 10^{-3} X + 1.610 \times 10^{-2}$	5	0–150
BSA	$Y = 2.742 \times 10^{-3} X + 4.000 \times 10^{-4}$	37	0–240
Casein	$Y = 3.911 \times 10^{-3} X - 2.381 \times 10^{-3}$	5	0–300
Mixtures:			
1 Gln–	$Y = 3.085 \times 10^{-3} X + 4.143 \times 10^{-3}$	13	0–150
1 BSA	$Y = 6.209 \times 10^{-3} X + 2.552 \times 10^{-2}$	13	0–150
1 Gln–	$Y = 3.192 \times 10^{-3} X + 2.707 \times 10^{-3}$	25	0–120
2 BSA	$Y = 3.947 \times 10^{-3} X + 3.280 \times 10^{-2}$	22	0–240
1 Gln–	$Y = 3.851 \times 10^{-3} X + 1.748 \times 10^{-2}$	5	0–150
1 casein	$Y = 7.384 \times 10^{-3} X - 8.286 \times 10^{-3}$	5	0–150
1 Gln–	$Y = 4.740 \times 10^{-3} X + 7.200 \times 10^{-3}$	5	0– 90
2 casein	$Y = 5.832 \times 10^{-3} X + 2.714 \times 10^{-3}$	5	0–300
1 Glu/	$Y = 2.840 \times 10^{-3} X + 1.420 \times 10^{-2}$	5	0–120
1 casein	$Y = 6.063 \times 10^{-3} X + 2.762 \times 10^{-2}$	5	0–150
1 Glu–	$Y = 3.710 \times 10^{-3} X + 1.280 \times 10^{-2}$	5	0– 90
2 Casein	$Y = 5.378 \times 10^{-3} X + 2.686 \times 10^{-2}$	5	0–300
1 Glu–	$Y = 2.835 \times 10^{-3} X + 1.119 \times 10^{-2}$	5	0–150
1 BSA	$Y = 5.923 \times 10^{-3} X + 1.395 \times 10^{-2}$	5	0–150
1 Glu–	$Y = 2.398 \times 10^{-3} X + 2.014 \times 10^{-2}$	5	0–150
2 BSA	$Y = 4.508 \times 10^{-3} X + 2.286 \times 10^{-2}$	5	0–300
1 Asn–	$Y = 4.186 \times 10^{-3} X + 1.860 \times 10^{-2}$	5	0– 90
1 casein	$Y = 9.718 \times 10^{-3} X + 1.448 \times 10^{-2}$	5	0–150
1 Asn–	$Y = 4.090 \times 10^{-3} X + 3.020 \times 10^{-2}$	5	0– 90
2 casein	$Y = 7.065 \times 10^{-3} X + 2.571 \times 10^{-2}$	5	0–300
1 Asn–	$Y = 3.943 \times 10^{-3} X + 1.830 \times 10^{-2}$	5	0– 90
1 BSA	$Y = 7.844 \times 10^{-3} X + 5.438 \times 10^{-2}$	5	0–150
1 Asn–	$Y = 3.930 \times 10^{-3} X + 1.740 \times 10^{-2}$	5	0– 90
2 BSA	$Y = 5.490 \times 10^{-3} X + 6.157 \times 10^{-2}$	5	0–300

100°C, it was observed that the products of the reaction between PBQ and proteins absorb at about 350 nm; for amino acids, the products of reaction absorb in the range 390–670 nm, but most of them at about 430–440 nm (Table 1). With the exceptions of lysine and cysteine, the absorption band shown by amino acids at 340 nm is of low intensity. On changing the pH to 6.0, 7.0 or 8.0, a shift of the maximum absorbance to shorter wavelengths was observed (spectra not shown). Birks and Slifkin [17] observed a similar shift to shorter wavelengths with tetrachloro-*p*-benzoquinone (chloranil), whereas Lin and Cheng [18] observed a shift to longer wavelengths; these discrepancies can be attributed to differences in the reaction conditions employed.

Table 2 shows the straight line equations and range of linearity (Beer's law) for the products of reaction between PBQ and proteins (BSA or casein) or amino acids (Gln, Glu, Asn). These amino acids were chosen because they are the most concentrated in several biological media (cerebrospinal fluid, culture media, protein hydrolysates); BSA and casein were chosen because they are commonly used as standards for protein determination. For the determination of amino acids the absorbance at 480 nm was used, despite the observation that the absorbance at 440 nm can be a maximum, because at 480 nm the best correlation coefficient of the straight line, with the least signal loss, was obtained for the products of the reaction between PBQ and either Gln alone or in a mixture with BSA. The absorbance of the products of the reaction between PBQ and mixtures of BSA and Gln (1:1 or 2:1, w/w) follows Beer's law, in the concentrations range shown in Table 2, at both 480 and 350 nm; the correlation coefficients for all the straight lines shown in Table 2 were at least 0.98.

The slopes of the straight lines for the products of the reaction between PBQ and either Gln or Gln–BSA are almost identical, but the slopes for BSA alone or in a mixture with Gln are different; this difference is attributed to an increase in the baseline due to the absorbance at 440 nm of the products of reaction between PBQ and Gln (Fig. 1). Another minor contribution to the observed difference between BSA alone and

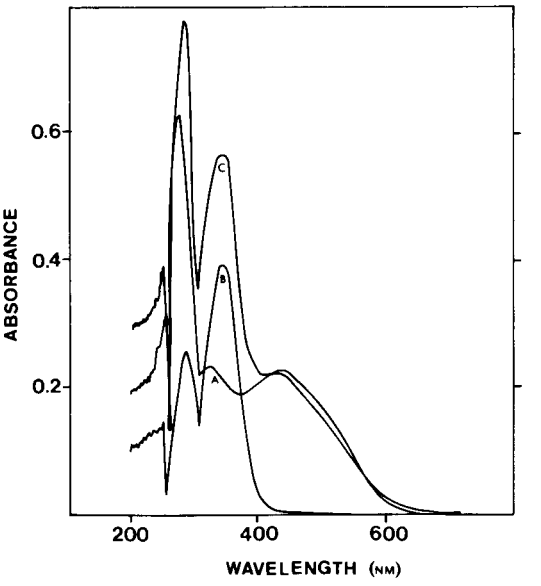

Fig. 1. Absorption spectra of the products of the reaction between PBQ and (a) Gln (60 μg ml^{-1}), (b) BSA (120 μg ml^{-1}) and (c) Gln (60 μg ml^{-1}) plus BSA (120 μg ml^{-1}). Samples were heated at 100°C for 20 min in a medium containing 1.0 mM PBQ and 0.1 M phosphate buffer (pH 6.0).

BSA–Gln comes from a low-intensity absorbance band at 340 nm shown by the products of the reaction of PBQ and Gln (Fig. 1). Similar effects were observed for the other mixtures of proteins and amino acids shown in Table 2. For concentrations of Gln greater than 120 μg ml^{-1}, the absorbance band at 440 nm shows a shift due to the increase in the intensity of the band at 280 nm.

The detection limits for BSA show that the PBQ method is about 18 times more sensitive than the biuret method, and about 4 times less sensitive than Lowry's method. For amino acids, the ninhydrin method is about 5.7 times more sensitive than that employing PBQ as proposed by Lorentz and Flatter [10], which in turn is about 6.3 times more sensitive than that proposed here. However, the sensitivity achieved with this proposed method is in the μg ml^{-1} range, which is sufficient for most analytical applications.

The absorbance of the products of the reaction between PBQ and either Gln or Gln–BSA changed by only a few percent during the first 2 h after the period of heating at 100°C, increasing

thereafter when the samples were kept at 30°C, or decreasing when they were kept at 5°C (Fig. 2). Absorption spectra (not shown) obtained at the same times as indicated in Fig. 2 showed no shifts of the wavelength of maximum absorbance for the whole period of study, at either 30 or at 5°C. As proposed by Lorentz and Flatter [10], the PBQ method for amino acids requires that the absorbances be read immediately after the reaction, or requires two extractions with diethyl ether and readings of absorbance within 1 h; the method proposed here has the advantge of greater stability, allowing the reading of absorbances within 2 h of the heating step.

Table 3 shows the specific and molar absorptivities of amino acids and proteins, respectively. As observed with other UV–visible spectrophotometric methods, the absorptivities are not constant among either amino acids or proteins. No change in absorbance was observed for the product of the reaction between PBQ and cysteine, as the absorption maximum of this product is at about 670 nm. Lorentz and Flatter [10] observed that the product of the reaction between PBQ and cysteine shows the smallest equivalent in relation to glycine, indicating that their measurements at 492 nm were not at the absorption maximum. For proline a change in absorbance was observed at 480 nm, despite the fact that its absorption maximum is at 590 nm, whereas Lorentz and Flatter observed a corresponding band at 525 nm.

The PBQ method was applied to the simultaneous determination of amino acids and proteins in a mixture resembling cerebrospinal fluid, that is, in a mixture containing a 2:1 ratio of BSA to total amino acids, with glutamine as the most concentrated amino acid. The sample recoveries with this mixture are given in Table 4. Using a calibration graph for a 2:1 (w/w) ratio of BSA to Gln, the recoveries of proteins and amino acids were 109.9% and 113.9%, respectively; using a

TABLE 3

Specific absorptivities of proteins and molar absorptivities of amino acids after reaction with 1.0 mM PBQ at 100°C for 20 min in 0.1 M phosphate buffer (pH 6.0)

Amino acids	Molar absorptivity at 480 nm ($l\ mol^{-1}\ cm^{-1}$)	Equivalent in glutamine	Protein	Specific absorptivity ($10^3\ cm^2\ \mu g$)	Equivalent in BSA
Ala	355.23	0.69	BSA [b]	2.56	1.00
Arg	571.78	1.11	casein [b]	2.11	0.81
Asn	635.04	1.23	Cytochrome *c*	8.84	3.38
Asp	323.60	0.63	HSA [b]	3.05	1.17
Cys [a]	–	–	OA [b]	2.59	0.99
Gln	515.82	1.00	Pepsin [b]	1.89	0.72
Glu	406.33	0.79	Trypsin [b]	5.33	2.84
Gly	749.39	1.45			
His	294.40	0.57			
Ile	632.60	1.23			
Leu	523.11	1.01			
Lys	676.40	1.31			
Met	749.39	1.45			
Phe	742.09	1.44			
Pro	420.92	0.82			
Ser	564.48	1.09			
Thr	637.47	1.24			
Trp	900.24	1.75			
Tyr	456.12	0.87			
Val	637.47	1.24			

[a] No band at 480 nm. [b] Published data [15].

TABLE 4

Recoveries from samples containing BSA, Gln or a mixture of BSA and amino acids ($\mu g\ ml^{-1}$) with composition similar to cerebrospinal fluid [16] [sample heated at 100°C for 20 min with 1.0 mM PBQ in 0.1 M phosphate buffer (pH 6.0)]

Parameter [a]	Sample [d]		Mixture [c]		Mixture [c]	
	BSA	Gln	BSA [d]	AAs [d]	BSA [b]	AAs [b]
M =	124.66	60.71	219.83	113.86	192.45	109.58
S =	8.69	3.92	15.44	12.07	17.40	9.12
E =	2.75	1.24	4.88	3.64	4.49	2.75

[a] M = mean; S = standard deviation; E = standard error of the mean. Number of samples, $n = 10$. [b] Calibration graph: BSA–Gln (1:1, w/w). [c] Mixture of amino acids and BSA. AAs = total amino acids. [d] Calibration graph: BSA–GLn (2:1, w/w).

1:1 ratio these recoveries were 96.2% and 109.6%, respectively. For a sample containing only BSA and Gln the recoveries of BSA and Gln were 103.9% and 101.2%, respectively. Thus, even using calibration graphs constructed with two different ratios of BSA to Gln the recovery was acceptable.

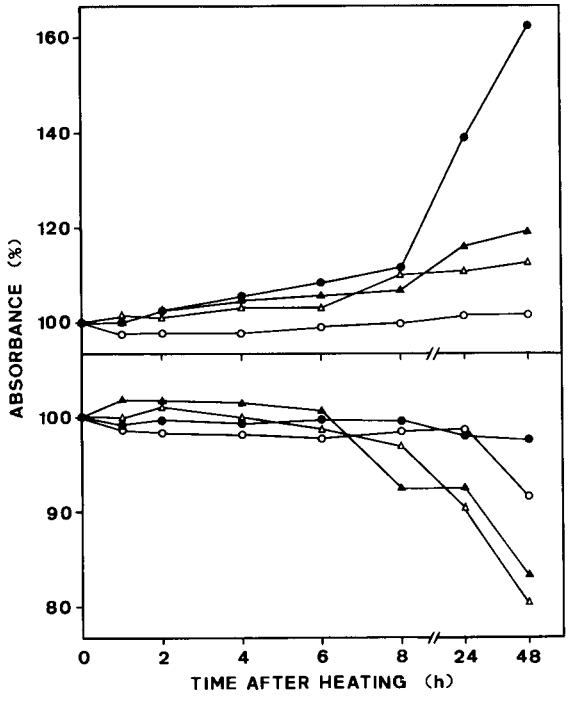

Fig. 2. Stability of the products of the reaction between PBQ and BSA or Gln. Samples were heated at 100°C for 20 min in a medium containing 1.0 mM PBQ in 0.1 M phosphate buffer (pH 6.0), and then kept at 5°C (bottom) or 30°C (top). ○ = BSA (120 $\mu g\ ml^{-1}$); ● = BSA (120 $\mu g\ ml^{-1}$) plus Gln (60 $\mu g\ ml^{-1}$), absorbance at 350 nm; △ = Gln (60 $\mu g\ ml^{-1}$); ▲ = BSA (120 $\mu g\ ml^{-1}$) plus Gln (60 $\mu g\ ml^{-1}$), absorbance at 480 nm.

Conclusion

The results show that, after heating at 100°C, the products of the reaction between PBQ and proteins have an absorbance band at 350 nm, whereas for most amino acids the corresponding band is at 440 nm; Beer's law is followed for most amino acids and proteins, either separated or in 1:1 or 2:1 (w/w) mixtures of proteins and amino acids. The products of the reaction between PBQ and Gln, PBQ and BSA, or PBQ and BSA plus Gln, are stable for several hours at either 5 or 30°C. Tests of sample recovery from a mixture with a composition resembling that of cerebrospinal fluid showed an adequate recovery for routine analysis. It is therefore suggested that the PBQ reaction proposed here can be used as a fast and simple spectrophotometric method for the simultaneous determination of proteins and amino acids in mixtures.

The authors thank Dr. Luis C.J. Gaziri for his interest, helpful criticism and help in the preparation of the manuscript, and Dr. Y. Kawano for permitting the use of the Hitachi Perkin-Elmer 139-0880 spectrophotometer.

REFERENCES

1 J.R. Whitaker and P.E. Granum, Anal. Biochem., 109 (1980) 156.
2 P. Wolf, Anal. Biochem., 129 (1983) 145.
3 A.G. Gornall, C.J. Bardawill and M.M. David, J. Biol. Chem., 177 (1949) 751.

4 O.H. Lowry, N.J. Rosebrough, A.L Farr and R.J. Randall, J. Biol. Chem., 193 (1951) 265.
5 M.M. Bradford, Anal. Biochem., 72 (1976) 248.
6 R.G. Martinek, Clin. Chem., 11 (1965) 441.
7 D.S. Miyada, V. Baysinger, S. Notrica and R.M. Nakamura, Clin. Chem., 18 (1972) 52.
8 W. Troll and R.K. Cannan, J. Biol. Chem., 200 (1953) 803.
9 L.J. Fisher, S.L. Bunting and L.E. Rosenberg, Clin. Chem., 9 (1963) 573.
10 K. Lorentz and B. Flatter, Clin. Chem., 20 (1974) 1553.
11 R. Foster, N. Kulevsky and D.S. Wanigasekera, J. Chem. Soc., Perkin Trans. 1, (1974) 1318.
12 M.A. Slifkin, H.A.K. Saaid and E. Fernandez-Dias, Spectrochim. Acta, Part A, 42 (1986) 827.
13 W.J. Barreto, M. De Aquino and D.A.M. Zaia, Anal. Lett., 23 (1990) 1279.
14 D.A.M. Zaia, M.M. Obara, S.R. Rockenbach, L.C.J. Gaziri, C.T.B.V. Zaia, W.J. Barreto and J. Lichtig, Braz. J. Med. Biol. Res., 25 (1992) 549.
15 D.A.M. Zaia, S.R. Rockenbach, M.M. Obara, W.J. Barreto, S. Arizawa, R. Curi and J. Lichtig, Anal. Lett., 25 (1992) 1225.
16 A.L. Lajtha, O.S. Maker and D.D. Clarke, in G.J. Siegel, R.W. Albers, B.W. Agranoff and R. Katzman (Eds.), Basic Neurochemistry, American Society for Neurochemistry, 1981, Chap. 17, p. 345.
17 J.B. Birks and M.A. Slifkin, Nature, 197 (1963) 42.
18 B.Y. Lin and K.L. Cheng, Anal. Chim. Acta, 120 (1980) 335.

Analytica Chimica Acta, 277 (1993) 97–101
Elsevier Science Publishers B.V., Amsterdam

Separation of chlorophenols by capillary isotachophoresis

Petr Praus

Chemical Laboratory of Povodí Odry, Varenská 51, 701 26 Ostrava (Czech Republic)

Václav Dombek

Institute of Industrial Landscape Ecology, Czech Academy of Sciences, Hladnovská 9, 710 00 Ostrava 2 (Czech Republic)

(Received 30th November 1992)

Abstract

Conditions for the isotachophoretic separation and determination of chlorophenols in test samples were studied. With the combination of two electrolytic systems ($pH_L = 6.20$ and 7.80), the total separation of chlorophenols is possible. Detection limits with a conductivity detector were 10 ng for pentachlorophenol and 2,4,6-trichlorophenol and 50 ng for 2,4,5-trichlorophenol and 2,4-dichlorophenol.

Keywords: Electrophoresis; Chlorophenols; Isotachophoresis

Chlorophenols are important pollutants in the environment because of their high toxicity and tendency for bioaccumulation. Many methods for their determination in different matrices have been developed, mostly chromatographic techniques. Paper chromatography (PC) [1] and thin-layer chromatography (TLC) [1,2] have now mainly been replaced by liquid chromatography (LC) [3–9] and gas chromatography (GC) [10–18]. The separation of chlorophenols by supercritical fluid chromatography (SFC) has also been described [19,20]. Recently, the application of electromigration methods, such as electrokinetic micellary chromatography (MECC) [21–23] and capillary zone electrophoresis (CZE) [24], has been reported.

The determination of phenol [25], nitrophenols [26,27] and aminophenols [28] by capillary isotachophoresis (ITP) has been described, but the use of ITP to determine chlorophenols has not so far been published.

The aim of this work was the study of conditions for the ITP separation and determination of chlorophenols. The four widespread [29–31] derivatives pentachlorophenol (PCP), 2,4,5-trichlorophenol (2,4,5-TCP), 2,4,6-trichlorophenol (2,4,6-TCP) and 2,4-dichlorophenol (2,4-DCP) were chosen for this work.

EXPERIMENTAL

Instrumentation

A CS ZKI 01 isotachophoretic analyser (VVZ PJT, Spišská Nová Ves, Czech Republic) using a one-capillary (150 × 0.3 mm i.d.) array was used. The driving current was reduced from 75 to 25 μA after 600 s of analysis time. The signal of the conductivity detector was recorded on a TZ 4200 two-channel recorder (Laboratorní přístroje, Prague) at a chart drive speed of 1 mm s^{-1}. pH measurements were performed using a digital pH

Correspondence to: P. Praus, Chemical Laboratory of Povodí Odry, Varenská 51, 701 26 Ostrava (Czech Republic).

meter (Radelkis, Budapest). Sampling was done with Hamilton microsyringes (maximum volume 10 μl).

Chemicals

The chemicals used were of analytical-reagent grade: hydrochloric acid, barium hydroxide, sodium hydroxide, methanol and ethanol (all from Lachema, Brno), methylhydroxyethylcellulose 30000 (MHEC) and tris(hydroxymethyl)aminoethane (Tris) (both from Serva, Heidelberg), 1,3-bis [tris(hydroxyethyl)aminopropane] (BTP) (Calbiochem, La Jolla, CA), L-asparagine monohydrate and 2-amino-2-methylpropane-1,3-diol (Ammediol) (both from Merck, Darmstadt) and trichloroacetic acid (Avondale Labs., Banbury, UK). Tris and BTP were purified by recrystallization from methanol and ethanol, respectively. MHEC was purified on a mixed-bed ion exchanger.

Standards of chlorophenols were prepared by dissolution of PCP, 2,4,5-TCP, 2,4,6-TCP and 2,4-DCP (all from Supelco, Bellefonte, PA) in 0.1 mol l^{-1} sodium hydroxide solution and dilution to volume with demineralized water (specific conductivity up to 2 μS cm^{-1}).

RESULTS AND DISCUSSION

A knowledge of the dissociation constants (pK_a) of chlorophenols is needed for setting the ITP separation conditions. The pH range of the leading electrolyte (pH_L) was chosen in accordance with the condition of ionization of the separands for anionic analysis pH > $pK_a - 1$ [32]. Different pK_a values are given in the literature (Table 1), especially for tri-, tetra- and pentachlorophenol.

The electrolyte systems for ITP separation must have a sufficient buffer capacity. Separation of chlorophenols was tested in the pH_L range 6.2–9.0 (Table 2). The separation order of chlorophenols at lower pH_L in system I (Table 2) is PCP, 2,4,6-TCP and 2,4,5-TCP, i.e., in order of their dissociation constants (separation according to pK_a). 2,4-DCP migrates in the terminating electrolyte zone ($pH_L = 6.2$). The zones of PCP

TABLE 1

pK_a values of chlorophenols

Compounds	pK_a		
	A [a]	B (20°C) [b]	C (25°C) [c]
Phenol	9.92	10.03 ± 0.03	10.02
o-Chlorophenol	8.52	9.13 ± 0.04	8.48
m-Chlorophenol	8.97	9.53 ± 0.08	9.02
p-Chlorophenol	9.37	9.70 ± 0.04	9.38
2,3-Dichlorophenol	7.71	8.52 ± 0.08	7.45 [d]
2,4-Dichlorophenol	7.90	8.51 ± 0.05	7.89
2,5-Dichlorophenol	7.51	7.69 ± 0.03	7.50
2,6-Dichlorophenol	6.78	7.15 ± 0.05	6.79
3,4-Dichlorophenol	8.62	8.87 ± 0.03	8.39 [d]
3,5-Dichlorophenol	8.25	8.54 ± 0.06	8.18
2,3,6-Trichlorophenol	5.80	6.10 ± 0.03	6.12
2,3,4-Trichlorophenol	6.97	7.34 ± 0.08	7.59
2,4,6-Trichlorophenol	5.99	6.51 ± 0.07	6.42
2,4,5-Trichlorophenol	6.72	7.20 ± 0.07	7.33
3,4,5-Trichlorophenol	7.55	7.57 ± 0.03	7.74
2,3,5,6-Tetrachlorophenol	5.03	5.76 ± 0.06	5.44
2,3,4,6-Tetrachlorophenol	5.22	5.53 ± 0.08	–
2,3,4,5-Tetrachlorophenol	5.64	5.92 ± 0.06	6.96
Pentachlorophenol	4.74	4.93 ± 0.03	5.26

[a] From [3]. [b] From [8]. [c] From [2]. [d] pK_a at 29°C.

TABLE 2

Operational systems

Parameter	Electrolytic system		
	I	II	III
Leading anion	Cl^-	Cl^-	Cl^-
Concentration (mM)	10	10	10
Counter ion	BTP	Tris	Ammediol
pH_L	6.2–7.5	7.5–8.5	9.0
Additive	MHEC	MHEC	MHEC
Concentration (%, w/v)	0.1	0.1	0.1
Terminating anion	Asparagine	Asparagine	Asparagine
Concentration (mM)	5	5	5
Counter ion	Ba^{2+}	Ba^{2+}	Ba^{2+}
pH_T	9.5–10.0	9.5–10.0	9.5–10.0

and 2,4,6-TCP make a mixed zone during the increase of pH_L and the zone of 2,4-DCP divides from the terminating electrolyte (Fig. 1a–c).

Separation of chlorophenols in operational system II (Table 2) was then tested. At $pH_L = 7.5$ a mixed zone of PCP and 2,4,6-TCP existed (Fig. 2a). During the increase of pH_L ($pH_L = 7.8$) all chlorophenols are separated (Fig. 2b) with the opposite order of PCP and 2,4,6-TCP, but only in the smallest concentration range. Subsequent increases of pH_L influence the zones of PCP and 2,4,5-TCP, which combine, and it is not possible to identify the individual zones with the conductivity detector (Fig. 2c and d).

The operational system with a higher pH_L (System III, Table 2) gave poor results and the chlorophenols were not separated.

On the basis of these results, the successful separation of all the chlorophenols studied over a wide concentration range on the ITP analyser with conductivity detection is not possible with one electrolyte system. System I is useful only for the determination of PCP and 2,4,6-TCP with consideration of the low sensitivity (weak dissociation) of 2,4,5-TCP. System II is useful for the determination of 2,4,5-TCP and 2,4-DCP. These conditions were used in subsequent work.

The zones were defined by the relative step heights (RSH) (Table 3) according to the equation

$$RSH = (h_i - h_L)/(h_s - h_L) \quad (1)$$

where h_i, h_L and h_s are the zones height of the chlorophenols, the leading ion and the standard (trichloroacetic acid), respectively.

The presence of an HCO_3^- zone in both systems does not have a disturbing effect (Figs. 1 and 2). It has sharp boundaries from the other zones and a constant length.

The determination of chlorophenols was tested using calibration graphs (Fig. 3). The length of the zones was measured from derivative records.

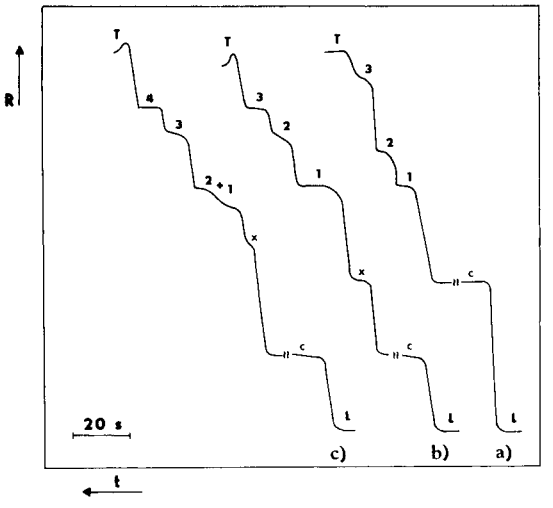

Fig. 1. Separation of chlorophenols at pH_L = (a) 6.20, (b) 7.00 and (c) 7.50. One-capillary array (150×0.3 mm i.d.); $I = 25$ μA; volume injected = 2 μl; chart speed = 1 mm s^{-1}: 1 = PCP; 2 = 2,4,6-TCP; 3 = 2,4,5-TCP; 4 = 2,4-DCP; c = HCO_3^-; x = impurities.

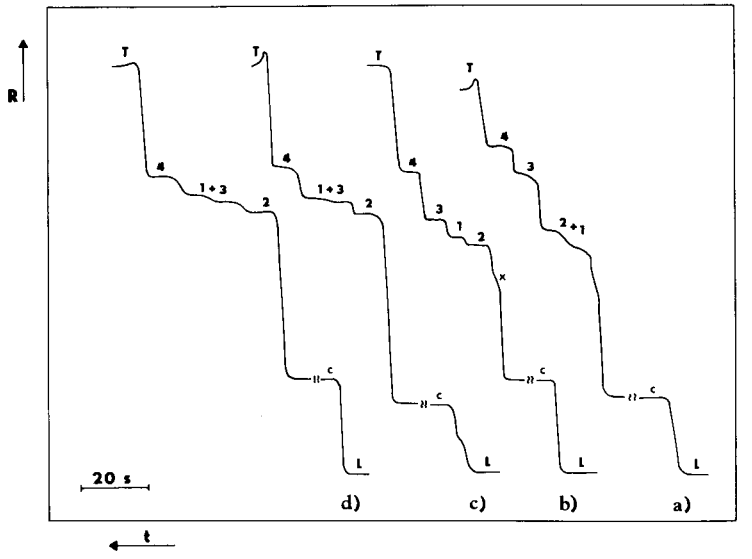

Fig. 2. Separation of chlorophenols at pH_L = (a) 7.50, (b) 7.80, (c) 8.20 and (d) 8.50. Conditions and identifications as in Fig. 1.

TABLE 3

Relative step heights (RSH) of chlorophenols

Compounds	RSH	
	System I (pH_L = 6.20)	System II (pH_L = 7.80)
Pentachlorophenol	1.60	1.69
2,4,6-Trichlorophenol	1.76	1.64
2,4,5-Trichlorophenol	2.69	1.81
2,4-Dichlorophenol	–	2.13

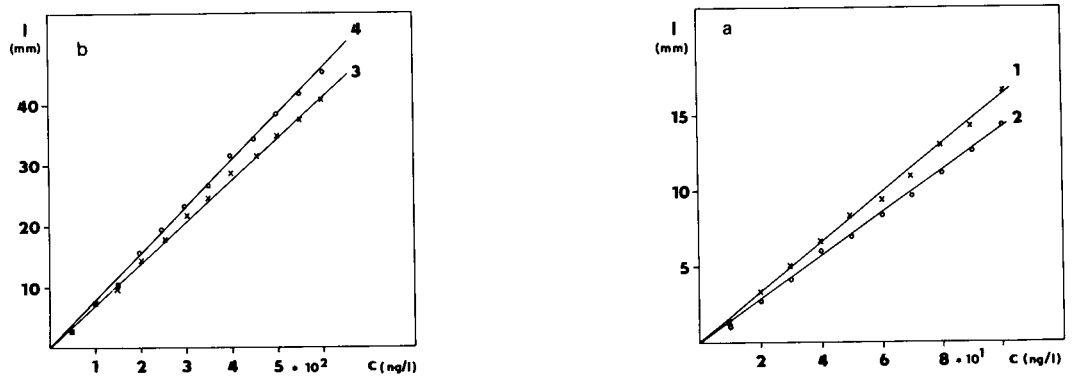

Fig. 3. Calibration dependences for (a) PCP and 2,4,6-TCP at pH_L = 6.20 and (b) 2,4,5-TCP and 2,4-DCP at pH_L = 7.80. 1 = PCP (correlation coefficient r = 0.9986); 2 = 2,4,6-TCP (r = 0.9991); 3 = 2,4,5-TCP (r = 0.9987); 4 = 2,4-DCP (r = 0.9993).

The detection limits (corresponding to a zone length of 1 mm) were 10 ng for PCP and 2,4,6-TCP and 50 ng for 2,4,5-TCP and 2,4-DCP.

Conclusions

The possibility of the ITP separation of chlorophenols was examined using test mixtures of the widespread pentachlorophenol, 2,4,6-trichlorophenol, 2,4,5-trichlorophenol and 2,4-dichlorophenol. On the basis of the results, capillary isotachophoresis seems to be a promising method for the separation and determination of these pollutants. After establishing the isolation and preconcentration steps, the determination of the chlorophenols will be tested in water and other environmental samples by this rapid and simple method.

REFERENCES

1 J. Gasparič and J. Churáček, Papírová a Tenkovrstvá Chromatografie Organických Sloučenin, SNTL, Prague, 1981, pp. 103–104.
2 L. Lepri, P.G. Desideri and D. Heimler, J. Chromatogr., 195 (1980) 339.
3 K. Ugland, E. Lundanes and T. Greibrokk, J. Chromatogr., 213 (1981) 83.
4 C.E. Werkhoven-Goewie, W.M. Boon, A.J.J. Praat, R.W. Frei, U.A.Th. Brinkman and C.J. Little, Chromatographia, 16 (1982) 53.
5 R.E. Shoup and G.S. Mayer, Anal. Chem., 54 (1982) 1164.
6 B. Rössner and G. Schwedt, Fresenius' Z. Anal. Chem., 315 (1983) 610.
7 F.P. Bigley and R.L. Grob, J. Chromatogr., 350 (1985) 407.
8 S. Li, M. Paleologou and W.C. Purdy, J. Chromatogr. Sci., 29 (1991) 66.
9 P.J.M. Kwakman, D.A. Kamminga, U.A.Th. Brinkman and G.J. De Jong, J. Chromatogr., 553 (1991) 345.
10 C.D. Chriswell, R.C. Chang and J.S. Fritz, Anal. Chem., 47 (1975) 1325.
11 L.L. Lamparski and T.J. Nestrick, J. Chromatogr., 156 (1978) 143.
12 R.T. Coutts, E.E. Hargesheimer and F.M. Pasutto, J. Chromatogr., 179 (1979) 291.
13 T.R. Edgerton, R.F. Moseman, E.M. Lores and L.H. Wright, Anal. Chem., 52 (1980) 1774.
14 C.E. Rostad, W.E. Pereira and S.M. Ratcliff, Anal. Chem., 56 (1984) 2856.
15 R.S.K. Buisson, P.W.W. Kirk and J.N. Lester, J. Chromatogr. Sci., 22 (1984) 339.
16 K. Norén and J. Sjövall, J. Chromatogr., 414 (1987) 55.
17 V. Janda and H. van Langenhove, J. Chromatogr., 472 (1989) 327.
18 EPA-604, Fed. Regist., 49 (1984) 58.
19 T.A. Berger and J.F. Deye, J. Chromatogr. Sci., 29 (1991) 54.
20 D. Thiebaut, J.P. Chervet, R.W. Vannoort, G.J. De Jong, U.A.Th. Brinkman and R.W. Frei, J. Chromatogr., 477 (1989) 151.
21 K. Terabe, K. Otsuka, K. Ichikawa, A. Tsuchiya and T. Ando, Anal. Chem., 56 (1984) 111.
22 K. Otsuka, K. Terabe and T. Ando, J. Chromatogr., 348 (1985) 39.
23 C.P. Ong, C.L. Ng, N.C. Chong, H.K. Lee and S.F.Y. Li, J. Chromatogr., 516 (1990) 263.
24 Ch.D. Gaitonde and P.V. Pathak, J. Chromatogr., 514 (1990) 389.
25 P.A. Pfeifer, G.K. Bonn and O. Bobleter, Fresenius' Z. Anal. Chem., 315 (1983) 205.
26 S. Čefová and P. Rajec, J. Radioanal. Nucl. Chem., Articles, 101 (1986) 17.
27 D. Kaniansky, V. Madajová, J. Marák, E. Šimuničová, I. Zelenský and V. Zelenská, J. Chromatogr., 390 (1987) 51.
28 S. Fanali, J. Chromatogr., 470 (1989) 123.
29 M. Veningerová, J. Uhnák, A. Kočan, K. Oprchalová, M. Svrčková, E. Nagyová and Y. Hudecová, Stanovenie Degradačných Produktov Herbicídov a ich Reziduí. Výzkumná Zpráva, Výzkumný Ústav Preventívného Lekárstva, Bratislava, 1985.
30 V. Gajdůšková, M. Machala, J. Palásek and J. Hofírková, Sledování Reziduí Rizikových Herbicidů Typu Chlorfenolů a Nitrofenolů v Potravinovém Řetězci. Výzkumná Zpráva, Výzkumný Ústav Veterinárního Lékařství, Brno, 1987.
31 V. Gajdůšková and M. Jiaxisová, Výskyt a Prevence Reziduí Chlorfenolů a Nitrofenolů v Potravinovém Řetězci. Výzkumná Zpráva, Výzkumný Ústav Veterinárního Lékařství, Brno, 1988.
32 P. Boček, M. Deml, P. Gebauer and V. Dolník, Analytická Kapilární Izotachoforéza, Academia, Prague, 1987, p. 91.

Analytica Chimica Acta, 277 (1993) 103–111
Elsevier Science Publishers B.V., Amsterdam

Simultaneous ion chromatographic determination of anions and cations by series conductivity and flame photometric detection

Wolfgang Frenzel

Institut für Technischen Umweltschutz, Fachgebiet Luftreinhaltung, Technische Universität Berlin, Str. d. 17. Juni 135, W-1000 Berlin 12 (Germany)

Dietrich Schepers and Gerhard Schulze

Institut für Anorganische und Analytische Chemie, Technische Universität Berlin, Str. d. 17. Juni 135, W-1000 Berlin 12 (Germany)

(Received 1st September 1992; revised manuscript received 8th December 1992)

Abstract

A method for the simultaneous determination of anions and cations using non-suppressed ion chromatography (NSIC) is proposed. Anions are separated on an ion-exchange column and determined with conductivity detection. In the same run the non-retained cations leaving the chromatographic system as a discrete sample zone are detected by a multi-element flame emission spectrometer which is coupled directly to the outlet. The principal analytical features of the proposed method are discussed and the experimental requirements of interfacing the two detection methods are outlined. System performance is evaluated for the high-speed NSIC of chloride, nitrate and sulphate and the multi-channel flame emission spectroscopic detection of sodium, potassium and calcium. The figures of merit are given and application to the analysis of tap, surface and mineral waters is presented.

Keywords: Ion chromatography; Anions; Cations

Since the introduction of modern ion chromatography (IC) in the mid-1970s [1], the method has quickly evolved and become a powerful tool for the determination of inorganic and organic ions. The speed, sensitivity and selectivity of analysis and the ability to determine simultaneously several ions at widely varying concentration levels are impressive characteristics. Recent developments [2–6] such as gradient techniques, coupling of detectors and in-line preconcentration provide improved resolution, extension of detectable ions and lowering of detection limits. Despite these features, there are still deficiencies in IC. For instance, the separation and detection of anions and cations is generally performed with independent IC systems using different columns, eluents and detectors. Several attempts have been undertaken to determine anions and cations simultaneously in a single run [7]. A trivial solution to this problem is the simultaneous injection of the sample solution in a dual-channel IC system [7,8], where the term "simultaneous" is hardly appropriate. Tandem operation [9–11] of anion- and cation-exchange colums in a single-channel IC system requires specialized hardware and sets stringent constraints on the choice of the mobile phase composition. The separation of anions to-

Correspondence to: W. Frenzel, Institut für Technischen Umweltschutz, Fachgebiet Luftreinhaltung, Technische Universität Berlin, Str. d. 17. Juni 135, W-1000 Berlin 12 (Germany).

gether with divalent cations (in the form of anionic complexes) [12,13] has been reported but is of limited applicability. Mixed-bed ion exchangers [14] or bifunctional exchange materials [15] have also been applied for the simultaneous determination of anions and cations, but these columns cannot compete with conventional separation techniques with respect to selectivity and resolution.

In this paper a totally different concept to achieve the goal of the simultaneous ion chromatographic determination of cations and anions is proposed. The basic principle is the series arrangement of at least two detectors, one of which being used in a conventional manner to detect the ions separated on the column, the other detecting the non-separated counter ions present in the void volume. A description of the concept is given and the potential analytical features are outlined. As a first example non-suppressed IC (NSIC) is presented for separation and conductivity detection of anions coupled with multi-element flame atomic emission detection (FAED) for cation determination. The instrumental requirements of interfacing the two methods are discussed and the optimum operating conditions are outlined. Application to the simultaneous high-speed determination of chloride, nitrate, sulphate, sodium, potassium and calcium in water samples is used to demonstrate the analytical utility of the approach.

BASIC PRINCIPLE

In IC, cations or anions are generally separated on the basis of ion-exchange reactions on an analytical separation column. In NSIC a suitable detector is directly connected to the outlet of the column and the change in the composition of the mobile phase or a characteristic feature of the separated ions is measured. Conductivity, direct and indirect UV absorption and amperometric detectors are commonly employed, the first being the most popular and versatile detection technique.

A characteristic of any chromatogram is the occurrence of the "solvent" or "injection" peak, which has been interpreted by several workers (e.g., [16,17]). It is represented by a discrete zone containing the solvent in which the sample has been dissolved, an equivalent amount of competing ions to the sum of all ions retained on the separation column and those components of the sample which show no interaction with the stationary phase. In anion chromatography the sample cations present are generally not retained and, hence, elute within the void volume. Owing to the constant flow conditions and low dead volumes of common chromatographic detectors, the cations leaving the detector may be subjected to further analysis by collection of this fraction of the mobile phase or, more conveniently, by direct coupling of a cation detector in series.

It appears that this concept has not previously been proposed for analytical purposes. As will be shown in a series of papers, there is a wide applicability of this approach, offering new opportunities in chromatographic detection. The main features recognized so far can be summarized as follows: true simultaneous determination of cations and anions becomes feasible without column switching using conventional commercially available chromatographic equipment; microanalytical capabilities are inherent in the method in that cations and anions are determined in the minute sample volume injected into the chromatographic system; mutual interferences of anions and cations are widely eliminated because of their physical separation which means, for instance, that irrespective of the original sample composition the cations leaving the anion separation column are accompanied solely by competing anions present in the mobile phase, non-ionic species that are not retained by adsorption can be detected likewise using a suitable detector in series, and using anion or cation separation columns potential interferences of the respective ions can be eliminated; and the retention behaviour of cations on anion-exchange stationary phases which might occur under special circumstances [18,19] can be studied in an elegant way. Additionally, the total analysis time is reduced compared with the sequential determination of anions and cations by two seperate methods. Finally, the direct coupling of detectors in

series is economic with respect to reagent consumption and instrumentation requirements and lends itself well to automation.

EXPERIMENTAL

Apparatus

A schematic diagram of the entire system is shown in Fig. 1. The ion chromatographic system consisted of a Model 64 LC pump (Knauer, Bad Homburg), a variable-volume injection valve (Knauer) and a Metrohm Model 690 conductivity detector. The separation column used throughout was a Hamilton (Darmstadt) PRP-X 100 (150 mm × 4.2 mm i.d.). Flame atomic emission measurements were performed using a Zeiss (Type FA-1) total consumption burner. A hydrogen–oxygen flame was employed throughout. The original detection system of the Zeiss instrument with lenses, monochromator and photomultiplier tube was replaced with a purpose-built detection unit that permits the simultaneous registration of light emission at different wavelengths.

Briefly, the present system consists of three optical fibres arranged circularly around the flame. The emission light is guided by the optical fibres to detectors which contain interference filters, photodiodes, current–voltage converter and associated electronics and allow independent amplification and zeroing of each channel. A detailed description of the detector will be published elsewhere [20]. In this work a three-channel version was used. Additional channels can be easily established when necessary. The transmission maxima of the interference filters used (Bruno Lange, Berlin) are 589, 770 and 622 nm for sodium, potassium and calcium, respectively. The output of the conductivity detector and the three outputs of the FAED are interfaced to a multi-channel strip chart (Linseis Series 2000) in order to permit the simultaneous recording of the respective signals. Evaluation of the signals was done manually by peak-height measurements. A combination glass pH electrode (Metrohm, Herisau) in connection with a Knick ion meter was used for the precise adjustment of the pH of the mobile phase.

Chemicals and solutions

All chemicals were of analytical-reagent grade. Doubly distilled water was used in the preparation of all solutions. Stock standard solutions of chloride, nitrate, sulphate, sodium, potassium and

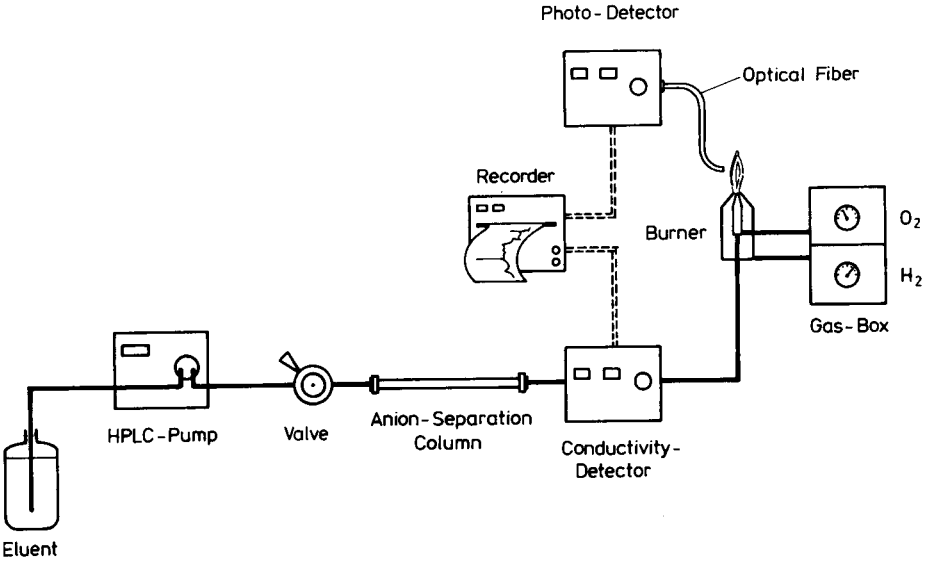

Fig. 1. Schematic diagram of the system.

calcium were prepared at a concentration of 1 g l^{-1} and diluted when required. The eluent for IC separation was prepared by dissolving 0.3323 g of phthalic acid in 1 l of water. Then ammonia solution (25%, w/w) (Merck) was added dropwise until a pH of 6.8 ± 0.05 was reached (ca. 1 ml is required). After membrane filtration and careful degassing by ultrasonic agitation under water suction vacuum, the eluent was ready for use.

RESULTS AND DISCUSSION

Interfacing IC with FAED

Detection methods in chromatography are inextricably linked to the separation method used. In order to apply the concept proposed in this work, the choice of chromatographic conditions requires thorough consideration of both detectors employed. Instrumental parameters, i.e., flow-rate and injection volume, and the selection of the mobile phase with respect to the nature of the competing ion, concentration and pH must be chosen for optimum separation of anions without sacrificing the FAED capabilities.

Flow-rate. The flow-rate plays an important role because retention time, separation efficiency and mechanical strain of the chromatographic material are strongly influenced. High flow-rates shorten the chromatographic run but adversely affect the separation efficiency and column lifetime. With respect to operation of the FAED and interfacing the two detectors, the flow-rate of the mobile phase should be in the range 2–5 ml min^{-1}. At lower flow-rates the burner works under starvation, which adversely affects the sensitivity and causes problems with outgassing of the eluent owing to the underpressure created at the outlet of the upstream conductivity detector [21]. According to manufacturers recommendation, only a few IC columns are suitable for working at these relatively high flow-rates. The Hamilton PRP-X 100 can be used at a maximum flow-rate of 8 ml min^{-1} and routinely at 3–6 ml min^{-1} without a noticeable decrease in lifetime [22,23]. Hence this column was selected for the present work.

Injection volume. The injection volume in IC is usually in the range 10–100 μl. Lower volumes substantially decrease the sensitivity, whereas higher volumes create problems with peak resolution and potential column overload. In conventional FAES the sample is continuously aspirated or pumped with a typical consumption of 1–5 ml of sample per analysis. Studies on flow-injection (FI) [24,25] and hydraulic high-pressure nebulization [26] sample introduction for atomic absorption and emission spectrometry and the use of these detection techniques in chromatography [27,28] have shown, however, that much smaller volumes can be used. Of course, a transient rather than continuous signal is obtained, the peak height or area of which can be related to concentration. Because the sample cations move through the separation column without retention, a discrete sample zone still exists at the outlet of the conductivity detector. The system, in principle, compares very well with FI sample introduction. Using terminology from this field of research [29], the column, the connecting tubing and the upstream detector can be regarded purely as dispersion elements. The sample injected undergoes dispersion during transportation to the FAED, the magnitude depending on the injection volume, flow-rate of the mobile phase and dimensions of the column and the transportation line. A quantitative measure of the sample distribution process during transportation is the dispersion coefficient [29], defined as the ratio of concentrations of the sample material before and after the dispersion process has taken place or, in other words, the ratio between analytical readouts of injected and continuously aspirated sample.

The contributions of injection volume and sample transport through the column, conductivity detector and connecting tubing on sample dispersion were studied in detail. In Fig. 2 the influence of injection volume on the dispersion coefficient is shown for FI sample introduction in FAED, i.e., without the chromatographic system. As can be seen, the peak height increases linearly up to 30 μl, levels off in the range 30–200 μl and becomes constant for higher volumes. Dispersion coefficients for injection volumes of 20 and 100 μl are 3.3 and 1.3, respectively. Repeating this

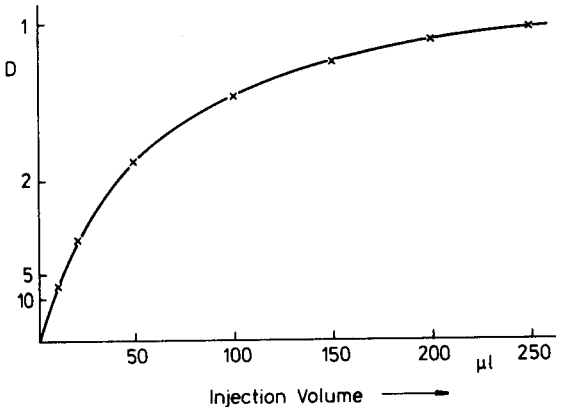

Fig. 2. Influence of injection volume on dispersion coefficient in flow-injection flame emission spectrometry. $D = 1$ corresponds to the signal obtained when the sample is continuously aspirated.

experiment with the chromatographic column and conductivity detector installed, the overall dispersion of the system was investigated for injection volumes of 20 and 100 µl. The dispersion coefficients obtained were 8.5 and 4.1, respectively, leading to a contributing factor of the chromatographic system of ca. 2.5.

For reasons of convenience of installation, the length of the connecting tubings between the column outlet and the conductivity detector and interfacing the two detectors was not reduced to the absolute minimum so that even lower dispersion coefficients could be obtained. From these data the general conclusion can be drawn that the dispersion of non-retained components can be kept comparatively low at moderate injection volumes.

Chromatographic considerations

NSIC has long been used for the simultaneous determination of inorganic anions and numerous papers are available in which optimum conditions for specific separation problems can be found (e.g., [2,22,23]). A commonly used eluent in NSIC is potassium hydrogenphthalate. The concentration and pH of the eluent are the two variables that markedly influence the retention time and resolution of adjacent peaks. In previous work [23,30,31] it was demonstrated that high-speed separations can be performed, permitting the determination of 3–5 anions within 3 min.

The presence of potassium ions in the mobile phase is disadvantageous if the FAED is used for the series detection of cations. It makes the determination of potassium impossible, of course, and the high spectral background interferes in the determination of other metals. Replacement of potassium with ammonium ions in the eluent was considered to avoid these problems. In fact, no significant changes in the chromatographic separation of anions were apparent. A typical chromatogram for the high-speed separation of chloride, nitrite, bromide, nitrate and sulphate evidencing baseline resolution is shown in Fig. 3. Under these conditions, fluoride and organic acid anions elute within the void volume and do not

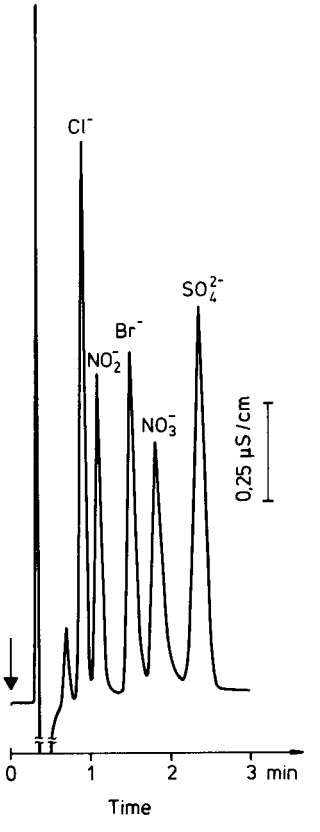

Fig. 3. Typical chromatogram for high-speed separation of five anions. Eluent, 2 mM phthalic acid (pH 6.8), adjusted with ammonia solution; flow-rate, 4 ml min^{-1}; injection volume, 20 µl.

interfere. In the presence of phosphate an additional peak occurs which partially overlaps with the bromide signal. Hydrogencarbonate was found to interfere at concentrations above 50 mg l^{-1}, giving rise to a negative peak overlapping with the chloride signal. The system peak often encountered in NSIC [2,32] does not occur owing to the relatively high pH of the mobile phase.

Optimization of FAED

The performance of the FAED was first optimized using a conventional sample aspiration technique. The gas flow-rates of oxygen and hydrogen (absolute and relative to each other) were optimized to provide maximum signal-to-noise ratios for the three elements investigated. Horizontal and vertical alignment of the optical fibres was carried out in order to find the position of maximum emission intensity yet avoiding excessive heat stress [20].

Continuous pumping of the sample solution at various flow-rates below and above the natural aspiration rate revealed no significant change in detector response in the range 2.5–4 ml min^{-1}. Higher flow-rates were not investigated. At lower flow-rates the sensitivity (peak-height measurements) decreased markedly. Further tests were performed using FI sample introduction with a flow-rate of 4 ml min^{-1}. The influence of injection volume on the FAED response has been discussed before. Another variable is the dimension (length and i.d.) of the connecting tubing between the injector and burner. With increasing length and i.d. the sample dispersion increases [29]. Using small-bore tubing (i.d. $\leqslant$ 0.5 mm) the effect of increasing length was, however, not very pronounced. On changing the length from 10 cm (which was the shortest practical length) to 270 cm the dispersion coefficient increased by a factor of 1 .3.

Potential interferences in FAED are well documented [33,34] and appropriate means of overcoming such shortcomings are known. In the determination of alkali metals the main problems are ionization at high flame temperatures, flame background emission of different origin and self-absorption phenomena at high metal concentrations. The determination of alkaline earth elements requires comparatively high temperatures and is strongly influenced by the presence of certain anions [33].

In this work, the simultaneous determination of sodium, potassium and calcium by a multichannel emission spectrometer was sought. Hence a compromise was required between the choice of flame temperature and optimum composition of the gas mixture. The hydrogen–oxygen flame employed is suitable in this respect. Background emission is corrected for in that the peak height of the transient signal is measured. Owing to the fast response, successive background and signal measurements are done in short time sequences. This, however, cannot eliminate background emission contributions from sample constituents. Anion interferences are virtually absent because of the physical separation, i.e., retention of anions on the chromatographic column [35].

Performance characteristics of the proposed method

The system described here was used for the simultaneous determination of chloride, nitrate, sulphate, sodium, potassium and calcium. Optimized chromatographic and flame emission conditions were set (see below) and the various analytical characteristics were evaluated.

Precision and stability. In order to verify the reproducibility, replicate injections of standard solutions at low and high concentration levels were made and peak heights were measured. Statistical evaluation revealed relative standard deviations (R.S.D.s) below 2% for all ions (ten injections). This is about the same as can be expected when these two methods are applied separately. Long-term stability was examined during routine operation of the system over a period of several days. The within-day reproducibility was usually better than 5% (R.S.D.) even when the instrument was shut down during working breaks. Day-to-day variations were more pronounced, obviously owing to small variations in the preparation of the mobile phase and fine tuning of the gas-flow regulation. With respect to resolution of the chromatographic separation and sensitivity these changes are, however, insignificant.

Measuring range and detectability. The working range for both detection methods is strongly dependent on the injection volume used. For 20-μl injections all ions except calcium can be determined in the range 1–100 mg l^{-1}. For calcium the accessible range is 10–200 mg l^{-1}. By increasing the injection volume to 100 μl the sensitivity (peak-height measurement) is increased by a factor of about five for all ions, with a concomitant shift of the working range to lower concentrations. The resolution of the IC separation is still sufficient with a 100-μl injection volume but becomes worse when larger volumes are used.

Detection limits were not evaluated by statistical treatment of the data because they depend on the injection volume and to a considerable extent on the noise level of the detectors employed. In conductivity detection noise is mainly created by temperature fluctuations. The excellent thermostating of the measuring cell of the Metrohm instrument and proper design of the flow cell allows the detection of very small conductivity differences. The noise of the FAED results almost exclusively from the high flow turbulences of the total consumption burner. The contributions of the photodetector (dark current) and ambient light are negligible. Effective noise reduction was achieved by the application of sophisticated analogue signal filtering [20,35].

Detectable signals for the respective ions could generally be obtained when the sample concentrations were five times lower than those given for the lower end of the working ranges.

Analysis time. In the proposed method the analysis time is determined solely by the retention time of the most strongly retained ion in the chromatographic separation. Hence the chromatographic conditions must be optimized in order to balance the required selectivity and resolution and the desired sampling frequency. In this work high-speed NSIC [23,30] was applied for the separation of chloride, nitrate and sulphate. This was done because in the intended application other ions of interest are not likely to be present and the running time of the FAED between cation measurements of successively run samples should be kept to the minimum.

As is evident from Fig. 3, the retention time of sulphate is about 2.2 min and the time necessary to establish a stable baseline after sample injection is 2.4 min. Because a subsequent sample can be filled into the injection loop during the chromatographic run of the previous sample, a true sampling frequency of 25 h^{-1} is obtainable.

Calibration data

Calibration of the method was done by injection of mixed ion standards covering the entire working range. The sensitivity settings of the conductivity detector and the three channels of the FAED were adjusted to give almost full-scale deflection for the highest standard concentration. Each sample was injected three times in random order. Linear correlations ($r \geqslant 0.9997$) between concentration and peak height were obtained for all ions except sodium. The sodium calibration graph was non-linear, which is believed to be a result of self-absorption at high concentrations. The results of the statistical treatment of calibration data for the five anions, potassium and calcium are summarized in Table 1.

TABLE 1

Calibration data for simultaneous determination of anions and cations using the proposed approach (peak-height measurements)

Parameter	Cl^-	NO_2^-	Br^-	NO_3^-	SO_4^{2-}	K^+	Ca^{2+}
Concentration range (mg l^{-1})	5–50	5–50	10–100	10–100	10–100	2–20	15–150
Slope [a]	0.038	0.022	0.013	0.010	0.014	138.8	48.1
Intercept [b]	0.02	−0.03	−0.02	−0.04	0.03	2.4	100.8
Residual standard deviation [b]	0.009	0.006	0.007	0.007	0.012	9.77	46.9
Relative standard deviation of the method (%)	0.82	1.03	1.01	1.17	1.46	0.64	1.18

[a] Units for anions and cations are μS l cm^{-1} mg^{-1} and mV l mg^{-1}, respectively. [b] Units for anions and cations are μS cm^{-1} and mV, respectively.

TABLE 2

Results of real sample analysis (left columns) and comparison with standard methods (right columns) [36] [a]

Sample	Chloride		Nitrate		Sulphate		Potassium		Sodium		Calcium	
Tap water	79.2	79.4	– [b]	2.8	169.2	168.5	5.9	7.2	44.2	45.8	127.4	121.4
Surface water	43.5	44.2	5.4	12.2	130.2	130.3	7.8	8.6	29.0	32.6	82.2	78.7
Mineral water (Irisquelle)	301.4	297.4	– [b]	– [b]	1467.5	1470.0	5.8	5.6	268.0	271.8	546.0	564.0
Mineral water (Irenenquelle)	112.2	105.0	– [b]	– [b]	1495.0	1473.0	4.2	5.3	51.6	56.3	495.5	546.0
Mineral water (St. Martin)	103.9	107.5	– [b]	– [b]	351.9	350.0	5.4	6.4	133.5	133.4	207.0	200.5

[a] All values in mg l^{-1}; means of three determinations. [b] Not detectable.

Real sample analysis

The proposed method was applied to the analysis of tap, surface and mineral waters. In the last instance excess carbon dioxide was removed by shaking a 10-ml sample for about 1 min prior to injection. The concentrations of the respective ions were calculated using a calibration graph. In Table 2 results obtained with the proposed method are given and compared with those obtained using standard methods of analysis. In general there is good agreement between the results. The large difference in the result for the nitrate content of surface water is obviously due to microbiological conversion which took place in the relatively long time span between analysis by the two methods.

Conclusion

Coupled conductivity and flame emission detection in ion chromatography has the capability to detect anions and cations simultaneously. The instrumentation used is relatively simple and the method offers high flexibility with respect to the choice of chromatographic conditions. Using high-speed NSIC and a multi-channel emission detector, chloride, nitrate, sulphate, sodium, potassium and calcium could be determined in the mg l^{-1} concentration range. The sample volume required is only 20 μl and the analysis time is below 3 min.

In addition to these impressive features there is obviously great potential for other applications. The number of accessible components that can be simultaneously determined may be increased using more sophisticated chromatographic separations and, for instance, plasma emission spectrometry for multi-element cation detection [35]. Another route would be the re-introduction of the sample zone containing the cations into a cation chromatographic system.

The authors are indebted to H. Rietdorf, G. Steinbrecher and T. Thele for technical assistance.

REFERENCES

1 H. Small, T.S. Stevens and W.C. Bauman, Anal. Chem., 47 (1975) 1801.
2 P.R. Haddad and P.E. Jackson, Ion Chromatography – Principles and Applications (Journal of Chromatography Library, Vol. 46), Elsevier, Amsterdam, 1990.
3 J. Weiss, Ionenchromatographie, Verlag Chemie, Weinheim, 2nd edn., 1991.
4 W.R. Jones, P. Jandik and A.L. Heckenberg, Anal. Chem., 60 (1988) 1977.
5 K. Slais, J. Chromatogr., 436 (1988) 413.
6 P.E. Jackson and P.R. Haddad, J. Chromatogr., 439 (1988) 37.
7 V. Cheam and A.S.Y. Chau, Analyst, 112 (1987) 993, and references cited therein.
8 G. Schwedt and B. Kondratjonok, Labor Praxis, 5 (1988) 540.
9 H. Small and T.E. Miller, Anal. Chem., 54 (1982) 462.
10 Z. Iskandarani and T.E. Miller, Anal. Chem., 57 (1985) 1591.
11 V.K. Jones and J.G. Tarter, Analyst, 113 (1988) 183.
12 M. Yamamoto, H. Yamamoto, Y. Yamamoto, S. Matsushita, N. Baba and T. Ikashige, Anal. Chem., 56 (1984) 832.
13 G. Schwedt and B. Konratjonok, Fresenius' Z. Anal. Chem., 332 (1989) 855.

14 D.J. Pietrzyk and D.M. Brown, Anal. Chem., 58 (1986) 2554.
15 T. Takeuche, E. Suzuki and D. Ishii, Chromatographia, 25 (1988) 480.
16 H. Hershcovitz, C. Yarnitzki and G. Schmuckler, J. Chromatogr., 244 (1982) 217.
17 T. Okada and T. Kuwamoto, Anal. Chem., 56 (1984) 2073.
18 D.R. Jenke and G.K. Pagenkopf, Anal. Chem., 55 (1983) 1168.
19 A. Siriaks, J.E. Girard and P.E. Buell, Anal. Chem., 59 (1987) 2665.
20 W. Frenzel and D. Schepers, in preparation.
21 D.R. Jones, H.C. Tung and S.E. Manaham, Anal. Chem., 48 (1976) 7.
22 P.R. Haddad, P.E. Jackson and A.L. Heckenberg, J. Chromatogr., 346 (1985) 139.
23 W. Frenzel, Fresenius' J. Anal. Chem., 340 (1991) 525.
24 J.L. Burguera (Ed.), Flow Injection Atomic Spectroscopy, Dekker, New York, 1989.
25 J.F. Tyson, Anal. Chim. Acta, 234 (1990) 3.
26 G. Weber and H. Berndt, Chromatographia, 29 (1990) 254.
27 P.C. White, Analyst, 109 (1984) 677.
28 R.M. Harrison and S. Rapsomanikis (Eds.), Environmental Analysis Using Chromatography Interfaced with Atomic Spectroscopy, Horwood, Chichester, 1989.
29 J. Ruzicka and E.H. Hansen, Flow Injection Analysis, Wiley, New York, 2nd edn., 1988.
30 A. Rauterberg, Diploma Thesis, Technical University of Berlin, Berlin, 1989.
31 W. Frenzel and A. Rauterberg, in preparation.
32 P.E. Jackson and P.R. Haddad, J. Chromatogr., 346 (1985) 125.
33 J.A. Dean, Flame Photometry, McGraw-Hill, New York, 1960.
34 R. Herrmann and C.T.J. Alkemade, Flammenphotometrie, Springer, Berlin, 2nd edn., 1960.
35 D. Schepers, Diploma Thesis, Technical University of Berlin, Berlin, 1992.
36 Deutsche Einheitsverfahren zur Wasser-, Abwasser- und Schlammuntersuchung, DIN 38405, Teil 19, Bestimmung von Anionen mit Ionenchromatographie (1988); DIN 38406, Teil 3, Bestimmung von Calzium und Magnesium mit Atomabsorptionsspektrometrie (1982); Teil 13, Bestimmung von Kalium mit Flammenemissionspektrometrie (1968); Teil 14, Bestimmung von Natrium mit Flammenemissionsspektrometrie (1968), Beuth, Berlin.

Analytica Chimica Acta, 277 (1993) 113–117
Elsevier Science Publishers B.V., Amsterdam

Coulometric determination of arsenic in gallium arsenide crystal wafers

M. Cullen and J.M.P. Mearns

R&T Department, ICI Chemicals and Polymers Group, The Heath, Runcorn, Cheshire WA7 4QD (UK)

(Received 18th September 1992; revised manuscript received 30th November 1992)

Abstract

The determination of small variations in the stoichiometry of undoped, semi-insulating gallium arsenide can be achieved by using constant current coulometry. Samples taken from a wafer are etched in HF, dissolved in NaOH–peroxide solution, then treated with a citric acid buffer. To convert the arsenic to arsenic(III), sulphurous acid is added. After removal of excess SO_2, the arsenic concentration of the solution is measured by coulometric generation of iodine at a platinum electrode. The dissolution in alkaline peroxide, and the controlled pH and coordinating properties of the citrate buffer, ensure that arsenic losses are decreased to an insignificant level. This method was routinely applied to the determination of arsenic in gallium arsenide wafers and gives a reproducibility of $\pm 0.002\%$ relative.

Keywords: Coulometry; Arsenic; Crystal wafers; Gallium arsenide; Wafers

In undoped semi-insulating gallium arsenide, the impurity content and variations in stoichiometry can have a marked effect on the electrical and optical properties of the material [1–3]. Trace elemental impurities can routinely be determined by many modern analytical techniques. The measurement of stoichiometry, however, has proved to be a more difficult problem. To produce meaningful data, very small variations in gallium or arsenic ($< \pm 0.005\%$ relative) need to be measured. Of the many approaches in the measurement of stoichiometry, coulometry is unique in that if offers absolute measurements based on the Faraday as well as being capable of the very high precision required. However, careful pretreatment is necessary to prepare gallium arsenide samples prior to analysis.

Coulometry was used by Marinenko and Taylor [4] to measure accurately As_2O_3 standard reference material. The use of coulometry to measure gallium arsenide stoichiometry has been previously reported. Terashima et al. [5] reported results and related them to the material characteristics but did not describe in detail their analytical procedure. The use of EDTA by Kuramoto et al. [6] to prevent precipitation of gallium hydroxide produced errors at the end point of the arsenic titration if any excess EDTA was present. Also, significant loss of arsenic was reported during sample preparation. It has been shown that acid/peroxide digestion of arsenic materials can produce loss of arsenic [7]. Kurusu et al. [8] measured gallium by reaction with EDTA and subsequent titration of excess EDTA with electrolytically generated cadmium ions. This required an accurate assay to standardise the EDTA before it was used.

The aim of this work was to develop an analytical method for the determination of arsenic with sufficient accuracy so that it could be used rou-

Correspondence to: M. Cullen, R&T Department, ICI Chemicals and Polymers Group, The Heath, Runcorn, Cheshire WA7 4QD (UK).

tinely to measure small variations in the stoichiometry of gallium arsenide wafers. This has been achieved by using an alkaline peroxide dissolution and reduction with SO_2 in citrate buffer, and by close attention to detail in the application of the method.

EXPERIMENTAL

Equipment and reagents

Coulometry at a constant current was carried out using an Electronic Development Co. (EDC) Model 100 traceable power supply and a current threshold detector which provided a TTL signal to remotely start/stop a Marconi counter/timer. The power supply was controlled externally by computer. The end point of the coulometric titration was determined by the use of a pair of platinum electrodes with 0.15 V applied by a mV source. The current from the detector was measured by the voltage drop across a series resistor on a Kipp and Zonen chart recorder. A Cahn micro balance was used to weigh samples to ± 1 μg.

Much of the sample preparation was carried out in a 100-ml iodine flask. During the sample dissolution a funnel with a ground glass joint was used. The introduction of a small amount of water to the funnel acts as a bubble trap, gently releasing any pressure and preventing any mechanical losses due to spray. During the boiling stage to remove SO_2, a special boiling rod with a "waist" that loosely fitted the flask neck was used. This prevented "bumping" and spray losses while boiling (Fig. 1).

The coulometry was carried out under conditions similar to that used by Marinenko and Taylor [4]. Platinum generating electrodes were used. The anode and cathode chambers were separated by a Vycor glass frit, sealed using heat shrink tubing. This was found to be better than agar gel for routine use. The filling solution for the cathode compartment was 3 M sulphuric acid–0.1 M sodium sulphate.

The titration cell electrolyte was 0.5 M Na_2HPO_4–0.5 M KH_2PO_4–0.4 M KI adjusted to pH 7.0 with 20% NaOH solution. All water used

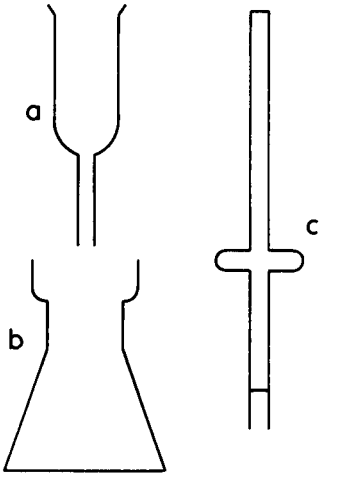

Fig. 1. (a) Bubble trap, (b) dissolution flask, (c) boiling rod.

was distilled followed by de-ionization. All chemicals used were Aristar or AnalaR grade (BDH, Poole).

Procedure

Preparing the wafer sample. A strip was cut by a scalpel from an unpolished wafer sample approximately 3–5 mm wide. This was cut into 8 equal pieces (Fig. 2). Each piece was transferred to a labelled plastic vial. The optimum weight for sample dissolution is 55 ± 5 mg.

HF etch. Each sample was washed in 2 ml of 40% HF for 30 s to remove any oxides from the surface. Then washed with water followed by methanol and dried with a nitrogen purge. Each

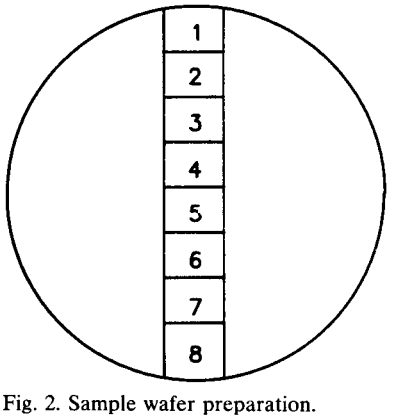

Fig. 2. Sample wafer preparation.

sample was weighed immediately to ± 1 μg and transferred to the dissolution flasks.

Sample dissolution. To each flask was added 1 ml of 20% NaOH and 1 ml of 30% H_2O_2. Then a wetted bubble trap funnel containing a small amount of water was placed on each flask and the flask set at an angle of about 45°. After 15 min a further 0.5 ml of 30% H_2O_2 was added. Complete dissolution normally occurred in about 25 min. If not, 0.2 ml of 30% H_2O_2 was added and the solution left for a further 10 min.

Removal of excess H_2O_2. 25 ml of 14% sodium sulphite solution was added and the flask put on a water bath at 70°C for 20 min, then cooled to room temperature.

Reduction of As(V) to As(III). 10 ml of 20% citric acid solution was added followed by 8.3 ml of 3 M H_2SO_4. Then the flask was cooled to about 4°C. 7 ml of SO_2 water (prepared by bubbling SO_2 gas through water until saturated) was added and flasks loosely stoppered. The solutions were then left at room temperature for a minimum of 12 h (e.g., overnight).

Removal of SO_2. A "waisted" boiling rod was added to each flask and the solution gently boiled. After 20 min most of the SO_2 was removed. At regular intervals the vapour above the flask was tested with a small piece of blue litmus paper held in tweezers until no colour change was observed. If any SO_2 could still be detected after boiling for 40 min the sample was discarded. The flask was cooled and the boiling rod washed down and removed. 2 ml of 40% formaldehyde solution was added and the solution neutralised using 20% NaOH solution.

Sample titration. 100 ml of phosphate buffer was added to the cell and titrated at 0.3 mA under a nitrogen purge until iodine has been in excess for 60 s. This was the blank excess titration. The sample solution was then transferred to the cell via a siphon using a nitrogen purge and washed in with water. This was titrated at 100 mA until about 98% had reacted. This work used a computer to control the power supply and calculate the time interval based on the sample weight (assuming 1 : 1 stoichiometry). The solution was then titrated at 0.3 mA to record the end point. This technique of 0.3 mA end point run and 100 mA bulk titration gives high resolution at the end point and a reasonably short total titration time.

From the recorded time intervals and currents, including the blank excess, the total amount of iodine used to react with the sample was calculated. From this and the sample weight the arsenic concentration (%, w/w) was calculated.

The titration was repeated for each of the eight sample segments using a fresh cell solution for each run. From this, the mean arsenic value, a standard deviation for the wafer and any variation in stoichiometry could be obtained.

TABLE 1

Determination of NBS As_2O_3 standard 83d (99.9926 $\pm$0.0030% As_2O_3)

Run No.	% (w/w) As_2O_3
1	99.995
2	99.993
3	99.991
4	99.985
5	99.996
6	99.993
7	99.990
8	99.995
9	99.995
10	99.989
Mean	99.992
S.D.	0.003

RESULTS AND DISCUSSION

The accuracy of the method was confirmed by using NBS standard reference material 83d As_2O_3 (Table 1). It was found during the course of this work that some samples of gallium arsenide gave more reproducible results than the As_2O_3. This may be because the As_2O_3 was not homogeneous and also that as a fine powder it was more difficult to weigh and transfer than segments of gallium arsenide.

HF washing of the gallium arsenide samples prior to weighing is important in order to remove any surface oxide layer. Also, the sample must be of a defined size and weight for the dissolution to be successful using the given quantities of

TABLE 2

Typical result of gallium arsenide wafer determination (Ingot JMPM/File42)

Segment No.	% (w/w) As
1	51.798
2	51.798
3	51.797
4	51.799
5	51.799
6	51.799
7	51.798
8	51.799
Mean	51.798
S.D.	0.001

NaOH–peroxide. The described conditions were found to give a complete dissolution without the reaction being too vigorous.

The addition of citrate not only prevented gallium precipitation during the titration, but also provided pH buffered conditions during removal of SO_2. It was found during the early stages of the development of this method that the control of pH was important when boiling the sample solution. If the solution was too acidic (pH < 1) arsenic could be lost. If the solution was insufficiently acidic (pH > 3.5) incomplete removal of SO_2 occurred. Determinations on As_2O_3 taken through the procedure of peroxide oxidation, sulphurous acid reduction, boiling to remove SO_2 and subsequent iodine titration gave an accurate recovery of arsenic when citrate was used as described in this method.

By taking sections across the diameter of a wafer and individually analyzing them local areas of non-stoichiometry could be identified. In order for this to be possible each measurement needed to be completely reliable, a difficult task as so much manipulation is involved in the course of the sample preparation. For the method to be successful, meticulous attention to detail was necessary. Careful manipulation and addition of reagents, along with the design of decomposition flask, bubble trap funnel, and boiling rod, combine to produce an accurate and precise method.

Samples of gallium arsenide were routinely repeated over the course of many months to assess if there were any long term changes in the results produced by this method. It was found that samples were repeatable to within ±0.001% (w/w) As. A typical result of a gallium arsenide wafer analysis is given in Table 2.

Samples of gallium arsenide crystals produced from varying melt compositions were analyzed by this method and any variations in the wafer stoichiometry determined. From the results of this work, it was shown that melt composition and other changes in growth conditions affected the mean stoichiometry of wafers and that the method described here could resolve variations in stoichiometry across the diameter of a wafer. In general, the standard deviation for the eight measurements taken per wafer was ±0.001% (w/w) As (±0.002% relative).

Occasionally samples from "unusual" growth conditions were analyzed. These sometimes gave rise to relatively large variations in arsenic concentration across the wafer and down the length of an ingot. This shows up as higher values of standard deviation on the mean wafer arsenic result (Table 3). "Ingot C" illustrates this effect and wafers analyzed from this ingot were found to be gallium rich near the edges.

This analytical method has been used on a regular basis to check the quality of ingots and

TABLE 3

Variation in mean %As of gallium arsenide wafers produced from normal and unusual growth conditions

Ingot	%As	S.D. [a] (%)	Comments
A	51.799	0.001	"Normal" growth
B	51.801	0.003	As rich melt
C	51.797	0.007	Single growth became polycrystalline as growth progressed Wafer edges gallium rich

[a] $n = 8$.

wafers produced during routine gallium arsenide manufacture.

The authors are grateful to ICI Wafer Technology for their support during this work.

REFERENCES

1 D.E. Holmes, R.T. Chen, K.R. Elliott and C.G. Kirkpatrick, Appl. Phys. Lett., 40 (1982) 46.
2 L.B. Ta, H.M. Hobgood, A. Rohatgi and R.N. Thomas, J. Appl. Phys., 53 (1982) 5771.
3 T. Sato, K. Terashima, H. Emori, S. Ozawa, M. Nakajima, T. Fukuda and K. Ishida, Jpn. J. Appl. Phys., 24 (1985) L488.
4 G. Marinenko and J.K. Taylor, Anal. Chem., 39 (1967) 1568.
5 K. Terashima, J. Nishio, A. Okada, S. Washizuka and M. Watanabe, J. Crystal Growth, 79 (1986) 463.
6 K. Kuramoto, T. Sato and K. Ishida, J. Electrochem. Soc., 134 (1987) 1286.
7 R. Bock, A Handbook of Decomposition Methods in Analytical Chemistry, International Textbook Company, 1979.
8 K. Kurusu, Y. Suzuki and H. Takami, J. Electrochem. Soc., 136 (1989) 1450.

Analytica Chimica Acta, 277 (1993) 119–135
Elsevier Science Publishers B.V., Amsterdam

Simultaneous determination of equivalence volumes and thermodynamic acid dissociation constants from data for the acidic region of potentiometric titration curves

G. Papanastasiou, I. Ziogas and G. Kokkinidis

Laboratory of Physical Chemistry, Department of Chemistry, Faculty of Sciences, University of Thessaloniki, 540–06 Thessaloniki (Greece)

(Received 25th August 1992; revised manuscript received 2nd December 1992)

Abstract

New iterative methods for the analysis of potentiometric titration data of weak monoprotic acids or of mixtures of two monoprotic acids are presented. These methods, using equations without approximations and data exclusively resulting from the acidic region of the titration curve, seem to be valid throughout the acidic strength range. In the titration of weak monoprotic acids, the proposed procedures are able to extract accurate values of the equivalence volume and also the thermodynamic dissociation constant. On the other hand, in the titration of mixtures of two monoprotic acids, the proposed approach is able to extract accurate values of the concentrations and the thermodynamic dissociation constants of the component acids even when their acidity strengths are similar. The test of the proposed procedures by means of ideal simulated data (free from any extraneous "noise") and Monte Carlo simulated data revealed that these methods are fairly applicable even when the titration data are considerably obscured by "noise". Further, for acids having $pK \geqslant 4$ the proposed procedures lead to accurate results even when the pH data contain an important systematic error. The proposed procedures were also successfully applied to experimental titration data for weak acids. A procedure for the analysis of titration data carried out in binary water–dimethylformamide solvent systems is also presented.

Keywords: Potentiometry; Titrimetry; Acid dissociation constants; Equivalence volumes; pH

This paper is part of continuing series on studies of the ionization of several mono- and polyprotic acids in various water–organic solvent systems with special reference to acid strength as a function of the solvent composition and the structure of the acid molecule [1–6]. An attempt has been made to extend the studies to binary water–dimethylformamide (DMF) solvent systems, these mixtures being suitable media for acid–base titrations [7].

To determine the thermodynamic acid dissociation constant, it is obviously necessary to know with sufficient accuracy the analytical concentration of the corresponding acid, a quantity which is usually determined by potentiometric titrations. However, preliminary potentiometric titrations with a glass electrode in water–DMF mixtures (especially with high contents of DMF) showed that the titration curves of various weak acids do not present a pronounced vertical portion corresponding to the end-point of the neutralization. On the other hand, the existence of multiple peaks in the immediate vicinity of the equivalence point of the differential titration curves introduces an uncertainty in the choice of the exact value of the equivalence volume (see Fig. 4). This behaviour could be attributed on two facts. First, the process of obtaining derivatives

Correspondence to: G. Papanastasiou, Laboratory of Physical Chemistry, Department of Chemistry, Faculty of Sciences, University of Thessaloniki, 540-06 Thessaloniki (Greece).

from experimental data usually results in a considerable decrease in accuracy [8]. Second, in the neighbourhood of the equivalence point the response of the glass–calomel electrode couple was slower than that observed in the buffer region of the same titration curve. Hence, in such solvent mixtures, it is very difficult to locate the end-point of the titration and to determine (or check) the accurate value of the analytical concentration of the acid concerned. In addition, in some instances of very weak acids, because of the contribution of the hydrolysis of the salt formed, the equivalence volume does not coincide with the inflection point of the titration curve; the difference is greater the weaker is the acid [9,10].

In an attempt to overcome these difficulties a new iterative technique was developed that permits the simultaneous determination of the thermodynamic constant and the equivalence volume of weak acids. This method, using equations derived here without approximations and data exclusively resulting from the buffer region of a titration curve, seems to be valid throughout the acidic strength range.

It should be noted that many methods have been devised for the determination of equivalence volumes from potentiometric acid–base titrations [11–18]. The more recent approaches use equations derived from the appropriate mass balance and equilibrium expressions. However, these equations are valid under conditions of constant ionic strength. Hence, the activity coefficients are not explicitly included in these equations, so it is not possible to derive from these approaches accurate thermodynamic constants of the examined acids.

However, it is considered that the determination of the accurate values of the thermodynamic dissociation constants, apart from its theoretical and analytical interest, provides information supporting the identification of the titrated acids.

EXPERIMENTAL

Conductivity water (conductance = 1.0×10^{-6} Ω^{-1} cm^{-1}) was used throughout. *N*,*N*-Dimethylformamide (Fluka, puriss., > 99%) was purified by vacuum distilation[19]; the middle fraction, comprising about 75%, was retained and stored over 3A molecular sieves. Analytical-reagent grade acids (Fluka, puriss. p.a., > 99.5%) were used without further purification; their purity was checked by potentiometric titrations. All sodium hydroxide solutions were prepared from stock solutions of known concentration (Merck, Titrisol). A nitrogen atmosphere was maintained above these solutions to avoid any contact with atmospheric carbon dioxide. In all titrations, the titrant was added to the working solution from a Metrhom piston burette (Dosimat) with a readability of 0.005 ml. All pH measurements were made by using the following cell:

glass electrode | working solution || concentrated KCl solution (aq.) || concentrated KCl solution (aq.) | Hg_2Cl_2, Hg

In order to avoid any influence of the measured solution of the working solution on the reversible potential of the calomel electrode, a sleeved electrode was used. For this purpose, a glass tube of slightly greater diameter was fitted over the calomel electrode, terminating in a small fritted-glass disc. The sleeve was filled with a concentrated aqueous solution of KCl. The electrode pair (Beckman, Type E-2, glass electrode–Ingold, Type 303-NS-EK, saturated calomel electrode) was connected to a Beckman Research pH meter, with a readability of 0.001 pH unit. Temperature was controlled at 25 ± 0.01°C and a nitrogen atmosphere was maintained above the working solution.

The electrode system was standardized against the aqueous buffer solutions recommended by the National Bureau of Standards [20]. Hence, the measured pH value of a solution is identified very closely with the conventional value of $-\log \alpha_H$ (where α_H is the corresponding hydrogen ion activity), provided that the total ionic strength is not greater than 0.1 and the pH is between 2.5 and 11.5 [21]. The glass electrode was confirmed to have a Nernstian pH response. However, with DMF–water mixtures, in order to determine the hydrogen ion activity referred to the standard state in the corresponding medium, the pH meter readings were corrected by a method reported previously [7].

POTENTIOMETRIC TITRATION OF WEAK MONOPROTIC ACIDS WITH STRONG BASES

Theoretical

Consider a volume V_o of any weak monoprotic acid HA of initial concentration C_o, which is titrated with a strong base MOH of concentration C_B. Assuming that all singly charged ions have the same activity coefficient y_1 and that the activity coefficients of uncharged species are unity, the thermodynamic acid constant of HA is given by

$$K_a = \frac{\alpha_H[A^-]y_1}{[HA]} \quad (1)$$

At any point on the buffer region of the titration curve the mass and charge balance are expressed by the equations

$$C = [HA] + [A^-] \quad (2)$$

$$[H^+] + [M^+] = [A^-] + [OH^-] \quad (3)$$

where the concentrations C and $[M^+]$ can be determined from the equations

$$C = \frac{C_B V_e}{V_o + V} = b_N C_B V_e \text{ and}$$

$$[M^+] = \frac{C_B V}{V_o + V} = b_N C_B V \quad (4)$$

where V is the volume of the added titrant, V_e the equivalence volume and $b_N = 1/(V_o + V)$.

Combining these equations and rearranging gives

$$\alpha_H\left(b_N C_B V y_1 + \alpha_H - \frac{K_w}{\alpha_H}\right) = K_a\left[b_N C_B(V_e - V) - \frac{\alpha_H}{y_1} + \frac{K_w}{\alpha_H y_1}\right] \quad (5)$$

where K_w is the autoprotolysis constant of the solvent used. For dilute solutions ($I < 0.1$ M) the activity coefficient y_1 can be calculated from the Debye–Hückel equation:

$$\log y_1 = -A\sqrt{I}/(1 + B\mathring{a}\sqrt{I}) \quad (6)$$

where A and B are constants, the values of which depend on the physical properties of the medium [22], I is the ionic strength of the solution and $\mathring{a}$ the distance of closest approach of the ions. In principle, $\mathring{a}$ is a function of the solvent and electrolyte, but in practice it is traditionally taken to be equal to 5 Å [23–25]. The ionic strength, at any point of the titration curve, is given by [1,23]

$$I = [M^+] + [H^+] = b_N C_B V + [H^+] \quad (7)$$

To determine y_1, it is obviously necessary to know the value of $[H^+] = \alpha_H/y_1$ and vice versa. The values of $[H^+]$ and y_1 may be obtained from the measured value of α_H by successive approximations [26]. Assuming first $y_1 = 1$, so that $\alpha_H = [H^+]$, it is possible to calculate I from Eqn. 7, and hence y_1 from Eqn. 6. This new value of y_1 can be used to refine the values of $[H^+]$, I and y_1. All these operations are repeated until y_1 converges (the criterion here being less than 0.00001 difference in I, between two subsequent cycles).

It is noted that Eqn. 5, including the thermodynamic dissociation constant of the titrated acid, is also valid under conditions of varying ionic strength during the titration. Equation 5 has the form

$$Y = K_a X \quad (8)$$

This equation predicts a linear relationship between Y and X with a gradient equal to K_a. Alternatively, the experimental confirmation of such a correlation, using V and pH data, supports the assumption that the titrated acid is monoprotic. Then, the thermodynamic acidity constant K_a can be deduced, by linear regression, from the slope of the corresponding straight line.

However, there is no way in which, without prior knowledge of V_e, the Y vs. X data can be plotted to give a linear graph. This is possible with the iterative method proposed in this investigation.

Iterative method for the determination of V_e and K_a

This method is based on the main principles of previously proposed procedures that have been successfully used for the determination of the rate constants of various chemical and electrochemical reactions [27–30].

It is assumed first that the value of V_e lies in an interval (a,b). Choosing arbitrarily from this

interval a value for V_e, it is possible to trace, by means of the experimental V and pH data, the curve $Y=f(X)$. This will approach a straight line to the extent where the chosen value of V_e also approaches the exact value of the equivalence volume. Hence, the best linearity that could be obtained, by means of the available experimental data, evidently corresponds to the best approximation to the exact value of the equivalence volume. Therefore, by seeking within the interval (a,b) the V_e value, it is possible to trace N curves $Y=f(X)$, N being the number of V_e values taken for these calculations. For each of these curves, the calculation of the square of the correlation coefficient, R^2, permits a comparison of the linearity of various $Y=f(X)$ plots and the curve $R^2=f(V_e)$ to be traced. This curve is expected to present a pronounced maximum at a value of V_e equal to V_e^{max}, which can be considered as the best approximation to the exact value of the equivalence volume. The slope of the straight line corresponding to V_e^{max}, is the best approximation to the exact value of K_a.

It is noted that this iterative procedure is a general method that can be applied, as will be seen below, even to more complicated titrations (e.g. mixtures of two acids). However, in the case of the titration of a monoprotic weak acid, V_e and K_a can be more easily determined by the following graphical method.

Graphical method for the determination of V_e and K_a

Equation 5 can be rewritten as

$$y = V_e - \frac{1}{K_a} \cdot x \tag{9}$$

where

$$y = V + \frac{1}{y_1 C_B b_N}\left(\alpha_H - \frac{K_w}{\alpha_H}\right) \tag{10}$$

and

$$x = \alpha_H\left(y_1 V + \frac{\alpha_H}{C_B b_N} - \frac{K_w}{\alpha_H C_B b_N}\right) \tag{11}$$

In this treatment, it is possible to calculate y and x directly from the experimental data resulting from the acidic region of the titration curve, and to determine V_e and K_a by linear regression from the coefficients of Eqn. 9.

It is noted that an analogous graphical procedure has been proposed by Johanson [15]. However, that approach was focused on the determination of V_e rather than K_a. Indeed, in Johanson's method the proposed equation, including the apparent dissociation constant of the titrated acid, is valid under conditions where the ionic strength remains constant during the titration. This condition is normally fulfilled by addition of a neutral salt in a sufficient amount. Hence, apparent dissociation constants derived from this method are not free from a possible salt effect. On the other hand, it is difficult to derive from these constants the accurate thermodynamic values; the usually used Debye–Hückel equation, for the calculation of activity coefficients, is not valid at such ionic strengths.

To establish the reliability of the proposed procedures, it must first be shown that they actually work by comparison with a system where the answer is already known. Experimentally, this implies that the proposed approaches, applied to an already reported system, give a reasonable (or even better) precision on the extraction of the sought parameters. In this respect, it was considered necessary to test the proposed methods first with simulated data corresponding to various values of pK_a and second to experimental data resulting from titrations of weak acids (of known pK_a) with strong bases.

Application of the methods using simulated data

Simulated V and pH ($pH = -\log \alpha_H$) data were derived by solving Eqn. 5 using the so-called secant method [31]. In all these calculations it was assumed that $V_o = 50$ ml, $V_e = 5.00$ ml, $C_B = 0.1$ M, $T = 298.15$ K and $pK_w = 14.0$.

First the titration of an acid with $pK_a = 4.80$ was considered. This value represents the mean pK_a value of the lower members of the series of aliphatic monocarboxylic acids [22,23]. The results obtained are reported in Table 1. Taking into account that the NBS buffer solutions used for the standardization of the pH meters are given to three decimal figures at most, the simu-

TABLE 1

Ideal and Monte Carlo (M-C) pH values of the titration of an acid with a strong base ($pK_a = 4.8$, $V_o = 50$ ml, $V_e = 5.00$ ml, $C_B = 0.1$ M, $T = 298.15$ K and $pK_w = 14.0$)

V	pH		V	pH		V	pH	
	Ideal [a]	M-C [b]		Ideal [a]	M-C [b]		Ideal [a]	M-C [b]
1.0	4.195	4.195	2.1	4.635	4.641	3.2	5.017	5.024
1.1	4.243	4.236	2.2	4.670	4.670	3.3	5.055	5.058
1.2	4.289	4.300	2.3	4.704	4.712	3.4	5.093	5.088
1.3	4.333	4.336	2.4	4.738	4.733	3.5	5.133	5.132
1.4	4.375	4.366	2.5	4.772	4.772	3.6	5.175	5.175
1.5	4.415	4.416	2.6	4.806	4.800	3.7	5.219	5.222
1.6	4.454	4.450	2.7	4.840	4.838	3.8	5.265	5.265
1.7	4.492	4.501	2.8	4.874	4.868	3.9	5.313	5.315
1.8	4.529	4.521	2.9	4.909	4.906	4.0	5.365	5.368
1.9	4.565	4.570	3.0	4.944	4.948			
2.0	4.600	4.606	3.1	4.980	4.992			

[a] Values that exactly fit Eqn. 5. [b] Mean values of four normally distributed deviates generated from the ideal data with standard deviation equal to 0.01 pH unit.

lated pH values were rounded to three decimal places. It is now examined whether it is possible, using these data and by means of the proposed methods, to extract the values $pK_a = 4.80$ and $V_e = 5.00$ ml.

In a first attempt the proposed iterative method was applied. The variation of R^2 with V_e is presented graphically in Fig. 1. It can be seen that the curve $R^2 = f(V_e)$ presents a pronounced maximum. Further, in the vicinity of the maximum ($4.9 \leqslant V_e \leqslant 5.1$), it was found that this curve can be perfectly fitted, by a least-squares analysis,

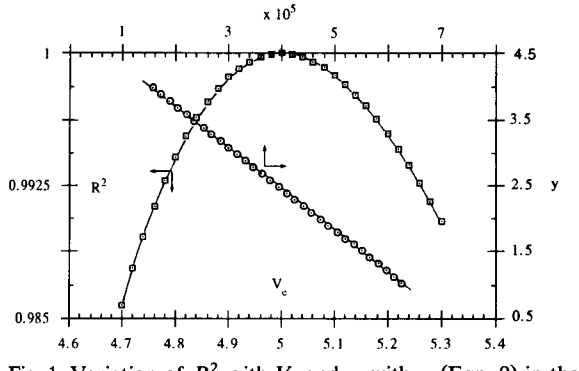

Fig. 1. Variation of R^2 with V_e and y with x (Eqn. 9) in the case of the simulated titration of 50 ml of 0.01 M acid ($pK_a = 4.80$) with 0.1 M NaOH at 25°C.

to the following polynomial (the square of the correlation coefficient was very close to unity):

$$R^2 = \sum_{n=0}^{4} A_n V_e^n$$
$$= -8.4884 + 4.0513 V_e - 0.28140\, V_e^2 - 6.9957 \times 10^{-2}\, V_e^3 + 8.0183 \times 10^{-3}\, V_e^4 \quad (12)$$

Consequently, the exact value of V_e at which R^2 reaches a maximum value can be determined from the solution of the following equation:

$$\frac{dR^2}{dV_e} = \sum_{n=0}^{4} n A_n V_e^{n-1}$$
$$= A_1 + 2A_2 V_e + 3A_3 V_e^2 + 4A_4 V_e^3 = 0 \quad (13)$$

From Eqn. 13 one obtains $V_e = 4.9988$ ml, which almost coincides with the theoretical value of the equivalence volume. The corresponding slope to this value of the straight line $Y = f(X)$ is equal to 1.5857×10^{-5} ($pK_a = 4.7998$). The very modest deviations between the theoretical and the determined values of V_e and pK_a, equal to 0.024% and 0.0042%, respectively, are due to the fact that the simulated pH data have been rounded to three decimal places.

In a second attempt, the graphical method was applied. In accordance with Eqn. 9, it was found that the plot of y vs. x was perfectly linear; the square of the correlation coefficient was very close to unity (Fig. 1). The following relationship was found:

$$y = (4.9988 \pm 0.0009) - (63.0629 \pm 0.0209) \times 10^3 x \quad (14)$$

where the standard deviations of the coefficients of the above regression equation have been evaluated by appropriate equations [32]. Comparison of this equation with Eqn. 9 leads to the values $V_e = 4.9988 \pm 0.0009$ and $pK_a = 4.7998 \pm 0.0001$. It is evident that the two proposed methods give identical results.

In an attempt to generalize the conclusions concerning the applicability of the proposed methods, these procedures were also applied to various simulated titration curves corresponding

to different pK_a values ($1.8 \leq pK_a \leq 6$). In all instances simulated data lying in the 20–80% neutralization range of the titration curve were used. The results obtained showed that the proposed methods reach the desired values of V_e and pK_a with fair accuracy.

The examples studied previously showed that the proposed approaches are able to extract V_e and pK_a values in the particular case where the V and pH data used, resulting from the buffer region of a titration curve, are free from experimental errors.

However, of more experimental interest is the question of how well the proposed techniques are able to cope with data containing random extraneous contributions, such as annoying experimental "noise". To investigate this, a Monte Carlo technique was used, which has been detailed in a previous paper [29] and need not be repeated here. The main idea of this procedure is based on the observation that, often, random experimental errors closely follow a Gaussian (or normal) distribution. Thus, at each point (V_i and pH_i) of the theoretical titration curve $pH = f(V)$, a number N of normally distributed random variables $pH_{i,j}$ with mean pH_i and standard deviation S_i were produced. At the experimental level, this implies the realization of N titrations with a precision equal to S_i. Using this technique, as an example, the titration of an acid with $pK_a = 4.80$ was again treated. In this treatment it was assumed that S_i is equal to 0.01 pH unit. At each volume V_i, four values $pH_{i,j}$ were created and the results were

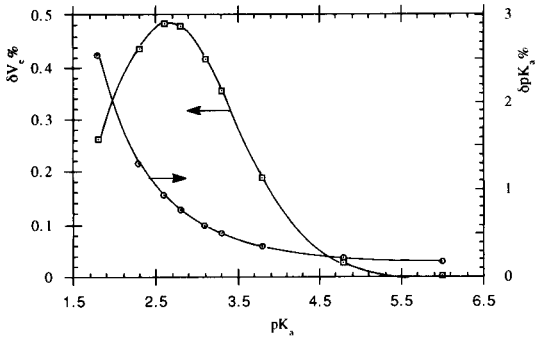

Fig. 2. Systematic titration errors in V_e and pK_a values resulting from a systematic deviation $\delta pH = 0.01$ in the pH values as a function of the strength of the titrated acid.

averaged. The mean values $\overline{pH}_{i,j}$ are summarized in Table 1. Evidently, these values would coincide with the corresponding pH_i values only in the case where the number N of the produced random variables $pH_{i,j}$ tended to infinity. Using these Monte Carlo $\overline{pH}_{i,j}$ data, both the proposed methods give the values $V_e = 4.9878$ and $pK_a = 4.7986$. These results are within 0.24% and 0.03%, respectively, of their true magnitudes. Evidently the proposed techniques are able to extract V_e and pK_a values, even when the pH data are considerably obscured by noise. However, these results can be improved by the following procedure, which is often used in the treatment of experimental data containing random errors. Thus, the $\overline{pH}_{i,j}$ values can be smoothed by means of a polynomial relating $\overline{pH}_{i,j}$ with V. In the case of the example treated here, it was found that the variation of $\overline{pH}_{i,j}$ with V can be perfectly fitted, by a least-squares analysis, to the following polynomial ($R^2 = 0.99973$):

$$\overline{pH}_{i,j} = 3.4649 + 1.0542V - 0.4453\,V^2 + 0.1435\,V^3 - 0.0252\,V^4 + 0.0020\,V^5 \quad (15)$$

Using smoothed data, calculated from Eqn. 15, one obtains by means of the proposed methods $V_e = 4.992$ and $pK_a = 4.799$. The agreement of these values with their true magnitudes is excellent.

Finally, the proposed methods were applied to various simulated titration curves, corresponding to different pK_a values, where the pH data contained a systematic error equal to 0.01 pH unit. Experimentally such errors are usually introduced by an erroneous standardization of the pH meter assembly. A systematic error in the pH values gives rise to systematic titration errors δV_e and δpK_a in the values of V_e and pK_a determined by

$$\delta V_e(\%) = \frac{V_{e/id} - V_{e/syst}}{V_{e/id}} \times 100 \quad (16)$$

$$\delta pK_a(\%) = \frac{pK_{a/id} - pK_{a/syst}}{pK_{a/id}} \times 100 \quad (17)$$

where $V_{e/id}$, $pK_{a/id}$, $V_{e/syst}$ and $pK_{a/syst}$ are the values of V_e and pK_a determined respectively

from ideal simulated data (rounded to three decimal places) and data containing a systematic error δpH in the pH values. These titration errors as a function of pK_a of the corresponding acid are given in Fig. 2.

Figure 2 shows that the titration errors δV_e and δpK_a, at constant δpH, are dependent on the strength of the acid that is being titrated. Also, it results from Fig. 2 that the titration error δV_e reaches a maximum value at the immediate vicinity of the pK_a value equal to 2.60. However, in all instances examined here, δV_e is less than 0.5%. Hence the proposed techniques are able to extract a value of V_e containing only a modest error, even when the pH data are obscured by an important systematic error $\delta pH = 0.01$ (about 5–10 times greater than the accuracy of a precision instrument).

It is noted that an analogous behaviour is observed when Hofstee's method is used to determine equivalence volumes of acids of varying acid strength [16].

The titration error in the pK_a value decreases as pK_a increases. For moderately strong acids (with $pK_a < 2.5$) this error takes values greater than 1.0%. In contrast, for acids with $pK_a \approx 4.8$ (such as the lower members of the series of aliphatic monocarboxylic acids) this error takes values equal to ca. 0.2%. For such acids the proposed techniques are able to extract the values V_e and pK_a with only a modest error ($\delta V_e \approx$ 0.03% and $\delta pK_a \approx 0.2\%$), even when the pH data contain an important systematic error δpH = 0.01. Finally, for acids with $pK_a > 3.8$, it can be shown that the titration error in the pK_a value is approximately equal to the error δpH in the pH values.

Application of the methods using experimental data

The very positive tests concerning the applicability of the iterative method using simulated data encouraged us to test this methodology on experimental data. For this purpose, two solutions of formic acid ($pK_a = 3.752$ at 25°C [22,23]) and propionic acid ($pK_a = 4.874$ at 25°C [22,23]) were prepared. Their exact concentrations, 0.01050 and 0.01029 M, respectively, were determined from at

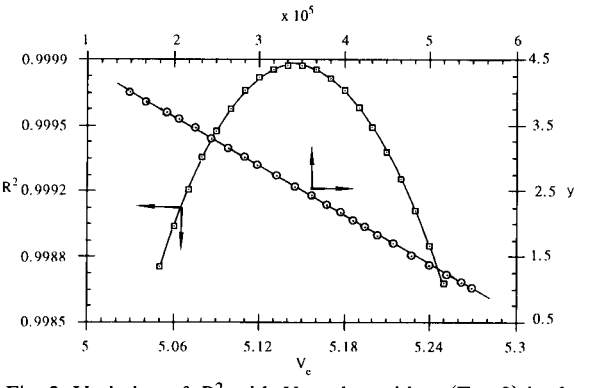

Fig. 3. Variation of R^2 with V_e and y with x (Eqn.9) in the case of the experimental titration of 50 ml of 0.01029 M propionic acid with 0.1 M NaOH at 25°C.

least five potentiometric titrations. For each of these solutions, a volume of 50 ml was titrated with 0.100 M NaOH. The measurements obtained, lying in the 20–80% neutralization range of the corresponding titration curve, are given in Table 2. As shown by the example in Fig. 3, the application of the iterative method revealed that the curves $R^2 = f(V_e)$ presented a very pronounced maximum. In both acids, it was found that these curves can be perfectly fitted, by a least-squares analysis, to a polynomial form of equation, the square of the correlation coefficient being very close to unity.

Thus, for formic acid the following polynomial was found ($5.15 \leqslant V_e \leqslant 5.35$):

$$R^2 = \sum_{n=0}^{5} A_n V_e^n$$

$$= -1.2769 - 0.82119 V_e + 0.66564\ V_e^2 - 6.6993 \times 10^{-2}\ V_e^3 - 9.2515 \times 10^{-3}\ V_e^4 + 1.2445 \times 10^{-3}\ V_e^5 \quad (18)$$

One obtains from this equation, as described previously, $V_e = 5.254$ ml ($C_o = 0.01051$ M). The corresponding gradient to this value of Eqn. 8 is equal to 1.7959×10^{-4} ($pK_a = 3.746$). It is noted that the corresponding titration curve presented a pronounced inflection in the vicinity of $V = 5.25$ ml.

For propionic acid the following polynomial was found ($5.05 \leqslant V_e \leqslant 5.25$):

$$R^2 = \sum_{n=0}^{5} A_n V_e^n$$
$$= -1.0068 - 0.73083 V_e + 0.60308\ V_e^2 - 6.0687 \times 10^{-2}\ V_e^3 - 8.9738 \times 10^{-3}\ V_e^4 + 1.2082 \times 10^{-3}\ V_e^5 \quad (19)$$

One obtains from this equation $V_e = 5.145$ ml ($C_o = 0.01029$ M). The corresponding gradient to this value of Eqn. 8 is equal to 1.3360×10^{-5} ($pK_a = 4.874$). It is noted that the corresponding titration curve presented a pronounced inflection in the immediate vicinity of $V = 5.15$ ml.

Also, the analysis of the experimental data in Table 2 by means of the graphical method revealed that the plots of y vs. x were perfectly linear, as shown by the example in Fig. 3. The following linear relationships (where the corresponding linear correlation coefficient was very close to unity) were found:

For formic acid:

$$y = (5.254 \pm 0.005) - [(5.5682 \pm 0.0109) \times 10^3]x \quad (20)$$

for propionic acid:

$$y = (5.144 \pm 0.007) - [(74.8359 \pm 0.192) \times 10^3]x \quad (21)$$

The comparison of these equations with Eqn. 9 leads to the following values: for formic acid, $V_e = 5.254 \pm 0.005$ ($C_o = 0.01051$ M) and $pK_a = 3.746 \pm 0.002$; and for propionic acid, $V_e = 5.144 \pm 0.007$ ($C_o = 0.01029$ M) and $pK_a = 4.874 \pm 0.003$.

The equivalence volumes of the examples treated here, determined by means of the proposed techniques, are in excellent agreement with the corresponding values determined by traditional potentiometric titrations. On the other hand, the determined values of pK_a virtually coincide with those reported in the literature [22,23].

As pointed in the Introduction it is very difficult to determine, by traditional potentiometric titrations, the accurate value of the analytical concentration of weak acids in DMF–water solvent mixtures (see Fig. 4). Consequently, the successful application of the proposed methods to such mixtures is of great interest. For this purpose, a stock solution of 0.1048 M *n*-butanoic acid in water was prepared; its concentration was checked by potentiometric titration. A working solution of 0.01048 M in DMF–water (1 + 1, v/v) was prepared by diluting the stock solution. The dielectric constant of this mixture, equal to 65.65, has been determined previously [7]. A volume of 50 ml was titrated with 0.100 M sodium hydroxide solution also prepared in the appropriate mixed solvent. The measurements obtained are given in Table 2. The determination of V_e and pK_a, by means of the proposed methods, requires of course an estimate of the term K_w/α_H (see Eqns. 5 and 10), where K_w is the autoprotolysis constant of the mixed solvent. This constant can be determined by a procedure described previously [6], using titration data lying beyond the equivalence point. However, the determination of K_w requires a knowledge of the values of K_a and V_e and vice versa. Generally, for acidic aqueous solutions the term K_w/α_H can be neglected [26], but for mixed solvents with a high content of organic solvent it is not evident that this condition is fulfilled. For this reason the following procedure of successive approximations was applied: assuming first $pK_w = 100$, so that $K_w/\alpha_H \approx 0$, it is possible to evaluate V_e and pK_a by treating the data of the buffer region of the

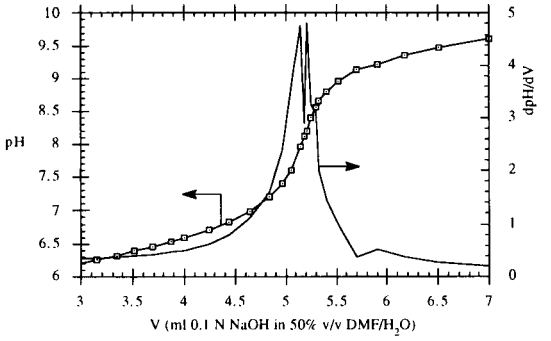

Fig. 4. Titration and differential titration curve of 50 ml of 0.01048 M *n*-butanoic acid with 0.1 M NaOH in DMF–water (1 + 1, v/v) at 25°C.

TABLE 2

Experimental titration data for formic acid ($C_o = 0.0105$ M) and propionic acid ($C_o = 0.0103$ M) in aqueous solutions and *n*-butanoic acid ($C_o = 0.0105$ M) in DMF–water (1+1, v/v) ($V_o = 50$ ml, $C_B = 0.1$ M, $T = 298.15$ K)

Formic acid		Propionic acid		*n*-Butanoic acid	
V	pH	*V*	pH	*V*	pH
1.00	3.243	1.01	4.256	1.02	5.481
1.14	3.289	1.10	4.300	1.15	5.546
1.29	3.337	1.22	4.355	1.35	5.631
1.41	3.375	1.36	4.418	1.54	5.706
1.53	3.415	1.53	4.484	1.71	5.770
1.68	3.462	1.71	4.550	1.88	5.830
1.80	3.497	1.83	4.595	2.06	5.894
2.00	3.558	1.97	4.641	2.21	5.942
2.12	3.593	2.07	4.676	2.38	5.999
2.23	3.627	2.18	4.714	2.59	6.066
2.35	3.665	2.30	4.753	2.80	6.137
2.50	3.708	2.44	4.799	2.98	6.196
2.64	3.752	2.59	4.848	3.15	6.255
2.81	3.801	2.74	4.900	3.34	6.320
2.93	3.839	2.91	4.957	3.51	6.383
3.05	3.877	3.03	4.998	3.69	6.452
3.19	3.921	3.17	5.046	3.87	6.527
3.33	3.970	3.31	5.098	4.00	6.589
3.45	4.011	3.46	5.151		
3.61	4.072	3.60	5.207	*Values after* V_e	
3.74	4.120	3.70	5.248	5.91	9.217
3.86	4.168	3.87	5.324	6.17	9.354
4.00	4.228	4.01	5.390	6.51	9.482
				7.00	9.615
				7.50	9.718
				8.00	9.794
				8.50	9.867
				9.00	9.921
				9.50	9.968
				10.00	10.015

titration curve. These values serve as a basis for the determination of the first approximation of K_w, by means of a method reported previously [6] and titration data after the equivalence point. All these operations are repeated until V_e, pK_a and pK_w converge.

However, it remains open to question whether this method actually converges to the desired values of V_e, pK_a and pK_w, even in the case where one starts from very different trial values of pK_w. To investigate this, the procedure was applied successively using ${}^{o}pK_w$ (initial estimate of pK_w) values of 10, 14, 100. The obtained sequences $\{{}^{n}V_e\}$, $\{{}^{n}pK_a\}$ and $\{{}^{n}pK_w\}$ are summarized in Table 3. It is evident that independent of the starting values, the procedure converges to the values $V_e = 5.235$ ml ($C_o = 0.01047$ M), $pK_a = 6.120$ and $pK_w = 12.185$.

The value of V_e (or C_o) obtained proves that the proposed technique is able to extract the concentration of the titrated solution with fair accuracy. Concerning the values of pK_a and pK_w, their interpretation is outside the scope of this investigation and this will be the subject of a future paper.

POTENTIOMETRIC TITRATION OF MIXTURES OF TWO WEAK ACIDS

Theoretical

The titration of mixtures of acids is a problem that has been treated by numerous workers in the past. Two acids in admixture with each other can simply be titrated if their pK values differ sufficiently. In such instances, the acids are neutralized serially in accord with their pK values. As a rule of thumb, a difference between the pK values of greater than 2 pK units is usually satisfactory to distinguish, by traditional titration, the

TABLE 3

Successive approximations to pK_w, V_e and pK_a values resulting from the titration of *n*-butanoic acid with 0.1 M NaOH in DMF–water (1 + 1, v/v) at 25°C.

n	${}^{n}pK_w$	${}^{n}V_e$	${}^{n}pK_a$	${}^{n}pK_w$	${}^{n}V_e$	${}^{n}pK_a$	${}^{n}pK_w$	${}^{n}V_e$	${}^{n}pK_a$
0	10.0			14.0			100.0		
1	12.113	4.9061	6.0906	12.186	5.2369	6.1205	12.186	5.2369	6.1205
2	12.185	5.2343	6.1203	12.185	5.2347	6.1203	12.185	5.2347	6.1203
3	12.185	5.2347	6.1203	12.185	5.2347	6.1203	12.185	5.2347	6.1203
4	12.185	5.2347	6.1203						

component acids. For smaller differences between the pK values, the acids will apparently be neutralized simultaneously and the evaluation of the titration will become increasingly difficult, yielding less reliable results. A wide variety of solutions to this problem have been suggested [17,33–37]. All these methods require an exact knowledge of the dissociation constants of the acids and most of them also require the sum of the concentrations of the acids. This situation encouraged us to develop a new method permitting the simultaneous determination of the thermodynamic dissociation constants and the concentrations of two monoprotic acids in admixture with each other even when the difference between their pK values is small. In this method, which requires only data resulting from the acidic region of the titration curve, the sum of the concentrations need not be known.

Consider a volume V_o of a mixture of n weak monoprotic acids HA_1, HA_2,..., HA_n of initial concentrations C_1^o, C_2^o,..., C_n^o which is titrated with a solution of a strong base MOH, of concentration C_B. Assuming again that all singly charged ions have the same activity coefficient y_1 and that the activity coefficients of uncharged species are unity, the dissociation constant of the acid HA_i is expressed by the equation

$$K_i = \frac{\alpha_H [A_i^-] y_1}{[HA_i]} \tag{22}$$

At any point on the acidic region of the titration curve the mass and charge balance are expressed by the equations

$$C_t = \sum_{i=1}^{n} [HA_i] + \sum_{i=1}^{n} [A_i^-] \tag{23}$$

$$\sum_{i=1}^{n} [A_i^-] = [M^+] + [H^+] - [OH^-] = F \tag{24}$$

where

$$C_t = \sum_{i=1}^{n} C_i = \frac{C_t^o V_o}{V_o + V} = \frac{C_B V_e}{V_o + V} = b_N C_t^o V_o = b_N C_B V_e \tag{25}$$

$$C_t^o = \sum_{i=1}^{n} C_i^o = C_B V_e / V_o \tag{26}$$

$$C_i = [HA_i] + [A_i^-] = [HA_i]\left(1 + \frac{K_i}{\alpha_H y_1}\right) = b_N C_i^o V_o \tag{27}$$

$$F = [M^+] + [H^+] - [OH^-] = b_N C_B V + \frac{\alpha_H}{y_1} - \frac{K_w}{\alpha_H y_1} \tag{28}$$

Combination of Eqns. 22–28 gives

$$C_t - F = \sum_{i=1}^{n} \frac{C_i}{1 + \frac{K_i}{\alpha_H y_1}} \tag{29}$$

For $n = 2$, Eqn. 29 yields

$$Y = A_o + A_1 X_1 + A_2 X_2 \tag{30}$$

where

$$A_o = K_1 K_2,\ A_1 = K_1,\ A_2 = K_2 \tag{31}$$

$$Y = (\alpha_H y_1)^2 (F/L) \tag{32}$$

$$X_1 = \alpha_H y_1 \frac{b_N C_1^o V_o - F}{L} \tag{33}$$

$$X_2 = \alpha_H y_1 \frac{b_N (C_t^o - C_1^o) V_o - F}{L} \tag{34}$$

and

$$L = C_t - F = b_N C_B (V_e - V) - \frac{\alpha_H}{y_1} + \frac{K_w}{\alpha_H y_1} \tag{35}$$

The activity coefficient y_1 introduced in the above relationships can be determined, as previously, from Eqn. 6 by successive approximations. Concerning the ionic strength I, a simple calculation gives

$$I = b_N C_B V + (\alpha_H / y_i) \tag{36}$$

Equation 30 predicts that the relationship $Y = f(X_1, X_2)$ is linear. Alternatively, the experimental confirmation of such a correlation, using V and pH data, supports the assumption that the titrated solution is a mixture of two monoprotic acids. Then, the thermodynamic acidity constants K_1 and K_2 may be obtained, by a multiple linear regression method, from the partial regression coefficients.

However, despite the fact that Eqn. 30 offers a theoretical basis to correlate the results, there is no way in which, without a prior knowledge of V_e (or C_t^o) and C_1^o, the values of X_1 and X_2 can be determined. This is possible with the iterative method proposed in this paper.

Iterative method for the determination of V_e, C_1^o, C_2^o, pK_1 and pK_2

This method is based on the particular property of Eqn. 30 that, at the true value of the equivalence volume V_e defined by Eqn. 26, this equation is linear, independent of the chosen value for C_1^o.

Indeed, in the particular case where one uses the correct value of V_e and an erroneous value for C_1^o equal to $\hat{C}_1^o = C_1^o + \delta C_1^o$, the variables X_1 and X_2 are transformed into $\hat{X}_1$ and $\hat{X}_2$ defined by the following equations:

$$\hat{X}_1 = \alpha_H y_1 \left(\frac{b_N \hat{C}_1^o V_o - F}{L} \right)$$

$$= X_1 + \left(\frac{\alpha_H y_1 b_N V_o}{L} \right) \delta C_1^o \quad (37)$$

$$\hat{X}_2 = \alpha_H y_1 \left[\frac{b_N (C_1^o - \hat{C}_1^0) V_o - F}{L} \right]$$

$$= X_2 - \left(\frac{\alpha_H y_1 b_N V_o}{L} \right) \delta C_1^o \quad (38)$$

Combination of Eqns. 33, 34, 37 and 38 yields

$$\frac{\alpha_H y_1 b_N V_o}{L} = \frac{\hat{X}_1 - \hat{X}_2}{2(C_1^o + \delta C_1^o) - C_t^o} \quad (39)$$

and combination of Eqns. 30 and 37–39 finally gives

$$Y = \hat{A}_o + \hat{A}_1 \hat{X}_1 + \hat{A}_2 \hat{X}_2 \quad (40)$$

where

$$\hat{A}_o = A_o = K_1 K_2 \quad (41)$$

$$\hat{A}_1 = K_1 + \frac{(K_2 - K_1)\delta C_1^o}{2(C_1^o + \delta C_1^o) - C_t^o} \quad (42)$$

$$\hat{A}_2 = K_2 - \frac{(K_2 - K_1)\delta C_1^o}{2(C_1^o + \delta C_1^o) - C_t^o} \quad (43)$$

It results from these equations that, using the true value of V_e and any value for C_1^o, the relationship $Y = f(\hat{X}_1, \hat{X}_2)$ remains linear. However, the corresponding coefficients $\hat{A}_1$ and $\hat{A}_2$ are different from those of Eqn. 30; the differences are greater, the greater is the value of δC_1^o. In the case when $\delta C_1^o = 0$, so that the selected value for C_1^o is the correct one, Eqns. 40 and 30 are identical with each other. This very important property may be used in order to determine the values of V_e and C_1^o as follows.

It is assumed first that V_e is unknown and that its true value lies in an interval (a,b). Let $\hat{C}_1^o$ be any trial value for C_1^o chosen arbitrarily from an interval (a',b') of possible values of this concentration.

Starting from this value, and taking from the interval (a,b) any value for V_e, it is possible to obtain, by means of the experimental V and pH data, the dependence $Y = f(\hat{X}_1, \hat{X}_2)$. This will approach a linear relationship to the extent where the chosen value of V_e also approaches the exact value of the equivalence volume. Hence, the best linearity which could be obtained, by means of the available experimental data, evidently corresponds to the best approximation to the exact value of the equivalence volume. Thus, by seeking within the interval (a,b) the V_e value, it is possible to obtain N relationships $Y = f(\hat{X}_1, \hat{X}_2)$, N being the number of V_e values taken for these calculations. For each of these relationships, the calculation of the square of the multiple correlation coefficient R^2, permits a comparison of the linearity of the various $Y = f(\hat{X}_1, \hat{X}_2)$ variations and the curve $R^2 = f(V_e)$ to be traced. This is expected to present a pronounced maximum at a value of V_e equal to V_e^{max} which can be considered as the best approximation to the exact value of the equivalence volume. At this value of V_e, the partial regression coefficients of the corresponding multiple regression equation will approach the coefficients of Eqn. 30 to the extent where the chosen value $\hat{C}_1^o$ also approaches the exact value of C_1^o.

In a second step, starting from the value V_e^{max}, and seeking within the interval (a',b') the $\hat{C}_1^o$ value, it is possible to obtain as previously N' relationships $Y = f(\hat{X}_1, \hat{X}_2)$, N' being the number

of $\hat{C}_1^o$ values taken for these calculations. For each of these relationships, it is possible to calculate the ratio

$$R_{cf} = \hat{A}_o / \hat{A}_1 \hat{A}_2 \quad (44)$$

This ratio may be equal to unity at a certain value of $\hat{C}_1^o$, which can be considered as the best approximation to the exact value of C_1^o. Evidently, C_2^o can be calculated from Eqn. 26, while pK_1 and pK_2 can be estimated from the coefficients of the corresponding multiple linear regression equation.

As previously, in the attempt to establish the reliability of the proposed procedure, it was considered necessary to test the proposed method, first on simulated titration data of various mixtures of two acids of varying acidity strength and second on experimental data resulting from titrations of mixtures of two acids (with known pK_1 and pK_2).

TABLE 4

Ideal and Monte Carlo (M-C) pH values for the titration of a mixture of two acids with a strong base ($pK_1 = 4.8$, $pK_2 = 3.8$, $V_o = 50$ ml, $C_1^o = 0.006$ M, $C_2^o = 0.004$ M, $C_B = 0.1$ M, $T = 298.15$ K and $pK_w = 14.0$)

V	pH		V	pH	
	Ideal [a]	M-C [b]		Ideal [a]	M-C [b]
1.0	3.681	3.682	2.6	4.445	4.440
1.1	3.734	3.731	2.7	4.490	4.490
1.2	3.786	3.790	2.8	4.535	4.531
1.3	3.836	3.832	2.9	4.579	4.574
1.4	3.886	3.887	3.0	4.624	4.621
1.5	3.936	3.940	3.1	4.669	4.667
1.6	3.984	3.982	3.2	4.715	4.710
1.7	4.032	4.029	3.3	4.761	4.757
1.8	4.080	4.075	3.4	4.807	4.806
1.9	4.127	4.128	3.5	4.855	4.854
2.0	4.173	4.174	3.6	4.905	4.907
2.1	4.219	4.216	3.7	4.955	4.960
2.2	4.265	4.265	3.8	5.008	5.012
2.3	4.311	4.312	3.9	5.063	5.057
2.4	4.356	4.351	4.0	5.121	5.121
2.5	4.401	4.395			

[a] Values that exactly fit Eqn. 30. [b] Mean values of four normally distributed deviates generated from the ideal data with standard deviation equal to 0.01 pH unit.

Application of the method using simulated data

Simulated V and pH data were derived by solving Eqn. 30 using, as previously, the so-called secant method [31]. In all these calculations it was assumed that $V_o = 50$ ml, $V_e = 5.00$ ml, $C_B = 0.1$ M, $T = 298.15$ K and $pK_w = 14.0$.

First, two weak monoprotic acids of initial concentrations $C_1^o = 0.006$ M, $C_2^o = 0.004$ M, $pK_1 = 4.80$ and $pK_2 = 3.80$ were considered. The results obtained, rounded to three decimal places, are reported in Table 4. It is now examined whether it is possible, using these data resulting from the acidic region of the titration curve and by means of the proposed method, to extract the desired pK and concentration values. In a first attempt the variation of R^2 with V_e was examined, the starting value for C_1^o being 0.002 M. Further, at each value of V_e, the adequacy of the fit of Eqn. 40 to the simulated data was examined by means of S_{yx} (standard error of the estimate) and F_{st} (F-statistic). These statistics are defined by the following equations [32]:

$$S_{yx} = \left[\frac{\sum_{i=1}^{N} (Y_i - Y_{est})^2}{N - p - 1} \right]^{1/2} \quad \text{and}$$

$$F_{st} = \frac{(N - p - 1) R^2}{p(1 - R^2)} \quad (45)$$

where Y_{est} is the estimated Y value, obtained by means of the corresponding regression equation, p the number of the independent variables of the multiple linear model (here $p = 2$) and N the number of the titration data used in the fit. At the true value of V_e, these statistics may reach a minimum and a maximum value, respectively [32]. The results obtained are presented graphically in Fig. 5. It should be emphasized that one obtains identical results independent of the starting value for C_1^o. Figure 5 shows that both the graphs $R^2 = f(V_e)$ and $F_{st} = f(V_e)$ present pronounced maxima at $V_e \approx 5.0$ ml. However, the maximum of the latter plot is much more accentuated than that of the former; the statistic F_{st}, equal to 1.9891×10^5 at $V_e = 4.90$ ml, is about 28 times as great for $V_e = 5.00$ ml ($F_{st} = 5.5316 \times 10^6$). In

contrast, the variation of S_{yx} with V_e passes through a minimum corresponding also to $V_e \approx 5.0$ ml. Further, for $4.9 < V_e < 5.1$, it was found that the curves $R^2 = f(V_e)$ and $1/F_{st} = f(V_e)$ can be perfectly fitted, by least squares, to the following polynomials (the squares of their correlation coefficients were very close to unity):

$$R^2 = \sum_{n=0}^{6} A_n V_e^n$$
$$= -16.284 + 5.5839 V_e + 1.2884 V_e^2 - 0.52412 V_e^3 - 2.6767 \times 10^{-2} V_e^4 + 2.0888 \times 10^{-2} V_e^5 - 1.6559 \times 10^{-3} V_e^6 \quad (46)$$

$$\frac{1}{F_{st}} = \sum_{n=0}^{6} B_n V_e^n$$
$$= 1.1987 - 0.38517 V_e - 9.0672 \times 10^{-2} V_e^2 + 3.6630 \times 10^{-2} V_e^3 + 1.8393 \times 10^{-3} V_e^4 - 1.4498 \times 10^{-3} V_e^5 + 1.1497 \times 10^{-4} V_e^6 \quad (47)$$

Consequently, the exact value of V_e at which R^2 and F_{st} reach maximum values can be determined by solving (using any numerical method) the following equations:

$$\frac{dR^2}{dV_e} = 0 \text{ and } \frac{d(1/F_{st})}{dV_e} = 0 \quad (48)$$

Both Eqns. 48 have as the root the value $V_e^{max} = 4.9994$ ml, which virtually coincides with the theoretical value of the equivalence volume; hence $C_t^o = 0.009999$ M.

In a second step, starting from this value of V_e, the variation of R_{cf} (Eqn. 44) with $\hat{C}_1^o$ was examined. The results obtained, summarized in Table 5, verify the theoretical analysis reported previously (Eqns. 40–43). Indeed, at the true value of V_e, the variation of Y with $\hat{X}_1$ and $\hat{X}_2$ remains perfectly linear ($R^2 = 0.999998$), independent of the chosen value of $\hat{C}_1^o$. Also, for all values of $\hat{C}_1^o$ used, the regression coefficient $\hat{A}_o$ remains constant, while $\hat{A}_1$ and $\hat{A}_2$ vary with $\hat{C}_1^o$.

Using the results in Table 5, it was found that the variation of $\hat{C}_1^o$ with R_{cf} can be perfectly fitted, by regression analysis, to the following

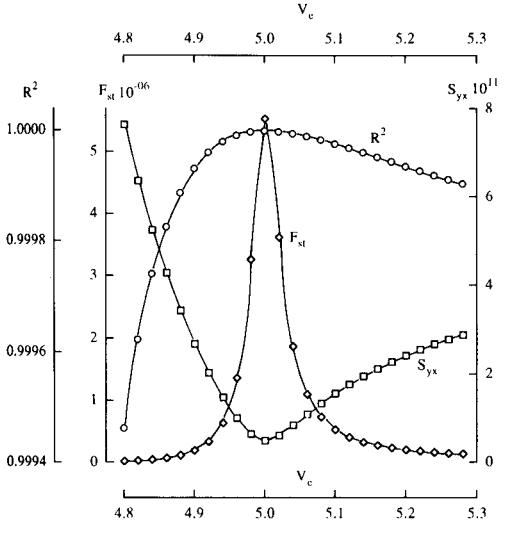

Fig. 5. Variation of R^2, F_{st} and S_{yx} with V_e in the case of the titration of 50 ml of a mixture of two acids ($C_1^o = 0.006$ M, $C_2^o = 0.004$ M, $pK_1 = 4.80$ and $pK_2 = 3.80$) with 0.1 M NaOH at 25°C.

TABLE 5

Values of the coefficients of the regression equation $Y = \hat{A}_o + \hat{A}_1\hat{X}_1 + \hat{A}_2\hat{X}_2$ fitting the ideal data in Table 4 and the parameter R_{cf}(V_e = 4.9994 ml).

$\hat{C}_1^o \times 10^3$	R^2	$\hat{A}_o \times 10^9$	$\hat{A}_1 \times 10^6$	$\hat{A}_2 \times 10^4$	R_{cf}
5.90	0.999998	2.5278	7.1852	1.6776	2.097
5.91	0.999998	2.5278	8.0669	1.6688	1.8778
5.92	0.999998	2.5278	8.9294	1.6602	1.7052
5.93	0.999998	2.5278	9.7734	1.6517	1.5659
5.94	0.999998	2.5278	10.599	1.6435	1.4511
5.95	0.999998	2.5278	11.408	1.6354	1.3549
5.96	0.999998	2.5278	12.200	1.6274	1.2732
5.97	0.999998	2.5278	12.975	1.6197	1.2028
5.98	0.999998	2.5278	13.735	1.6121	1.1416
5.99	0.999998	2.5278	14.479	1.6047	1.0880
6.00	0.999998	2.5278	15.209	1.5974	1.0405
6.01	0.999998	2.5278	15.924	1.5902	0.9983
6.02	0.999998	2.5278	16.625	1.5832	0.9604
6.03	0.999998	2.5278	17.312	1.5763	0.9263
6.04	0.999998	2.5278	17.987	1.5696	0.8954
6.05	0.999998	2.5278	18.648	1.5630	0.8673
6.06	0.999998	2.5278	19.297	1.5565	0.8416
6.08	0.999998	2.5278	20.559	1.5439	0.7964
6.10	0.999998	2.5278	21.775	1.5317	0.7579
6.12	0.999998	2.5278	22.947	1.5200	0.7247
6.14	0.999998	2.5278	24.078	1.5087	0.6959

polynomial (the square of the correlation coefficient being very close to unity):

$$10^3\hat{C}_1^o = 7.9266 - 5.8203R_{cf} + 7.2517R_{cf}^2 - 4.6705R_{cf}^3 + 1.5156R_{cf}^4 - 0.19607R_{cf}^5 \quad (49)$$

From this polynomial and for $R_{cf} = 1$ one obtains $\hat{C}_1^o = C_1^o = 0.006009$ M. This value, being within 0.15% of its true magnitude, is the best approximation to the exact value of C_1^o. Also, it results from Eqn. 26 that $C_2^o = C_t^o - C_1^o = 0.00399$ M. Finally, using the resulting values of V_e and C_1^o, one obtains from the coefficients of the corresponding multiple linear regression equation: $pK_1 = 4.799$ and $pK_2 = 3.798$. The minor differences between the theoretical and the determined values of V_e, C_1^o, C_2^o, pK_1 and pK_2 are due to the fact that the simulated pH data have been rounded to three decimal places.

In an attempt to generalize the conclusions concerning the applicability of the proposed methods, this procedure was also applied to various mixtures containing two acids of different strength and concentration. In all instances simulated data lying in the 20–80% neutralization range of the titration curve were used. It was found that the proposed procedure is fairly applicable even when the difference between the pK of the acids is equal to 0.5 pK unit. For smaller values of the pK difference, the proposed procedure requires more accurate titration data (pH values correct to four decimal places) in order to obtain reliable results. For such small differences, calculations could be carried out as if only one acid, having a pK equal to the average pK and a concentration equal to the sum of the concentrations, were present.

The proposed technique was also applied to data containing random extraneous contributions, such as annoying experimental "noise". As in the titration of one monoprotic acid, at each point (V_i and pH_i) of the theoretical titration curve, a number N of normally distributed random variables $pH_{i,j}$ with mean pH_i and standard deviation S_i was produced. Using this Monte Carlo technique, as an example, the ideal data in Table 4 were treated again, assuming $S_i = 0.01$ pH unit. At each volume V_i four normally distributed deviates $pH_{i,j}$ were created and the results were averaged. The mean values $\overline{pH}_{i,j}$ are summarized in Table 4. Using these Monte Carlo data for $\overline{pH}_{i,j}$, the proposed method gives the values $V_e = 5.014$ ml ($C_t^o = 0.01003$ M), $C_1^o = 5.892 \times 10^{-3}$ M, $C_2^o = 4.138 \times 10^{-3}$ M, $pK_1 = 4.814$ and $pK_2 = 3.817$. These results are within 0.3%, 1.8%, 3.5%, 0.3% and 0.45%, respectively, of their true magnitudes. As in the the titration of a monoprotic acid, these results can be improved by smoothing the titration data, using as smoothing function a polynomial form equation relating $\overline{pH}_{i,j}$ with V. The following polynomial (with $R^2 = 0.99995$) was found:

$$\overline{pH}_{i,j} = 3.1539 + 0.50788\,V + 5.5126 \times 10^{-2}\,V^2 - 4.3937 \times 10^{-2}\,V^3 + 9.4133 \times 10^{-3}\,V^4 - 5.3340 \times 10^{-4}\,V^5 \quad (50)$$

Using smoothed data, one obtains $V_e = 4.976$ ml ($C_t^o = 9.952 \times 10^{-3}$ M), $C_1^o = 5.955 \times 10^{-3}$ M, $C_2^o = 3.997 \times 10^{-3}$ M, $pK_1 = 4.789$ and $pK_2 = 3.803$. These results are within 0.48%, 0.75%, 0.08%, 0.23% and 0.08%, respectively, of their true magnitudes.

Finally, the proposed methods were applied to various simulated titration curves where the pH data contain a systematic error equal to $\delta pH = 0.01$ pH unit. The difference between the pK values of the component acids was retained equal to 1.0 pK unit ($pK_1 = pK_2 + 1$).

A systematic error in the pH values gives rise to systematic titration errors in the parameters to be evaluated. These errors can be determined by

$$\delta V_e(\%) = \frac{V_{e/id} - V_{e/syst}}{V_{e/id}} \times 100 \quad (51)$$

$$\delta C_i^o(\%) = \frac{C_{i/syst}^o - C_{i/id}^o}{C_{i/id}^o} \times 100 \quad (52)$$

$$\delta pK_i(\%) = \frac{pK_{i/id} - pK_{a/syst}}{pK_{i/id}} \times 100 \quad (53)$$

where $V_{e/id}$, $C_{i/id}^o$ $pK_{i/id}$, $V_{e/syst}$, $C_{i/syst}^o$ and $pK_{i/syst}$ are the values of V_e, C_i^o and pK_i (with $i = 1$ or 2) determined respectively from ideal simulated data (rounded to three decimal places)

and data containing a systematic error δpH in the pH values. These titration errors were calculated for various simulated titrations curves, where $\delta pH = 0.01$, corresponding to different values of pK_1 ($pK_2 = pK_1 - 1$).

The results obtained showed an analogous behaviour to that observed in the titration of monoprotic acids. Thus, the titration errors δV_e, δC_i^o and δpK_i, at constant δpH, were functions of the strength of the component acids. Hence, taking into account that $pK_1 = pK_2 + 1$ (for the examples treated here), we can write

$$\delta E(\%) = f(pK_1, pK_2) = f(u) \quad (54)$$

where

$$u = \sqrt{(pK_1 - 1)^2 + pK_2^2}$$
$$= pK_2\sqrt{2} = (pK_1 - 1)\sqrt{2} \quad (55)$$

and $\delta E(\%) = \delta V_e(\%)$, $\delta C_i^o(\%)$, $\delta pK_i(\%)$.

It was found that δV_e was maximum in the immediate vicinity of the value of $u = 4.67$ ($pK_1 = 4.3$ and $pK_2 = 3.3$). However, in all instances examined here, δV_e was $\leqslant 0.20\%$, while the titration errors δpK_i and δC_i^o decreased as u increased. For mixtures with $u > 6.08$ ($pK_1 = 5.3$ and $pK_2 = 4.3$) these errors were less than 0.37%.

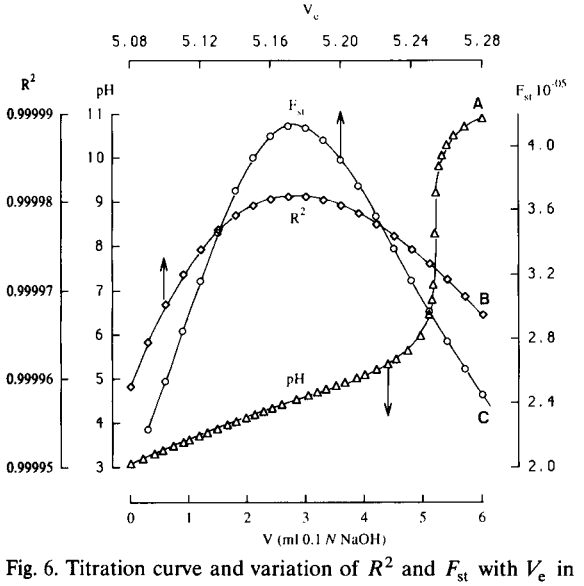

Fig. 6. Titration curve and variation of R^2 and F_{st} with V_e in the case of the titration of 50 ml of a mixture of propionic and formic acid with 0.1 M NaOH at 25°C. The mixture was prepared by mixing 30 ml of 0.01029 M propionic acid with 20 ml of 0.01051 M formic acid.

TABLE 6

Experimental titration of an aqueous mixture of 30 ml of 0.01029 *M* propionic acid and 20 ml of 0.01051 *M* formic acid with 0.1 M NaOH at $T = 298.15$ K

V	pH	V	pH
1.00	3.639	2.59	4.432
1.17	3.727	2.84	4.545
1.31	3.800	3.04	4.638
1.48	3.888	3.20	4.710
1.65	3.975	3.35	4.778
1.80	4.050	3.52	4.860
1.97	4.133	3.67	4.932
2.12	4.207	3.87	5.036
2.27	4.278	4.01	5.107
2.42	4.348		

Hence, for such mixtures the proposed technique is able to extract the values of V_e, C_i^o and pK_i with only a modest error ($\delta V_e \leqslant 0.04\%$, $\delta C_1^o \leqslant 0.17\%$, $\delta C_2^o \leqslant 0.37\%$, $\delta pK_1 \leqslant 0.22\%$ and $\delta pK_1 \leqslant 0.29\%$) even when the pH data contain an important systematic error $\delta pH = 0.01$ (about 5–10 times greater than the accuracy of a precision instrument).

Application of the methods on experimental data

In an attempt to test this methodology on experimental data, a mixture was prepared by mixing 30 ml of 0.01029 M propionic acid with 20 ml of 0.01051 M formic acid. This mixture was titrated with 0.100 M sodium hydroxide. As shown in Fig. 6, the titration curve presents only one pronounced inflection (at $V \approx 5.18$ ml) corresponding to the total neutralization of the mixture. The measurements, carried out in the acidic neutralization range of the mixture, are given in Table 6. It was found that the plots of $R^2 = f(V_e)$ and $F_{st} = f(V_e)$ presented pronounced maxima.

The following polynomials were found ($5.08 \leqslant V_e \leqslant 5.28$):

$$R^2 = \sum_{n=0}^{6} A_n V_e^n$$
$$= -8.8752 + 5.3268\ V_e - 0.67377\ V_e^2 - 5.1405 \times 10^{-2}\ V_e^3 + 2.8774 \times 10^{-3}\ V_e^4 + 2.9221 \times 10^{-3}\ V_e^5 - 2.8269 \times 10^{-4}\ V_e^6 \quad (56)$$

$$\frac{1}{F_{st}} = \sum_{n=0}^{6} B_n V_e^n$$

$$= 1.2482 - 0.66860\ V_e + 7.9863 \times 10^{-2}\ V_e^2 + 8.8802 \times 10^{-3}\ V_e^3 - 8.9562 \times 10^{-4}\ V_e^4 - 3.1027 \times 10^{-4}\ V_e^5 + 3.3127 \times 10^{-5}\ V_e^6 \quad (57)$$

By combining these equations with Eqns. 48, one obtains the root $V_e^{max} = 5.172$ ml ($C_t^o = 0.01034$ M), which is the best approximation to the desired value of V_e.

In a second step, starting from this value of V_e, the variation of $\hat{C}_1^o$ with R_{cf} was examined. For $0.00610\ M \leqslant \hat{C}_1^o \leqslant 0.00625$ M, the following polynomial (with the square of the correlation coefficient very close to unity) was found:

$$10^3 \times \hat{C}_1^o = 7.3866 - 3.7954\ R_{cf} + 4.9682\ R_{cf}^2 - 3.4283\ R_{cf}^3 + 1.2084\ R_{cf}^4 - 0.17165\ R_{cf}^5 \quad (58)$$

From this polynomial and for $R_{cf} = 1$ one obtains $\hat{C}_1^o = C_1^o = 6.168 \times 10^{-3}$ M. This value is the best approximation to the exact value of C_1^o. Also, it results that $C_2^o = C_t^o - C_1^o = 4.176 \times 10^{-3}$ M. These values are in excellent agreement with the expected values of C_1^o ($= 30 \times 0.01029/50 = 6.174 \times 10^{-3}$) and C_2^o ($= 20 \times 0.01051/50 = 4.204 \times 10^{-3}$). Finally, using the determined values of V_e and C_1^o, one obtains from the coefficients of Eqn. 30 $pK_1 = 4.877$ and $pK_2 = 3.742$, which are very close to the corresponding values (4.874 and 3.752 at 25°C) reported in the literature [22,23].

Conclusions

The proposed iterative methods for the analysis of potentiometric acid–base titration data of weak monoprotic acids and of mixtures of two weak monoprotic acids are fairly applicable even when the data are considerably obscured by extraneous "noise". For some acids ($pK \geqslant 4.0$) the proposed techniques lead to accurate results even when the pH data contain an important systematic error $\delta pH = 0.01$ (about 5–10 times greater than the accuracy of a precision instrument). The proposed procedures are also valid under conditions of varying ionic strength. Hence, it is not necessary to add an inert electrolyte to the titrated solution to keep the ionic strength constant. Therefore, the pK values obtained are free from any possible salt effect. On the other hand, the simultaneous determination of accurate values of concentrations and thermodynamic dissociation constants of the titrated acids, in addition to its theoretical and analytical interest, provides information supporting the identification of the titrated acids. Hence, the proposed procedure for mixtures of weak acids could also be used in the analysis and identification of solutions containing two isomeric acids, produced during an isomerization reaction, with similar acidic strength.

Despite the fact that the proposed methods require laborious calculations, they can be easily applied with the opportunities offered today by high-speed computers. Thus, using a common personal computer, the analysis of the titration of a mixture of acids requires only a few minutes to achieve the correct results. Further investigations concerning the development of similar methods applicable to more complicated titrations are in progress.

REFERENCES

1 G. Papanastasiou, G. Stalidis and D. Jannakoudakis, Bull. Soc. Chim. Fr., (1985) 255.
2 G. Papanastasiou and I. Ziogas, Bull. Soc. Chim. Fr., (1985) 725.
3 G. Papanastasiou, I. Ziogas and I. Moumtzis, Anal. Chim. Acta, 186 (1986) 213.
4 G. Papanastasiou and I. Ziogas, Anal. Chim. Acta, 222 (1989) 189.
5 G. Papanastasiou and I. Ziogas, Talanta, 36 (1989) 977.
6 G. Papanastasiou, Anal. Chim. Acta, 229 (1990) 261.
7 G. Papanastasiou and I. Ziogas, Anal. Chim. Acta, 221 (1989) 295.
8 E. Grunwald, J. Am. Chem. Soc., 73 (1951) 4934.
9 E.J. King, Acid–Base Equilibria, Pergamon, Oxford, 1965, p. 83.
10 H. Freiser and Q. Fernando, Ionic Equilibria in Analytical Chemistry, Wiley, New York, 1966, p. 240.
11 G. Gran, Acta Chem. Scand., 4 (1950) 559.
12 G. Gran, Analyst, 77 (1952) 661.

13 B.H.J. Hofstee, Science, 131 (1960) 39.
14 F. Ingman and E. Still, Talanta, 13 (1966) 1431.
15 A. Johanson, Analyst, 95 (1970) 535.
16 L. Pehrson, F. Ingman and A. Johanson, Talanta, 23 (1976) 769.
17 L. Pehrson, F. Ingman and S. Johanson, Talanta, 23 (1976) 781.
18 A. Olin and B. Wallén, Talanta, 28 (1981) 919.
19 D.D. Perrin, W.L.F. Armarego and D.R. Perrin, Purification of Laboratory Chemicals, Pergamon, Oxford, 1980.
20 R.G. Bates, J. Res. Natl. Bur. Stand., Sect. A, 66 (1962) 179.
21 K.G. Ong, R.A. Robinson and R.G. Bates, Anal. Chem., 36 (1964) 1971.
22 R.A. Robinson and R.H. Stokes, Electrolyte Solutions, Butterworths, London, 2nd edn., 1968, pp. 230, 517.
23 A. Albert and L.P. Serjeant, The Determination of Ionization Constants, Chapman and Hall, London, 2nd edn., 1971, pp. 28, 84.
24 A.L. Bacarella, E. Grunwald, H.P. Marshall and E.L. Purlee, J. Org. Chem., 20 (1955) 747.
25 C.L. De Ligny, P.F.M. Luykx, M. Rehbah and A.A. Wieneke, Recl. Trav. Chim. Pays-Bas, 79 (1960) 713.
26 H. Rossotti, The Study of Ionic Equilibria, Longman, London, 1978, p. 19.
27 P. Cayzergues, C. Georgoulis and G. Papanastasiou, J. Chim. Phys., 74 (1977) 1112.
28 A. Papoutsis, G. Papanastasiou, C. Georgoulis and D. Jannakoudakis, J. Chim. Phys., 82 (1985) 907.
29 G. Papanastasiou, G. Kokkinidis and N. Papadopoulos, J. Electroanal. Chem., 305 (1991) 19.
30 G. Kokkinidis, G. Papanastasiou, C. Hasiotis and N. Papadopoulos, J. Electroanal. Chem., 309 (1991) 263.
31 G. Dahlquist and A. Björck, Numerical Methods, Prentice-Hall, Englewood Cliffs, NJ, 1969, p. 227.
32 S. Chatterjee and B. Price, Regression Analysis by Example, Wiley, New York, 1977, pp. 3, 51.
33 A. Frisque and V.W. Meloche, Anal. Chem., 26 (1954) 468.
34 N. Purdie, M.B. Thomson and G.K. Cook, Anal. Chem., 44 (1972) 1525.
35 J.J. Kankare, Anal. Chem., 45 (1973) 1877.
36 F. Ingman, A. Johanson, S. Johanson and R. Karlsson, Anal. Chim. Acta, 64 (1973) 113.
37 A. Ivaska, Talanta, 22 (1975) 995.

Analytica Chimica Acta, 277 (1993) 137–144
Elsevier Science Publishers B.V., Amsterdam

Voltammetric behaviour of marine hydrophobic copper complexes: effect of adsorption processes at a mercury electrode

Gioacchino Scarano and Emilia Bramanti

Istituto di Biofisica, Consiglio Nazionale della Ricerche, Via S. Lorenzo 26, Pisa 56100 (Italy)

(Received 3rd August 1992; revised manuscript received 22nd December 1992)

Abstract

The voltammetric behaviour of copper in the presence of marine hydrophobic organic matter and soil fulvic acid was examined by differential-pulse anodic stripping voltammetry (DPASV) in sodium perchlorate. These organic substances strongly adsorb on a mercury electrode, thereby affecting the peak current. The extent of this interference is related to the charge on the electrode during the plating step, but the mechanism of the influence on the anodic peak is mainly connected with the stripping step. A cathodic potential step whereby the effects of adsorption can be removed is described. This modified DPASV method was used to evaluate the lability of copper–organic complexes and to elucidate the effects on the anodic current due to the adsorption process.

Keywords: Stripping voltammetry; Copper; Hydrophobic complexes; Sea water

Adsorption of surface-active substances on mercury electrodes may influence the redox properties of metals, affecting peak currents and potentials in anodic stripping voltammetry (ASV) [1–3]. This surface process may cause a serious interference when the ASV diagnostic parameters are used for speciation purposes, as many natural complexing agents involved in metal speciation are also surface-active substances [4,5].

Complexation and adsorption processes may act simultaneously in such a manner that their individual effects cannot be easily differentiated. Indeed, both processes may hinder metal reduction during the plating step or change the reversibility of metal oxidation during the stripping step [1]. Voltammetric studies of metal interactions with organic surface-active complexing substances can help to differentiate between the effect of surface interactions and those due to complexation properties in bulk solution [6–9].

Many papers have shown that the voltammetric behaviour of copper is altered when natural organic matter such as fulvic acids [10–13] and extracellular polymeric substances [14] or model organic compounds such as soluble proteins and polysaccharides [15] are present in solution. Peak distortion, appearance of subsidiary peaks and shifts of the baseline represent the alterations of the ASV response and they have been attributed to the adsorption of organics at the mercury/water interface [10–15].

The use of gelatin as a reagent in the differential-pulse anodic stripping voltammetry (DPASV) of estuarine waters [16,17], linear ASV with ring collection [18] and sampled-d.c. versus pulse voltammetry [19,20] all have been exploited in order to avoid or compensate for the effect of sorption on the anodic current.

Correspondence to: G. Scarano, Istituto di Biofisica, Consiglio Nazionale delle Ricerche, Via S. Lorenzo 26, Pisa 56100 (Italy).

This paper presents the results of a voltammetric investigation of marine hydrophobic copper complexes isolated by a solid-phase extraction technique employing prepacked Sep-Pak C_{18} cartridges [21–24]. The influence of this fraction of marine organic matter (MOM) on the voltammetric behaviour of the bound copper was studied by DPASV at a hanging mercury drop electrode (HMDE).

Experimental evidence for interference with the peak current due to the adsorption of these uncharacterized organic substances on the mercury surface is reported. The usefulness of a selected potential step procedure for improving the electrochemical response is presented. The behaviour of copper in the presence of soil fulvic acid was also examined by this technique.

EXPERIMENTAL

Voltammetric measurements were carried out with a Metrohm Model 646 VA processor in conjunction with a model 647 VA stand. A conventional three-electrode arrangement, consisting of a glassy carbon rod as an auxiliary electrode, an Ag/AgCl/KCl (3 M) double-junction electrode as a reference electrode and a Metrohm multi-mode electrode (MME) used in the hanging mercury drop mode (HMDE), was used.

Voltammetric measurements were carried out in the DPASV mode with 0.5 M $NaClO_4$ (pH 6) as the supporting electrolyte. Metal–ligand solutions were obtained by adding selected amounts of the Sep-Pak extract solution to the cell. A 2-h equilibration time was used before analysis. The instrumental settings were as follows: deposition potential (E_{dep}), -0.25 V vs. Ag/AgCl; scan rate, 12 mV s^{-1}; pulse duration, 40 ms; pulse repetition time, 0.5 s; modulation amplitude, 25 mV; and mercury drop size, 0.55 mm^2.

In organic-free 0.5 M $NaClO_4$, the copper peak potential (E_p) was -1 ± 2 mV, the half-width ($w_{1/2}$) was 58 ± 4 mV and the sensitivity, measured as $i_p C_M^{-1} t_{dep}^{-1}$, was $(1.75 \pm 0.85) \times 10^{-3}$ nA l $nmol^{-1}$ s^{-1}.

Stripping polarography [25–28] was performed by varying E_{dep} at 10-mV intervals from the rising part of the i_p (nA) vs. E_{dep} (V) curve to the copper reduction plateau and then at 50–100-mV intervals until $E_{dep} = -1.4$ V. After plating, the voltage was switched to -0.25 V and scanned in the differential-pulse mode.

Reversed-phase trifunctional Sep-Pak t-C_{18} cartridges (Waters) were used to isolate the hydrophobic copper–organic complexes from sea-water samples. The method involves the passage of 1 l of natural sea water (pH 8) through a precleaned (10 ml of methanol, 10 ml of 3×10^{-4} M HCl solution and 20 ml of Milli-Q-purified water) Sep-Pak cartridge at a flow-rate of 10 ml min^{-1}. After rinsing, the cartridges were eluted with 10 ml of methanol–water (80 + 20), the eluate was vacuum dried and the residue was dissolved in water.

The copper concentration in this solution was measured by atomic absorption spectrometry (AAS) using a Perkin-Elmer Model 1100 B spectrophotometer equipped with Model HGA 700 graphite furnace. The amount of copper adsorbed on the Sep-Pak cartridge after the passage of 1 l of sea water was 65 ± 7 ng and < 0.2 ng for untreated (pH 8) and UV-irradiated samples, respectively.

Total organic carbon (TOC) was determined using a DC-190 high-temperature TOC analyser (Rosemount Analytical, Dohrmann). The amount of TOC adsorbed on the Sep-Pak cartridge (1 l of untreated sea water) was 60 ± 7 μg.

Sea-water samples were collected in the Tyrrhenian sea (close to the Tuscan Archipelago) using clean sampling techniques according to the precautions recommended by Mart [29,30], then filtered through membrane filters (0.45 μm), stored in the dark at 4°C and utilized within 2 months of collection.

Photooxidation of sea water was accomplished by exposing the sample to a 1-kW UV lamp for 8 h.

A copper stock solution was prepared by dissolving analytical-reagent grade copper(II) sulphate in water and diluting to give the desired copper concentration. $NaClO_4$ solution was prepared from the AnalaR reagent (BDH). Methanol was of LC grade. All solutions were prepared

with water purified with a Milli-Q purification system (Millipore).

Characterized soil fulvic acid [31] was kindly provided by Professor J. Weber, Department of Chemistry, University of New Hampshire (USA).

RESULTS AND DISCUSSION

Preliminary investigations on the voltammetric determination of copper in the presence of Sep-Pak-extractable marine organic matter (SPE-MOM) showed that this hydrophobic fraction of marine organic matter strongly affects the copper stripping peak.

At a deposition potential (E_{dep}) of −0.25 V, corresponding to the diffusion-limited plateau of copper in organic-free 0.5 M $NaClO_4$, the following general effects (Fig. 1) were observed in the presence of SPE–MOM: an increase in the slope of the baseline which increases with both the deposition time (t_{dep}) and the modulation amplitude of the pulse, ΔE (mV); at low copper concentrations ([Cu] $< 5 \times 10^{-8}$ M) the copper peak appears broadened and shifted towards more positive potentials (Fig. 1, curve b) in comparison with the peak shape and position of copper in a ligand-free solution (Fig. 1, curve a); and the current peak (i_p) was not linearly correlated to deposition time (t_{dep}).

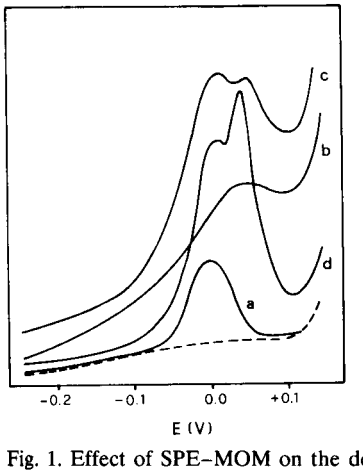

Fig. 1. Effect of SPE–MOM on the determination of copper by DPASV. (a) Copper ion in organic-free 0.5 M $NaClO_4$; (b) copper in the presence of SPE–MOM at pH 6, [Cu] $< 3 \times 10^{-8}$ M; (c) copper in the presence of SPE–MOM at pH 6, [Cu] $> 1 \times 10^{-7}$ M; (d) copper in the presence of SPE–MOM at pH 2, [Cu] $> 1 \times 10^{-7}$ M.

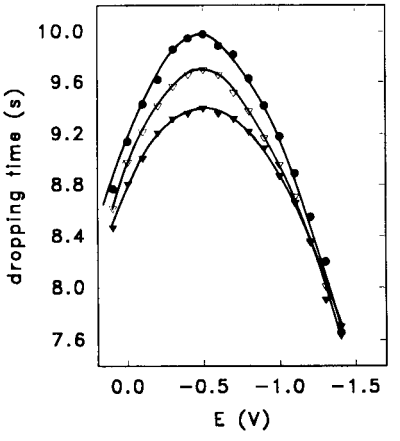

Fig. 2. Influence of the concentration of Sep-Pak C_{18}-extractable marine organic matter (SPE–MOM) on the electrocapillary curve. 0.5 M $NaClO_4$, pH 6. TOC concentration: ● = 0; ▽ = 6; ▼ = 12 mg l^{-1}.

With increasing copper additions, the stripping peak was modified by the appearence of an additional unresolved peak at more negative potential ($\Delta E_p \approx 40$ mV) until a "double peak" configuration was attained (Fig. 1, curve c). This more cathodic peak is set at the potential of the Cu^0–Cu^{2+} reaction, increases with copper addition and behaves as a diffusion peak. The double-peak configuration was also found when the solution was acidified to pH 2 (with $HClO_4$). At this pH, the more anodic peak displays the characteristics of an adsorption post-wave (Fig. 1, curve d).

Adsorption of hydrophobic organic matter at the mercury electrode was investigated by means of electrocapillary measurements. The drop time (t_d) was recorded as a function of the potential (E) for two different concentrations of SPE–MOM. The results are shown in Fig. 2 for TOC concentrations of 6 and 12 mg l^{-1} in 0.5 M $NaClO_4$ (pH 6).

The lowering of t_d confirms the adsorption of SPE–MOM at the mercury electrode over a wide potential range. This effect becomes more marked as the TOC increases and it appears more pronounced on the positive side of the electrocapillary maximum where the drop is positively

charged. In contrast, weaker adsorption occurs for $E < -1$ V. A similar behaviour was observed in acidified solutions.

The effects of E_{dep} on the copper stripping peak were investigated at copper concentrations of 5×10^{-8} and 1.5×10^{-7} M. After the deposition step at the selected E_{dep}, the scan was started from -0.25 V. At low copper concentrations, where the broadened and shifted peak occurs, the shape and height of the peak depended on the deposition potential. The slope of the baseline decreased when the potential was set at more negative values and, from -0.8 to -1.4 V, a better resolved peak, rising from a flattened baseline, and an increase in the measurable current were found. At higher copper concentrations, the deposition potential produces a marked effect on the double peak: at E_{dep} between -1.0 and -1.6 V the more anodic peak decreases and finally disappears. The shape of the resulting peak and its peak potential (E_p) were similar to those of copper ion in organic-free $NaClO_4$.

These results could be explained on the basis of the electrocapillary curve. At $E_{dep} = -0.25$ V, the net charge on the mercury electrode with respect to the electrocapilllary zero is positive. This positive charge permits the accumulation of the adsorbed ligands on the electrode surface. When E_{dep} is set at more cathodic values, the charge on the drop becomes negative and the adsorption processes decrease [32]. Because the starting potential of the anodic scan was -0.25 V also when cathodic desorption potentials were selected as the plating potential, the above-mentioned behaviour seems to indicate that the adsorption processes should not occur to a significant extent during the scan. Therefore, it seems that the factors determining the adsorption of the organics should be the value of E_{dep}, which fixes the charge of the electrode, and the deposition time, which determines the surface concentration of adsorbed organic ligands on the mercury drop.

In order to establish whether the adsorption processes affecting the anodic peak are mainly connected with the deposition or the stripping step, the plating was performed at a reduction potential where the adsorbed layer is formed ($E_{dep} = -0.25$ V). The strirring was then stopped

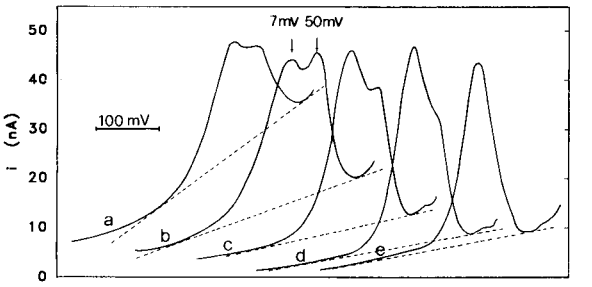

Fig. 3. Effect of cathodic rest potential (E_{rest}) on the copper stripping peak in the presence of SPE–MOM. [Cu] = 8×10^{-8} M; $\Delta E = 25$ mV; scan rate = 12 mV s^{-1}; $E_{dep} = -0.25$ V; $t_{dep} = 300$ s; $t_{rest} = 15$ s. E_{rest}: (a) -0.25; (b) -1; (c) -1.2; (d) -1.4; (e) -1.6 V.

and, as an additional step, a cathodic potential was superimposed during the rest period (t_{rest}). After this step the electrode was charged again at -0.25 V and, after 3 s, the scan was started.

The effect of these cathodic rest potentials (E_{rest}) on the stripping peaks is shown in Fig. 3. The solution was prepared by adding the Sep-Pak extract (from 1 l of sea water) and an amount of copper sufficient to obtain a "double peak" to the supporting electrolyte. When E_{rest} was set more negative in the range -1.2 to -1.6 V, the shape of the peak improved and, at $E_{rest} = -1.6$ V, the peak with the more positive E_p value disappeared. E_p and $w_{1/2}$ assumed values similar to those for ionic copper in organic-free $NaClO_4$. The same effect on the double peak also occurred at pH 2. Figure 4 shows the effect of the potential step at -1.6 V on the copper peak when the deposition time was varied from 1 to 10 min. The i_p vs. t_{dep} relationship shows a linear behaviour (Fig. 4B).

These results show that this additional cathodic potential step removes the effect on i_p of the adsorption of organic matter during the plating step. A possible mechanism could be the desorption of the organic film due to an electrostatic effect of the negative value of the charge on the electrode.

The effectiveness of this procedure on the resolution of the copper peak is shown in Fig. 5, where increasing amounts of SPE–CuMOM complexes were added to 0.5 M $NaClO_4$ at pH 6. All

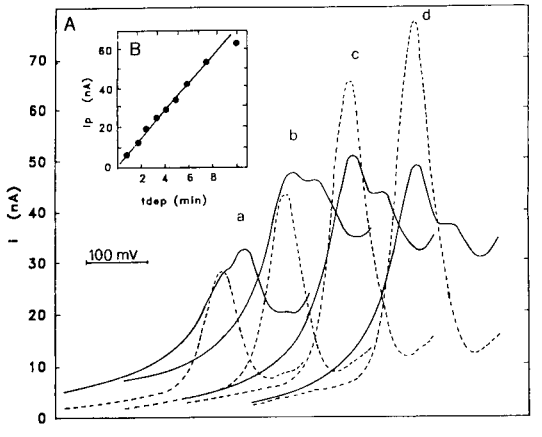

Fig. 4. Effect of deposition time on the copper stripping peak in the presence of SPE–MOM. (A) Solid lines, $E_{dep} = E_{rest} = -0.25$ V; dashed lines, $E_{dep} = -0.25$ V, $E_{rest} = -1.6$ V. t_{dep}: (a) 150; (b) 300; (c) 450; (d) 600 s. (B) i_p (nA) vs. t_{dep} after $E_{rest} = -1.6$ V. $E_p = 2$ mV.

the plots were obtained with $E_{dep} = -0.25$ V and $t_{dep} = 300$ s. The calculated total copper concentrations in solution were 0.8, 1.6, 2.4 and 3.2×10^{-8} M Cu. The double peak reported above does not appear at these low copper concentrations; nevertheless, at $E_{dep} = E_{rest} = -0.25$ V, the peak is ill-defined and difficult to quantify (Fig. 5A). A second analysis was performed by setting the potential at -1.4 V during the rest time (15 s). At these copper concentrations this lower potential was found to be sufficient to improve the baseline. This value (-1.4 V) was preferred to the higher value (-1.6 V) because it reduced the hydrogen evolution current during this step. In this instance, the peak was well defined and the current precisely measurable (Fig. 5B).

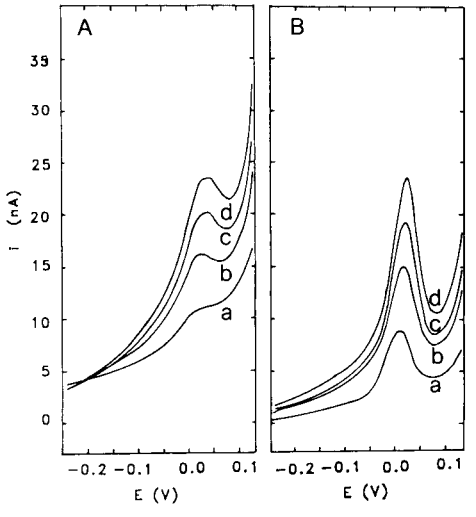

Fig. 5. DPASV of SPE–CuMOM complexes. $t_{dep} = 300$ s; $t_{rest} = 15$ s; $\Delta E = 25$ mV; scan rate = 12 mV s^{-1}. (a) 0.8; (b) 1.6; (c) 2.4; (d) 3.2×10^{-8} M total copper. (A) $E_{dep} = E_{rest} = -0.25$ V, $E_p = 45 \pm 5$ mV. (B) $E_{dep} = -0.25$ V, $E_{rest} = -1.4$ V, $E_p = 15 \pm 3$ mV, $w_{1/2} = 62 \pm 5$ mV.

This modified DPASV procedure was tentatively used for evaluating the lability of SPE–CuMOM complexes in 0.5 M $NaClO_4$ at pH 6. The voltammetric current peak was related to the total copper concentration in the cell measured by a non-electrochemical method. The voltammetric conditions were $E_{dep} = -0.25$ V, $t_{dep} = 180$ s, $E_{rest} = -1.4$ V and $t_{rest} = 15$ s.

Ten different natural sea water (pH 8) samples (1 l) were passed through Sep-Pak cartridges. $[Cu]_{tot}$ in the water-dissolved Sep-Pak eluates was measured by AAS, then known aliquots of this solution were added to $NaClO_4$ without any ionic copper addition. This calibration should also clarify if the reduction of some adsorbed SPE–CuMOM complexes occurs during the potential step at -1.4 V, so contributing to the peak current. The final total copper concentration in the polarographic cell ranged from 0.8×10^{-8} to 5×10^{-8} M. The TOC concentration ranged from 2 to 6 mg^{-1}.

The results are shown in Fig. 6. The plot of i_p vs. $[Cu]_{tot}$ was linear in the tested range ($r^2 = 0.986$, $n = 19$) with a sensitivity of 1.69×10^{-3} nA l $nmol^{-1}$ s^{-1}. Because this sensitivity is comparable to that found for ionic copper in the organic-free medium (see Experimental), the reduction of SPE–CuMOM complexes seems to occur at the same rate as the Cu^{2+}–Cu^0 reaction. This result also indicates that the copper reduced during the potential step at -1.4 V must be negligible with respect to the copper plated at -0.25 V. Hence the SPE–CuMOM complexes seem to be labile in 0.5 M $NaClO_4$ at pH 6 under the conditions of low overpotential ($E_{dep} = -0.25$ V).

Because the highly negative potential step acts only after the end of the plating step, the results indicate that this type of surfactant does not

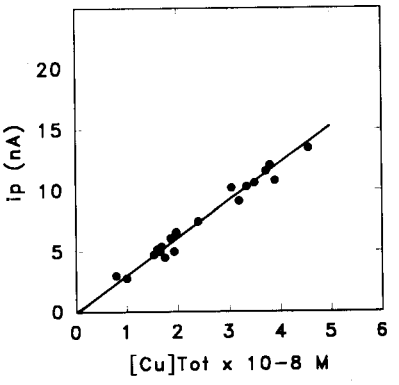

Fig. 6. Plot of i_p vs. $[Cu]_{tot}$ for SPE–CuMOM complexes. Symbols, DPASV with potential reduction step to −1.4 V; solid line, calibration plot of copper in organic-free 0.5 M $NaClO_4$.

hinder the metal reduction. As a consequence, the organic layer adsorbed during the plating step seems mainly to interfere with the anodic process, probably owing to the pulsed nature of the stripping step [11,19].

This modified DPASV procedure might be a useful test for discriminating between the effects of complexation on the peak current and those due to interfering adsorption processes. This was accomplished by using stripping polarography.

Figure 7 (curve a) shows the relationship between i_p and E_{dep} at a constant t_{dep} for a solutions containing 3.8×10^{-8} M copper as SPE–CuMOM at pH 6. When the ASV cycles were performed at $E_{dep} = E_{rest}$ the pseudo-polarogram did not reach a plateau but showed a continuous increase of i_p at $-E_{dep} > 0.2$ V corresponding to the limiting peak current (i_{pL}) for ionic copper. When the potential step at −1.4 V was applied, the current assumed the limiting value in the range $0.2 < -E_{dep} < 1.2$ V, as expected for ionic copper. Moreover, i_p reached the value 12.3 ± 0.5 nA, equal to that reported in Fig. 6 for the same copper concentration. The linearity with t_{dep} was also verified. In addition, copper determination was performed ($E_{dep} = -0.25$ V and $E_{rest} = -1.4$ V) by adding three spikes of 0.25×10^{-8} M ionic copper. The regression line of i_p vs. added Cu allowed a copper concentration of 3.5×10^{-8} M to be calculated.

A more complex pseudo-polarographic behaviour was found for a solution containing 4.5×10^{-8} M copper as SPE–CuMOM at pH 2. In particular, when $E_{rest} = E_{dep}$, i_p assumes, over a wide potential range, higher values than those expected (Fig. 7, curve b). In addition, i_p did not vary linearly with t_{dep} at $E_{dep} = E_{rest} = -1$ V. At this pH all the copper can be considered to be ionic, and a current value of 14.5 ± 0.5 nA, which is that corresponding to an organic-free copper solution, should be obtained. When $E_{rest} = -1.4$ V a nearly constant expected value of $i_p = 15.4 \pm 0.9$ nA was obtained in the range $0.2 < -E_{dep} < 1.2$ V, and i_p was also found to vary linearly with t_{dep} at $E_{dep} = -1$ V. The standard addition method gave a copper concentration of 4.2×10^{-8} M.

From these results, together with those in Fig. 6, curves a and b in Fig. 7 must be regarded as an artefact due to adsorption interferences. This conclusion seems to be of interest because the behaviour at pH 6 could be erroneously attributed to the presence of a large number of different reducible copper complexes that need a high overvoltage for their reduction. On the other hand, the behaviour at pH 2 suggests that care must be taken when the non-reducible copper

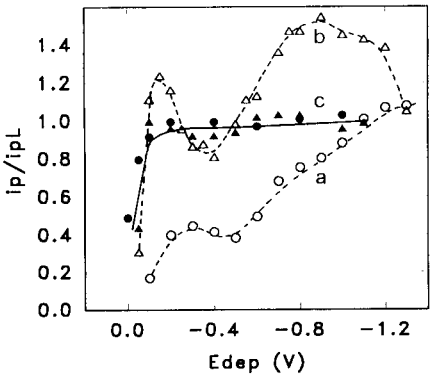

Fig. 7. Relationship between applied deposition potential and copper peak current for SPE–CuMOM solutions. $t_{dep} = 180$ s; i_{pL} refers to the limiting current obtained by applying the cathodic potential step after plating. (a) pH 6, $[Cu]_{tot} = 3.8 \times 10^{-8}$ M, $E_{dep} = E_{rest}$, $E_p = +27 \pm 1.5$ mV; (b) pH 2, $[Cu]_{tot} = 4.5 \times 10^{-8}$ M, $E_{dep} = E_{rest}$, $E_p = +20 \pm 3$ mV; (c) ● = pH 6, $E_{rest} = -1.4$ V, $i_{pL} = 12.3 \pm 0.5$ nA, $E_p = +15 \pm 3$ mV; ▲ = pH 2, $E_{rest} = -1.4$ V, $i_{pL} = 15.7 \pm 0.8$ nA, $E_p = -4 \pm 1.3$ mV.

complexes are defined by the i_p difference between complexing and non-complexing conditions obtained by a pH change. Such a two-point method should clearly be considered unsuitable for defining the amount of the metal present in SPE–CuMOM as non-labile complexes.

The behaviour of soil fulvic acid (SFA) was also briefly investigated. These compounds are known to be complexing agents subject to adsorption at the charged mercury surface [8,26]. In Fig. 8 the copper peak obtained in organic-free $NaClO_4$ is compared with that obtained after addition of SFA (0.5 mg l^{-1}). At $E_{dep} = -0.25$ V, the peak appeared broadened, showing an apparent decrease in i_p. When the plating step was followed by the E_{rest} potential step at -1.4 V, the copper peak overlapped that obtained in the organic-free solution with i_p assuming a constant value in the range $0.25 < -E_{dep} < 1.4$ V. When 0.5 mg l^{-1} SFA was added to the copper solution only during oxidation step (15 s before the end of the plating time), the stripping peak was only slightly broadened with about the same i_p value. This effect reflects the slowness of adsorption process and it indicates that, at this concentration of SFA, the adsorption occurring during the stripping step is negligible. Only at SFA concentrations higher than 2 mg l^{-1} were the peak shape and the current value noticeably affected.

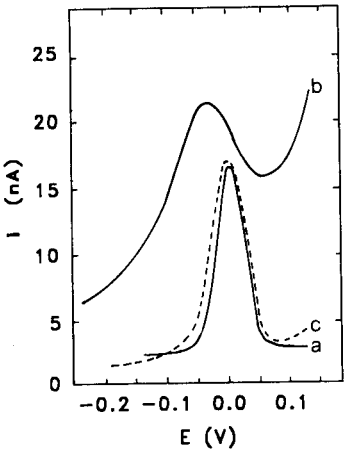

Fig. 8. DPASV of copper in the presence of fulvic acid. (a) Organic-free 0.5 M $NaClO_4$, pH 6, [Cu] = 5×10^{-8} M, $E_{dep} = E_{rest} = -0.25$ V, $t_{dep} = 180$ s; (b) after addition of 0.5 mg l^{-1} FA; (c) as (b) but $E_{rest} = -1.4$ V.

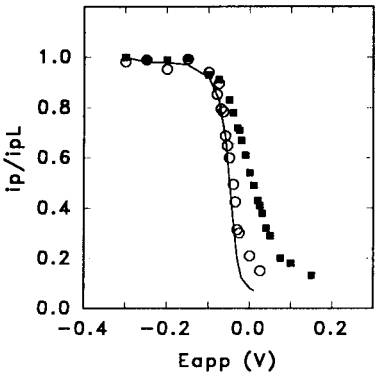

Fig. 9. Differential-pulse stripping polarograms ($E_{rest} = -1.4$ V) of copper in the presence of (○) FA and (■) SPE–MOM. Solid line, copper in organic-free $NaClO_4$.

The pseudo-polarographic approach used in Fig. 7 (curve c) was applied to obtain the i_p vs. E_{dep} relationship on the rising part of the reduction wave of copper in the presence of SPE–MOM and SFA (Fig. 9).

This relationship cannot be considered as a true pseudo-polarogram owing to the cathodic potential step at -1.4 V performed after each E_{dep}, hence additional considerations must be taken into account. When the limiting current of the pseudo-polarogram is considered (as in Fig. 7, curve c), the effects of the reducing characteristics of E_{rest} on i_{pL} can be neglected because at $E_{dep} = -0.25$ V the SPE–CuMOM complexes were found to be labile (Fig. 6). Along the rising part of the reduction wave, where E_{dep} assumes values more anodic than -0.25 V, an additional reduction might take place during the potential step owing to the presence of adsorbed copper species on the electrode, so contributing to the peak current. Hence the results reported here are only examined from a qualitative point of view.

The reduction wave of copper in SFA solution behaves very similarly to that of the ionic copper with a half-wave potential ($E_{1/2}$) close to -50 mV and a slope of 34 mV. Apart from the minor deviation at the bottom of the curve, probably due to the negative value of E_{rest}, this behaviour shows that the interferences are effectively removed when the cathodic potential step is ap-

plied. The reduction wave of copper in SPE–MOM solution also exibits a narrow sigmoid-shaped curve at E_{dep} ranging from +0.1 to −0.25 V, but it shows a 60 mV positive shift of $E_{1/2}$ and a broadened rising part of the wave. This could suggest a different reduction mechanism with respect to that of ionic copper or, alternatively, a more pronounced influence of the reducing E_{rest} value on i_p.

Conclusion

The use of an additional selected cathodic potential step in the determination of copper by DPASV decreases the effect of the adsorption of naturally occurring organic matter on the mercury electrode. For marine hydrophobic organic matter and soil fulvic acid this was achieved by negatively charging the drop using a rest potential of −1.4 V during the rest time of the DPASV cycle. This improves the electrochemical response and allows a lower overpotential to be used in the plating step.

The study of the electrocapillary curves and a knowledge of the relationship between the peak current and the charge on the electrode surface could be a helpful preliminary step when voltammetric methods are used for complexation studies of naturally occurring organic matter. In fact, when the complexation and adsorption phenomena simultaneously affect the voltammetric response, the capability of ASV to detect speciation is strongly decreased.

The authors thank Professor A. Zirino for comments and suggestions.

REFERENCES

1 J. Buffle, Complexation Reactions in Aquatic Systems: an Analytical Approach, Horwood, Chichester, 1988, Chap. 9.
2 Z. Lukaszewski, M.K. Pawlak and A. Ciszewski, J. Electroanal. Chem. Interfacial Electrochem., 103 (1979) 217.
3 J. Buffle, A.M. Mota and M.L.S. Simoes Goncalves, J. Electroanal. Chem. Interfacial Electrochem., 223 (1987) 235.
4 F.L. Greter, J. Buffle and W. Haerdi, J. Electroanal. Chem. Interfacial Electrochem., 101 (1979) 211.
5 J. Buffle and F.L. Greter, J. Electroanal. Chem. Interfacial Electrochem., 101 (1979) 231.
6 M. Plavsic, B. Cosovic and S. Miletic, Anal. Chim. Acta, 255 (1991) 15.
7 M. Plavsic and B. Cosovic, Mar. Chem., 36 (1991) 39.
8 J. Buffle and A. Cominoli, J. Electroanal. Chem. Interfacial Electrochem., 121 (1981) 273.
9 J. Buffle, J.J. Vuilleumier, M.L. Tercier and N. Parthasarathy, Sci. Total. Environ., 60 (1987) 75.
10 S.A. Wilson, T.C. Huth, R.E. Arndt and R.K. Skogerboe, Anal. Chem., 52 (1980) 1515.
11 R.M.F.J. Cleven, P. del Castillo and P.M. Wolfs, Environ. Technol. Lett., 9 (1988) 869.
12 M. Boussemart, C. Benamou, M. Richou and J.Y. Benaim, Mar. Chem., 28 (1989) 27.
13 T. Ugapo and W.F. Pickering, Talanta, 32 (1985) 131.
14 G.E. Batley, Anal. Chim. Acta, 189 (1986) 371.
15 P.L. Brezonik, P.A. Brauner and W. Stumm, Water Res., 10 (1976) 605.
16 A. Nelson and R.F.C. Mantoura, J. Electroanal. Chem. Interfacial Electrochem., 164 (1984) 265.
17 A. Nelson, Anal. Chim. Acta, 169 (1985) 273.
18 C. Brihaye and G. Duyckaerts, Anal. Chim. Acta, 146 (1983) 37.
19 J.E. Gregor and H.K.J. Powell, Anal. Chim. Acta, 211 (1988) 141.
20 T.M. Florence, Anal Chim. Acta, 119 (1980) 217.
21 G.L. Mills and J.G. Quinn, Mar. Chem., 10 (1981) 93.
22 X. Zhou and P.J. Wangersky, Mar. Chem., 26 (1989) 21.
23 G.S. Douglas, G.L. Millis and J.G. Quinn, Mar. Chem., 19 (1986) 161.
24 J.R. Donat, P.J. Statham and K.W. Bruland, Mar. Chem., 18 (1986) 85.
25 A. Zirino and S.P. Kounaves, Anal. Chem., 49 (1977) 56.
26 M. Shuman and J.L. Cromer, Anal. Chem., 51 (1979) 1546.
27 M. Branica, D. Novak and S. Bubic, Croat. Chem. Acta, 49 (1977) 539.
28 M. Lovric and M. Branica, Croat. Chem. Acta, 53 (1980) 477.
29 L. Mart, Fresenius' Z. Anal. Chem., 296 (1979) 350.
30 L. Mart, Fresenius' Z. Anal. Chem., 299 (1979) 97.
31 J.W. Weber and S.A. Wilson, Water Res., 9 (1975) 1079.
32 B. Raspor, Sci. Total Environ., 81/82 (1989) 319.

Analytica Chimica Acta, 277 (1993) 145–151
Elsevier Science Publishers B.V., Amsterdam

Polarographic determination of total iron, iron(II) and iron(III) in zinc plant electrolyte

A.M. Bond and B.V. Pfund

Department of Chemistry, La Trobe University, Bundoora, Victoria 3083 (Australia)

O.M.G. Newman

Pasminco-EZ Co. of Australia Ltd., GPO Box 377D, Hobart, Tasmania 7001 (Australia)

(Received 9th June 1992)

Abstract

Polarographic methods for the determination of iron(II), iron(III) and total iron in zinc plant electrolyte have been investigated. To provide a suitable medium for the determination, an aliquot of zinc plant electrolyte is added to a 0.1 M citrate–0.1 M EDTA solution and adjusted to pH 6.0 with ammonia. Polarograms recorded under these conditions provide a reversible $Fe(III) + e^- \rightleftarrows Fe(II)$ response which is essentially independent of whether iron(II) or iron(III) standard solutions are used for calibration purposes. The media used eliminates interference from copper and precipitation of insoluble materials which occurs with more commonly used electrolytes for the polarographic determination of iron. Measurement of the differential pulse and current sampled dc polarograms followed by sequential addition of iron(II) and iron(III) iron standards provides an efficient method for the simultaneous determination of total iron, iron(II) and iron(III) in the 30–100 mg l^{-1} range. However, while the results for the total iron method can be validated, it has not been possible to establish whether or not transport of plant electrolyte circulating at elevated temperatures to a polarographic cell maintained at ambient temperature modifies the ratio of the two oxidation states.

Keywords: Polarography; Iron; Plant electrolyte; Zinc

The electrolytic recovery of metallic zinc requires the electrochemical reduction of zinc ions from purified zinc sulphate plant electrolyte. The presence of metals such as copper and cadmium in the plant electrolyte, either lowers the efficiency of the zinc electrolysis or leads by codeposition to a poorer quality product, or both. Consequently, the monitoring of metal impurities at trace levels, especially those metal ions which are more readily reduced than zinc, is required at all stages of the production of zinc.

Correspondence to: A.M. Bond, Department of Chemistry, La Trobe University, Bundoora, Victoria 3083 (Australia).

In view of the fact that the production of zinc is based on electrochemical methods, it is not surprising that electroanalytical methods have been widely considered for the determination of impurities such as cadmium, cobalt, antimony, nickel and copper [1–3]. For example, work in these laboratories has led to the development of an on-line voltammetric method for continuous monitoring of these metals which has now been used in the Pasminco Metals-EZ (PMEZ) plant for several years [3].

Iron occurs in leach solutions used for zinc production at concentrations in excess of 20 g l^{-1}, the dominant form being iron(III). At the PMEZ

plant, it is removed from iron rich solutions as jarosite, a basic iron sulphate. However, iron is incompletely removed by this process and an additional iron removal step is required which involves the precipitation of hydrated iron oxide at pH 5.2, under aerated conditions, so that any iron(II) is oxidised to iron(III). Iron-purified solutions typically contain 1–50 mg l^{-1} iron partly in solution and partly as suspended particulates, the plant operating ideally involving the lower end of this range.

Polarographic methods for the determination of iron have been developed for many matrices [4,5]. However, application to zinc plant electrolyte presents a range of problems not usually encountered in other matrices. For example, the widely used oxalic acid electrolyte, in which a reversible well-defined $Fe(III) + e^- \rightleftarrows Fe(II)$ response is observed [6], is unsatisfactory because the presence of saturated solutions of calcium sulphate in the zinc plant electrolyte leads to precipitation of calcium oxalate. Additionally, the presence of many electroactive species other than iron means that achieving adequate resolution of the iron response is difficult. Standard complexing agents which might be used to mask the interferences in zinc plant electrolyte do not work because they complex preferentially with the large excess of zinc, rather than with the iron or interfering elements of interest.

This paper describes the results of an investigation into the development of a reagent combination which enables the direct determination of total iron in zinc plant electrolyte and which enables information on the distribution between iron(III) and iron(II) to be obtained. The method has been developed so that, if required, it could be readily implemented in the on-line mode described elsewhere [3], although at this stage, it has only been employed in an off-line mode on typical samples available at the PMEZ plant.

EXPERIMENTAL

Chemicals

Trisodium citrate, disodium diaminoethanetetraacetic acid (EDTA) and ammonia (33% solution) required to prepare the reagent combination used for the determination of iron were of analytical grade purity, as were ammonium iron(II) sulphate, iron(III) nitrate, copper(II) nitrate and cadmium nitrate from which standard solutions were prepared. Zinc plant electrolyte solutions were obtained from the PMEZ plant and either acidic leach solutions containing about 10 g l^{-1} sulphuric acid (high iron levels) or near neutral iron purified solutions (low iron levels) were examined.

Instrumentation

Voltammograms (polarograms) for determining total iron, copper and cadmium were obtained with a Metrohm Model 646 VA processor and Model 647 VA stand. The multi-mode mercury electrode was used in the dropping mercury format for polarography and in the hanging mercury drop format for stripping voltammetry. The reference and auxiliary electrodes were Ag/AgCl (3 M KCl) and glassy carbon electrodes respectively. The pH was measured with a Metrohm E520 pH meter. Oxygen was removed by degassing with high purity nitrogen and the temperature was maintained at 20 ± 1°C throughout the course of the determination of iron.

For the simultaneous determination of total iron(II) and iron(III), either a PAR Model 174 polarographic analyser modified [7] so that current sampled d.c. and differential pulse polarograms could be measured in a single experiment was used or alternatively the Metrohm equipment described above was used with dc and differential pulse polarograms being recorded sequentially.

Determination of total iron

An aliquot of zinc plant electrolyte (acidic or neutral) was added to 20 ml of reagent solution (0.1 M sodium citrate–0.1 M EDTA) and adjusted to pH 6.0 with ammonia. After 5 min degassing of the solution with nitrogen to remove oxygen, a differential pulse polarogram (drop time = 0.8 s, pulse amplitude = −50 mV) recorded over the potential range of 0.10 to −0.30 V vs. Ag/AgCl gives an extremely well-defined response with a peak potential, E_p, of -0.09 ± 0.02 V vs. Ag/AgCl. Additionally, copper and

cadmium may be determined simultaneously with total iron via the use of their well resolved reduction processes which have peak potentials at -0.37 ± 0.02 and -0.59 ± 0.02 V vs. Ag/AgCl, respectively, under the above-mentioned conditions. Differential pulse voltammetry at a stationary mercury drop may be used as an alternative to the polarographic method in order to conserve mercury.

RESULTS AND DISCUSSION

Determination of total iron

Ideally, for the sensitive determination of total iron by differential pulse polarography, a reversible process (Eqn. 1) would be used:

$$Fe(III) + e^- \rightleftharpoons Fe(II) \quad (1)$$

In the presence of commonly used complexing agents such as oxalate, tartrate or citrate, the half-wave potential ($E_{1/2}$) for reduction of Fe(III) and oxidation of Fe(II) are identical as theoretically expected for a reversible process, assuming equal diffusion coefficients for iron(II) and iron(III) ions. Total iron can be determined in such media by techniques such as differential pulse polarography, because at least in their commonly used forms, such methods do not distinguish between oxidative and reductive currents. Methods such as current sampled dc polarography which have the capability of measuring the sign of the current may be used to determine iron(II) and iron(III).

In zinc plant electrolyte, neither oxalate or tartrate electrolytes can be used for the determination of iron because of precipitation of insoluble calcium salts, PMEZ solutions being saturated with calcium sulphate. While citrate electrolytes do not suffer from this problem, resolution from the process for reduction of copper (Eqn. 2) is inadequate if a purely citrate electrolyte is employed:

$$Cu(II) + 2e^- \overset{Hg}{\rightleftharpoons} Cu(Hg) \quad (2)$$

To achieve adequate resolution of the iron and copper responses, EDTA, which shifts the copper reduction to significantly more negative potentials than the iron process, may be added to the zinc plant electrolyte solution along with a buffer. However, the concentrations of citrate and EDTA as well as the pH and buffering capacity must be very carefully controlled as the half-wave potentials of the iron, as well as copper, cadmium and other potential interferents, are all sensitive to variations in these parameters. Additionally, the volume ratio of zinc plant electrolyte to analytical reagents used for the determination is critical. The high concentrations of zinc in the plant electrolyte needs to be diluted prior to the determination, so that complexation with the vast excess of zinc does not preclude sufficient complexation taking place with iron and copper.

After an extensive investigation of the influence of the variation of pH and buffer capacity and the concentration of citrate and EDTA as well as the ratio of volumes of zinc plant electrolyte to reagent, the procedure for total iron given above is recommended.

In reagent solution only (no zinc present), an iron(II) standard gave a linear calibration graph with a slope of 75 nA l mg^{-1} and a correlation coefficient of 0.9998 ($n = 6$) via standard regression analysis over the range 1–20 mg l^{-1}. The corresponding values for a calibration graph prepared from the iron(III) standard solution were 72 nA l mg^{-1} and 0.9993 ($n = 6$). These data demonstrate that total iron can be determined by use of either an iron(III) or an iron(II) standard. The iron(II) standard was used for the determination of total iron as it was prepared from an ammonium sulphate salt and is therefore completely compatible with the matrix. However, the method of standard additions was used in preference to direct calibration to minimise any problems associated with the matrix which may vary considerably in samples obtained from different stages of the zinc production.

Figure 1 shows responses for the simultaneous determination of total iron, copper and cadmium when 1 ml of high iron "acidic" zinc plant electrolyte containing 10 g l^{-1} sulphuric acid is added to 20 ml of the reagent solution. Extremely well defined and separated peaks were obtained for each metal. The cadmium concentration in this particular sample was determined by anodic

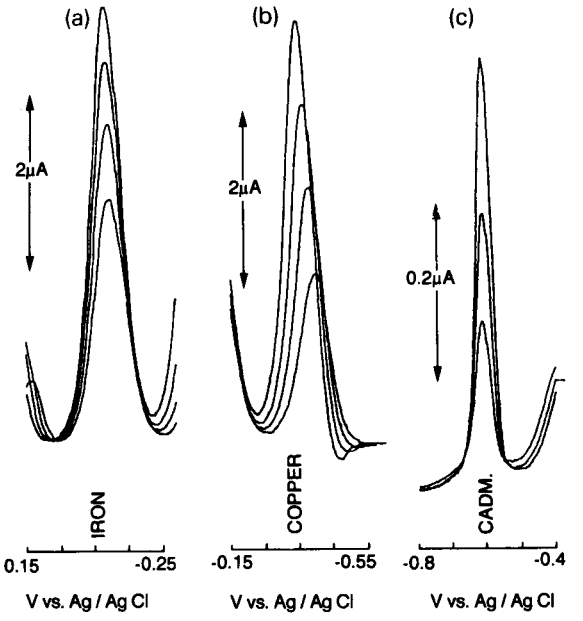

Fig. 1. Simultaneous determination of total (a) iron, (b) copper and (c) cadmium by (a, b) differential pulse polarography (pulse amplitude = −50 mV, drop time = 0.8 s); and (c) differential pulse anodic stripping voltammetry (pulse amplitude = 50 mV, duration between pulses = 0.6 s, plating time with stirring = 20 s, equilibration time = 5 s) in high iron "acidic" zinc plant electrolyte. Curves (lowest to highest) refer to addition of 0, 1, 2 and 3×200 μl of 1.00 g l^{-1} iron(II), copper and cadmium standards. Other experimental parameters and details are presented in the text.

stripping voltammetry as the concentration was too low to be determined accurately by polarography. Figure 2 shows voltammetric curves obtained on the low iron "neutral" zinc plant electrolyte in which 5 ml of sample was added to 20 ml of reagent solution. In this sample, which involves less dilution of plant electrolyte, the polarographic method could be applied directly to the determination of cadmium as well as the other elements. As can be seen from data contained in Table 1, the slopes of the standard addition calibration data change markedly when the volume ratio of plant sample to reagent is altered from 1:20 to 5:20. However, the slope of the iron peak current response in supporting electrolyte reagent alone and with a zinc plant electrolyte solution to supporting electrolyte ratio of 1:20 are not markedly different. While the simultaneous determination of total iron, copper and cadmium may be achieved with the use of the reagent developed in this work, the determination of cadmium and copper may be better achieved by the on-line method described elsewhere [2,3] where the matrix variation is removed by a matrix exchange procedure applicable to metals that can be reduced to the metallic (amalgam) state at a hanging mercury drop electrode.

TABLE 1

Representative data obtained for the determination of total iron, iron(II), iron(III), copper and cadmium in 0.1 M citrate–0.1 M EDTA (pH 6.0) by differential pulse polarography [a]

Solution	Element	Concentration [b] (mg l^{-1})	Standard addition slope (nA l mg^{-1})	Correlation coefficient (n = 6)
Reagent	Fe(II)	–	75	0.9998
only	Fe(III)	–	72	0.9993
With addition				
of 1 ml "acidic"	Fe(total)	688	74	0.9990
zinc plant	Cu	301	107	0.9987
electrolyte [c]	Cd [d]	189	15	0.9968
With addition				
of 5 ml "neutral"	Fe(total)	31.0	289	0.9981
zinc plant	Cu	148	85	0.9938
electrolyte [c]	Cd	225	109	0.9989

[a] Method of standard additions used in all cases for the determinations in zinc plant electrolyte. Experimental parameters for all measurements are given in the text. [b] In zinc plant electrolyte prior to dilution. [c] Added to 20 ml of supporting electrolyte [d] By anodic stripping voltammetry, all other determinations by differential pulse polarography.

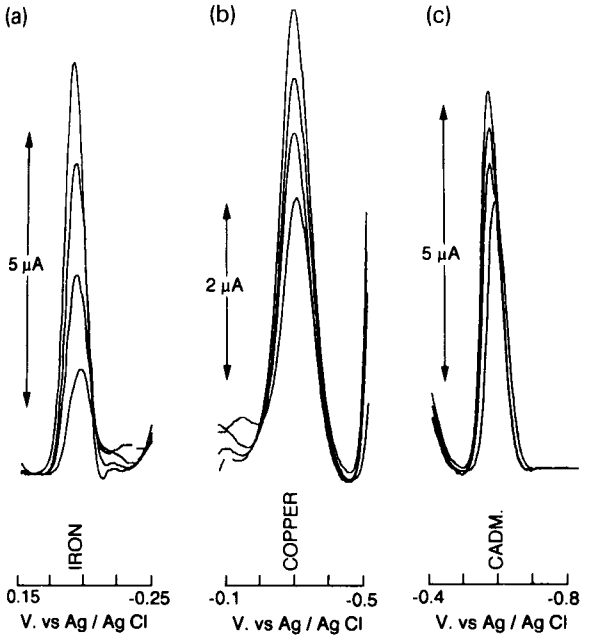

Fig. 2. Simultaneous determination of total (a) iron, (b) copper and (c) cadmium by differential pulse polarography (pulse amplitude = −50 mV, drop time = 0.8 s) in low iron "neutral" zinc plant electrolyte. Other details are as for Fig. 1.

Determination of total iron, iron(II) and iron(III) in zinc plant electrolyte

A transient polarographic (voltammetric) technique, such as the differential pulse method described above, may not be used for the determination of iron(II) and iron(III) when the electrode process is reversible because no distinction between oxidative and reductive components of the experiments is possible. However, a steady-state method such as dc polarography may be used. With d.c. polarography, the reduction current represents the iron(III) concentration as measured from the $Fe(III) + e^- \rightleftarrows Fe(II)$ component and the oxidation current represents the iron(II) concentration as measured by the $Fe(II) \rightleftarrows Fe(III) + e^-$ component.

The differential pulse experiment is obtained by adding a pulse component to the d.c. voltage ramp used in d.c. polarography and recording the difference between the current before and after the application of the pulse [7]. Inherently, the differential pulse measurement actually therefore contains the relevant information required to simultaneously determine the d.c. and differential

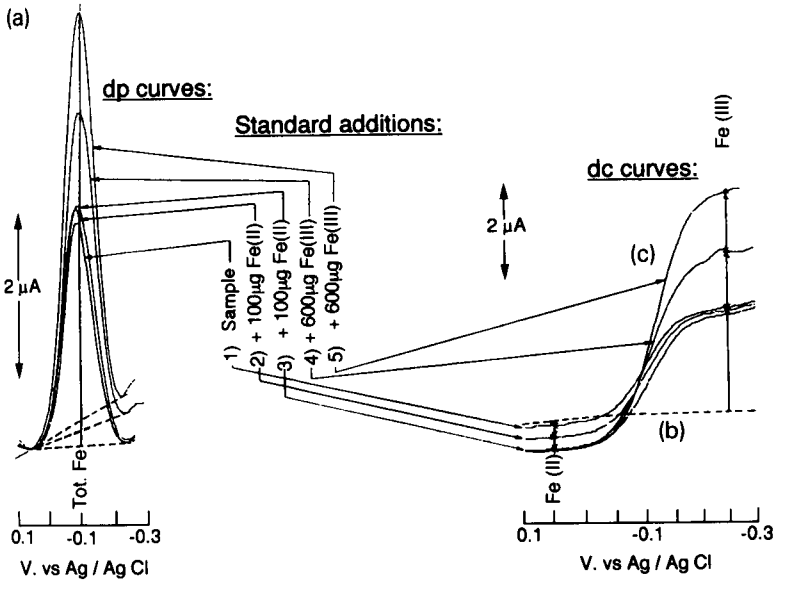

Fig. 3. Simultaneous determination of (a) total iron by differential pulse polarography (pulse amplitude = −50 mV, drop time = 0.8 s) and (b) iron(II) and iron(III) by d.c. polarography with sequential addition of iron(II) and iron(III) standard solutions. Other experimental parameters and details are described in the text.

pulse polarograms from the same experiment. Instrumentation suitable for this purpose is readily constructed in digital or analog format [7]. Alternatively, of course, sequential recording of d.c. and differential pulse polarograms may be used.

To determine total iron, as well as iron(II) and iron(III) in a single experiment using an efficient calibration procedure, a 1.5-ml aliquot of zinc electrolyte was added to 20 ml of 0.1 M sodium citrate–0.1 M EDTA reagent and the pH adjusted to 6.0 with ammonia. d.c. and differential pulse polarograms were recorded either simultaneously or sequentially on the same solution. Standard addition experiments with iron(II) were then used to determine both total iron and iron(II) and standard addition with iron(III) was used to determine iron(III). The baseline reference point (or zero Faradaic current) in the d.c. experiment was ascertained from experimental data obtained by using 1.5 ml of a synthetic zinc solution made from analytical reagent grade zinc sulphate at the approximate zinc concentration present in the plant electrolyte and at the same pH as the solution to be determined.

Figure 3 illustrates the responses obtained from the method as applied to a high iron acidic zinc plant electrolyte solution. In the first experiment, the differential pulse and d.c. polarograms are recorded. Two standard additions of iron(II) followed by two standard additions of iron(III) then enable total iron, iron(II) and iron(III) to be determined. Linear calibration plots are obtained. In the solution used to obtain the data presented in Fig. 3, four determinations gave values (mean $\pm$ S.D.) of 1032 ± 48, 50 ± 12 and 907 ± 53 mg l^{-1} for total iron, iron(II) and iron(III), respectively. For this solution and after transfer to the polarographic cell, the iron is predominantly iron(III). Furthermore, when the method was applied to the "low iron" neutral zinc plant electrolyte no iron(II) could be detected within the limit of experimental error. However, in the plant situation which operates at around 70°C the situation with respect to iron(II) and iron(III) may be different, relative to the situation prevailing after samples are collected from the plant stream, cooled, stored and then diluted in an off-line analytical method. In contrast, the total iron concentration determined should be directly relevant to the plant conditions, irrespective of whether the distribution between iron(II) and iron(III) changes. The methodology described in this paper therefore extends the range of trace elements that may be monitored in zinc plant electrolyte by polarographic procedures.

The validity of the total iron measurement method was confirmed by comparison of data obtained polarographically with established spectrophotometric methods [8,9] in which iron(III) is reduced to iron(II) using tin(II) chloride and the iron(II) is determined by titration with potassium dichromate in acid solution with diphenylamine as an indicator. In the spectrophotometric method, iron(II) is determined directly without addition of tin(II) chloride and iron(III) by difference [8,9]. With the spectrophotometric method and when high copper concentrations are present, the iron has to be separated from the copper as hydrated iron(III) oxide. Agreement between the polarographic and spectrophotometric methods was within $\pm 5\%$, $\pm 10\%$ and $\pm 20\%$ for total iron, iron(III) and iron(II), respectively for a range of samples. Unfortunately, in the present instance it was not possible to confirm the fidelity of the iron(II) and iron(III) measurements obtained in the laboratory with either polarographic or spectrophotometric methods with respect to the possible introduction of errors introduced by the sampling procedures. Such errors are a constant cause for concern, but in on-line applications where the time for sampling and measurement is small compared with the solution residence time in the plant, the problem may not be severe.

REFERENCES

1 E.S. Pilkington, C. Weeks and A.M. Bond, Anal. Chem., 48 (1976) 1665; and references cited therein.
2 A.M. Bond, R.W. Knight and O.M.G. Newman, Anal. Chem., 60 (1988) 2445; and references cited therein.
3 A.M. Bond, R.W. Knight, B.R. Champion and O.M.G. Newman, Extraction Metallurgy 1989, Institute of Mining and Metallurgy, London, 1989, pp 301–313.

4 I.M. Kolthoff and J.J. Lingane, Polarography, Interscience, New York, 1952; and references cited therein.
5 G. Henze and R. Neeb, Elektrochemische Analytik, Springer Verlag, Berlin, 1986; and references cited therein.
6 M.E. Beyer, A.M. Bond and R.J.W. McLaughlin, Anal. Chem., 47 (1975) 479; and references cited therein.
7 J.E. Anderson and A.M. Bond, Anal. Chem., 52 (1980) 1439.
8 A.I. Vogel, A Textbook of Quantitative Inorganic Analysis, Longmans, London, 3rd edn., 1961.
9 W.H. Scott, in N.H. Furman (Ed.), Standard Methods of Chemical Analysis, Van Nostrand–Reinhold, New York, 5th edn., 1939, pp. 471–474.

Analytica Chimica Acta, 277 (1993) 153–155
Elsevier Science Publishers B.V., Amsterdam

Remote analysis of motorboat exhausts using Fourier transform infrared spectrometry

Junde Wang, Yunhua Luo, Zuoru Chen, Yurang Lu, Su Pan and Xuemei Wang

Laboratory of Advanced Spectroscopy, East China Institute of Technology, Nanjing 210014 (China)

(Received 3rd November 1992)

Abstract

Infrared absorption spectra of motorboat exhausts were remotely recorded by means of remote-source Fourier transform infrared spectrometer with 4 cm^{-1} spectral resolution in the spectral range 4000–800 cm^{-1}, which covers mainly the spectral bands of methanol, carbon monoxide, carbon dioxide and water vapor. A method for quantitative remote identification is described. The concentrations found for methanol, carbon monoxide and carbon dioxide in the exhaust were 0.17, 4.26 and 0.32%, respectively.

Keywords: Infrared spectrometry; Engine exhausts

Remote-sensing Fourier transform infrared (FTIR) absorption spectrometry requires no sampling or sample handling, and no contamination can occur. Such measurements can simultaneously determine several pollutants more sensitively than IR emission spectrometry. Hence methods of this type have been extensively applied for, e.g., the determination of gaseous fluorides, such as SiF_4 and/or HF, emitted from a phosphate fertilizer plant gypsum pond, the exhausts of jet engines and air pollutants from an oil refinery [1,2], air pollution by large brick manufacturing facilities [3] and exhausts of motorcycles [4] and aircraft [5].

The fuel of high-speed engines used in racing motorboats usually consists of 75% methanol and 25% castor oil. When the combustion of the fuel is incomplete, amounts of vapour of harmful gaseous species are formed which not only pollute the environment but may also seriously affect the crew. This paper describes the determination of the various components in the exhausts of motorboats by remote-sensing FTIR absorption spectrometry. Through these quantitative measurements it would be possible and convenient to modify the burning conditions of the engine to reduce environmental pollution and to protect the health of the persons involved.

Correspondence to: Junde Wang, Laboratory of Advanced Spectroscopy, East China Institute of Technology, Nanjing 210014 (China).

EXPERIMENTAL

Apparatus

The spectrometer used was a Nicolet RS-170 remote-sensing FTIR system. This system is designed for absorption and/or emission studies of hot sources (jet exhausts, plumes, etc.) or long-path environmental transmission studies using remote IR sources. The instrumental components and operating conditions are given in Table 1. A more detailed description of this apparatus has been presented elsewhere [4].

TABLE 1

Instrumentation and operating conditions

Spectrometer	Continuous-scan Michelson interferometer with dual air bearings mounted at the geometric centre of mass of the scanning mirror carriage
Beamsplitter	Germanium-coated zinc selenide optimized for the spectral range 5400–700 cm^{-1}
Telescope	2-in refractive with zinc selenide optics
Detector	Liquid nitrogen-cooled mercury cadmium telluride (MCT) optimized for the spectral range 5400–700 cm^{-1}
Aperture	5 mm nominal diameter
Resolution	4 cm^{-1} in the range 5400–700 cm^{-1}
Scan velocity	Scan rate 1.5 s^{-1} at 4 cm^{-1} resolution
Standard IR source	Globar with optimized emissivity for the spectral range 5400–400 cm^{-1}

Procedure

For measuring the absorption of the exhaust from a motorboat engine, the standard IR source (Globar source) and remote-sensing FTIR system are located so as to provide an optical path perpendicular to the engine axis. The distance between the standard IR source and spectrometer is about 14 m.

The distance between the engine and spectrometer is about 10 m. Measurements are made with the engine operated at idling and afterburner power. The exhaust absorption path measured is about 10 cm. The receiver telescope is aimed at the nozzle exit plane of the engine. The absorption spectrum is the result of four cumulated scans.

The temperature of the exhaust of the sailing motorboat is measured by a semiconductor-connecting thermometer. In this work, the measured temperature was 353 K.

RESULTS AND DISCUSSION

The absorption spectrum obtained in the spectral region 4000–800 cm^{-1} at idling power of motorboat engine is shown in Fig. 1. At least five absorption bands of the methanol are observed, corresponding to 3740–3600, 3100–2765, 2070, 1400–1235 and 1080–974 cm^{-1}. The absorption band at 2349 cm^{-1} is due to carbon dioxide. The absorption band of carbon monoxide occurs at 2200–2100 cm^{-1}. The bands at 1800–1500 cm^{-1} are due to IR absorption of H_2O.

The exhaust component concentrations can be measured from absorption spectra through Beer's law:

$$\tau(\nu) = \exp[-K(\nu)C'L]$$

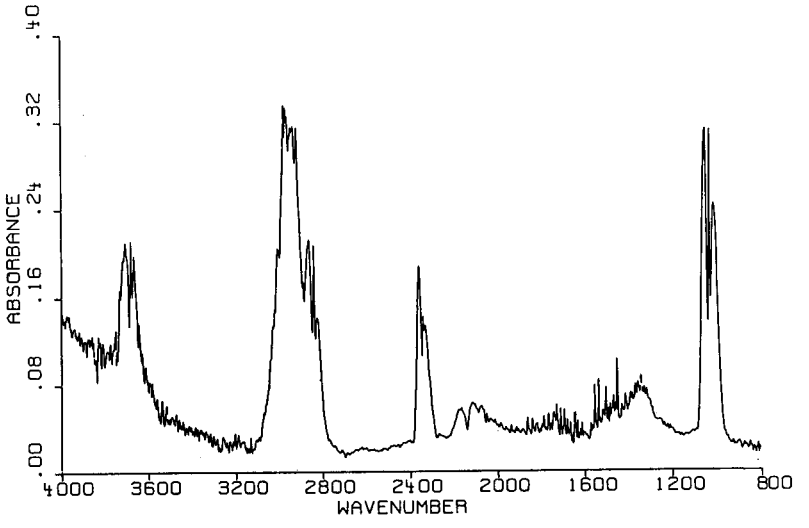

Fig. 1. Absorption spectrum of motorboat exhaust at idling power.

where $\tau(\nu)$ is the transmittance at the wavenumber ν, $K(\nu)$ is spectral absorption coefficient at the wavenumber ν, C' is the gas concentration uncorrected for gas temperature and L is the absorption path of the exhaust.

The gas concentration can be corrected for temperature differences by using the following equation:

$$C = C'(T/273)$$

where T is the gas temperature.

Table 2 gives the spectral absorption coefficients of gas components in the exhaust at room temperature. The concentrations of exhaust gases are given in Table 3.

Table 3 shows that carbon monoxide concentration at idling power is higher than at afterburner power, but the carbon dioxide and methanol concentrations at afterburner power are higher than at idling power. The relative standard deviations ($n = 12$) for carbon monoxide, carbon dioxide and methanol are 2.1, 8.8 and 2.5%, respectively.

TABLE 2

Spectral absorption coefficients $K(\nu)$ at room temperature

Species	Measurement frequency (cm^{-1})	Absorption coefficient ($atm^{-1}\ cm^{-1}$)
Carbon monoxide	2165	0.19
Carbon dioxide	2360	5.60
Methanol	1033	25

TABLE 3

Species concentrations in motorboat engine exhaust

Species	Concentration (%)	
	Idling power	Afterburner power
Carbon monoxide	4.26	1.05
Carbon dioxide	0.32	2.17
Methanol	0.17	0.38

This project was supported by the National Science Foundation of China.

REFERENCES

1 W.F. Herget, in J.R. Ferraro and L.J. Basile (Eds.), Fourier Transform Infrared Spectroscopy, Applications to Chemical Systems Vol. 2, Academic Press, New York, 1979, pp. 111–127.
2 W.F. Herget, Appl. Opt., 21 (1982) 635.
3 W.F. Herget and J.D. Brasher, Opt. Eng., 19 (1980) 508.
4 J.-D. Wang, H.-Y. Bian, Z.-R. Chen and Y.-H. Luo, Spectrosc. Lett., 21 (1988) 935.
5 J.-D. Wang, H.-Y. Bian, Z.-R. Chen, Y.-H. Lou and C. Ma, Fenxi Huaxue, 18 (1990) 435.

Analytica Chimica Acta, 277 (1993) 157–162
Elsevier Science Publishers B.V., Amsterdam

Determination of trace zirconium and hafnium in high-purity scandium oxide by inductively coupled plasma atomic emission spectrometry and extraction chromatography

Xiao-Jin Yang and Jing-Su Guan

Laboratory of Analytical Chemistry, Institute of Atomic Energy, P.O. Box 275(88), Beijing 102413 (China)

Tai-Jun Shen

Second Research Institute of Ministry of Public Security, Beijing (China)

(Received 10th June 1992)

Abstract

Inductively coupled plasma atomic emission spectrometry in combination with extraction chromatography was applied to the determination of trace amounts of zirconium and hafnium in high-purity scandium oxide. The chromatographic column separation procedure was carried out with 1-phenyl-3-methyl-4-benzoylpyrazol-5-one as the stationary phase and hydrochloride acid as the mobile phase. Optimum column operating conditions were established. The enrichment factor based on 0.1 g of scandium oxide was over 2000. The results obtained agreed well with those obtained by spark-source mass spectrometry without the separation of scandium. For a sample mass of 0.3 g, the detection limits for zirconium and hafnium were 0.14 and 0.17 $\mu g\ g^{-1}$, respectively. The proposed method could be applied to the analysis of scandium oxide of laser grade and 99.9995% purity.

Keywords: Atomic emission spectrometry; Inductively coupled plasma spectrometry; Liquid chromatography; Extraction; Hafnium; Scandium oxide; Zirconium

High-purity scandium has important applications in the electronic, atomic energy and laser industries, etc. Zirconium and hafnium are the main impurities in scandium oxide and the determination of trace amounts of these elements is important. However, there are few methods for the determination of traces of zirconium and hafnium in high-purity scandium oxide. In recent years, inductively coupled plasma atomic emission spectrometry (ICP-AES) has been applied extensively to the analysis of high-purity substances [1], but the method for the direct determination of traces of zirconium and hafnium in the presence of a large amount of a scandium matrix by ICP-AES [2] lacks satisfactory sensitivity because of spectral interferences and matrix effects, and large amounts of expensive Specpure scandium oxide are used for the matched matrix. In order to increase the sensitivity of the determination and to avoid spectral interference, chemical separation and preconcentration prior to ICP-AES determination are necessary.

In previous studies, it was found [3] that zirconium could be separated from scandium using a

Correspondence to: Xiao-Jin Yang, Laboratory of Analytical Chemistry, Institute of Atomic Energy, P.O. Box 275(88), Beijing 102413 (China).

cation-exchange resin with ammonium thiocyanate–hydrochloric acid as the eluent, but this method of separation is very tedious and ammonium thiocyanate will affect the ICP-AES determination. Deorkar and Khopkar [4] reported that a mixture of zirconium (25 μg), hafnium (25 μg) and scandium (50 μg) could be separated by extraction with dicyclohexyl-18-crown-6; however, it is difficult to apply this method to the analysis of high-purity scandium oxide.

1-Phenyl-3-methyl-4-benzoylpyrazol-5-one (PMBP) is a chelating extractant that has been used for the extraction of zirconium and hafnium [5], but it has not been applied in extraction chromatography for the separation of zirconium and hafnium from scandium. In this work the PMBP extraction chromatographic separation and ICP-AES determination of traces of zirconium and hafnium at the μg g^{-1} level in high-purity scandium oxide were investigated.

EXPERIMENTAL

Apparatus and conditions

ICP-AES determinations were made on ARL Model 3560 ICP spectrometer. The instrumental facilities and operating conditions used are summarized in Table 1. A PDP 11/23 computer controlled all instrument functions.

TABLE 1

Instrumentation and operating conditions for ICP-AES

ICP spectrometer	ARL 3560
RF generator:	
Frequency	27.12 MHz
Forward power	1.2 kW
Reflected power	< 5 W
Argon flow-rates:	
Coolant gas	12 l min^{-1}
Plasma gas	0.8 l min^{-1}
Carrier gas	1 l min^{-1}
Nebulizer	Meinhard TR-30-A_3 concentric glass nebulizer
Sample uptake rate	1.5 ml min^{-1}
Observation height	15 mm above load coil
Flush time	20 s
Signal integration time	10 s
Integration cycle	2
Wavelengths used:	
Zr	343.82 nm
Hf	264.14 nm
Sc	255.23 nm

For chromatographic separations, a borosilicate glass tube of i.d. 1 cm was filled with PMBP Levextral resin to give a resin bed height of 10 cm (in water). Before use, the resin column was pre-equilibrated with 15 ml of 6 M hydrochloric acid.

Reagents and materials

All chemicals were of analytical-reagent grade. Distilled, deionized water was used throughout.

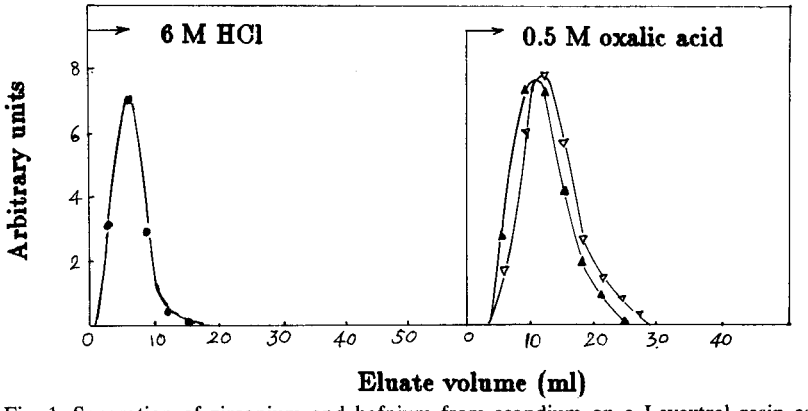

Fig. 1. Separation of zirconium and hafnium from scandium on a Levextrel resin column (10 cm × 1 cm i.d.). ● = Sc; ▲ = Zr; ▽ = Hf. Loading, 0.1 g of scandium oxide, 5 μg of Zr and 5 μg of Hf; flow-rate, 1 ml cm^{-2} min^{-1} for 6 M HCl, 0.8 ml cm^{-2} min^{-1} for 0.5 M oxalic acid.

Instrument calibration standards were prepared in 1 M HCl from commercially available 1 mg ml^{-1} stock standard solutions. Levextrel resin (75–120 mesh) was supplied by Beijing Research Institute of Chemical Engineering and Metallurgy. A 4-g amount of the resin was sufficient to give a bed height of 10 cm.

High-purity scandium oxide (99.99%) was used as a base matrix for the study of the elution behaviour and the recovery tests. Specpure scandium oxide was obtained from Johnson Matthey Chemicals (Royston, UK).

Procedure for investigation of chromatographic separation

An aliquot of solution containing 5 μg of zirconium, 5 μg of hafnium and 0.1 g of scandium oxide was mixed with 3 ml of 6 M hydrochloric acid. The solution was loaded on top of the column previously treated with 6 M HCl and eluted with 6 M HCl at a flow-rate of 1 ml cm^{-2} min^{-1}. The zirconium and hafnium were retained on the column while iron, calcium and unwanted elements and the matrix scandium were eluted with 6 M HCl. Twenty 3-ml fractions were collected and the scandium in each fraction was determined by EDTA titrimetry [6]. The zirconium and hafnium extracted with PMBP were stripped from the stationary phase with 0.5 M oxalic acid at a flow-rate of 0.8 ml cm^{-2} min^{-1}. Fifteen 3-ml fractions were collected and analysed by ICP-AES after eliminating the oxalic acid. The elution curves for scandium, zirconium and hafnium are given in Fig. 1.

Column regeneration

The used chromatographic columns were regenerated by washing with 15 ml of water at a flow-rate of 1 ml cm^{-2} min^{-1} followed by 15 ml of 6 M hydrochloric acid. The column was stored in water for further use.

RESULTS AND DISCUSSION

Effect of hydrochloric acid concentration

The extraction of scandium, zirconium and hafnium with PMBP was studied as a function of hydrochloric acid concentration and the results are given in Fig. 2. The optimum hydrochloric acid concentration range for the quantitative extraction of scandium is from 10^{-2} to 10^{-4} M. When the concentration is >2 M scandium is hardly extracted, whereas zirconium and hafnium are completely extracted from 2 to 7 M HCl. On basis of these results the chromatographic separation was carried out with 6 M hydrochloric acid as the mobile phase. Under these conditions calcium, aluminium and other unwanted elements were also separated from zirconium and hafnium.

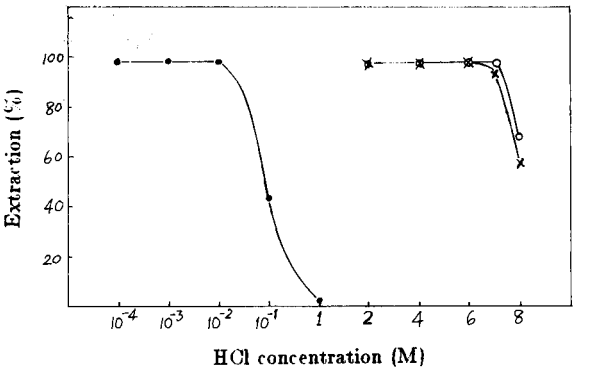

Fig. 2. Effect of hydrochloric acid concentration on the extraction of (●) scandium, (○) zirconium and (×) hafnium.

Effect of resin bed height

Three resin bed heights (5, 10 and 15 cm) were tested. Three aliquots of solution containing 0.1 g of scandium oxide, 10 μg of zirconium and 10 μg of hafnium in 6 M HCl medium were loaded on the columns and eluted with 6 M HCl at a flow-rate of 1 ml cm^{-2} min^{-1}. The results showed that 15 ml of eluent could wash more than 99% of the scandium oxide at any of the bed heights. The elution curves are shown in Fig. 3. After 80 ml of eluent had passed through, the concentration of scandium in the eluate determined by ICP-AES was less than 1 μg ml^{-1}. However, the recoveries of zirconium and hafnium were low for a 5-cm but good for 10- and 15-cm of bed heights. Therefore, a 4-g amount of resin, i.e., a 10-cm bed height, was adopted for the separation of zirconium and hafnium from scandium oxide. Under these conditions the extracted zirconium and

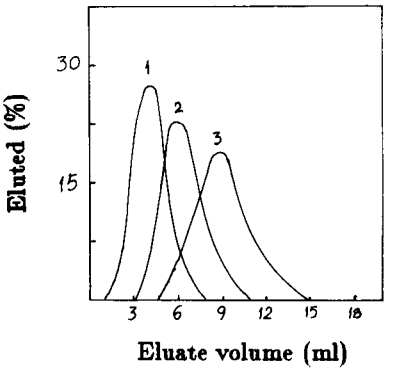

Fig. 3. Elution curves for scandium as a function of resin bed height (1 cm i.d. column) with 6 M HCl as the eluent. Bed height: (1) 5; (2) 10; (3) 15 cm. Flow-rate: 1 ml cm^{-2} min^{-1}.

hafnium on the column were found not to percolate through the column after elution with 100 ml of 6 M hydrochloric acid.

Effect of amount of scandium oxide

Feed solutions prepared with 5 ml of 6 M hydrochloric acid containing 0.1, 0.2 and 0.3 g of scandium oxide were passed through the column with a 10-cm bed height. The elution curves are shown in Fig. 4. The results showed that the concentration of scandium in the eluate after elution with 80 ml of 6 M HCl was less than 1 μg ml^{-1} in each instance. Accordingly, the amount of scandium oxide sample taken for the analysis could be 0.1–0.3 g.

Effect of stripping agent

No mineral acid at low concentration was effective for stripping the absorbed zirconium and hafnium. Although concentrated hydrochloric or nitric acid could strip these elements, the resin of the column was so severely degraded by concentrated acids that the resin could not be reused. Oxalic acid was preferred as the stripping agent because of the formation of oxalate complexes. The elution curves for zirconium as a function of oxalic acid concentration are shown in Fig. 5. Subsequently, 0.5 M oxalic acid was utilized as the stripping agent for zirconium and hafnium.

Effect of flow-rate

The flow-rate was varied from 0.4 to 1.5 ml cm^{-2} min^{-1}. It was found that flow-rates up to 1 ml cm^{-2} min^{-1} did not affect the retention of zirconium and hafnium and the elution of the matrix scandium with 6 M HCl as eluent but that the flow-rate of the stripping agent (0.5 M oxalic acid) had some effect on the stripping of zirconium and hafnium, as shown in Fig. 6. Hence, flow-rates of 1 and 0.8 ml cm^{-2} min^{-1} were adopted for scandium elution with 6 M HCl and zirconium and hafnium stripping with 0.5 M oxalic acid, respectively.

Effect of scandium and oxalic acid

Because the stripping solution used for the determination was 0.5 M oxalic acid containing trace analytes and residual scandium, it was important to examine the effect of scandium and oxalic acid on the ICP-AES determination. This was done by aspirating 0.5 μg ml^{-1} solutions of zirconium and hafnium containing scandium and oxalic acid into the plasma and measuring the emission intensities at the wavelengths used for the analyte determinations. It was found that the tolerance limit for scandium, if significant interference effects are to be avoided, is 25 μg ml^{-1} and that a solution containing oxalic acid de-

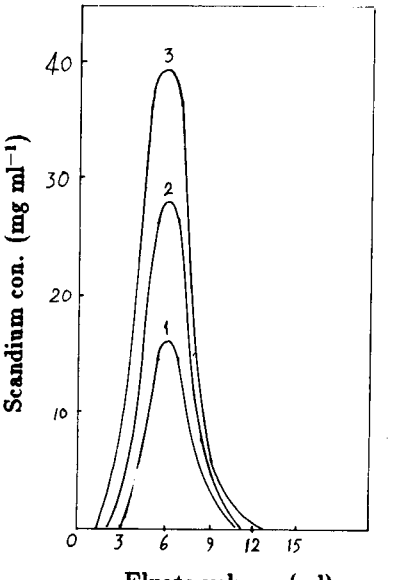

Fig. 4. Elution curves for scandium as a function of the amount of scandium oxide with 6 M HCl as the eluent: (1) 0.1; (2) 0.2; (3) 0.3 g. Flow-rate: 1 ml cm^{-2} min^{-1}.

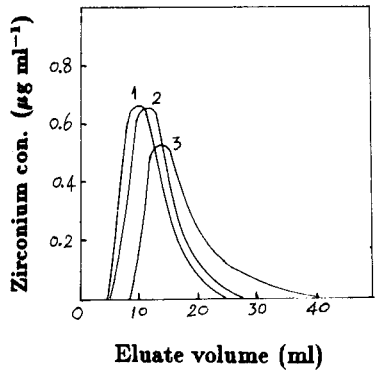

Fig. 5. Elution curves for zirconium as a function of oxalic acid concentration: (1) 1 M oxalic acid; (2) 0.5 M oxalic acid; (3) 0.1 M oxalic acid + 1.5 M HCl. Flow-rate: 0.8 ml cm^{-2} min^{-1}.

creases the emission intensities (see Fig. 7). Therefore, the oxalic acid present in the solution containing the analytes was eliminated prior to determination by heating the solution with addition of 0.5 ml of concentrated perchloric acid on a hot-plate and evaporating until almostly complete termination of the evolution of white fumes of perchloric acid. The residue was dissolved in 5 ml of 1 M hydrochloric acid, which was used for the analysis by ICP-AES. The concentration of scandium in the 5-ml volume of 1 M HCl solution was determined by ICP-AES and found to be less than 10 μg ml^{-1}. Accordingly, the enrichment factor based on 0.1 g of scandium oxide was over 2000. This low concentration of scandium of 10 μg ml^{-1} does not interfere with the ICP-AES

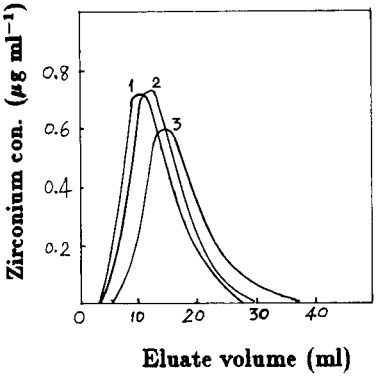

Fig. 6. Elution curves for zirconium as a function of flow-rate of 0.5 M oxalic acid; (1) 0.4; (2) 0.8; (3) 1.5 ml cm^{-2} min^{-1}.

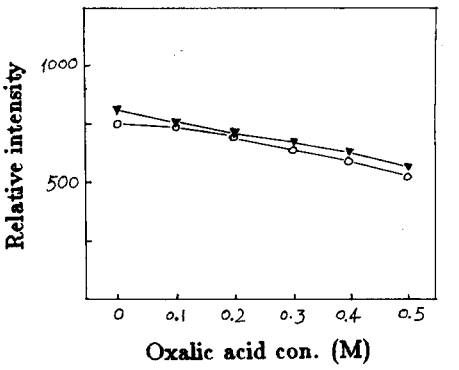

Fig. 7. Effect of oxalic acid concentration on the emission intensities of (▼) Zr and (○) Hf.

determination according to the tolerance limit for scandium. The efficiency of the separation is satisfactory.

Final analytical procedure

High-purity scandium oxide (0.1–0.3 g) was placed in a 50-ml beaker and 1.5 ml of concentrated hydrochloric acid was added. The beaker was gently heated on a hot-plate and a 0.2-ml volume of hydrogen peroxide (3%, v/v) was added carefully in small portions to accelerate dissolution of the sample. After dissolution was complete, the solution was evaporated to dryness and the residue was dissolved in 5 ml of 6 M HCl, and then the solution was passed through the column previously equilibrated with 6 M HCl. After scandium had been eluted with 80 ml of 6 M HCl at a flow-rate of 1 ml cm^{-2} min^{-1}, the extracted zirconium and hafnium on the column were quantitatively desorbed with 30 ml of 0.5 M oxalic acid at a flow-rate of 0.8 ml cm^{-2} min^{-1}. The eluate was treated as described above to eliminate oxalic acid and then diluted to volume with 1 M HCl in a 5-ml volumetric flask. Subsequently, the concentrations of zirconium and hafnium in this 1 M HCl solution were determined by ICP-AES under the operating conditions given in Table 1.

Detection limits

Detection limits are defined by the instrument's software as the concentration of an element giving a signal equal to twice the standard

TABLE 2

Detection limits, lowest determinable concentrations (LDC) of zirconium and hafnium and the specification values in high-purity scandium oxide

Element	Detection limit		LDC ($\mu g\ g^{-1}$) [a]	Specification value [b] ($\mu g\ g^{-1}$)	
	$\mu g\ ml^{-1}$	$\mu g\ g^{-1}$ [a]		Laser grade	99.9995% purity
Zr	0.008	0.14	0.4	5 [c]	10 [c]
Hf	0.01	0.17	0.5		

[a] Based on 0.3 g of sample in a final volume of 5 ml. [b] Presented by Hunan Research Institute of Rare Earth Metal Materials. [c] Total concentration of zirconium and hafnium.

deviation of the blank solution under the operating conditions adopted. The lowest determinable concentration (LDC) of zirconium and hafnium in scandium oxide based on a 0.3-g sample was taken to be that corresponding to about three times the detection limit [7]. The LDC were well below the specification values for zirconium and hafnium in high-purity scandium oxide. The results are summarized in Table 2. From these results, it can be confirmed that the proposed method used for the analysis of high-purity scandium oxide of laser grade and 99.9995% purity is effective.

TABLE 3

Recoveries of zirconium and hafnium added to high-purity scandium oxide by the proposed method

Element	Amount (μg)			Recovery (%)
	Initial	Added	Found	
Zr	0.605	2.0	2.55	97
Hf	< 0.05	2.0	1.82	91

TABLE 4

Results of the analysis of high-purity scandium oxide (means of three determinations)

Purity of scandium oxide	Element	Proposed method ($\mu g\ g^{-1}$)	SSMS [a] ($\mu g\ g^{-1}$)	Stated [b] ($\mu g\ g^{-1}$)
99.99%	Zr	8.90	7.25	< 10
	Hf	8.50	7.57	< 10
Specpure	Zr	8.10	8.20	< 10
	Hf	< 0.5	< 3.0	< 10

[a] Spark-source mass spectrometry. [b] Stated by the manufacturer.

Recoveries of zirconium and hafnium

The validity of the proposed analytical procedure was assessed by measuring the recoveries of added zirconium and hafnium. The synthetic samples used here were prepared by adding known amounts of zirconium and hafnium to high-purity scandium oxide and carried through the proposed procedure. The recoveries were > 91% (Table 3).

Analysis of high-purity scandium oxide

The proposed method was applied to the analysis of two samples. The results were compared with those obtained by a direct spark-source mass spectrometric method and are summarized in Table 4. The results showed good agreement.

REFERENCES

1 V.Z. Krasilshchik, ICP Inf. Newsl., 16 (1991) 640.
2 H.-P. Zhong and J.-L. Wang, SpectroLabo, 8 (1991) 36.
3 H. Hamayuchi, R. Kuroda, K. Aoki, R. Sugisita and N. Onuma, Talanta, 10 (1963) 153.
4 N.V. Deorkar and S.M. Khopkar, Anal. Chim. Acta, 245 (1990) 27.
5 O. Navratil and B.S. Jensen, J. Radioanal. Chem., 5 (1970) 313.
6 S.-C. Hung and S.-C. Liang, Acta Chim. Sin., 30 (1964) 1.
7 P.W.J.M. Boumans, Fresenius' Z. Anal. Chem., 299 (1979) 333.

PUBLICATION SCHEDULE FOR 1993

	S'92	O'92	N'92	D'92	J	F	M	A	M	J	J	A
Analytica Chimica Acta	267/1 267/2	268/1 268/2	269/1 269/2	270/1 270/2	271/1 271/2	272/1 272/2 273/1–2	274/1 274/2	275/1–2 276/1 276/2	277/1 277/2	278/1 278/2	279/1 279/2	280/1 280/2
Vibrational Spectroscopy		4/1			4/2		4/3	5/1		5/2		5/3

INFORMATION FOR AUTHORS

Manuscripts. The language of the journal is English. English linguistic improvement is provided as part of the normal editorial processing. Authors should submit three copies of the manuscript in clear double-spaced typing on one side of the paper only. *Vibrational Spectroscopy* also accepts papers in English only.

Abstract. All papers and reviews begin with an Abstract (50–250 words) which should comprise a factual account of the contents of the paper, with emphasis on new information.

Figures. Figures should be prepared in black waterproof drawing ink on drawing or tracing paper of the same size as that on which the manuscript is typed. One original (or sharp glossy print) and two photostat (or other) copies are required. Attention should be given to line thickness, lettering (which should be kept to a minimum) and spacing on axes of graphs, to ensure suitability for reduction in size on printing. Axes of a graph should be clearly labelled, along the axes, outside the graph itself. All figures should be numbered with Arabic numerals, and require descriptive legends which should be typed on a separate sheet of paper. Simple straight-line graphs are not acceptable, because they can readily be described in the text by means of an equation or a sentence. Claims of linearity should be supported by regression data that include slope, intercept, standard deviations of the slope and intercept, standard error and the number of data points; correlation coefficients are optional.

Photographs should be glossy prints and be as rich in contrast as possible; colour photographs cannot be accepted. Line diagrams are generally preferred to photographs of equipment.

Computer outputs for reproduction as figures must be good quality on blank paper, and should preferably be submitted as glossy prints.

Nomenclature, abbreviations and symbols. In general, the recommendations of the International Union of Pure and Applied Chemistry (IUPAC) should be followed, and attention should be given to the recommendations of the Analytical Chemistry Division in the journal *Pure and Applied Chemistry* (see also *IUPAC Compendium of Analytical Nomenclature, Definitive Rules*, 1987).

References. The references should be collected at the end of the paper, numbered in the order of their appearance in the text (*not* alphabetically) and typed on a separate sheet.

Reprints. Fifty reprints will be supplied free of charge. Additional reprints (minimum 100) can be ordered. An order form containing price quotations will be sent to the authors together with the proofs of their article.

Papers dealing with vibrational spectroscopy should be sent to: Dr J.G. Grasselli, 150 Greentree Road, Chagrin Falls, OH 44022, U.S.A. Telefax: (+1-216) 2473360 (Americas, Canada, Australia and New Zealand) or Dr J.H. van der Maas, Department of Analytical Molecule Spectrometry, Faculty of Chemistry, University of Utrecht, P.O. Box 80083, 3508 TB Utrecht, The Netherlands. Telefax: (+31-30) 518219 (all other countries).

0003-2670/93/$06.00

This issue is printed on acid-free paper.

PRINTED IN THE NETHERLANDS

Announcement from the Publisher

Elsevier Science Publishers encourages submission of articles on floppy disk.

All manuscripts may now be submitted on computer disk, with the eventual aim of reducing production times still further.

- The preferred storage medium is a 5¼ or 3½ inch disk in MS-DOS format, although other systems are welcome, e.g. Macintosh.
- After **final acceptance**, your disk plus one final, printed and exactly matching version (as a printout) should be submitted together to the editor. **It is important that the file on disk and the printout are identical.** Both will then be forwarded by the editor to Elsevier.
- Illustrations should be provided in the usual manner.
- Please follow the general instructions on style/arrangement and, in particular, the reference style of this journal as given in 'Instructions to Authors'.
- Please label the disk with your name, the software & hardware used and the name of the file to be processed.

Contact the Publisher for further information:

Elsevier Science Publishers
Analytica Chimica Acta
P.O. Box 330
1000 AH Amsterdam, The Netherlands
Phone: (+31-20) 5862 791 Fax: (+31-20) 5862 459

ELSEVIER SCIENCE PUBLISHERS

711\414\140\079\03

0003-2670(19930515)277:1;1-A